

Universiteit
Leiden
The Netherlands

Immune cell complexity in the tumor microenvironment of breast cancer

Salvagno, C.

Citation

Salvagno, C. (2019, October 22). *Immune cell complexity in the tumor microenvironment of breast cancer*. Retrieved from https://hdl.handle.net/1887/79824

Version:	Publisher's Version
License:	Licence agreement concerning inclusion of doctoral thesis in the Institutional Repository of the University of Leiden
Downloaded from:	https://hdl.handle.net/1887/79824

Note: To cite this publication please use the final published version (if applicable).

Cover Page



Universiteit Leiden



The handle http://hdl.handle.net/1887/79824 holds various files of this Leiden University dissertation.

Author: Salvagno, C.
Title: Immune cell complexity in the tumor microenvironment of breast cancer
Issue Date: 2019-10-22

IMMUNE CELL COMPLEXITY IN THE TUMOR MICROENVIRONMENT OF BREAST CANCER

Camilla Salvagno

About the cover
During my PhD I became very interested in understanding the role of macrophages in tumor progression. Macrophages are very plastic cells and are highly affected by the environment they reside and by external stimuli they receive. The cover of this thesis represents the tumor microenvironment as a factory that is actively changing the status of macrophages.

Cover concept: Camilla Salvagno and Giovanni Marinovich

Cover design: Giovanni Marinovich

Lay-out and printing: ProefschriftMaken

ISBN: 978-94-6380-439-4

The printing of this thesis was financially supported by the NKI-AvL.

© 2019 by Camilla Salvagno. All rights reserved. No part of this thesis may be reproduced, stored in a retrieval system or transmitted in any form or by any means without prior permission of the author and the publisher holding the copyright of the articles.

The research described in this thesis was performed at the division of Immunology and at the division of Tumor Biology & Immunology of the Netherlands Cancer Institute – Antoni van Leeuwenhoek Hospital (NKI-AvL), Amsterdam, The Netherlands.

IMMUNE CELL COMPLEXITY IN THE TUMOR MICROENVIRONMENT OF BREAST CANCER

Proefschrift

ter verkrijging van de graad van Doctor aan de
Universiteit Leiden
op gezag van
Rector Magnificus

Prof. Mr. C.J.J.M. Stolker

volgens besluit van het College voor Promoties
te verdedigen op dinsdag

22 oktober 2019 klokke 11:15 uur

Door
Camilla Salvagno

Geboren te Venetië
In 1987

Promotor:
Prof.dr. K. E. de Visser

Co-supervisor:
Dr. S. B. Coffelt (Cancer Research UK Beatson Institute)

Promotiecommissie:
Prof.dr. J. Borst
Prof.dr. J. Jonkers
Prof.dr. J. van Rheenen (Utrecht University)
Prof.dr. S. H. van der Burg

Table of Contents

Chapter 1 11

Scope of the thesis
Unpublished

Chapter 2 27

Purification of Immune Cell Populations from Freshly Isolated Murine Tumors and Organs by Consecutive Magnetic Cell Sorting and Multi-parameter Flow Cytometry-Based Sorting

Camilla Salvagno and Karin E. de Visser
Methods Mol Biol. 2016;1458:125-35

Chapter 3 41

Transcriptional signatures derived from murine tumor-associated macrophages predict outcome in breast cancer patients

Sander Tuit*, Camilla Salvagno*,Theodore S. Kapellos*, Cheei-Sing Hau, Lea Seep, Marie Oestereich, Kathrin Klee, Karin E. de Visser, Thomas Ulas and Joachim L. Schultze
* These authors contributed equally
Manuscript submitted for publication

Chapter 4 79

Exploiting the immunomodulatory properties of chemotherapeutic drugs to improve the success of cancer immunotherapy

Kelly Kersten[†], Camilla Salvagno[†] and Karin E. de Visser
[†]These authors contributed equally
Front Immunol. 2015 Oct 7;6:516.

Chapter 5 111

Therapeutic targeting of macrophages enhances chemotherapy efficacy by unleashing type I interferon response

Camilla Salvagno, Metamia Ciampricotti*, Sander Tuit*, Cheei-Sing Hau, Antoinette van Weverwijk, Seth B. Coffelt, Kelly Kersten, Kim Vrijland, Kevin Kos, Thomas Ulas, Ji-Ying Song, Chia-Huey Ooi, Dominik Rüttinger, Philippe A. Cassier, Jos Jonkers, Joachim L. Schultze, Carola H. Ries and Karin E. de Visser
*These authors contributed equally
Nat Cell Biol. 2019 Apr;21(4):511-521

Chapter 6 167

hMRP8-ATTAC mice: a new model for conditional and reversible neutrophil ablation

Camilla Salvagno, Lisanne Raeven, Kim Vrijland, Marjolein C. Stip, Cheei-Sing Hau, Colin Pritchard, Linda Henneman, Rahmen Bin Ali, Ivo Huijbers, Karin E. de Visser
Unpublished

Chapter 7 203

Discussion

Chapter 8 - Addenda 225

English Summary
Dutch Summary
Curriculum Vitae
Publications

CHAPTER 1

Scope of the thesis

Breast cancer is the most prevalent tumor type in women, accounting for 28% of all cancers in female patients[1]. It is estimated that 1 in 8 women will receive a diagnosis of breast cancer during her lifetime[2]. Breast cancer is a heterogeneous disease that includes several subtypes defined by histological and molecular features. Histological type, hormone receptor status (estrogen, progesterone receptor), HER2 receptor status, tumor grade and size are all aspects of the disease that affect the prognosis, the selection of treatment options and the response to therapy. Chemotherapy represents one of the main treatments that breast cancer patients receive, however, response rates differ among patients. For example, patients with invasive lobular carcinoma (ILC), a histological subtype accounting for 10% of breast cancers, respond poorer to chemotherapy compared to patients with invasive ductal carcinoma (IDC), when administered before tumor resection (neoadjuvant setting)[3]. It was proposed that this was due to the enrichment of estrogen receptor positive/HER2 negative tumors in ILC patients, which are less sensitive to chemotherapy[4]. Because pathologic response to neoadjuvant chemotherapy of the primary breast tumor is associated with long-term survival[5,6], it is essential to discover new therapeutic strategies that improve the success rate of chemotherapy.

Since Theodor Boveri hypothesized the existence of a causal link between chromosomal abnormalities and tumor growth in 1914[7], the idea that tumors arise solely as a consequence of mutations in healthy cells and that their genetic aberrations are the determinants of therapy response dominated the oncology field for decades. However, this concept of cancer as a "disease of the genome", does not fully explain tumor progression and therapy outcome. In the 1970s, researchers started to acknowledge the tumor microenvironment (TME) as a key component able to influence tumor behavior[8]. Alongside cancer cells, tumors include different cell populations, such as immune cells, fibroblasts and endothelial cells. In addition, their secreted inflammatory mediators like cytokines, chemokines and metabolites, and elements of the extracellular matrix play a central role in the TME. It is now well established that the components of the TME are active players in tumor development and progression[9]. Of particular interest are immune cells because of their opposing abilities to interfere or promote tumor growth[10,11]. Indeed, in the past years, great emphasis was placed on understanding the impact of immune cells in tumor initiation, progression and metastasis formation that led to the development of different types of immunotherapies[12].

Tumor-associated inflammation

The immune system includes cells from the innate and adaptive arm which, by communicating with each other, protect the human body against foreign pathogens in a fine-tuned and regulated fashion. The immune system has developed in such a way that, upon perturbation of tissue homeostasis, it sets in motion a chain of

events that leads to the elimination of the assaulting agents and that culminates in wound healing and resolution of inflammation. Cells from the innate immune compartment, also called myeloid cells, like monocytes/macrophages, neutrophils, eosinophils, mast cells, dendritic cells (DCs) and NK cells, represent the first line of defense against foreign pathogens. They are also pivotal in bridging the innate and adaptive immune system by helping the activation of CD8+ and CD4+ T cells and B cells. Differently from the unspecific responses of myeloid cells, adaptive immune cells provide antigen-specific responses against pathogen-infected cells.

When the immune system fails to clear the initiating stimulus, chronically activated immune cells persist and induce tissue damage that may, in some cases, increase the risk of cancer development[10]. The first awareness of this concept was by Rudolph Virchow in 1863, when he proposed a causal link between inflammation and cancer after the observation that solid tumors are infiltrated by leukocytes[13]. Indeed, in some instances, inflammation can trigger tumorigenesis. For example, infections with the bacteria Helicobacter Pylori or the Hepatitis B and Hepatitis C viruses may lead to chronic gastritis and hepatitis, respectively, that may result in gastric or liver cancers[14,15]. Besides infectious pathogens, toxic agents and irritants that cause inflammation are also linked to tumor development, e.g. asbestos and malignant mesothelioma[16]. In addition to inflammation-induced cancers, many tumors induce inflammation, which can further promote tumor progression. Similar to a chronic infection, cancer is often described to be chronically inflamed or as a "wound that does not heal" due to the failed resolution of the original damage[17]. For decades, researchers have acknowledged that the majority of neoplastic lesions are highly infiltrated by cells of both the innate and adaptive immune system, resembling a chronic infection-induced inflammatory state. Tumor-associated chronic inflammation is characterized by accumulation of pro-inflammatory and pro-tumorigenic innate immune cells that produce cytokines, free radicals, growth and angiogenic factors, that sustain tumor growth and progression[10]. In addition, chronic inflammation supports immunosuppression in the TME, able to negate the anti-tumor cytotoxic activity of adaptive immune cells, such as CD8+ T cells[10]. Notably, the tumor-promoting capacity of inflammation was added to the list of hallmarks of cancer[18].

Macrophages, whose infiltration into tumors was already described in the late 70s – early 80s[19-21], represent one of the main immune cell types studied in the immune-oncology field. In a healthy organism, macrophages are found in every tissue with unique properties critical for the physiological function of a specific organ. Tissue-resident macrophages derive from the yolk sac and fetal liver during embryogenesis, but in certain conditions like infection or injury, damaged tissues recruit inflammatory monocytes from the circulation, blood and bone marrow which differentiate into macrophages[22]. Likewise, in mouse models for breast

cancer, tumor-associated macrophages (TAMs) have been proposed to derive from CCR2+ inflammatory monocytes[23], although local proliferation of differentiated macrophages has also been suggested[24]. Although early in vitro studies considered macrophages as tumoricidal cells[25], it is now appreciated that TAMs frequently function as orchestrators of tumor progression and metastatic disease via several mechanisms including support of angiogenesis, stimulation of tumor cell proliferation and migration, and suppression of anti-tumor immune responses[26]. Indeed, the majority of tumor types are densely populated by these cells, and for most of them, like breast, ovarian and oral cancers, the presence of macrophages is a negative prognostic factor[27-29]. Initially, TAMs were simplistically described as being either anti-tumoral (M1) or pro-tumoral (M2) by the expression of few markers. However, this dual definition has left room for a more complicated, but realistic view of macrophage phenotype. Indeed, using single cell RNA sequencing analysis, a recent study reported both M1- and M2-associated genes in the same macrophage isolated from the tumor of breast cancer patients[30]. TAMs, like tissue resident macrophages in general, are characterized by a remarkable plastic behavior; they adapt their phenotype depending on the environment they reside. Different stimuli, such as cyokines, metabolites and growth factors, derived from cancer cells or from stromal/immune cells can affect the macrophage polarization status and function in a dynamic and continuous fashion. This implies that macrophages are a heterogeneous population that differ between and within tumor types.

Apart from the role of inflammation in promoting tumor development, recent studies have shown that cancer cells are also able to dictate the intratumoral immune landscape and to induce systemic inflammation[31]. As the first cells that arrive in an inflamed site, neutrophils are well known to be mediators of inflammation. They are constantly produced in the bone marrow, in a process termed granulopoiesis, under control of the granulocytes-colony stimulating factor (G-CSF), the key regulator of neutrophil formation and differentiation[32,33]. Under critical circumstances, like cancer, malignant cell- and stromal cell-derived G-CSF stimulates the bone marrow and other organs (emergency granulopoiesis) to increase neutrophil generation[34,35]. Interestingly, this action also induces the release of immature neutrophils that have a less hypersegmented nucleus and that retain cKIT expression, which is usually found on progenitor cells[34]. Once in the circulation, the half-life of neutrophils is only about 7 hours, but it is increased to 17 hours in cancer patients[36]. Despite being short-lived cells, neutrophils can influence tumor progression[35]. Although a few preclinical studies showed an anti-tumorigenic role for neutrophils, the vast majority of preclinical studies reported a tumor-promoting function for these cells[35]. This effect is also mirrored in the clinic where a high neutrophil-to-lymphocyte ratio in the circulation of patients with several types of cancer is associated with worse disease outcome[37,38]. Like macrophages, also neutrophil phenotype is believed to

be constantly influenced by the environment, although our insights into neutrophil plasticity are still limited. Therefore, it is important to understand the function of neutrophils in each tumor settings in order to design new therapeutic strategies.

Not all cells of the immune system have pro-tumorigenic properties. For example, cytotoxic T cells are capable of killing cancer cells and controlling tumor progression. To obtain a successful anti-tumor response a process termed cancer-immunity cycle should be fulfilled[39]. Upon release of antigens from cancer cells and subsequent antigen uptake by dendritic cells (DCs), T cells are primed and activated. Effector T cells then infiltrate the tumor and kill the target cancer cells after recognizing the complex formed by a peptide and a major histocompatibility class I (MHC-I) molecule on the surface of malignant cells through their T cell receptor (TCR). The release of new antigens upon T cell-mediated killing of tumor cells reinforces the progression of the cycle. However, the generation of effective anti-tumor immunity is hampered by a series of bottlenecks, including paucity of released antigens, improper DC and T cell activation, and immunosuppressive mechanisms like the presence of myeloid cells and regulatory T cells (Tregs) that hamper the activity of cytotoxic T cells. Finding new ways to overcome these obstacles is essential in order to mount an effective immune response. Thus, the TME represents a complex dynamic environment in which immune cells paradoxically influence tumor growth in opposite ways. The pro- and anti-tumoral effects of the innate and adaptive immune system, respectively, often result in a tilted balance in favor of cancer progression.

The interplay between chemotherapy and immune system

The first chemotherapeutic drug, nitrogen mustard, a DNA alkylating agent, was discovered in the early 1940s and from that time on new chemotherapeutic agents and new combinations of cytotoxic drugs were used as standard of care in the clinic[40]. Apart from DNA damaging agents, other chemotherapies interfere with the DNA replication machinery or block cell mitosis. Although for a very long time chemotherapy was considered to solely target highly proliferating cancer cells, studies have shown that chemotherapeutic agents themselves have the capacity to modify the composition of the tumor microenvironment and the phenotype and function of intratumoral immune cells[41]. Because the immunomodulatory effects of some conventional cytotoxic therapies include inhibition of immunosuppressive cells, they could be strategically used in combination with immunotherapeutic agents to enhance anti-tumor immunity[41].

Although chemotherapeutic agents are frequently used for the treatment of the majority of tumor types, their anti-cancer effects are, most of the time, temporary. Cancer cells can escape the treatment regime because of the emergence of drug-resistant cells that, for instance, carry mutations in the target enzyme or enhance

DNA damage repair pathways, or overexpress drug efflux pumps[42]. Besides these cancer cell-intrinsic mechanisms, it is now clear that the tumor microenvironment also influences chemotherapy sensitivity[43]. Among the cells of the TME, macrophages have been the focus of a large number of studies addressing their role in response to chemotherapy. In breast cancer patients, a high intratumoral macrophage-to-CD8+ T cell ratio predicts poor response to chemotherapy[44,45]. In support of a detrimental function of macrophages in chemotherapy efficacy, preclinical mouse studies have shown that the elimination of these cells increased the efficacy of various chemotherapeutic drugs[45-52]. Several mechanisms have been accounted for the role of macrophages in limiting chemotherapy efficacy, including secretion of cathepsins that protect tumor cells from chemotherapy-induced cell death[51], production of lysophospholipids that affect the DNA damage response[46], and secretion of IL-10 that indirectly suppresses the cytotoxic activity of CD8+ T cells by inhibiting dendritic cell functions[50].

One clinically relevant strategy to deplete macrophages is to interfere with the CSF-1/CSF-1R signaling pathway, which is crucial for macrophage homeostasis, proliferation and survival[53]. Therapeutic agents include antibodies against CSF-1 or against the receptor, or small molecules inhibitors of the tyrosine kinase domain of CSF-1R[54]. Thus far, monotherapy with these drugs in clinical trials have shown limited efficacy in solid tumors, except for the high response rate of one particular cancer type, the diffuse-type tenosynovial giant cell tumor, characterized by CSF-1 overexpression and recruitment of CSF-1R+ cells[54]. In order to improve the therapeutic success of these drugs, it is crucial to understand the effects of these molecules on the TME and to identify their optimal therapeutic partner for combination treatment.

Similar to macrophages, neutrophils are also able to affect the response to chemotherapy. Although it was reported that depletion of neutrophils using the neutrophil-specific anti-Ly6G antibody modestly reduced the efficacy of doxorubicin in mice bearing inoculated cancer cells[55], other studies have shown that preventing their recruitment via inhibitors of the chemokine receptor CXCR2 in combination with chemotherapy decreased tumor growth in several mouse tumor models[56-58]. In line with these experimental data, clinical studies showed a better prognosis and a decreased recurrence risk in breast cancer patients that underwent chemotherapy-induced neutropenia[59,60]. It is thus important to understand in which settings neutrophils affect chemotherapy response and the underling mechanisms.

It is now clear that tumors hijack myeloid cells to sustain their growth and to hinder the anti-cancer efficacy of chemotherapy. Thus, targeting these cells represent a compelling strategy in combination with cytotoxic agents. However, understanding the mechanisms behind the effects of myeloid cells on therapy response is critical to design novel and more specific therapeutic strategies.

Description of the chapters in this thesis

Work described in this thesis aims to understand the role of myeloid cells in tumor progression and therapy response of breast cancer. Utilizing transgenic mouse models for breast cancer, I explored methodologies to study the role and phenotype of intratumoral immune cells, with a focus on how the tumor milieu affects macrophage phenotype. Moreover, I mechanistically addressed how immune cells impact the chemotherapy response of breast cancer.

The immune system is not a static component of the tumor microenvironment, but it constantly changes and adapts, co-evolving with the tumor during its initiation and progression. To study how cancer cells shape the phenotype of tumor-infiltrating immune cells, it is important to directly isolate the immune cells from freshly isolated tumors. In this regard, **chapter 2** describes a methodology to isolate immune cells from murine mammary tumors and other organs. This method is based on antibody-mediated enrichment of immune cells by magnetic cell sorting followed by purification of selected immune cell populations with multi-color flow cytometry-based sorting. By using this methodology, we studied in **chapter 3** whether and how distinct breast cancer models differently affect the phenotype of intratumoral macrophages. TAMs from two distinct genetically engineered mouse models (GEMMs) for *de novo* mammary tumorigenesis, *i.e. K14cre;Cdh1$^{F/F}$;Trp53$^{F/F}$* and *MMTV-NeuT* mouse models which resemble human ILC and HER2-overexpressing tumors, respectively[61,62], were compared at the transcriptomic level. Computational analysis of RNA sequencing data showed that although clustering together with macrophages from the mammary gland, these TAM populations showed a common signature as well as a breast cancer type-specific core signature. Interestingly, a selection of the genes derived from the model-specific core gene signature from the *K14cre;Cdh1$^{F/F}$;Trp53$^{F/F}$* model correlated with worse clinical outcome in two independent cohorts of ILC patients, while the core signature of TAMs derived from the *MMTV-NeuT* mammary tumors failed to predict prognosis in the same ILC patient cohort. These data highlight that the tumor of two independent GEMMs have such a strong impact on the transcriptome profile of intratumoral macrophages.

The second part of this thesis focuses on the impact of chemotherapy on the immune system and vice versa. There is growing evidence that chemotherapeutic drugs do not only target cancer cells, but also have immunomodulatory effects. **Chapter 4** reviews the preclinical and clinical studies investigating the impact of chemotherapeutic agents on various immune cell populations. For example, some chemotherapeutic agents target the lymphoid compartment, like low doses of cyclophosphamide that reduce regulatory T cells (Treg)[63], while other

chemotherapies influence the myeloid compartment like gemcitabine that reduces myeloid-derived suppressor cells (MDSC)[64] or trabectedin that selectively ablates monocytes and macrophages[65]. Because of the influence that chemotherapeutic agents have on these immunosuppressive immune cells, in this chapter we propose to rationally combine certain chemotherapies with immunotherapy in order to boost anti-tumor immunity.

As macrophage-targeting agents are under clinical investigation, **chapter 5** aims to maximize the success of these compounds and to uncover the mechanisms by which these agents can increase the sensitivity of breast cancer to chemotherapeutic drugs. By using a spontaneous mouse model for breast cancer, the *K14cre;Cdh1$^{F/F}$;Trp53$^{F/F}$* mouse model, we reveal that anti-CSF-1R synergizes with platinum-containing drugs by inducing an intratumoral type I interferon response. In particular, we discovered that anti-CSF-1R on one hand depletes the majority of TAMs and on the other hand changes the activation status of the remaining intratumoral macrophages into a type I interferon-producing phenotype. We further uncovered that the establishment of a type I interferon-enriched milieu and the elimination of immunosuppressive neutrophils were both critical to support anti-tumor immunity upon cisplatin treatment.

The most relevant method to study the role of immune cells in tumorigenesis or in chemotherapy response is to deplete these cells by either genetic manipulation of key factors involved in their recruitment to the tumor site or in their development (like chemokine receptors or transcription factors) or via antibody-mediated depletion. While for most immune cells this can be successfully achieved, the long-term depletion of neutrophils still remains challenging.
The most commonly used methods to target neutrophils *in vivo* are antibody-based techniques, which, however, lack specificity or fail to provide long-lasting depletion. Few genetic models have been generated of which the most satisfactory rely on the expression of the diphtheria toxin (DT) receptor in neutrophils and administration of DT to induce neutrophil apoptosis[66]. Nevertheless, durable depletion with this system is not achieved because of the generation of a neutralizing immune response against DT[67,68]. In order to overcome these limitations, in **chapter 6** we generated a novel mouse model for the conditional and reversible depletion of neutrophils using the Apoptosis Through Targeted Activation of Caspase 8 (ATTAC) approach[69]. This mouse model relies on the activation of apoptosis specifically in neutrophils upon injection of a compound. This chapter describes the model and characterizes the efficiency of neutrophil depletion, both in a homeostatic and in a cancer setting.

Finally, in **chapter 7** I contextualize the findings of this thesis in regards to the current literature. I also discuss the implications of my data concerning the current and future clinical strategies with immunomodulatory compounds.

In conclusion, in this thesis I focus on the non-cancer cell autonomous mechanisms that govern tumor progression and response to anti-cancer therapies, with a major emphasis on macrophages and neutrophils. I highlight the complex relationship between myeloid cells and tumor cells that might lead to the discovery of new therapeutic strategies.

References

1. www.cijfersoverkanker.nl.
2. https://seer.cancer.gov/data/.
3. Cristofanilli, M., et al. Invasive lobular carcinoma classic type: response to primary chemotherapy and survival outcomes. J Clin Oncol 23, 41-48 (2005).
4. Lips, E.H., et al. Lobular histology and response to neoadjuvant chemotherapy in invasive breast cancer. Breast Cancer Res Treat 136, 35-43 (2012).
5. Cortazar, P., et al. Pathological complete response and long-term clinical benefit in breast cancer: the CTNeoBC pooled analysis. Lancet 384, 164-172 (2014).
6. Symmans, W.F., et al. Long-Term Prognostic Risk After Neoadjuvant Chemotherapy Associated With Residual Cancer Burden and Breast Cancer Subtype. J Clin Oncol 35, 1049-1060 (2017).
7. Boveri, T. Concerning the origin of malignant tumours by Theodor Boveri. Translated and annotated by Henry Harris. J Cell Sci 121 Suppl 1, 1-84 (2008).
8. Prehn, R.T. The immune reaction as a stimulator of tumor growth. Science 176, 170-171 (1972).
9. Hanahan, D. & Coussens, L.M. Accessories to the crime: functions of cells recruited to the tumor microenvironment. Cancer Cell 21, 309-322 (2012).
10. de Visser, K.E., Eichten, A. & Coussens, L.M. Paradoxical roles of the immune system during cancer development. Nat Rev Cancer 6, 24-37 (2006).
11. Quail, D.F. & Joyce, J.A. Microenvironmental regulation of tumor progression and metastasis. Nat Med 19, 1423-1437 (2013).
12. Galluzzi, L., et al. Classification of current anticancer immunotherapies. Oncotarget 5, 12472-12508 (2014).
13. Schmidt, A. & Weber, O.F. In memoriam of Rudolf virchow: a historical retrospective including aspects of inflammation, infection and neoplasia. Contrib Microbiol 13, 1-15 (2006).
14. Brechot, C. Pathogenesis of hepatitis B virus-related hepatocellular carcinoma: old and new paradigms. Gastroenterology 127, S56-61 (2004).
15. Wroblewski, L.E., Peek, R.M., Jr. & Wilson, K.T. Helicobacter pylori and gastric cancer: factors that modulate disease risk. Clin Microbiol Rev 23, 713-739 (2010).
16. Liu, G., Cheresh, P. & Kamp, D.W. Molecular basis of asbestos-induced lung disease. Annu Rev Pathol 8, 161-187 (2013).
17. Dvorak, H.F. Tumors: wounds that do not heal. Similarities between tumor stroma generation and wound healing. N Engl J Med 315, 1650-1659 (1986).
18. Hanahan, D. & Weinberg, R.A. Hallmarks of cancer: the next generation. Cell 144, 646-674 (2011).
19. Haskill, S., Becker, S., Fowler, W. & Walton, L. Mononuclear-cell infiltration in ovarian cancer. I. Inflammatory-cell infiltrates from tumour and ascites material. Br J Cancer 45, 728-736 (1982).
20. Hersh, E.M., Mavligit, G.M., Gutterman, J.U. & Barsales, P.B. Mononuclear cell content of human solid tumors. Med Pediatr Oncol 2, 1-9 (1976).
21. Russel, S.W., Doe, W.F. & Cochrane, C.G. Number of macrophages and distribution of mitotic activity in regressing and progressing Moloney sarcomas. J Immunol 116, 164-166 (1976).
22. Wynn, T.A., Chawla, A. & Pollard, J.W. Macrophage biology in development, homeostasis and disease. Nature 496, 445-455 (2013).

23. Franklin, R.A., et al. The cellular and molecular origin of tumor-associated macrophages. Science 344, 921-925 (2014).
24. Tymoszuk, P., et al. In situ proliferation contributes to accumulation of tumor-associated macrophages in spontaneous mammary tumors. Eur J Immunol 44, 2247-2262 (2014).
25. Fidler, I.J. & Schroit, A.J. Recognition and destruction of neoplastic cells by activated macrophages: discrimination of altered self. Biochim Biophys Acta 948, 151-173 (1988).
26. Mantovani, A., Marchesi, F., Malesci, A., Laghi, L. & Allavena, P. Tumour-associated macrophages as treatment targets in oncology. Nat Rev Clin Oncol 14, 399-416 (2017).
27. Yuan, X., et al. Prognostic significance of tumor-associated macrophages in ovarian cancer: A meta-analysis. Gynecol Oncol 147, 181-187 (2017).
28. Zhang, Q.W., et al. Prognostic significance of tumor-associated macrophages in solid tumor: a meta-analysis of the literature. PLoS One 7, e50946 (2012).
29. Zhao, X., et al. Prognostic significance of tumor-associated macrophages in breast cancer: a meta-analysis of the literature. Oncotarget 8, 30576-30586 (2017).
30. Azizi, E., et al. Single-Cell Map of Diverse Immune Phenotypes in the Breast Tumor Microenvironment. Cell 174, 1293-1308 e1236 (2018).
31. Wellenstein, M.D. & de Visser, K.E. Cancer-Cell-Intrinsic Mechanisms Shaping the Tumor Immune Landscape. Immunity 48, 399-416 (2018).
32. Liu, F., Wu, H.Y., Wesselschmidt, R., Kornaga, T. & Link, D.C. Impaired production and increased apoptosis of neutrophils in granulocyte colony-stimulating factor receptor-deficient mice. Immunity 5, 491-501 (1996).
33. Richards, M.K., Liu, F., Iwasaki, H., Akashi, K. & Link, D.C. Pivotal role of granulocyte colony-stimulating factor in the development of progenitors in the common myeloid pathway. Blood 102, 3562-3568 (2003).
34. Coffelt, S.B., et al. IL-17-producing gammadelta T cells and neutrophils conspire to promote breast cancer metastasis. Nature 522, 345-348 (2015).
35. Coffelt, S.B., Wellenstein, M.D. & de Visser, K.E. Neutrophils in cancer: neutral no more. Nat Rev Cancer 16, 431-446 (2016).
36. Steinbach, K.H., et al. Estimation of kinetic parameters of neutrophilic, eosinophilic, and basophilic granulocytes in human blood. Blut 39, 27-38 (1979).
37. Templeton, A.J., et al. Prognostic role of neutrophil-to-lymphocyte ratio in solid tumors: a systematic review and meta-analysis. J Natl Cancer Inst 106, dju124 (2014).
38. Wei, B., et al. The neutrophil lymphocyte ratio is associated with breast cancer prognosis: an updated systematic review and meta-analysis. Onco Targets Ther 9, 5567-5575 (2016).
39. Chen, D.S. & Mellman, I. Oncology meets immunology: the cancer-immunity cycle. Immunity 39, 1-10 (2013).
40. Chabner, B.A. & Roberts, T.G., Jr. Timeline: Chemotherapy and the war on cancer. Nat Rev Cancer 5, 65-72 (2005).
41. Galluzzi, L., Senovilla, L., Zitvogel, L. & Kroemer, G. The secret ally: immunostimulation by anticancer drugs. Nat Rev Drug Discov 11, 215-233 (2012).

42. Holohan, C., Van Schaeybroeck, S., Longley, D.B. & Johnston, P.G. Cancer drug resistance: an evolving paradigm. Nat Rev Cancer 13, 714-726 (2013).
43. Coffelt, S.B. & de Visser, K.E. Immune-mediated mechanisms influencing the efficacy of anticancer therapies. Trends Immunol 36, 198-216 (2015).
44. Campbell, M.J., et al. The prognostic implications of macrophages expressing proliferating cell nuclear antigen in breast cancer depend on immune context. PLoS One 8, e79114 (2013).
45. DeNardo, D.G., et al. Leukocyte complexity predicts breast cancer survival and functionally regulates response to chemotherapy. Cancer Discov 1, 54-67 (2011).
46. Houthuijzen, J.M., et al. Lysophospholipids secreted by splenic macrophages induce chemotherapy resistance via interference with the DNA damage response. Nat Commun 5, 5275 (2014).
47. Mitchem, J.B., et al. Targeting tumor-infiltrating macrophages decreases tumor-initiating cells, relieves immunosuppression, and improves chemotherapeutic responses. Cancer Res 73, 1128-1141 (2013).
48. Olson, O.C., Kim, H., Quail, D.F., Foley, E.A. & Joyce, J.A. Tumor-Associated Macrophages Suppress the Cytotoxic Activity of Antimitotic Agents. Cell Rep 19, 101-113 (2017).
49. Paulus, P., Stanley, E.R., Schafer, R., Abraham, D. & Aharinejad, S. Colony-stimulating factor-1 antibody reverses chemoresistance in human MCF-7 breast cancer xenografts. Cancer Res 66, 4349-4356 (2006).
50. Ruffell, B., et al. Macrophage IL-10 blocks CD8+ T cell-dependent responses to chemotherapy by suppressing IL-12 expression in intratumoral dendritic cells. Cancer Cell 26, 623-637 (2014).
51. Shree, T., et al. Macrophages and cathepsin proteases blunt chemotherapeutic response in breast cancer. Genes Dev 25, 2465-2479 (2011).
52. Weizman, N., et al. Macrophages mediate gemcitabine resistance of pancreatic adenocarcinoma by upregulating cytidine deaminase. Oncogene 33, 3812-3819 (2014).
53. Stanley, E.R. & Chitu, V. CSF-1 receptor signaling in myeloid cells. Cold Spring Harb Perspect Biol 6(2014).
54. Cannarile, M.A., et al. Colony-stimulating factor 1 receptor (CSF1R) inhibitors in cancer therapy. J Immunother Cancer 5, 53 (2017).
55. Ma, Y., et al. Anticancer chemotherapy-induced intratumoral recruitment and differentiation of antigen-presenting cells. Immunity 38, 729-741 (2013).
56. Acharyya, S., et al. A CXCL1 paracrine network links cancer chemoresistance and metastasis. Cell 150, 165-178 (2012).
57. Di Mitri, D., et al. Tumour-infiltrating Gr-1+ myeloid cells antagonize senescence in cancer. Nature 515, 134-137 (2014).
58. Nywening, T.M., et al. Targeting both tumour-associated CXCR2(+) neutrophils and CCR2(+) macrophages disrupts myeloid recruitment and improves chemotherapeutic responses in pancreatic ductal adenocarcinoma. Gut 67, 1112-1123 (2018).
59. Han, Y., et al. Prognostic value of chemotherapy-induced neutropenia in early-stage breast cancer. Breast Cancer Res Treat 131, 483-490 (2012).

60. Ma, R.M., et al. Prognostic Value of Chemotherapy-Induced Neutropenia at the First Cycle in Invasive Breast Cancer. Medicine (Baltimore) 95, e3240 (2016).
61. Boggio, K., et al. Interleukin 12-mediated prevention of spontaneous mammary adenocarcinomas in two lines of Her-2/neu transgenic mice. J Exp Med 188, 589-596 (1998).
62. Derksen, P.W., et al. Somatic inactivation of E-cadherin and p53 in mice leads to metastatic lobular mammary carcinoma through induction of anoikis resistance and angiogenesis. Cancer Cell 10, 437-449 (2006).
63. Lutsiak, M.E., et al. Inhibition of CD4(+)25+ T regulatory cell function implicated in enhanced immune response by low-dose cyclophosphamide. Blood 105, 2862-2868 (2005).
64. Le, H.K., et al. Gemcitabine directly inhibits myeloid derived suppressor cells in BALB/c mice bearing 4T1 mammary carcinoma and augments expansion of T cells from tumor-bearing mice. Int Immunopharmacol 9, 900-909 (2009).
65. Germano, G., et al. Role of macrophage targeting in the antitumor activity of trabectedin. Cancer Cell 23, 249-262 (2013).
66. Reber, L.L., et al. Neutrophil myeloperoxidase diminishes the toxic effects and mortality induced by lipopolysaccharide. J Exp Med 214, 1249-1258 (2017).
67. Rombouts, M., et al. Long-Term Depletion of Conventional Dendritic Cells Cannot Be Maintained in an Atherosclerotic Zbtb46-DTR Mouse Model. PLoS One 12, e0169608 (2017).
68. Wang, J., Siffert, M., Spiliotis, M. & Gottstein, B. Repeated Long-Term DT Application in the DEREG Mouse Induces a Neutralizing Anti-DT Antibody Response. J Immunol Res 2016, 1450398 (2016).
69. Pajvani, U.B., et al. Fat apoptosis through targeted activation of caspase 8: a new mouse model of inducible and reversible lipoatrophy. Nat Med 11, 797-803 (2005).

CHAPTER 2

Purification of Immune Cell Populations from Freshly Isolated Murine Tumors and Organs by Consecutive Magnetic Cell Sorting and Multi-parameter Flow Cytometry-Based Sorting

Camilla Salvagno and Karin E. de Visser

Division of Immunology, Netherlands Cancer Institute, Amsterdam, The Netherlands

Methods Mol Biol. 2016;1458:125-35

Abstract

It is well established that tumors evolve together with nonmalignant cells, such as fibroblasts, endothelial cells, and immune cells. These cells constantly entangle and interact with each other creating the tumor microenvironment. Immune cells can exert both tumor-promoting and tumor-protective functions. Detailed phenotypic and functional characterization of intratumoral immune cell subsets has become increasingly important in the field of cancer biology and cancer immunology. In this chapter, we describe a method for isolation of viable and pure immune cell subsets from freshly isolated murine solid tumors and organs. First, we describe a protocol for the generation of single-cell suspensions from tumors and organs using mechanical and enzymatic strategies. In addition, we describe how immune cell subsets can be purified by consecutive magnetic cell sorting and multiparameter flow cytometry-based cell sorting.

Key words

Tumor microenvironment
Immune cells
Myeloid cells
Magnetic cell sorting
Enrichment Fluorescence-activated cell sorting (FACS)
Solid tumor
Preclinical mouse model

1. Introduction

It is now well established that immune cells present in the tumor microenvironment play a critical role in tumor development and progression [1]. Most human and experimental tumors are abundantly infiltrated with various immune cell types. The presence of some of these immune cells, including regulatory T cells, macrophages, and myeloid-derived suppressor cells, is frequently associated with a poor prognosis [2, 3, 4], while other immune cells, including CD8+ T cells and NK cells, frequently correlate with good prognosis [5, 6]. Experimental studies using transgenic mouse models for de novo tumorigenesis have been instrumental in identifying the functional significance of the various immune cell subsets in tumor development, progression, and therapy response [4, 7, 8, 9, 10, 11]. In these transgenic tumor models, tumors develop spontaneously in their natural microenvironment and immune cells evolve together with tumor cells, thus closely recapitulating tumor development in the human setting [12]. For these reasons, careful phenotypic and functional characterization of the complexity of the inflammatory tumor microenvironment has been increasingly important.

There are various methods for the assessment of the type, the phenotype, and/or the activation status of immune cells in tumors and other organs. It is possible to either directly analyze freshly generated single-cell suspension by multi-parameter flow cytometry or isolate specific immune cell population by flow cytometry-based cell sorting for further culturing, protein, or RNA extraction analyses. Regardless of which of these techniques will be performed, single-cell suspensions need to be generated from tumor and organs. Here, we describe a protocol to mechanically and enzymatically process tumors and other organs to generate single-cell suspensions and to prepare the samples for flow cytometry analysis. Flow cytometry-based sorting is the ultimate method for the isolation of specific cell populations. However, depending on the number and percentage of the immune cells of interest, the actual sorting procedure might be time consuming. In order to accelerate the sorting procedure and to obtain a high purity of the desired cells, we have described a two-step method for isolation of several myeloid cell subsets from tumors. Briefly, we first enrich the samples for myeloid immune cells by the use of magnetic cell sorting; then, we isolate immune cell subpopulations by flow cytometry-based sorting. A schematic overview of the protocol is depicted in Fig. 1. Although here we focus on the isolation of myeloid immune cells, researchers can adapt this protocol for the isolation of other type of cells, such as lymphocytes.

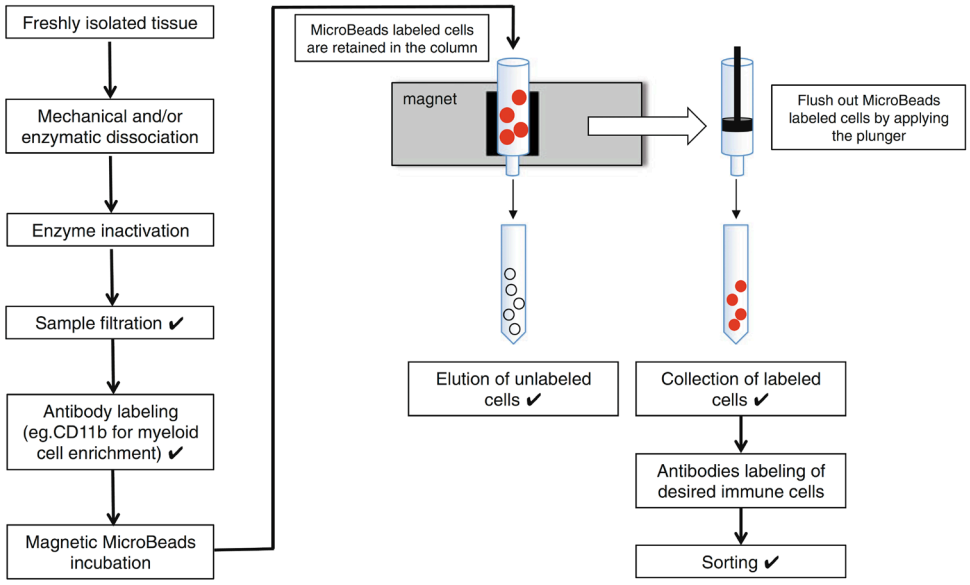


Fig. 1 | Schematic workflow of the immune cell subset isolation by magnetic cell sorting and multi-parameter flow cytometry-based cell sorting. Ticks (√) indicate steps to collect a small sample of cells that will be analyzed by flow cytometry at the end of the protocol

2. Materials

2.1. Generation of Single-Cell Suspensions from Freshly Isolated Solid Tumors and Organs

1. McIlwain Tissue Chopper (Ted Pella, Inc.) (*see* **Note 1**).
2. Enzyme digestion mix 1: 3 mg/mL Collagenase A in DMEM (serum free) (*see* **Notes 2** and **3**).
3. Enzyme digestion mix 2: 100 µg/mL Liberase in DMEM (serum free).
4. DMEM medium supplemented with 8 % fetal bovine serum (FBS), 100 IU/mL penicillin, 100 µg/mL streptomycin (P/S), and 0.5 mM EDTA.
5. DMEM medium supplemented with 8 % FBS, P/S.
6. Sorting buffer: IMDM, 2 % FBS, 0.5 % β-mercaptoethanol, 0.5 mM EDTA.
7. Erylysis buffer: 155 mM NH4Cl, 10 mM KHCO3, 0.1 mM EDTA in H2O, pH 7.2–7.4.
8. 5000 U.I./mL Heparin sulfate.
9. Deoxyribonuclease I from bovine pancreas (DNase) dissolved to 10 µg/µL in1× PBS.
10. FACS buffer: 0.5 % BSA in 1× PBS.
11. Plunger from a 2 mL syringe.
12. Water bath or MACSmix™ tube rotator from Miltenyi Biotec.

2.2. Purification of Immune Cell Subsets by Consecutive Magnetic Cell Sorting and Multi-parameter Fluorescence-Activated Cell Sorting (FACS)

1. AutoMACS™ Rinsing Solution supplemented with 0.5 % BSA from Miltenyi Biotec (*see* **Note 4**).
2. Magnetic Micro Beads (Miltenyi Biotec) conjugated to an antibody with specificity for the fluorochrome of the antibody used in Subheading 3.3, step 3 (*see* **Notes 4** and **5**).
3. QuadroMACS™ separator from Miltenyi Biotec (*see* **Notes 4** and **6**).
4. LS columns from Miltenyi Biotec (*see* **Notes 4** and **7**).
5. Antibodies: For the antibody combination used to isolate different myeloid cell populations, see Table 1 (*see* **Notes 8** and **9**).

Table 1 | Example of an antibody panel for the purification of several myeloid cell populations by consecutive magnetic cell sorting and flow cytometry-based cell sorting

Antigen	Marker for	Fluorochromes/ dye
CD11b	Myeloid cells	APC
F4/80	Macrophages	PE
Ly6G (1A8)	Neutrophils	FITC
Ly6C	Monocytes and neutrophils	eFluor450
	Live/dead	405 excitation

2.3. Other Materials

1. 96-Well U-bottom plates.
2. 70 µm Filter cell strainers that fit on top of a 50 mL tube.
3. 15 and 50 mL Polypropylene tubes (see **Note 19**).
4. 5 mL Polypropylene tubes.
5. Antibodies: For the antibody combination used for quantitative and/or phenotypic characterization of immune cells, see Table 2 (see **Note 9**).
6. Flow cytometer (see **Note 10**).
7. Sorter (see **Note 11**).

Table 2 | Examples of antibody panels for the quantitative and phenotypic characterization of myeloid and lymphoid cell populations

Antigen	Marker for	Fluorochromes/dye
Lymphoid panel		
CD45	Immune cells	eFluor605NC
CD11b	Myeloid cells	APC-Cy7 eFluor780 (damp channel)
CD3	Lymphocytes	PE-Cy7
CD19	B cells	FITC
CD4	$CD4^+$ T cells	PE-Cy5
CD8	$CD8^+$ T cells	PerCP
CD49b	NK cells	APC
Granzyme B[a]	Lymphocyte activation	PE
IFNγ[a,b]	Lymphocyte activation	eFluor450
	Live/dead	Dye eFluor780
Antigen	Marker for	Fluorochromes and dye
Myeloid panel		
CD45	Immune cells	PerCP
CD11b	Myeloid cells	APC-Cy7 eFluor780
CD3	Lymphocytes	PE-Cy7
Ly6G (1A8)	Neutrophils	FITC
Ly6C	Monocytes and neutrophils	eFluor450
F4/80	Macrophages	PE
	Live/dead	Dye 405 excitation

[a]These are intracellular markers. For intracellular staining, we have good experience with BD Cytofix/Cytoperm Fixation/Permeabilization kit from BD Bioscience. Follow the manufacturer's instruction for the intracellular staining

[b]For IFNγ staining, before starting with Subheading 3.2, step 3, cells need to be stimulated with 50 ng/mL PMA, 1 μM ionomycin and GolgiPlug in IMDM, 8 % FBS, and 0.5 % β-mercaptoethanol for 3 h in the incubator at 37 °C

3. Methods

Throughout the protocol, it is important to keep the samples on ice as much as possible, unless stated otherwise. Freshly harvested tissues should be collected in 1× PBS on ice and immediately processed. Single-cell suspensions are prepared as follows.

3.1. Tissue Digestion and Single-Cell Suspension

1. Mammary gland and mammary gland tumors: Chop the sample in a tissue chopper three times or until the tumor is dissociated (see Note 1). It is recommended to cut the tissues in smaller pieces with a scalpel before chopping to facilitate the procedure. Once chopped, incubate the sample in 10 mL enzyme digestion mix 1 with 25 µg/mL DNase in a 50 mL tube for 1 h at 37 °C in a shaking water bath (see Notes 2, 3, and 12). After digestion, stop the reaction by adding 20 mL DMEM, 8 % FBS, P/S, and 0.5 mM EDTA and filter the sample through a 70 µm cell strainer in a 50 mL tube at 4 °C. Wash the cell strainer with 5 mL of DMEM, 8 % FBS, P/S, and 0.5 mM EDTA to collect residual cells, centrifuge 300 × g for 10 min at 4 °C, and discard supernatant. Immediately continue through Subheading 3.2 or 3.3.
2. Lungs: Chop the lungs three times in a tissue chopper (see Note 1) and incubate the sample in 2 mL digestion mix 2 in a 15 mL tube for 30 min at 37 °C in a shaking water bath (see Note 12). Stop the reaction by adding 5 mL DMEM, 8 % FBS, and P/S and filter the sample through a 70 µm cell strainer in a 50 mL tube at 4 °C. Wash the cell strainer with 5 mL DMEM, 8 % FBS, and P/S to collect residual cells, centrifuge at 300 × g for 10 min at 4 °C, and discard supernatant. Immediately continue through Subheading 3.2 or 3.3.
3. Spleen and lymph nodes: Disperse the tissue through a 70 µm cell strainer (pre-wetted with 1× PBS) in a 50 mL tube by smashing it with a plunger while adding 1× PBS. Wash the cell strainer with 5 mL 1× PBS in order to collect residual cells. Centrifuge at 300 × g for 10 min at 4 °C and discard supernatant. Resuspend the pellet of the spleen in 5 mL erylysis buffer for 5–10 min at RT in order to eliminate erythrocytes that might interfere with flow cytometry analyses. Filter the cells through a 70 µm cell strainer, centrifuge at 300 × g for 10 min, and discard supernatant. Immediately continue through Subheading 3.2 or 3.3.
4. Blood: Collect 1 mL of blood in 50 µL heparin sulfate. Add 5 mL erylysis buffer and incubate for 5–10 min at RT in a 15 mL tube. Centrifuge at 300 × g for 10 min at 4 °C and pour off the supernatant. Add again 5 mL erylysis buffer for 5–10 min at RT, centrifuge at 300 × g for 10 min at 4 °C, and pour off the supernatant. Immediately continue through Subheading 3.2.

Once the single-cell suspensions have been prepared, the samples can either be directly analyzed by flow cytometry in order to quantitatively and phenotypically characterize cell populations (see Subheading 3.2) or prepared for cell sorting (see Subheading 3.3).

3.2. Quantitative and/or Phenotypic Characterization of Immune Cells by Multi-parameter Flow Cytometry

1. Resuspend single cells in 5–10 mL FACS buffer (for a small tumor and for one lymph node we recommend 5 mL; for large tumors, spleen, and lung, we recommend 10 mL) and count the cells. Plate ≈ 2 × 106 cells per antibody combination in a 96-well plate U-bottom shape.
2. Centrifuge the plate in a cold plate—centrifuge at 300 × g for 2 min and flick out supernatant.
3. Add 50 µL of antibody mix (see **Note 9**), gently mix by pipetting, and incubate the cells for 30 min at 4 °C in the dark. In Table 2, an example of an antibody combination for myeloid and lymphoid cells is shown.
4. Wash the wells twice with 150 µL of FACS buffer, centrifuge the plate at 300 × g for 2 min, and flick out supernatant. Resuspend in 50–100 µL of FACS buffer and analyze the sample with a flow cytometer (see **Notes 9** and **10**).

Although immune cell subsets can be directly sorted by flow cytometry from the prepared single-cell suspensions, it is our experience that a better yield and purity can be obtained by a two-step process involving pre-enrichment for total myeloid immune cells by magnetic cell sorting, followed by purification of the desired immune cell subset(s) by multi-parameter flow cytometry-based cell sorting. Throughout the protocol, we advise to collect small samples of cells for analysis by flow cytometry at the end of the procedure to check the enrichment by the column and the purity of the sorted cells.

3.3. Immune Subset Purification by Consecutive Magnetic Cell Sorting (See Note 4) and Multi-parameter Flow Cytometry-Based Cell Sorting

1. Resuspend single cells in 5–10 mL of sorting buffer (for a small tumor and for one lymph node we recommend 5 mL; for large tumors, spleen, and lung, we recommend 10 mL) and count cells.
2. Centrifuge cells at 300 × g for 10 min at 4 °C and discard supernatant.
3. To enrich the sample for myeloid cells, we use the marker CD11b (see **Note 8**). Resuspend the sample in sorting buffer containing the fluorochrome-conjugated CD11b antibody (e.g.: CD11b-APC) and incubate for 30 min at 4 °C in the dark. Use 50 µL of antibody mix per 107 cells (see **Note 13**). We advise to collect a small sample (≈50,000 cells) and store it in the 96-well plate at 4 °C. This sample will be used later for flow cytometry analyses and will be referred to as the "labeled" fraction.
4. Wash cells with 1–2 mL of sorting buffer per 107 cells (see **Note 13**). Centrifuge the cells at 300 × g for 10 min at 4 °C and discard supernatant.

5. Resuspend cell pellet in 80 µL of sorting buffer per 107 cells (see **Note 13**). Add 20 µL per 107 cells of magnetic Micro Beads conjugated with an antibody against the CD11b-fluorochrome used in Subheading 3.3, step 3 (e.g.: anti-APC Micro Beads) (see **Notes 5**, **13**, and **14**). Incubate for 20 min on ice in the dark.
6. Wash cells by adding 1–2 µL of sorting buffer per 107 cells (see **Note 13**). Centrifuge the cells at 300 × g for 10 min at 4 °C and discard supernatant.
7. Resuspend up to 108 cells in 500 µL of AutoMACS™ Rinsing Solution and filter the cell suspension through a 70 µm cell strainer on a 50 µL tube to eliminate clumps that might obstruct the column (see **Note 15**). Wash the cell strainer with 100 µL of AutoMACS™ Rinsing Solution to collect residual cells.
8. Depending on the number of labeled cells, choose the appropriate column, and place it in the magnetic field of a MACS separator (see **Notes 6** and **7**). Prepare empty 15 mL tubes underneath the column in order to collect the flow-through.
9. After rinsing the column with 3 mL of AutoMACS™ Rinsing Solution, apply cell suspension once the flow-through has stopped. Let the column empty by gravity.
10. Wash column three times with 3 mL of AutoMACS™ Rinsing Solution and collect the flow-through that contains the CD11b− cells. Add new buffer only when column reservoir is empty.
11. Remove the column from the magnetic field and place it into a new 15 mL tube. Pipette 6 mL of AutoMACS™ Rinsing Solution into the column and immediately flush out the CD11b+ cells by firmly pressing the plunger into the column (see **Note 16**).
12. Count both CD11b+ and CD11b− cell fractions. We advise to collect a small sample (≈50,000 cells) to put in the 96-well plate at 4 °C. These samples will be used later for flow cytometry analyses and will be referred to as “CD11b−” and “CD11b+” fractions.
13. Spin down CD11b+ cells at 300 × g for 10 min at 4 °C and discard supernatant.
14. Resuspend the CD11b+ cell fraction in the AutoMACS™ Rinsing Solution containing antibodies specific for the immune cell populations of interest. An example can be found in Table 1. Calculate 50 µL antibody mix per 107 cells (see **Notes 9** and **13**). If the number of cells is low, use at least 5 µL of antibody mix. Incubate cells for 30 min on ice in the dark.
15. Wash cells by adding 1–2 mL of AutoMACS™ Rinsing Solution per 107 cells (see **Note 13**). Centrifuge the cells at 300 × g for 10 min at 4 °C and discard supernatant. Resuspend cells in AutoMACS™ Rinsing Solution at a concentration of 20 × 106 cells per mL (see **Notes 17** and **18**), add live/dead marker if necessary, and take it to the sorter (see **Note 11**). Collect sorted cells in 5 ml DMEM and 8 % FBS in polypropylene tubes (see **Note 19**).
16. An example of a gating strategy to sort macrophages, neutrophils, and monocytes with markers described in Table 1 is shown in Fig. 2. After gating out duplets and gating on live cells, plot CD11b and F4/80. After

gating on the CD11b+ F4/80− population, plot Ly6G and Ly6C. CD11b+ F4/80+ cells are macrophages; Ly6G+ Ly6C+ cells are neutrophils; Ly6G− Ly6C+ cells are monocytes.

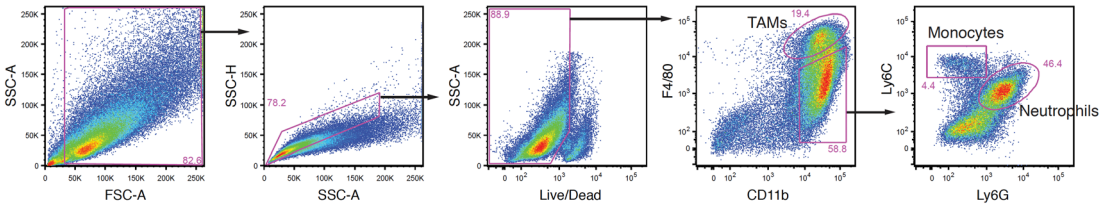


Fig. 2 | Dot plots of a murine mammary gland tumor illustrating the flow cytometry gating strategy. After gating out duplets and dead cells, the macrophage population is gated as CD11b+ F4/80+. In the CD11b+ F4/80− fraction, neutrophils are Ly6G+ Ly6C+ and monocytes are Ly6C+ Ly6G−

17. We advise to collect a small sample of each sorted cell type (≈50,000 cells) and put it in the 96-well plate at 4 °C. These samples will be used for flow cytometry analysis.
18. Analyze the samples collected in Subheading 3.3, **steps 3**, **12**, and **17** by flow cytometry. These samples will give an estimation of the CD11b enrichment by the column and the sorting purity. See Fig. 3 for an example.

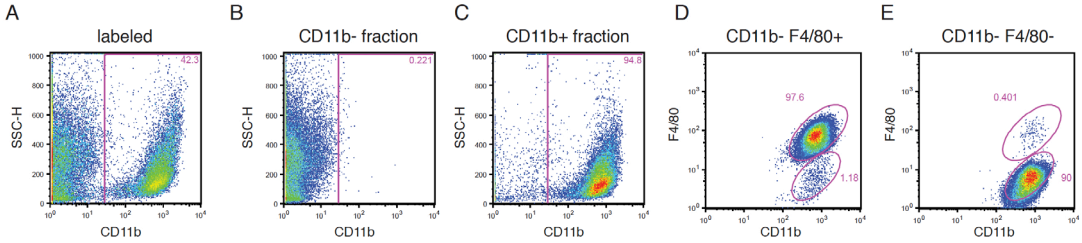


Fig. 3 | Dot plots of murine mammary gland tumor samples collected during the pre-enrichment procedure for myeloid immune cells by magnetic cell sorting and after the isolation by flow cytometry-based sorting. In this example, F4/80+ and F4/80− cells were isolated from the tumor. **(a)** Panel **a** depicts the dot plot and gating of CD11b+ myeloid cells before the magnetic column pre-enrichment. (**b**) and (**c**) show the CD11b− and CD11b+ fractions, respectively, obtained after the magnetic column pre-enrichment procedure. The comparison between (**a**) and (**c**) shows the enrichment of CD11b+ cells by the magnetic column. (**d**) and (**e**) show the purity of F4/80+ and F4/80− cells, respectively, after isolation by flow cytometry-based sorting

4. Notes

1. Researchers can adjust cutting speed, blade force, and blade travel on the tissue chopper. We have good experience with maximum cutting speed and blade force, and 5–10 µm blade travel. As an alternative to the tissue chopper, researchers can use razor blades, scissors, or scalpels to chop the tumors into very small fragments.
2. We have optimized the digestion mix for mammary tumors. For other tumor types, different composition of the enzyme digestion mix and different incubation time might be needed. An example for prostate cancer and subcutaneous B16 melanoma can be found in [13].
3. If the sample is not properly digested, it is also possible to add trypsin at the final concentration of 1.5 mg/mL to the digestion mix. Trypsin might cleave some surface markers that can be of interest for sorting or other type of analysis. For this reason, before proceeding with the experiment, it should be established if the marker of interest is cleaved by trypsin.
4. We have good experience with the MACS cell separation reagents from Miltenyi Biotec. However, researchers can also purchase magnetic separation columns from other vendors.
5. This protocol describes an indirect method for magnetically labeling the cells of interest. Researchers should select the Micro Beads based on the fluorochrome conjugated to the antibody used for column enrichment. For example, if the antibody is conjugated with allophycocyanin (APC), researchers are advised to use anti-APC Micro Beads.
6. MACS separators are strong magnets with holders for columns. Since there are different column sizes, researchers should match the correct separator with the correct column holder (see **Note 7**).
7. Based on the number of expected magnetically labeled cells, researchers should select the correct column capacity. For example, LS columns from Miltenyi Biotec can hold up to 108 magnetically labeled cells from up to 2 × 109 total cells. Make sure to match the correct MACS separator format (see **Note 6**).
8. We have good experience with the pan-myeloid marker CD11b conjugated to APC for column enrichment. However, it is also possible to use other markers for immune cells, like CD45, or CD3 for the isolation of lymphocytes.
9. According to the immune cell populations of interest, researchers should design their own antibody combinations. The choice of the fluorochromes conjugated to the antibodies is dependent on the flow cytometer used. Make sure that the flow cytometer contains the right lasers and detectors to excite and read the fluorochromes. An overview of our frequently used antibody combinations can be found in Tables 1 and 2.
10. We have good experience with BD LSRII Flow Cytometer with DIVA software (BD Biosciences, USA). Other machines can be used as long as they can detect the antibody combination used (see **Note 9**).

11. We have good experience with BD FACSARIA II sorter with DIVA software (BD Biosciences, USA). Other machines can be used as long as they can detect the antibody combination used (see **Note 9**).
12. Alternatively, we also have good experience using the MACSmix™ tube rotator from Miltenyi Biotec located in an incubator at 37 °C.
13. Round up the number of counted cells and use this value to calculate the amount of antibodies, sorting buffer or Micro Beads in order to ensure that all cells are labeled. For example, if the researcher counts 1.2 × 106 cells, round it up to 2 × 106.
14. Prior to use, resuspend the Micro Beads by vortexing.
15. Scale up the volume of sorting buffer according to the total number of cells.
16. Miltenyi Biotec provides the correct plunger together with the column.
17. This is the optimal concentration for cell sorting for the BD FACSARIA II in our facility. We suggest asking your FACS facility for optimal cell concentration. In case of very few cells, do not add less than 500 µL of AutoMACS™ Rinsing Solution in order for the sorter to have enough volume.
18. Use AutoMACS™ Rinsing Solution for sorting because it is colorless. Phenol red in medium may interfere with fluorochromes.
19. Cells easily attach to the wall of polystyrene tubes. To avoid this, polypropylene tubes are recommended for collection of sorted cells. Researchers should choose the size of the polypropylene tube accordingly to the tube holder of the sorter machine.

Acknowledgements

We thank Kim Vrijland and Tisee Hau for insightful comments on the manuscript. Work in the lab is supported by grants from the European Union (FP7 MCA-ITN 317445 TIMCC), the European Research Council (ERC consolidator award INFLAMET 615300), the Beug Foundation for Metastasis Research, and the Dutch Cancer Society (2011-5004).

References

1. Quail DF, Joyce JA (2013) Microenvironmental regulation of tumor progression and metastasis. Nat Med 19:1423–1437
2. Bates GJ, Fox SB, Han C, Leek RD, Garcia JF, Harris AL, Banham AH (2006) Quantification of regulatory T cells enables the identification of high-risk breast cancer patients and those at risk of late relapse. J Clin Oncol 24:5373–5380
3. Chevolet I, Speeckaert R, Schreuer M, Neyns B, Krysko O, Bachert C et al (2015) Clinical significance of plasmacytoid dendritic cells and myeloid-derived suppressor cells in melanoma. J Transl Med 13:9
4. DeNardo DG, Brennan DJ, Rexhepaj E, Ruffell B, Shiao SL, Madden SF et al (2011) Leukocyte complexity predicts breast cancer survival and functionally regulates response to chemotherapy. Cancer Discov 1:54–67
5. Ishigami S, Natsugoe S, Tokuda K, Nakajo A, Che X, Iwashige H et al (2000) Prognostic value of intratumoral natural killer cells in gastric carcinoma. Cancer 88:577–583
6. Mahmoud SM, Paish EC, Powe DG, Macmillan RD, Grainge MJ, Lee AH et al (2011) Tumor-infiltrating CD8+ lymphocytes predict clinical outcome in breast cancer. J Clin Oncol 29:1949–1955
7. Coffelt SB, Kersten K, Doornebal CW, Weiden J, Vrijland K, Hau CS et al (2015) IL-17-producing gammadelta T cells and neutrophils conspire to promote breast cancer metastasis. Nature 522:345–348
8. Coussens LM, Raymond WW, Bergers G, Laig-Webster M, Behrendtsen O, Werb Z et al (1999) Inflammatory mast cells up-regulate angiogenesis during squamous epithelial carcinogenesis. Genes Dev 13:1382–1397
9. Lin EY, Nguyen AV, Russell RG, Pollard JW (2001) Colony-stimulating factor 1 promotes progression of mammary tumors to malignancy. J Exp Med 193:727–740
10. Ciampricotti M, Hau CS, Doornebal CW, Jonkers J, de Visser KE (2012) Chemotherapy response of spontaneous mammary tumors is independent of the adaptive immune system. Nat Med 18:344–346
11. Bald T, Quast T, Landsberg J, Rogava M, Glodde N, Lopez-Ramos D et al (2014) Ultraviolet-radiation-induced inflammation promotes angiotropism and metastasis in melanoma. Nature 507:109–113
12. Junttila MR, de Sauvage FJ (2013) Influence of tumour micro-environment heterogeneity on therapeutic response. Nature 501:346–354
13. Watkins SK, Zhu Z, Watkins KE, Hurwitz AA (2012) Isolation of immune cells from primary tumors. J Vis Exp 64:e3952

CHAPTER 3

Transcriptional signatures derived from murine tumor-associated macrophages predict outcome in breast cancer patients

Sander Tuit[1,2,*], Camilla Salvagno[3,*], Theodore S. Kapellos[1,*], Cheei-Sing Hau[3], Lea Seep[1], Marie Oestereich[1], Kathrin Klee[1], Karin E. de Visser[3,#], Thomas Ulas[1,#] and Joachim L. Schultze[1,4,#]

[1] Genomics and Immunoregulation, LIMES Institute, University of Bonn, Carl-Troll-Str. 31, 53113 Bonn, Germany
[2] Department of Anatomy and Embryology, Leiden University Medical Center, Einthovenweg 20, 2333 ZC Leiden, The Netherlands
[3] Division of Tumor Biology & Immunology, Oncode Institute, the Netherlands Cancer Institute, Plesmanlaan 121, 1066 CX Amsterdam,The Netherlands
[4] Platform for Single Cell Genomics and Epigenomics (PRECISE) at the German Center for Neurodegenerative Diseases and the University of Bonn, Sigmund-Freud-Str. 27, 53127 Bonn, Germany
[*] shared first authorship
[#] shared last authorship

Corresponding authors: E-mail: j.schultze@uni-bonn.de, tel: (+49) 228 7362787;
E-mail: k.d.visser@nki.nl, tel: (+31) 20 5126104

Submitted for publication

Abstract

Tumor-associated macrophages (TAMs) are frequently the most abundant immune cells in murine and human cancers and are associated with poor survival. Here we generated TAM molecular signatures from K14cre;Cdh1flox/flox;Trp53flox/flox (KEP) and MMTV-NeuT (NeuT) transgenic mice which resemble human invasive lobular carcinoma (ILC) and HER2+ tumors, respectively. Determination of TAM-specific signatures in breast cancer required relationship analysis with healthy mammary tissue macrophages, since comparison with other macrophage populations overestimated TAM-specific gene expression. TAMs from the two models featured a distinct transcriptomic profile and KEP-derived signatures reliably predicted outcome in ILC patients, indicating that translation of murine TAM signatures to patients warrants consideration of the cancer subtype. Collectively, we show that a transgenic mouse tumor model can be utilized to derive a TAM signature for human breast cancer outcome prediction and we provide a generalizable strategy for determining and applying immune cell signatures provided the murine model reflects the human disease.

Introduction

The immune system plays an important role during tumor development, progression and therapy response and immune cells have evolved into attractive targets of therapeutic manipulation in cancer patients [1–3]. Ongoing and future attempts to fine-map the immune cell landscape of tumors will give us a full picture of the tumor microenvironment (TME) and may provide novel biomarkers and therapeutic targets [4]. Myeloid cells and, in particular, tumor-associated macrophages (TAMs) are a major component of the TME [5]. In the majority of cancer types, TAMs are often described as pro-tumorigenic and an enrichment of TAMs - as defined by immunohistochemistry and flow cytometry - has been linked to poor clinical outcome in several cancer types, including breast and lung cancers [6,7].

More recently, large multi-omics datasets from different cancer types consisting of thousands of human samples have been used to classify tumors based on immune cell-derived molecular signatures that could potentially be exploited in the future to improve patient stratification and therapeutic strategies [8–10]. For example, in colorectal cancer and T cell lymphomas, T cell-related gene signatures based on transcriptomic data were successfully used to diagnose, classify and predict disease outcome [11,12]. However, despite the enormous progress in the deconvolution of such data [13], the association of TAMs with clinically predictive signatures is not yet resolved.

Previous approaches to define might have been hampered by the fact that macrophages possess a tissue-specific transcriptional profile [14–16]. Consequently, the identification of TAM-specific signatures is not possible without access to healthy tissue macrophages of the same organ. Such reference data are still very limited [17] and efforts, such as the Human Cell Atlas[18] are not yet ready to provide such information. Whether or not the generation of cell type-specific signatures by single-cell transcriptomics [19–23] will be sufficient to infer TAM-specific signatures is currently not clear, considering the sparse nature of single-cell RNA-seq data.

In light of current shortcomings, we propose an alternative approach to define TAM-specific signatures and test their clinical applicability for outcome prediction. We first defined TAM signatures in well-defined murine tumor models by comparison with macrophages from different organs including the organ of tumor origin. For proof-of-principle, we generated TAM signatures from the K14cre;Cdh1flox/flox;Trp53flox/flox (KEP) murine breast cancer model [24] which recapitulates human ILC, the second most common histotype in humans, accounting for 10-15% of all breast cancers and the MMTV-NeuT (NeuT) breast cancer model[25] which has been indicated to resemble HER-2 positive breast cancers. Beside showing a shared transcriptional profile, TAMs from the two models present unique molecular signatures, illustrating the impact of the tumor subtype on TAMs. Tumor model-specific TAM signatures were then applied to clinical samples from large existing multi-omics studies[26,27] to assess the value of these TAM-specific signatures for predicting clinical outcome.

Results

Characterization of TAMs in two murine breast cancer models

We first characterized TAMs isolated from two spontaneous murine breast cancer models; the KEP (FVB background)[24] and the NeuT (Balb/c background) models [25] (Fig. 1a). Tumorigenesis in KEP mice is driven by the stochastic loss of E-cadherin and p53 by Keratin 14-specific Cre expression. These mice develop mammary tumors between 6-8 months of age and the disease resembles ILC in its pathology and progression [24]. In contrast, NeuT mice develop mammary tumors at 4 months of age due to the transgenic overexpression of the activated form of the rat oncogene *Neu* (ortholog of the human *HER2*) [25], previously indicated to resemble HER2^{+} breast tumors.

Assessment of the myeloid cell compartment in mammary tumors of both breast cancer models identified a CD11b^{hi}F4/80$^{low/-}$ population which contained Ly-6C^{hi} monocytes and Ly-6G^{hi}Ly-6C^{low} neutrophils and a CD11b^{hi}F4/80^{hi} macrophage population, hereafter referred to as TAMs (Fig. 1b-c). Next, we compared by immunohistochemistry the prevalence of macrophages in the mammary glands of age-matched WT mice, KEP and NeuT mice bearing early lesions and KEP and NeuT mice bearing tumors and found that both models were characterized by an increased accumulation of TAMs (Fig. 1d). Quantification of their numbers showed that CD11b^{hi}F4/80^{hi} macrophages represented 30% and 6% of the total live cells in the KEP and NeuT mammary tumors, respectively (Fig. 1e).

Further characterization of the macrophage phenotype showed that TAMs from the KEP and not from the NeuT model have lower expression of the mannose receptor CD206, while a higher proportion of TAMs in the NeuT model and not in the KEP model expresses higher levels of MHC-II compared to macrophages from the mammary gland of WT mice (Suppl. Fig. 1a-d). In addition, a significant increase in the frequency of Ki67^{+} TAMs was observed only in the KEP model compared to macrophages from healthy mammary glands of wild type FVB mice, (Suppl. Fig. 1e-f). Based on these data, we defined and sorted CD11b^{hi}F4/80^{hi} breast cancer TAMs, as well as tissue-resident macrophages from the mammary gland of KEP and NeuT mice (MTMs (KEP model), MTMs (NeuT model)), mammary tissue macrophages from KEP mice containing early neoplastic lesions, but not palpable tumors (MTMs (PRE-KEP model)) and spleen and bone marrow of WT and mammary tumor-bearing mice (WT spleen/BM (KEP/NeuT model) and spleen/BM (KEP/NeuT model)) for genome-wide assessment of transcriptional regulation (Suppl. Fig. 2a-h).

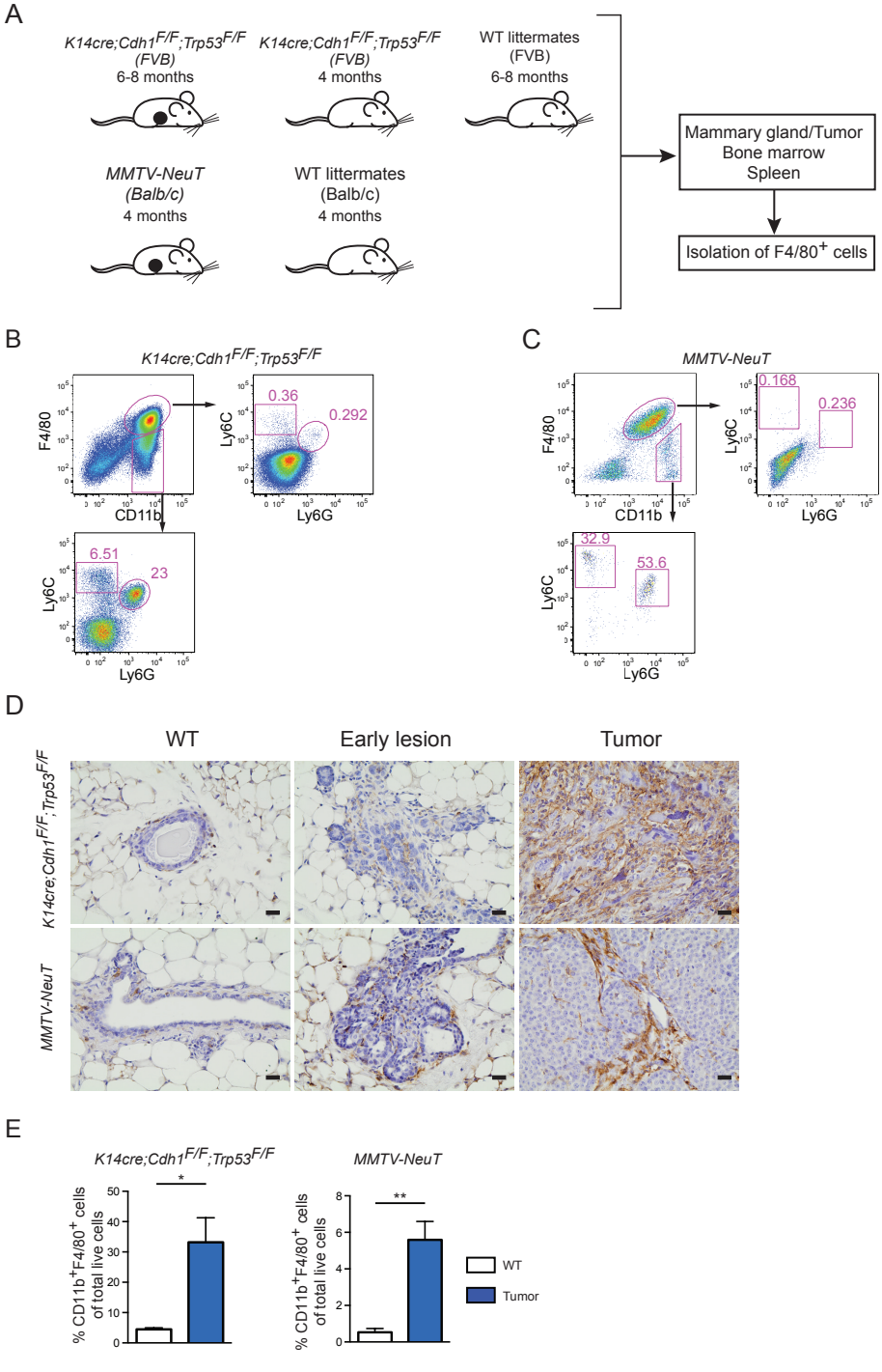

A
K14cre;Cdh1F/F;Trp53F/F (FVB) 6-8 months
K14cre;Cdh1F/F;Trp53F/F (FVB) 4 months
WT littermates (FVB) 6-8 months
MMTV-NeuT (Balb/c) 4 months
WT littermates (Balb/c) 4 months
Mammary gland/Tumor
Bone marrow
Spleen
Isolation of F4/80+ cells
B
K14cre;Cdh1F/F;Trp53F/F
F4/80
CD11b
Ly6C
Ly6G
0.36
0.292
6.51
23
C
MMTV-NeuT
0.168
0.236
32.9
53.6
D
WT
Early lesion
Tumor
K14cre;Cdh1F/F;Trp53F/F
MMTV-NeuT
E
K14cre;Cdh1F/F;Trp53F/F
MMTV-NeuT
% CD11b+F4/80+ cells of total live cells
WT
Tumor

Fig. 1 | Mammary tumorigenesis in two transgenic mouse models is characterized by macrophage influx. (a) Schematic representation of the macrophage sample collection for RNA sequencing. (b-c) Representative dot plots of a KEP mammary tumor (b) and a NeuT tumor (c) stained for F4/80 and CD11b, confirming absence of monocytes (Ly-6G$^-$Ly-6C$^+$) and neutrophils (Ly-6G$^+$Ly-6C^{low}) in the F4/80$^+$CD11b$^+$ TAM population. Dot plots are gated on CD45$^+$ cells. (d) Representative images of immunohistochemical F4/80 staining of a mammary gland from a WT FVB mouse, an early lesion in the mammary gland of a 4 months old KEP mouse and a KEP tumor (upper row); and of a mammary gland of a WT Balb/c mouse, an early lesion in the mammary gland of a 2 months old NeuT mouse and an NeuT mammary tumor (lower row), scale bar= 20 um. (e) Average percentage of CD11b$^+$ F4/80$^+$ macrophages gated on live cells in mammary glands and mammary tumors of KEP mice (left graph) and in mammary glands and mammary tumors of NeuT mice (right graph). Data are mean ± SEM from n=5-6 animals per group and were analyzed with a Mann-Whitney test, *$p < 0.05$, **$p < 0.001$.

Tissue origin dictates transcriptional regulation of TAMs

Considering findings demonstrating that tissue macrophages are characterized by organ-specific transcriptional regulation [16], we first compared the transcriptome profiles of the TAMs derived from the two breast cancer models (KEP, NeuT) with publicly available TAM profiles of two lung cancer models (Lewis lung carcinoma cell line and lung adenocarcinoma cell line) and with the profiles of tissue-resident macrophages of the mammary gland or lung, respectively. In addition, macrophages harvested from seven organs derived from either WT, mammary tumor-bearing or helminth-infected mice as well as other immune and epithelial cells [16,28–31] were used as controls (Fig. 2a and Suppl. Fig. 3a-b). Cells of the macrophage/monocyte lineage clustered together, separated from T cells, neutrophils, NK cells and epithelial cells (Suppl. Fig. 3c).

To elaborate the relationship between the different tissue-resident macrophages and cancer models, we performed sample-sample co-expression network analysis (CNA) based on Pearson correlation (cutoff 0.977) on all present genes. CNA showed a distinct cluster consisting of mammary gland tissue macrophages (MTMs) and TAMs derived from both breast cancer models, strongly suggesting that the tissue of origin dictates most of the transcriptional regulation in TAMs (Fig. 2b). This was similarly true for the lung cancer TAMs isolated from the two cancer cell line-based models which clustered together with the healthy lung-derived macrophages. To computationally validate these findings, we performed hierarchical clustering (HC) on the 1,000 genes with the highest variance within the dataset (Fig. 2c) and generated a Pearson correlation coefficient matrix (PCCM) (Fig. 2d). Both approaches supported our initial findings, clearly indicating that the TAMs of the two breast cancer models and the two lung cancer models were part of the mammary gland or lung clusters, respectively. Similarly, macrophages derived from spleen or bone marrow of tumor-bearing KEP or NeuT mice also clustered with the respective organ (Fig. 2c-d). Moreover, we observed that the transcriptional differences between TAMs and their respective healthy tissue counterparts were less pronounced than those between healthy and helminth-infected animals (Fig. 2c-d).

As an alternative to statistical models, we employed CNA on all genes and created a scale-free network (R^2= 0.772) based on a Pearson correlation cutoff of 0.87 (Suppl. Fig. 4a-b). A total of 28 clusters were identified in the Co-expression Network Analysis (CoCena[2]) cluster-condition heatmap (Fig. 2e) and specific gene signatures for each of the macrophage samples were discovered in this network as depicted in Suppl. Fig. 4c. We detected modules associated with classic macrophage functions,

such as scavenger receptors (*Cd163*, *Mrc1*, *Cd36*) and transcription factors (*Maf*) in MTMs, whereas we identified genes, such as the pro-inflammatory *Il12b*, the integrin *Itgb8* and the G protein-coupled receptor *Gpr31b* mainly associated with breast cancer TAMs (Fig. 2f). Taken together, our data suggest that the tissue of origin dictates not only the transcriptomes of healthy tissue-resident macrophages, but also of TAMs and dictates their transcriptional programs.

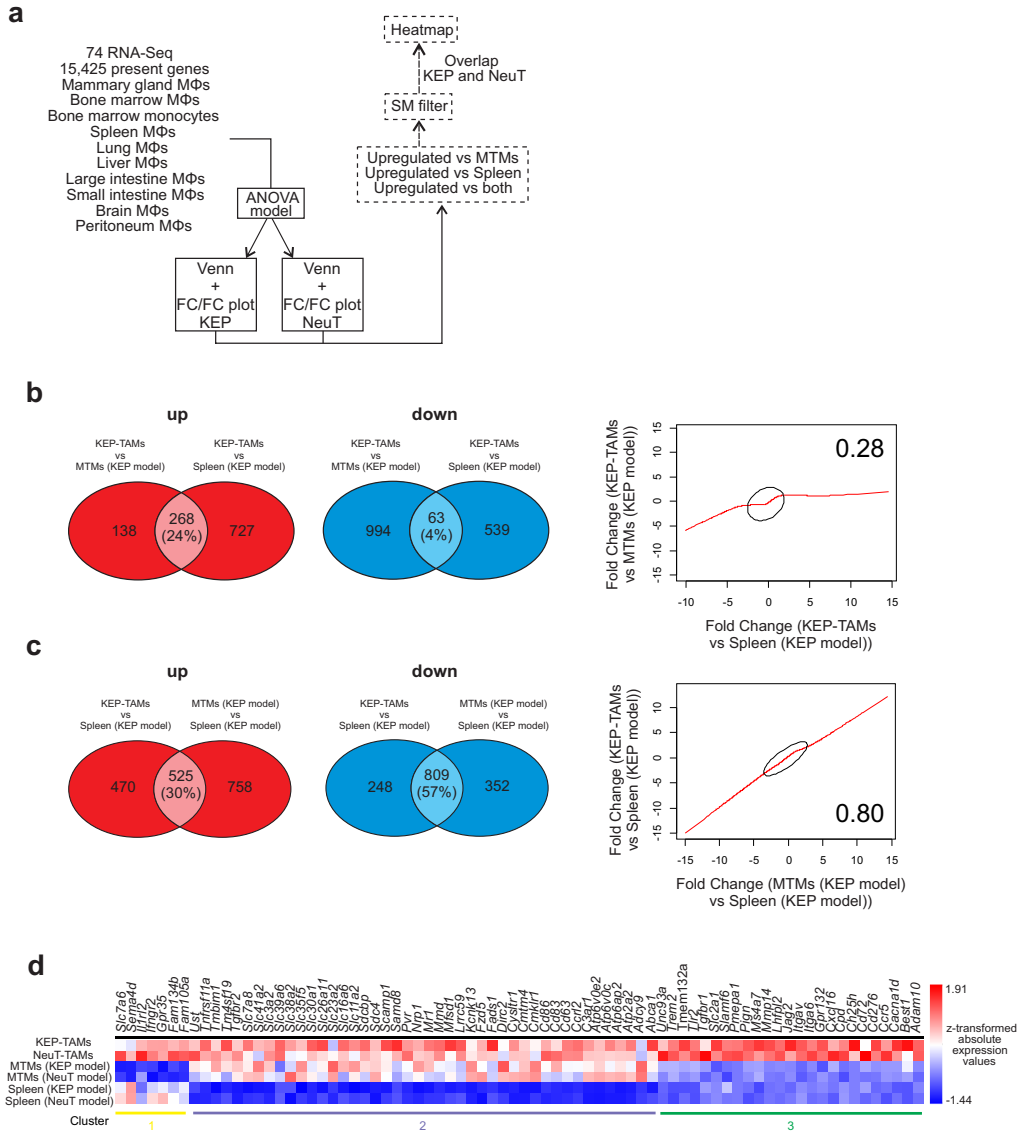


Fig. 2 | Tissue of origin determines the fate of the macrophage phenotype. (a) Schematic representation depicting the bioinformatics workflow. (b) Network visualization of sample-centered correlation analysis where each node represents one sample. (c-d) HC and PCCM maps based on the 1,000 genes with the highest variance within the dataset. Indicated in bold (d) are the disease state macrophages. (e) CoCena[2] cluster-condition heatmap and (f) CoCena[2] visualization of all present co-expressed genes in all tissues. Tissue-specific clusters for mammary gland/tumors are colored according to the clustering as seen in cluster-condition heatmap. Representative cluster-specific genes are noted next to them, GFC; Group Fold Change.

Identification of TAM-specific transcripts

Although the comparison of TAMs with different tissue-resident macrophage populations revealed that the tissue of origin is the major driver of the global transcriptome in TAMs, we were also interested to determine truly TAM-specific gene expression profiles. In previous reports, TAM functionalities have been compared to macrophages isolated from a different tissue than the tumor origin[32,33]. We, in contrast, defined such genes by direct comparison of breast cancer TAMs with macrophages from age-matched healthy mammary gland tissue and related them to those derived from comparisons of TAMs with other tissue-resident macrophages (Fig. 3). We employed Venn diagrams to compare KEP-TAMs with either MTMs or splenic macrophages (KEP model) (Fig. 3b), as well as splenic macrophages (KEP model) with either KEP-TAMs or MTMs (KEP model) (Fig. 3c). We found that the fold change of differentially expressed (DE) genes in the TAMs versus splenic macrophages correlated better with the fold change of DE genes in the MTMs versus splenic macrophages (KEP model) (r=0.8) as opposed to the fold change of DE genes in the TAMs versus MTMs (KEP model) (r=0.28), indicating an overestimation of differential gene expression by TAMs when comparing to splenic macrophages (Fig. 3b-c). This was also reflected in the respective FC/FC plots where many genes were similarly DE when plotting KEP-TAMs versus either MTMs (KEP model) or splenic macrophages (Suppl. Fig. 5a). Plotting KEP-TAMs versus splenic macrophages against MTMs indicated that the TAMs and MTMs displayed a transcriptome profile substantially different from that of splenic macrophages (Suppl. Fig. 5b). Similarly, the same pattern was observed in the NeuT model (Suppl. Fig. 5c-d) or when splenic macrophages were replaced with bone marrow macrophages in both breast cancer models (Suppl. Fig. 5e-h).

To identify truly TAM-associated cell surface markers, we plotted genes elevated in TAMs in comparison to either MTMs or splenic macrophages from both models (Fig. 3d). This analysis revealed a small set of genes that was DE against both MTMs and splenic macrophages (cluster 3). Moreover, we also identified genes which were DE only against splenic macrophages (cluster 2) or MTMs (cluster 1) and which would wrongfully be included or excluded from downstream analysis if splenic macrophages were to be used as the reference macrophage population. Collectively, these analyses further support the notion that the determination of TAM transcriptomic profiles requires comparison to macrophages derived from the same tissue and strongly argue for the careful selection of reference macrophage populations.

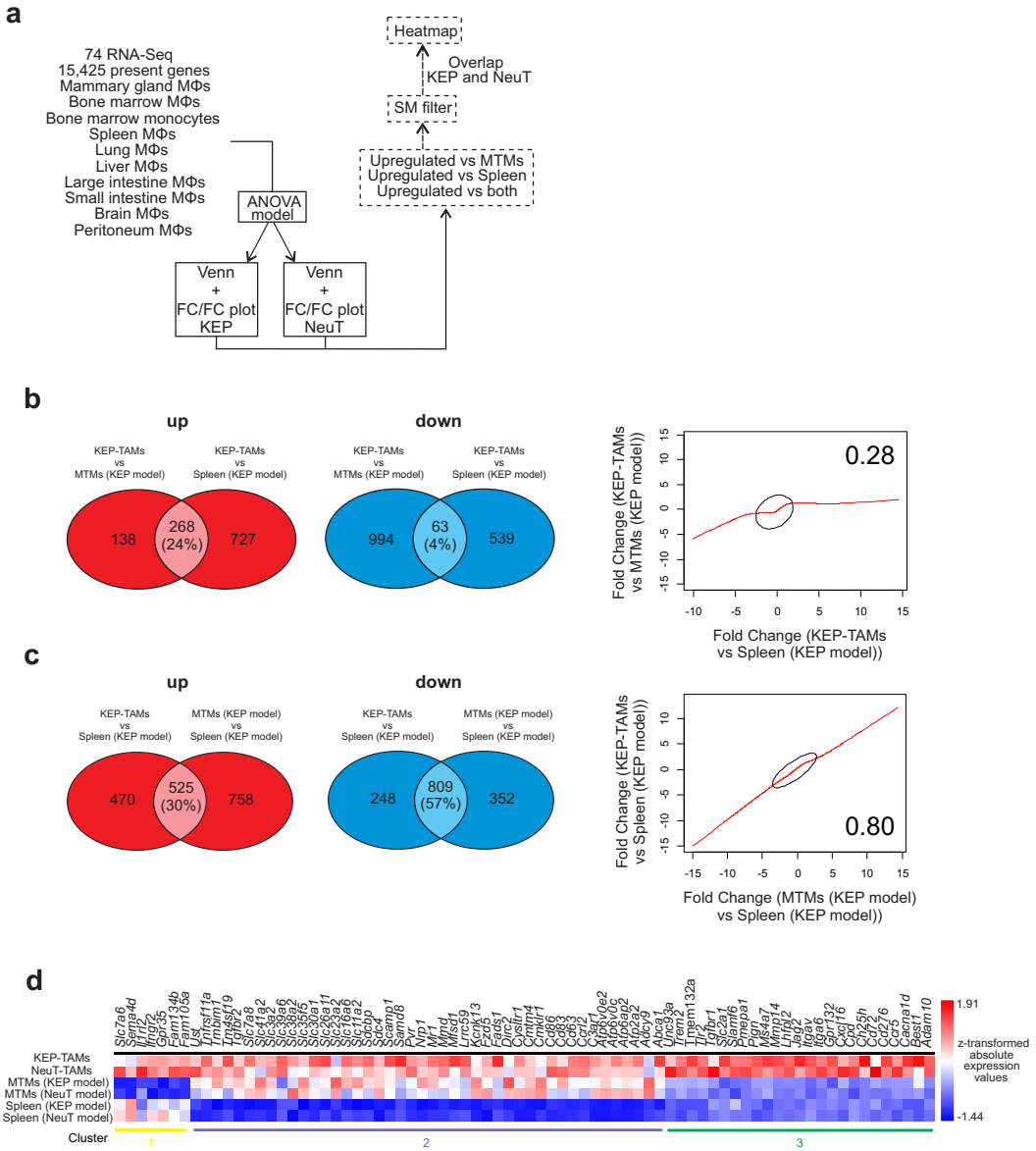


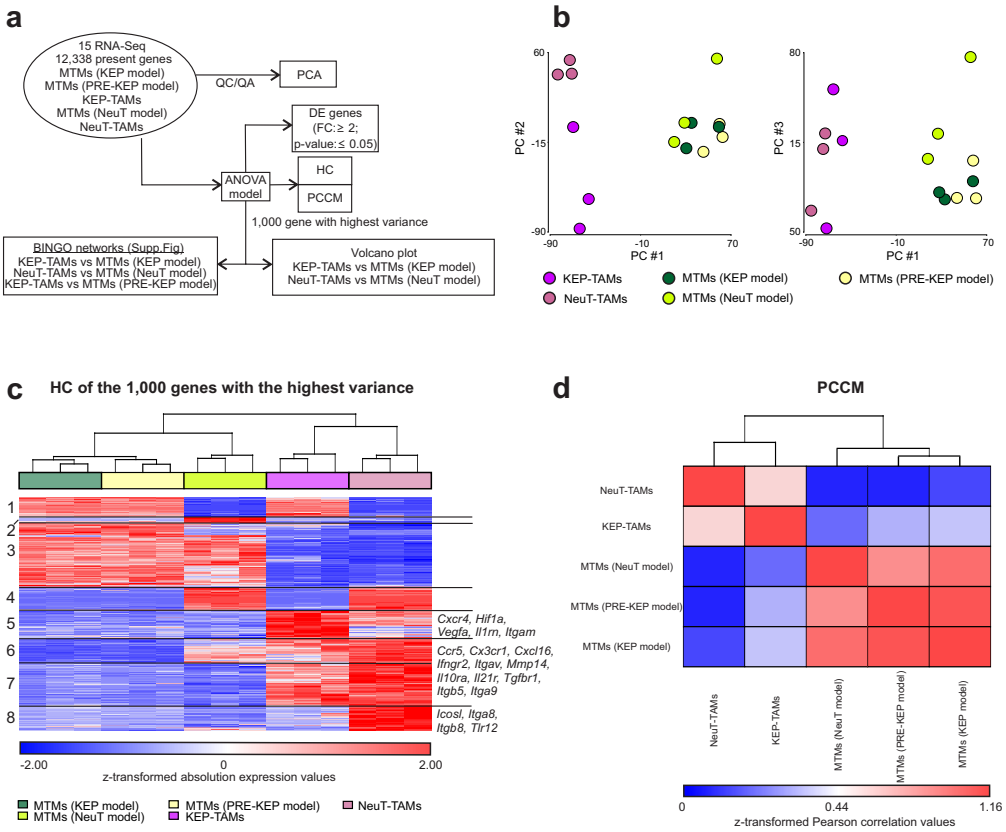
Fig. 3 | Inter-tissue comparison leads to false interpretation of changes in TAMs. (a) Schematic representation outlining the bioinformatics approach. (b-c) Venn diagrams of the comparisons of KEP-TAMs with MTMs and splenic macrophages (KEP model) (b) and splenic macrophages with KEP-TAMs and MTMs (KEP model) (c). Correlation plots of the fold changes of the DE genes in the aforementioned comparisons are shown (right) for both Venn diagrams. (d) Heatmap visualization of z-transformed surface marker (SM) absolute expression values. Overlapping DE genes from KEP and NeuT models were extracted from FC/FC plots, filtered for SMs and plotted.

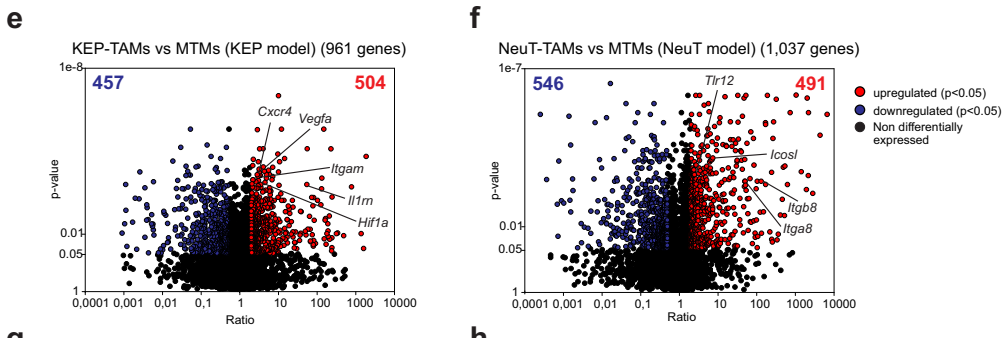
TAM transcriptomes differ between different breast cancer models

Our experimental setting also allowed us to define tumor model-specific regulation of macrophages (Fig. 4a). To define differences in TAM transcriptomes between the KEP and the NeuT model, we performed principal component analysis (PCA) (Fig. 4b), HC of the 1,000 genes with the highest variance (Fig. 4c) and PCCM (Fig. 4d). All three approaches demonstrated that TAMs from both breast cancer models are more closely related to each other than to MTMs from healthy or early neoplastic lesions. However, we also identified tumor model-specific gene alterations in TAMs as depicted in the HC analysis of KEP and NeuT models (Fig. 4c, clusters 5 and 8, respectively), implying that the tumor subtype also shapes the transcriptional regulation of TAMs. Two clusters (1 and 4) are related to the different genetic backgrounds of the models as the same up or downregulated genes in KEP-TAMs and NeuT-TAMs were also seen in MTMs (KEP model) and MTMs (NeuT model),respectively. Representative genes from clusters 5 (*Hif1a*, *Vegfa*, *Itgam*, *Cxcr4*, *Il1rn*) and 8 (*Tlr12*, *Itga8*, *Itgb8*, *Icosl*) of the HC are depicted in the model-specific Volcano plots of Fig. 4e-f.

We next visualized the DE genes from the comparison of KEP-TAMs and NeuT-TAMs to the respective MTMs in Venn diagrams to determine the overlap between the two models and found a small overlap in both the upregulated (17%, upper diagram) and downregulated (26%, lower diagram) DE genes (Fig. 4g). Since we also had the opportunity to isolate MTMs (PRE-KEP model), we could determine whether there were already transcriptional changes in macrophages at this stage. However, the transcriptional changes of MTMs (PRE-KEP model) to KEP-TAMs were comparable to those of healthy MTMs to KEP-TAMs as shown in the respective Venn diagrams for upregulated (70%, upper diagram) and downregulated (50%, lower diagram) DE genes, suggesting that they are similar to each other (Fig. 4h).

Based on the DE genes in both tumor models, we inferred overall biological changes by gene ontology enrichment analysis (GOEA) (Suppl. Fig. 6a-c). Common breast cancer TAM ontology terms included proliferation-related processes, regulation of innate immune responses and cell migration properties, wound healing processes and T cell activation processes (Suppl. Fig. 6a), whereas vasculature development and cell cycle-related processes (KEP-TAMs) and regulation of cell growth and angiogenesis-related processes (NeuT-TAMs) were associated with model-specific TAM populations (Suppl. Fig. 6b-c). Notably, the cell cycle-related processes were only significantly enriched in KEP-TAMs which is in line with the phenotypical observations of Suppl. Fig. 1e-f. In conclusion, our data show that the breast cancer subtype contributes to TAM transcriptional differences in different murine models.


a
15 RNA-Seq
12,338 present genes
MTMs (KEP model)
MTMs (PRE-KEP model)
KEP-TAMs
MTMs (NeuT model)
NeuT-TAMs
QC/QA
PCA
DE genes
(FC:≥ 2;
p-value:≤ 0.05)
ANOVA
model
HC
PCCM
1,000 gene with highest variance
BINGO networks (Supp.Fig)
KEP-TAMs vs MTMs (KEP model)
NeuT-TAMs vs MTMs (NeuT model)
KEP-TAMs vs MTMs (PRE-KEP model)
Volcano plot
KEP-TAMs vs MTMs (KEP model)
NeuT-TAMs vs MTMs (NeuT model)
b
PC #2
PC #1
PC #3
PC #1
KEP-TAMs
MTMs (KEP model)
MTMs (PRE-KEP model)
NeuT-TAMs
MTMs (NeuT model)
c
HC of the 1,000 genes with the highest variance
Cxcr4, Hif1a, Vegfa, Il1rn, Itgam
Ccr5, Cx3cr1, Cxcl16, Ifngr2, Itgav, Mmp14, Il10ra, Il21r, Tgfbr1, Itgb5, Itga9
Icosl, Itga8, Itgb8, Tlr12
z-transformed absolution expression values
MTMs (KEP model)
MTMs (NeuT model)
MTMs (PRE-KEP model)
KEP-TAMs
NeuT-TAMs
d
PCCM
NeuT-TAMs
KEP-TAMs
MTMs (NeuT model)
MTMs (PRE-KEP model)
MTMs (KEP model)
z-transformed Pearson correlation values


e
KEP-TAMs vs MTMs (KEP model) (961 genes)
457
504
Cxcr4
Vegfa
Itgam
Il1rn
Hif1a
p-value
Ratio
f
NeuT-TAMs vs MTMs (NeuT model) (1,037 genes)
546
491
Tlr12
Icosl
Itgb8
Itga8
upregulated (p<0.05)
downregulated (p<0.05)
Non differentially expressed

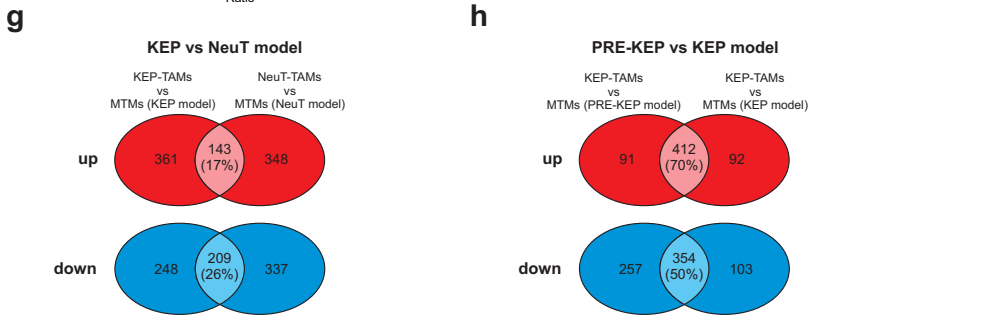

g
KEP vs NeuT model
KEP-TAMs vs MTMs (KEP model)
NeuT-TAMs vs MTMs (NeuT model)
up
361
143 (17%)
348
down
248
209 (26%)
337
h
PRE-KEP vs KEP model
KEP-TAMs vs MTMs (PRE-KEP model)
KEP-TAMs vs MTMs (KEP model)
up
91
412 (70%)
92
down
257
354 (50%)
103

Fig. 4 | Breast cancer subtype influences TAM phenotype - conventional approach. (a) Schematic representation outlining the bioinformatics approach. (b) PCA using all present (12338) genes with principle components (PC1-2 and PC1-3) plotted in two-dimensional graphs. (c) HC map based on the 1,000 genes with the highest variance within the dataset.
Representative cluster-specific genes are noted next to them. (d) PCCM map based on the 1,000 genes with the highest variance within the dataset. (e) Volcano plot of the DE genes from the comparison KEP-TAMs with MTMs (KEP model). (f) Volcano plot of the DE genes from the comparison NeuT-TAMs with MTMs (NeuT model). DE genes (FC ≥ 2, FDR-adjusted p-value ≤ 0.05) are indicated in red and representative upregulated DE genes are noted. (g) Venn diagram of the comparisons of KEP-TAMs with MTMs (KEP model) and NeuT-TAMs with MTMs (NeuT model). (h) Venn diagram of the comparisons of KEP-TAMs with MTMs (PRE-KEP model) and KEP-TAMs with MTMs (KEP model).

Identification of TAM-associated hubs by CNA

To link our information concerning differential transcriptional regulation within TAMs of different models to potential regulatory circuits, we utilized co-regulation of gene expression as our model and applied CNA on the DE genes between TAMs and MTMs in at least one of the breast cancer models (Fig. 5). The scale-free network (Fig. 5b, R^2=0.714) comprised 8 modules and confirmed that the transcriptomes of KEP-TAMs and NeuT-TAMs consisted of genes which followed shared (turquoise module) and model-specific expression patterns (blue and magenta modules) (Fig. 5c). Immune-related DE genes which were co-expressed are shown for the turquoise (*Ccr5*, *Cx3cr1*, *Cxcl16*, *Ifngr2*, *Itgav*, *Mmp14*), blue (*Cxcr4*, *Hif1a*, *Itgam*) and magenta (*Icosl*, *Itga8*, *Itgb8*, *Tlr12*) modules in Fig. 5d.
We then went one step further and investigated the potential hierarchies in TAM-associated gene regulation by building Intraclusteral Gene Interaction Networks (I-GINs) which extend the network approach. From the previous network analysis, we first focused on the gene module changed in both TAM models (turquoise module). We visualized the top 25% nodes based on degree and correlation and the top 25% correlation-ranked edges to identify known interactions from the STRING protein-protein interactions database (Fig. 5e). Subsequently, all edges to hubs were kept allowing a maximum of two edges between hubs. Already 46% of the identified interactions within the common breast cancer TAM network were known based on protein-protein interaction databases. Among the selected candidates, we detected cytokine receptors (*Ifngr2*), chemokines (*Cxcl16*) and metalloproteinases (*Mmp14*) which reflect the immune activation of breast cancer TAMs in the TME (Fig. 5f). Further assessment of the KEP-TAM- and NeuT-TAM-specific modules revealed the co-regulation of hypoxia factor (*Hif1a*) and scavenger receptors (*Msr1*) in the KEP-TAM dataset and pathogen recognition receptors (*Tlr12*), co-stimulatory molecules (*Icosl*) and integrins (*Itgax*) in the NeuT-TAM dataset (Suppl. Fig. 7). Finally, the co-expressed genes detected here presented a remarkably high degree of overlap with the DE genes identified by statistical models in Fig. 4c, further strengthening their relevance as breast cancer model-specific biomarkers in TAMs.

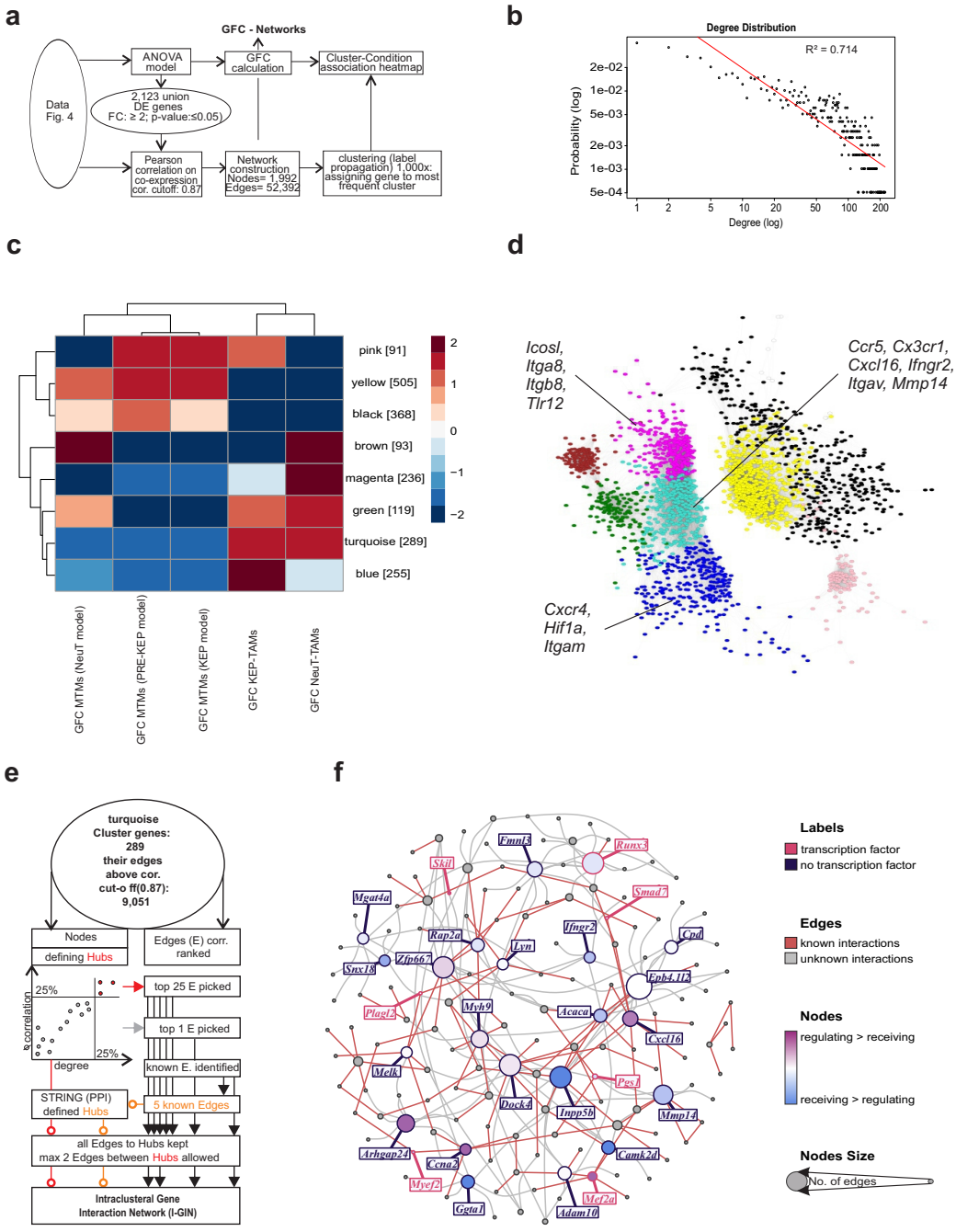

a
GFC - Networks
Data
Fig. 4
ANOVA
model
GFC
calculation
Cluster-Condition
association heatmap
2,123 union
DE genes
FC: ≥ 2; p-value:≤0.05)
Pearson
correlation on
co-expression
cor. cutoff: 0.87
Network
construction
Nodes= 1,992
Edges= 52,392
clustering (label
propagation) 1,000x:
assigning gene to most
frequent cluster
b
Degree Distribution
R² = 0.714
Probability (log)
2e-02
1e-02
5e-03
2e-03
1e-03
5e-04
1
2
5
10
20
50
100
200
Degree (log)
c
pink [91]
yellow [505]
black [368]
brown [93]
magenta [236]
green [119]
turquoise [289]
blue [255]
2
1
0
−1
−2
GFC MTMs (NeuT model)
GFC MTMs (PRE-KEP model)
GFC MTMs (KEP model)
GFC KEP-TAMs
GFC NeuT-TAMs
d
Icosl,
Itga8,
Itgb8,
Tlr12
Ccr5, Cx3cr1,
Cxcl16, Ifngr2,
Itgav, Mmp14
Cxcr4,
Hif1a,
Itgam
e
turquoise
Cluster genes:
289
their edges
above cor.
cut-o ff(0.87):
9,051
Nodes
defining Hubs
Edges (E) corr.
ranked
25%
top 25 E picked
top 1 E picked
25%
degree
known E. identified
STRING (PPI)
defined Hubs
5 known Edges
all Edges to Hubs kept
max 2 Edges between Hubs allowed
Intraclusteral Gene
Interaction Network (I-GIN)
f
Fmnl3
Runx3
Skil
Mgat4a
Smad7
Rap2a
Ifngr2
Cpd
Lyn
Snx18
Zfp667
Epb4.1l2
Plagl2
Myh9
Acaca
Cxcl16
Melk
Pex1
Dock4
Inpp5b
Mmp14
Arhgap24
Ccna2
Camk2d
Myef2
Mef2a
Ggta1
Adam10
Labels
transcription factor
no transcription factor
Edges
known interactions
unknown interactions
Nodes
regulating > receiving
receiving > regulating
Nodes Size
No. of edges

Fig. 5 |Breast cancer subtype influences TAM phenotype - co-expression-based approach. (a) Schematic representation outlining bioinformatics workflow. (b) CoCena[2] logged network degree distribution with linear fitting. (c) CoCena[2] cluster-condition heatmap. (d) CoCena[2] visualization of all present co-expressed genes. Network nodes are colored according to their cluster membership and representative cluster-specific genes are noted. (e) Schematic representation outlining bioinformatics workflow for I-GIN construction for breast cancer TAM-specific genes (turquoise cluster). (f) I-GIN node coloring represents regulatory or receiving status obtained from a Bayesian approach and points out highly co-expressed genes and their known or proposed links to strongest correlated neighbors. Candidate genes mentioned in the text are highlighted in yellow boxes. GFC; Group Fold Change

Model-specific TAM gene signatures predict disease outcome in humans

To determine the clinical relevance of the identified murine model-specific TAM signatures, we next set out to translate our findings to humans. For this purpose, we generated a unique list of TAM-associated genes defined by statistical and co-expression models (Fig. 6a), identifying 198 KEP-TAM associated genes, 227 NeuT-associated genes and 116 common breast cancer TAM genes (Fig. 6b). As a next step, we interrogated RNA-seq samples derived from ILC patients within the TCGA (n=125) [26] and the METABRIC (n=147) [27] databases for their macrophage content (Fig. 6c and Suppl. Fig. 8a). We used linear support vector regression (LSVR) and the LM22 macrophage gene signature set [34] to describe the immune cell content of these samples. When ranking the samples for predicted macrophage content, it became clear that ILC patients have quite variable amounts of macrophages within their tumor microenvironment (Fig. 6c). We also tested whether the specific murine TAM signatures could be identified (Suppl. Fig. 8a). Indeed, when applying LSVR using signatures derived from KEP-TAMs, NeuT-TAMs and respective MTMs, the KEP-TAM signatures represented a major part in most of the ILC patients (TCGA cohort), while the NeuT-TAM signatures were present to a lower extent in most of the cases (Suppl. Fig. 8a), indicating that the murine KEP-TAM signatures might better reflect the biology of TAMs in ILC patients.

Based on these encouraging results, we assessed the predictive value of these breast cancer model-specific TAM signatures for disease outcome. Kaplan-Meier analysis showed that the KEP-TAM signatures correlated with worse clinical outcome (p=0.037) of ILC patients from the TCGA cohort (Fig. 6d) and the METABRIC cohort (p=0.048) (Suppl. Fig. 8b). Importantly, the NeuT-TAM signatures were not enriched in ILC patients or did not correlate with better or worse overall survival in both patient cohorts (Fig. 6e and Suppl. Fig. 8c). To further prove the validity of these findings, we used gene signatures from the comparison of KEP-TAMs with splenic macrophages, random signatures and LSVR-derived total human macrophage signatures and assessed whether they were predictive of the outcome in the TCGA and METABRIC ILC cohorts (Fig. 6f-g, Suppl. Fig. 8d-g). In fact, none of these signatures showed a predictive value of disease outcome of ILC patients (separation of Kaplan-Meier groups or gene signature enrichment z score) in both cohorts. Collectively, these data indicate that the generation of meaningful gene signatures for outcome prediction derived from TAMs requires a clinically relevant murine model (here the KEP model for ILC) and the comparison of TAMs with their healthy tissue counterparts -here MTMs- instead of unrelated macrophage sources such as spleen or bone marrow.

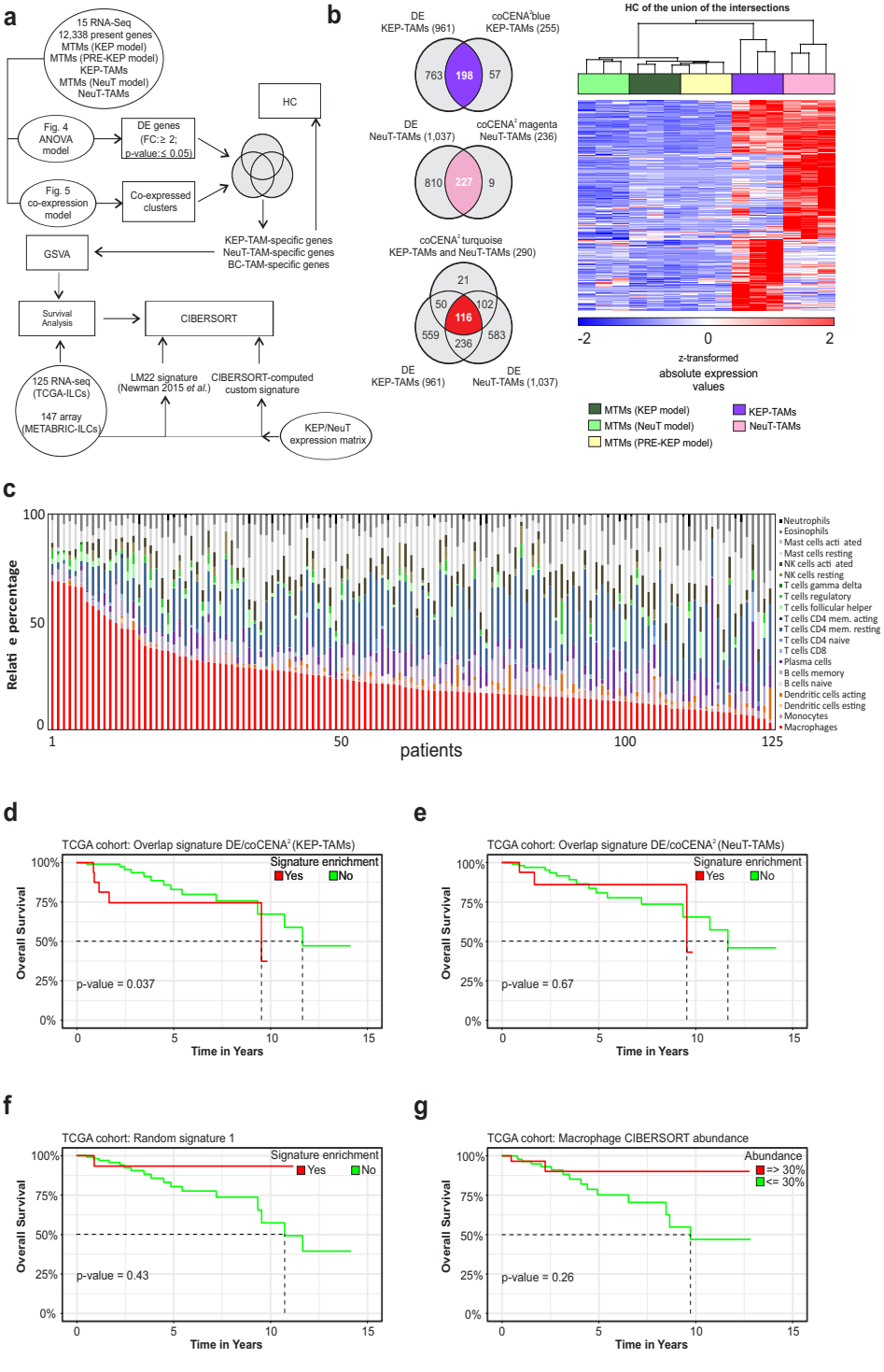

a
15 RNA-Seq
12,338 present genes
MTMs (KEP model)
MTMs (PRE-KEP model)
KEP-TAMs
MTMs (NeuT model)
NeuT-TAMs
Fig. 4 ANOVA model
DE genes (FC:≥ 2; p-value:≤ 0.05)
Fig. 5 co-expression model
Co-expressed clusters
HC
KEP-TAM-specific genes
NeuT-TAM-specific genes
BC-TAM-specific genes
GSVA
Survival Analysis
CIBERSORT
125 RNA-seq (TCGA-ILCs)
147 array (METABRIC-ILCs)
LM22 signature (Newman 2015 et al.)
CIBERSORT-computed custom signature
KEP/NeuT expression matrix
b
DE KEP-TAMs (961)
coCENA2blue KEP-TAMs (255)
763
198
57
DE NeuT-TAMs (1,037)
coCENA2 magenta NeuT-TAMs (236)
810
227
9
coCENA2 turquoise KEP-TAMs and NeuT-TAMs (290)
21
50
102
116
559
236
583
DE KEP-TAMs (961)
DE NeuT-TAMs (1,037)
HC of the union of the intersections
-2
0
2
z-transformed
absolute expression values
MTMs (KEP model)
MTMs (NeuT model)
MTMs (PRE-KEP model)
KEP-TAMs
NeuT-TAMs
c
Relati e percentage
100
50
0
1
50
100
125
patients
Neutrophils
Eosinophils
Mast cells acti ated
Mast cells resting
NK cells acti ated
NK cells resting
T cells gamma delta
T cells regulatory
T cells follicular helper
T cells CD4 mem. acting
T cells CD4 mem. resting
T cells CD4 naive
T cells CD8
Plasma cells
B cells memory
B cells naive
Dendritic cells acting
Dendritic cells esting
Monocytes
Macrophages
d
TCGA cohort: Overlap signature DE/coCENA2 (KEP-TAMs)
Signature enrichment
Yes
No
Overall Survival
100%
75%
50%
25%
0%
p-value = 0.037
0
5
10
15
Time in Years
e
TCGA cohort: Overlap signature DE/coCENA2 (NeuT-TAMs)
Signature enrichment
Yes
No
Overall Survival
p-value = 0.67
Time in Years
f
TCGA cohort: Random signature 1
Signature enrichment
Yes
No
Overall Survival
p-value = 0.43
Time in Years
g
TCGA cohort: Macrophage CIBERSORT abundance
Abundance
=> 30%
<= 30%
Overall Survival
p-value = 0.26
Time in Years

Fig. 6 | KEP-TAM-specific signatures predict overall survival in ILC patients. (a) Schematic representation depicting the bioinformatics approach. (b) Venn diagrams of overlapping CoCena[2]- and ANOVA-derived gene sets for KEP-TAMs (up), NeuT-TAMs (middle) and breast cancer TAMs (bottom) (left), HC map of the union of KEP-TAM-, NeuT-TAM- and breast cancer TAM-specific genes (right). (c) The "LM22" signatures (Newman et al. 2015) were used as input to identify the relative fraction of several immune cell populations in the ILC specimens (TCGA cohort, n=125). (d-g) Kaplan-Meier survival analysis of TCGA ILC patients. ILC specimens having a significant enrichment for KEP-TAMs signature (d), NeuT-TAMs signature (e), random signature (f) and CIBERSORT macrophage signature (g) are visualized in red line and numbers. The rest of ILC patients are visualized in green line and numbers. Z score above 2 marks significant enrichment of gene signatures.

Discussion

It is widely acknowledged that the immune system plays an important role in cancer development and progression [2]. Macrophages are one of the major components within the TME [35] and accumulating evidence indicates that their abundance is linked to disease outcome [36]. Here we provide a strategy to derive TAM-specific gene signatures and demonstrate that signatures derived from a transgenic murine tumor model for ILC can be used to predict outcome in two independent ILC cohorts (TCGA, METABRIC). These signatures could only be generated by proper comparison with the healthy tissue-resident macrophage counterparts, here MTMs, but not by comparison with macrophages derived from unrelated tissues, e.g. spleen or bone marrow. Moreover, we show that the global transcriptome of TAMs is mainly defined by tissue signals, although the tumor subtype also plays a crucial role in shaping the TAM transcriptional networks. Collectively, our approach illustrates how transcriptional regulation of TAMs derived from a murine model closely resembling the human disease (here ILC) [24] can be successfully translated into clinically meaningful disease outcome prediction.

Previous studies have defined TAM gene signatures by comparing TAMs to healthy tissue macrophages derived from tissues, such as the spleen [32,33]. However, recent evidence highlighted the diversity of the transcriptomes and epigenomes of the several tissue-resident macrophage populations [14,16]. With these findings at hand, it was conceivable to address whether such definitions would indeed lead to TAM-specific signatures. We provide compelling evidence that TAMs still share most genes with their healthy tissue counterparts both in breast and lung and that the comparison of TAMs with macrophage populations derived from other organs or tissue sites mainly reflect tissue differences rather than TAM-specific gene expression. As a consequence, we strongly propose to study TAMs in the context of their healthy tissue counterparts when searching for truly TAM-related changes in gene expression and functions. Clearly, this can be easier achieved in murine model systems compared to human cancer samples where healthy tissue from the same organ is often not accessible. More recently, Cassetta *et al*. reported on a 37-gene TAM signature derived from four breast cancer patients [17]. This signature was mainly enriched in the Her2 breast cancer subtype or the 'Claudin-low' molecular subtype as defined by the PAM50 classification [37]. Comparable to our results, this TAM signature could also be linked to worse outcome prediction of disease, albeit not specified for a particular breast cancer subtype which might be of importance for the development of new diagnostic and therapeutic strategies.

Indeed, another important finding of our study is the observation that only TAM-specific signatures derived from the KEP model were predictive for outcome in ILC patients. Although the two breast cancer models shared tumor-associated changes, such as the upregulation of genes associated with regulation of immune cells, we also observed functionality differences between the two murine models, such as the cell cycle. Differences in functions between breast cancer TAM populations have been previously described [38,39]. For instance, breast cancer TAM populations in different tumor models have been shown to differ in migratory behaviour and their ability to uptake fluorescent dextran [40]. Similarly, macrophage function can differ with varying oxygen levels across different tumor models [41,42]. Moreover, in the *MMTV-PyMT* mouse model both MTMs and TAMs are found in the mammary tumors, but only TAMs play a role in tumor progression [43,44]. Collectively, our findings show that the tumor subtype affects the phenotype of TAMs inducing a unique TAM signature in the two models.

While concerns have been raised about the validity of murine cancer models [45], we demonstrate here that a carefully designed cancer model, such as the KEP model can directly lead to clinically translatable results – here the generation of outcome prediction signatures based on TAM transcriptomes. For example, these signatures or marker genes (derived from such signatures) could now be tested in prospective clinical trials to assess their performance on outcome prediction. In this context, it is important to stress that only the KEP-TAM-derived, but not the NeuT-TAM-based gene signatures were informative for the ILC patient cohorts, further illustrating the requirement for murine tumor models that match with the patient tumor subtype. Such models are then ideally suited to address further questions concerning the role of the myeloid cell compartment within the TME [46].

While we could successfully translate population level information derived from the KEP model to a clinical question –namely outcome prediction–, other questions might need higher resolution analysis as it can be provided by single-cell -omics technologies [47]. Such a question in our study is the assessment of the underlying heterogeneity in the MTMs (PRE-KEP model). It is very likely that although these cells were found to be transcriptionally very similar to MTMs at the bulk population level, substructure analysis might reveal concealed homogeneous subsets with distinct transcriptomic profiles that follow a spectrum ranging from those of MTMs to KEP-TAMs. In this light, single-cell RNA-seq data from less than a hundred macrophages derived from 11 patients were described in an initial study [48] and a more recent study profiled more than 45,000 $CD45^+$ cells from 8 patients also including macrophages [23]. While particularly the second study highlighted the enormous heterogeneity of the immune cell compartment in breast cancer corroborating previous findings [11,12], it is too early to link this rich information to patient outcome prediction. Clearly, further studies are required that link approaches as presented here with these exciting new single cell -omics technologies to evaluate their clinical potential for diagnosis, subclassification of disease or outcome prediction.

Materials and methods

Animals

The generation and characterization of *K14cre;Cdh1$^{F/F}$;Trp53$^{F/F}$* mice have been previously described in detail [24]. The mice were backcrossed onto the FVB/N background and genotype was confirmed by PCR [24,49]. *MMTV-NeuT* mice on a Balb/c background [25] were purchased from Charles River Laboratories (Calco, Italy) and were bred in house. Female *K14cre;Cdh1$^{F/F}$;Trp53$^{F/F}$ and MMTV-NeuT* mice were monitored twice every week for the onset of mammary tumor formation by caliper and palpation measurement starting at 2 or 4 months of age, respectively. Mice were kept in open cages with food and water provided *ad libitum* at a 12-hour light/dark cycle. Animal experiments were approved by the Animal Ethics Committee of the Netherlands Cancer Institute (Amsterdam, Netherlands) and performed in accordance with institutional, national and European guidelines for Animal Care and Use (CCD license: AVD3010020172688).

Macrophage isolation

Macrophages were isolated according to [50]. Briefly, mammary glands or mammary tumors (size±225mm^2), spleen and bone marrow were harvested from 4 month old *K14cre;Cdh1$^{F/F}$;Trp53$^{F/F}$* female mice containing early lesions, 6-8 months old tumor-bearing *K14cre;Cdh1$^{F/F}$;Trp53$^{F/F}$*, 4 month old tumor-bearing *MMTV-NeuT* female mice and age- and sex-matched FVB/N and Balb/c mice. Tumors and mammary glands were mechanically chopped with a McIlwain Tissue Chopper (Ted Pella, Inc, CA, USA) and were enzymatically digested for 1 hour at 37°C with 3 mg/ml collagenase type A (Roche) and 1.5 mg/ml porcine pancreatic trypsin (BD Biosciences) in serum-free DMEM medium. Digestion was stopped by the addition of DMEM supplemented with 8% FBS and the suspension was disaggregated through a 70 µm cell strainer. Spleens and bone marrow cells from tibiae and femora were harvested and disaggregated through a 70 µm cell strainer. Splenic suspensions were subsequently treated twice with NH_4Cl erythrocyte lysis buffer for 3 min at room temperature. All single-cell suspensions were stained for 20 min at 4°C in the dark with anti-mouse F4/80 (1:200; BM8; eBioscience) and anti-mouse CD11b (1:200; M1/70; eBioscience) in IMDM supplemented with 2% FBS, 0.5% beta-mercaptoethanol, 0.5mM EDTA, Pen/Strep. Cells were then washed and incubated with magnetic MicroBeads (Miltenyi Biotec) following the manufacturer's guidelines. Isolation of F4/80$^+$ cells from the CD11b$^+$-enriched fraction was performed on a BD FACS ARIA II sorter with Diva software (BD Biosciences). DAPI was added to select viable cells. Sorted macrophages were stored at -80°C in TRIzol (Invitrogen). Cell purity was determined on a FACSCalibur using CellQuestPro software (BD Biosciences) and data were analyzed using FlowJo software v9.9.

Immunohistochemistry

Immunohistochemical analysis was performed by the Animal Pathology facility at the Netherlands Cancer Institute. Briefly, formaline-fixed paraffine-embedded tissues were blocked with 4% BSA/5% normal goat serum in PBS and stained with anti-mouse F4/80 (1:300; Cl:A3-1; AbD Serotec) after antigen retrieval with 20 ug/

ml Proteinase K (Sigma-Aldrich) at 37°C for 20 min. Endogenous peroxidase activity was neutralized in 3% H_2O_2 in methanol for 20 min at room temperature. Slides were then incubated with biotinylated goat anti-rat secondary antibody (1:100; SouthernBiotech) followed by DAB detection. Samples were visualized with a BX43 upright microscope (Olympus) and images were acquired in brightfield using cellSens Entry software (Olympus) at 40X magnification.

Flow cytometry

Single-cell suspensions were stained with anti-mouse CD45 (1:200; 30-F11; BD Biosciences), anti-mouse CD45 (1:200; 30-F11; eBioscience), anti-mouse CD11b (1:400; M1/70; Biolegend), anti-mouse CD11b (1:200; M1/70; eBioscience), anti-mouse F4/80 (1:200; BM8; eBioscience), anti-mouse CD206 (1:100; MR5D3; AbD Serotec), anti-mouse Ly-6C (1:400; HK1.4; eBioscience), anti-mouse Ly-6G (1:200; 1A8; BD Biosciences), anti-mouse Ly-6G (1:200; 1A8; Biolegend) and anti-mouse MHC-II (1:200; M5/114.15.2; eBioscience) for 20 min at 4°C in the dark in PBS supplemented with 0.5% BSA. 7AAD (1:20; eBioscience) or Fixable Viability Dye (1:1000; eBioscience) or Fixable aqua dead cell dye (1:100, ThermoFisher Scientific) were added to exclude dead cells. For Ki67 detection in macrophages, cells were fixed and permeabilized with the Foxp3/transcription factor staining Buffer set kit (ThermoFisher Scientific) as manufacturer's recommendations, followed by incubation with Fc block (CD16/CD32 purified; 1:50; 2.4G2; BD Biosciences) and stained with Ki67 or anti-mouse IgG2a. Experiments were performed using a LSRII flow cytometer (BD Biosciences) and data analysis were performed using FlowJo software v9.9.

Library preparation

Total RNA was extracted using the RNeasy Mini and Micro Kits (Qiagen). RNA (10 ng) was converted into cDNA libraries using the Ovation RNA-Seq system V2 and Encore Rapid library systems protocols (NuGEN) and samples were sequenced on a HiSeq 1500 system (Illumina).

Standard bioinformatic analysis

Publicly available datasets [16,28–31] were trimmed using fastx trimmer (*-l 50 -i Sample.fastq -o Sample_trim50.fastq*) to 50 bp reads to match our experimental settings. Our and the pre-processed publicly available data were aligned against the murine mm10 reference genome using TopHat2 (v2.0.11) default parameters [51]. The breast cancer datasets are available under GSE126268. Altogether three different datasets were composed; one containing only our two breast cancer models, one including our dataset and further available tissue macrophage datasets and another including our dataset and other tissue macrophage and immune cell types. The aligned reads were then imported into Partek Genomics Suite v6.6 (PGS) separately to deduct gene and transcript information before performing normalization using the DESeq2 package [52] in R (v3.0.2). Normalized read counts were floored to a value of at least 1 after batch correction. Finally, the datasets were filtered to a minimum value of 10 counts per group. The 1000 genes with the highest variance and DE gene calculations were performed utilizing a one-way ANOVA model in PGS. Genes with FC ≥ 2 and FDR ≤ 0.05 were defined as differentially expressed and were

visualized in volcano plots and FC/FC plots using SigmaPlot (v12.0) (Systat Software) and correlation plots. For more detailed analysis, the ANOVA model was filtered based on the respective gene lists [53]. TAM-specific surface marker expression was visualized in a heatmap using Mayday [54].

Comparative and biological function-related bioinformatic analysis
Global similarity comparisons between macrophage populations were performed by correlation analysis based on Pearson correlation coefficients (Pearson correlation ≥ 0.977) using BioLayout Express3D [55]. The correlation network was visualized in Cytoscape (http://www.cytoscape.org/). The structure of our breast cancer dataset was visualized utilizing PCA on all expressed genes. HC and PCCM were performed on the 1000 genes with the highest variance within the dataset using default settings in PGS. To link DE genes to known biological functions, GOEA was applied on DE gene sets extracted from FC/FC plots. Subsequently, Cytoscape was used to visualize GOEA results in a global view using the plug-ins BiNGO [56], EnrichmentMap[57] and Word Cloud[58].

CoCena²
To define differences and similarities in transcript expression patterns among the different groups, CoCena² (Construction of co-expression Network Analysis - automated) was performed based on Pearson correlation. Either all 15,425 present genes or the union of DE genes (2,123 genes) from the three comparisons KEP-TAMs versus MTMs from the KEP model, NeuT-TAMs versus MTMs from the NeuT model and KEP-TAMs versus MTMs from the PRE-KEP model were used as the input. Pearson correlation was performed using the R package Hmisc (v4.1-1). To increase data quality, only significant ($p<0.05$) correlation values were kept. A Pearson correlation coefficients cutoff of 0.878 (all present genes; 7,610 nodes and 310,789 edges) and of 0.87 (union DE genes; 1,992 nodes and 52,392 edges) was chosen to construct scale-free networks. The nodes were colored based on the Group Fold Change (GFC), the mean of each condition versus overall mean for each gene respectively, for each group separately. Unbiased clustering was performed using the "label propagation" algorithm in igraph (v1.2.1) and was repeated 1000 times. Genes assigned to more than 5 different clusters during the iterations got no cluster assignment. The mean GFC expression for each cluster and condition were visualized in the Cluster/Condition heatmap. Clusters smaller than 10 genes were not shown.

I-GIN (Intraclusteral Gene Interaction Network)
To further investigate condition-specific clusters (KEP and NeuT model shared signatures: turquoise [289 genes], NeuT-specific signatures: magenta [236 genes] and KEP-specific signatures: blue [255 genes]), an I-GIN was constructed based on the CoCena² results To enhance the structure and information access of the respective networks, hub genes were identified for each network separately. A gene was defined as hub gene, having a mean correlation greater or equal 75% of the connected edges. Maximal the top 25 most correlated and the two highest correlated edges with other hubs edges were visualized. All edges were classified as either already known or unknown via STRING database v1.20.0. Genes having

more than 5 known connections were additionally defined and labeled as hubs. All known interactions to hubs were kept and the resulting network nodes were sized according to their degree of connectivity in the resulting network. All edges in the network were colored grey and only known interactions were colored red. Hub genes were colored based on their property being regulating (purple) or being regulated (blue) by another gene. This information was calculated using Bayesian Network Analysis.

Bayesian Network Analysis

Bayesian Network Analysis is a probabilistic model that uses statistical dependencies and independencies between features to infer and describe their causal relations within the network. In this study, Bayesian Network Analysis was used to calculate the causal relationship of each gene pair within the cluster of interest defined by CoCena[2], providing additional information about the direction of regulation between two connected nodes within the I-GIN network. Bayesian Network Analysis extracted information from the turquoise, the blue and the magenta clusters and a greedy-search hill-climbing algorithm from the R-package "bnlearn" v4.4 [59] was used to create a network that best fits the observed data and represents the conditional dependencies and independencies between the genes within the cluster of interest. The network structure was then used to determine the regulatory status of each gene, classifying it as receiving if its number of parent nodes exceeded its number of children or as regulating if its number of children exceeded its number of parents. Genes were color-coded with respect to their regulatory status. We classified genes as "hot spots" with high regulatory potential, if their children-to-parent ratio (CP-ratio) exceeded the value 5.

Identification of TAM core signatures

Core signatures for breast cancer TAMs, KEP-TAMs, NeuT-TAMs were defined by overlapping CoCena[2] clusters and the respective DE genes. The breast cancer TAM core signatures are the intersection between the turquoise cluster and the common upregulated genes between KEP-TAMs versus MTMs (KEP model) and NeuT-TAMs versus MTMs (NeuT model). The KEP-TAM core signatures are the intersection between the blue cluster and the upregulated genes between KEP-TAMs versus MTMs (KEP model) and the NeuT-TAMs core signatures are the intersection between the magenta cluster and the upregulated genes between NeuT-TAMs versus MTMs (NeuT model). Subsequently, the union of the core signatures was visualized in a HC map using PGS.

CIBERSORT deconvolution analysis

CIBERSORT [34] was employed to characterize the relative contribution of immune cell populations to the TME of ILC patients. The normalized gene expression table of the TCGA ILC cohort was utilized as input mixture file and the published immune cell signatures "LM22" was used to compute the relative immune cell populations within bulk ILC samples (1,000 permutations). For custom signature generation by CIBERSORT, a gene expression matrix containing KEP-TAM and NeuT-TAM data was used as input.

TAM enrichment analysis

Bulk RNA-sequenced ILC TCGA specimens [27] were accessed through the Genomic Data Commons (https://gdc.cancer.gov/; phs000178.v9.p8) and were aligned against the human hg19 reference genome using TopHat2 (v2.0.11) default parameters. The data were normalized with DESeq2 in R (v3.0.2) and floored to a value of at least 1. Access to bulk ILC microarray specimens of the METABRIC cohort [26] was granted through the EGA depository (EGAD00010000162). The dataset was imported into PGS, quantile-normalized following log2 transformation of absolute expression values and subsequently filtered for probe sets exerting the highest variance. Genes were defined as expressed if the maximum value over all group means utilizing the classification in [27] was higher than 10 (TCGA) or 6.5 (log2 transformed; METABRIC). Before being able to ask whether the KEP-TAM or the NeuT-TAM signatures are enriched in the human TCGA or METABRIC datasets, the signatures were translated into human orthologues using the BioMart package [60] v2.36.1. The signature enrichment analysis for the human TCGA and METABRIC datasets was calculated using GSVA (v1.28.0) using the z-score method [61]. Enrichment analysis were performed for the KEP-TAM core signatures, NeuT-TAM core signatures, KEP-TAMs versus splenic macrophage core signatures (intersection of the blue cluster and KEP-TAM upregulated genes comparing KEP-TAMs versus splenic macrophages) and random signatures. Random gene signatures were generated by sampling a total of 450 genes from the union of signatures (breast cancer TAMs, KEP-TAMs and NeuT-TAMs) and randomly assigning them to three groups, each holding 150 genes. For each patient and each combination of dataset (TCGA and METABRIC) and signature, an enrichment score was calculated. The tool Cutoff Finder [62] was used to define the optimal enrichment score cutoff where a patient shows an enrichment of the respective signatures.

Kaplan Meier survival analysis

Kaplan-Meier survival analysis was performed utilizing the survival package in R (v3.0.2).

Acknowledgments

We thank H-S. Sow for technical assistance. We would like to acknowledge the flow cytometry facility, the animal facility and the animal pathology facility at the Netherlands Cancer Institute. Research in the KEdV lab is supported by the European Union (FP7 MCA-ITN 317445 TIMCC), the Dutch Cancer Society (NKI10623), the European Research Council (ERC consolidator award INFLAMET 615300) and Oncode. JLS is supported by the DFG (EXC 2151/1), the Helmholtz-funded project Sparse2Big, and the European Union (H2020, No 733100: SYSCID, A systems medicine approach to chronic inflammatory diseases).

Authors contributions

JLS, KEdV and TU designed the study. ST, CS and CSH performed experiments. ST, CS, LS, MO, KK and TU performed analysis. TSK wrote the manuscript with input from all authors.

Competing interests

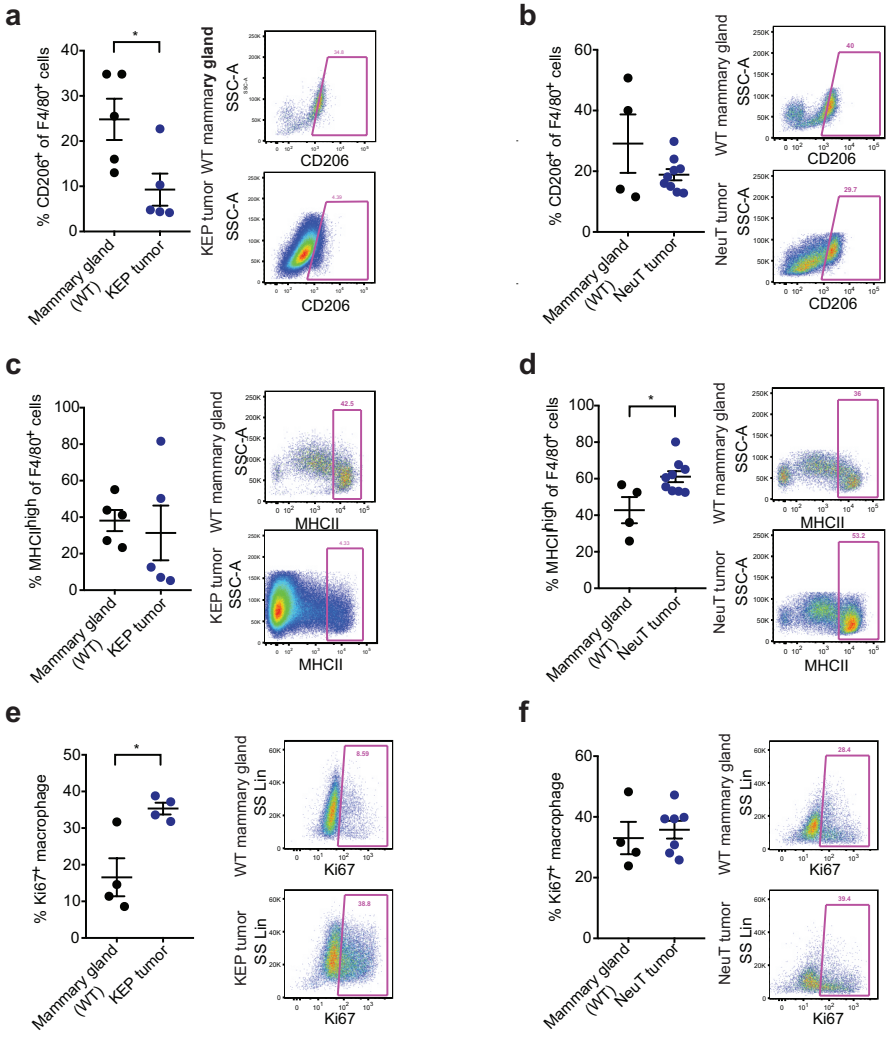
The authors declare no competing interests.

References

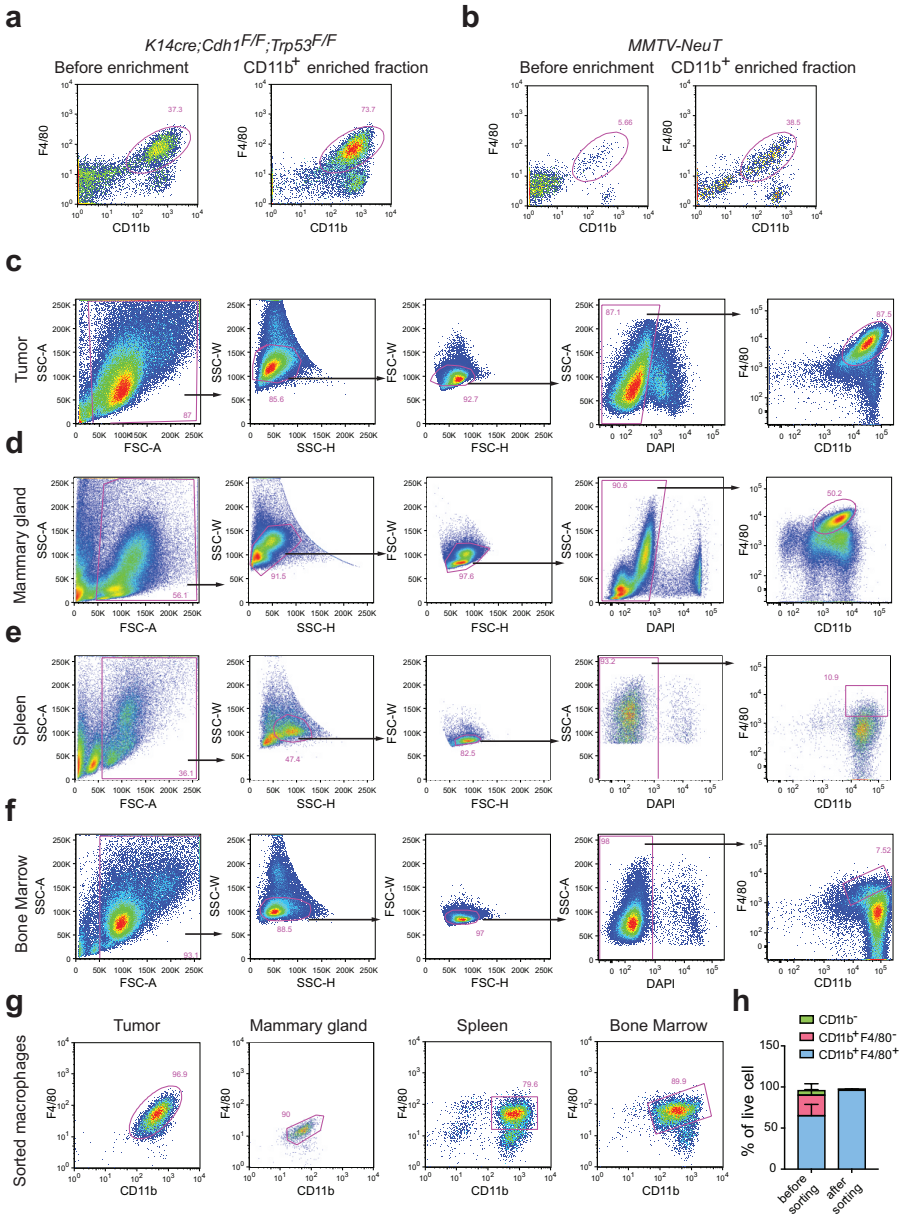
1. Chen, D. S. & Mellman, I. Oncology Meets Immunology: The Cancer-Immunity Cycle. *Immunity* **39,** 1–10 (2013).
2. Shalapour, S. & Karin, M. Immunity, inflammation, and cancer: an eternal fight between good and evil. *J. Clin. Invest.* **125,** 3347–55 (2015).
3. The Nobel Prize in Physiology or Medicine 2018. Available at: https://www.nobelprize.org/prizes/medicine/2018/summary/. (Accessed: 17th October 2018)
4. Ruffell, B. *et al.* Leukocyte composition of human breast cancer. *Proc. Natl. Acad. Sci. U. S. A.* **109,** 2796–801 (2012).
5. Noy, R. & Pollard, J. W. Tumor-Associated Macrophages: From Mechanisms to Therapy. *Immunity* **41,** 49–61 (2014).
6. Quatromoni, J. G. & Eruslanov, E. Tumor-associated macrophages: function, phenotype, and link to prognosis in human lung cancer. *Am. J. Transl. Res.* **4,** 376–89 (2012).
7. Zhao, X. *et al.* Prognostic significance of tumor-associated macrophages in breast cancer: a meta-analysis of the literature. *Oncotarget* **8,** 30576–30586 (2017).
8. Hoadley, K. A. *et al.* Cell-of-Origin Patterns Dominate the Molecular Classification of 10,000 Tumors from 33 Types of Cancer. *Cell* **173,** 291–304.e6 (2018).
9. Thorsson, V. *et al.* The Immune Landscape of Cancer. *Immunity* **48,** 812–830.e14 (2018).
10. Gentles, A. J. *et al.* The prognostic landscape of genes and infiltrating immune cells across human cancers. *Nat. Med.* **21,** 938–945 (2015).
11. Iqbal, J. *et al.* Molecular signatures to improve diagnosis in peripheral T-cell lymphoma and prognostication in angioimmunoblastic T-cell lymphoma. *Blood* **115,** 1026–36 (2010).
12. Johdi, N. A., Ait-Tahar, K., Sagap, I. & Jamal, R. Molecular Signatures of Human Regulatory T Cells in Colorectal Cancer and Polyps. *Front. Immunol.* **8,** 620 (2017).
13. Lyons, Y. A., Wu, S. Y., Overwijk, W. W., Baggerly, K. A. & Sood, A. K. Immune cell profiling in cancer: molecular approaches to cell-specific identification. *NPJ Precis. Oncol.* **1,** 26 (2017).
14. Gosselin, D. *et al.* Environment Drives Selection and Function of Enhancers Controlling Tissue-Specific Macrophage Identities. *Cell* **159,** 1327–1340 (2014).
15. Mass, E. *et al.* Specification of tissue-resident macrophages during organogenesis. *Science* **353,** aaf4238-aaf4238 (2016).
16. Lavin, Y. *et al.* Tissue-Resident Macrophage Enhancer Landscapes Are Shaped by the Local Microenvironment. *Cell* **159,** 1312–1326 (2014).
17. Cassetta, L. *et al.* Human Tumor-Associated Macrophage and Monocyte Transcriptional Landscapes Reveal Cancer-Specific Reprogramming, Biomarkers, and Therapeutic Targets. *Cancer Cell* (2019). doi:10.1016/j.ccell.2019.02.009
18. Regev, A. *et al.* The Human Cell Atlas. *Elife* **6,** (2017).
19. Lavin, Y. *et al.* Innate Immune Landscape in Early Lung Adenocarcinoma by Paired Single-Cell Analyses. *Cell* **169,** 750–765.e17 (2017).
20. Lambrechts, D. *et al.* Phenotype molding of stromal cells in the lung tumor microenvironment. *Nat. Med.* **24,** 1277–1289 (2018).
21. Tirosh, I. *et al.* Dissecting the multicellular ecosystem of metastatic melanoma by single-cell RNA-seq. *Science (80-.).* **352,** 189–196 (2016).
22. Savas, P. *et al.* Single-cell profiling of breast cancer T cells reveals a tissue-resident memory subset associated with improved prognosis. *Nat. Med.* **24,** 986–993 (2018).
23. Azizi, E. *et al.* Single-Cell Map of Diverse Immune Phenotypes in the Breast Tumor Microenvironment. *Cell* **174,** 1293–1308.e36 (2018).
24. Derksen, P. W. B. *et al.* Somatic inactivation of E-cadherin and p53 in mice leads to metastatic lobular mammary carcinoma through induction of anoikis resistance and angiogenesis. *Cancer Cell* **10,** 437–49 (2006).

25. Boggio, K. *et al.* Interleukin 12-mediated prevention of spontaneous mammary adenocarcinomas in two lines of Her-2/neu transgenic mice. *J. Exp. Med.* **188,** 589–96 (1998).
26. Curtis, C. *et al.* The genomic and transcriptomic architecture of 2,000 breast tumours reveals novel subgroups. *Nature* **486,** 346–52 (2012).
27. Ciriello, G. *et al.* Comprehensive Molecular Portraits of Invasive Lobular Breast Cancer. *Cell* **163,** 506–19 (2015).
28. Squadrito, M. L. *et al.* miR-511-3p modulates genetic programs of tumor-associated macrophages. *Cell Rep.* **1,** 141–54 (2012).
29. Choi, H. *et al.* Transcriptome analysis of individual stromal cell populations identifies stroma-tumor crosstalk in mouse lung cancer model. *Cell Rep.* **10,** 1187–201 (2015).
30. Lu, L.-F. *et al.* A Single miRNA-mRNA Interaction Affects the Immune Response in a Context- and Cell-Type-Specific Manner. *Immunity* **43,** 52–64 (2015).
31. Thomas, G. D. *et al.* The biology of nematode- and IL4Rα-dependent murine macrophage polarization in vivo as defined by RNA-Seq and targeted lipidomics. *Blood* **120,** e93–e104 (2012).
32. Biswas, S. K. *et al.* A distinct and unique transcriptional program expressed by tumor-associated macrophages (defective NF-kappaB and enhanced IRF-3/STAT1 activation). *Blood* **107,** 2112–22 (2006).
33. Ojalvo, L. S., King, W., Cox, D. & Pollard, J. W. High-density gene expression analysis of tumor-associated macrophages from mouse mammary tumors. *Am. J. Pathol.* **174,** 1048–64 (2009).
34. Newman, A. M. *et al.* Robust enumeration of cell subsets from tissue expression profiles. *Nat. Methods* **12,** 453–7 (2015).
35. Aras, S. & Zaidi, M. R. TAMeless traitors: macrophages in cancer progression and metastasis. *Br. J. Cancer* **117,** 1583–1591 (2017).
36. Poh, A. R. & Ernst, M. Targeting Macrophages in Cancer: From Bench to Bedside. *Front. Oncol.* **8,** 49 (2018).
37. Parker, J. S. *et al.* Supervised risk predictor of breast cancer based on intrinsic subtypes. *J. Clin. Oncol.* **27,** 1160–7 (2009).
38. Qian, B.-Z. & Pollard, J. W. Macrophage diversity enhances tumor progression and metastasis. *Cell* **141,** 39–51 (2010).
39. Kim, I. S. & Zhang, X. H.-F. One microenvironment does not fit all: heterogeneity beyond cancer cells. *Cancer Metastasis Rev.* **35,** 601–629 (2016).
40. Egeblad, M. *et al.* Visualizing stromal cell dynamics in different tumor microenvironments by spinning disk confocal microscopy. *Dis. Model. Mech.* **1,** 155–167 (2008).
41. Movahedi, K. *et al.* Different tumor microenvironments contain functionally distinct subsets of macrophages derived from Ly6C(high) monocytes. *Cancer Res.* **70,** 5728–39 (2010).
42. Casazza, A. *et al.* Impeding macrophage entry into hypoxic tumor areas by Sema3A/Nrp1 signaling blockade inhibits angiogenesis and restores antitumor immunity. *Cancer Cell* **24,** 695–709 (2013).
43. Franklin, R. A. *et al.* The cellular and molecular origin of tumor-associated macrophages. *Science (80-.).* **344,** 921–925 (2014).
44. Tymoszuk, P. *et al.* In situ proliferation contributes to accumulation of tumor-associated macrophages in spontaneous mammary tumors. *Eur. J. Immunol.* **44,** 2247–2262 (2014).
45. Mak, I. W., Evaniew, N. & Ghert, M. Lost in translation: animal models and clinical trials in cancer treatment. *Am. J. Transl. Res.* **6,** 114–8 (2014).
46. Salvagno, C. *et al.* Therapeutic targeting of macrophages enhances chemotherapy efficacy by unleashing type I interferon response. *Nat. Cell Biol.* **21,** 511–521 (2019).
47. Papalexi, E. & Satija, R. Single-cell RNA sequencing to explore immune cell heterogeneity. *Nat. Rev. Immunol.* **18,** 35–45 (2017).
48. Ferreri, A. J. M., Illerhaus, G., Zucca, E., Cavalli, F. & Group, on behalf of the I. E. L. S. Flows and flaws in primary central nervous system lymphoma. *Nat. Rev. Clin. Oncol.* **7,** 1–2 (2010).
49. Coffelt, S. B. *et al.* IL-17-producing γδ T cells and neutrophils conspire to promote breast cancer metastasis. *Nature* **522,** 345–348 (2015).

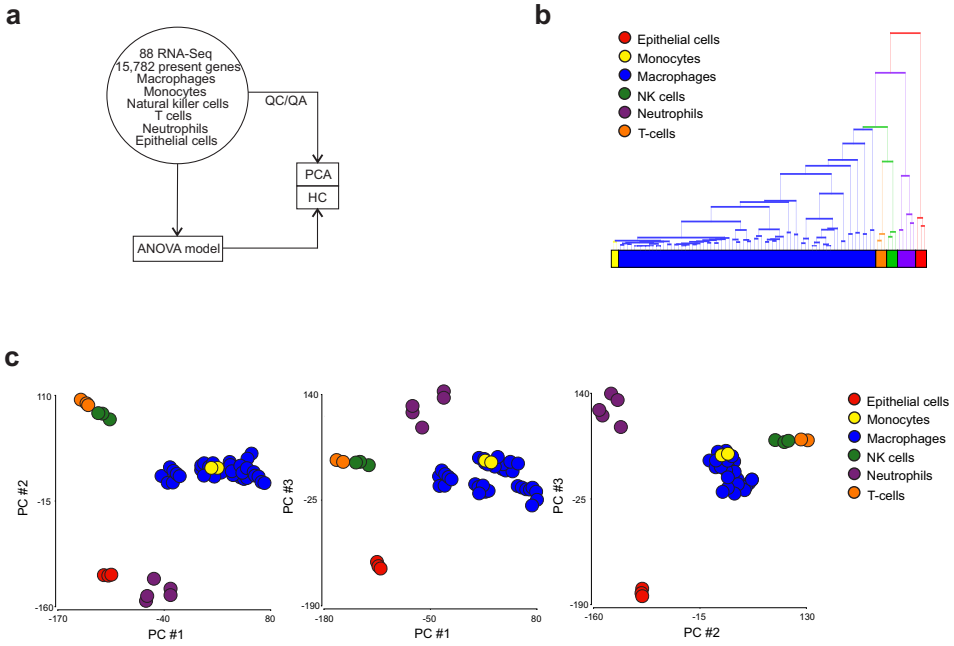
50. Salvagno, C. & de Visser, K. E. Purification of Immune Cell Populations from Freshly Isolated Murine Tumors and Organs by Consecutive Magnetic Cell Sorting and Multi-parameter Flow Cytometry-Based Sorting. *Methods Mol. Biol.* **1458,** 125–35 (2016).
51. Kim, D. *et al.* TopHat2: accurate alignment of transcriptomes in the presence of insertions, deletions and gene fusions. *Genome Biol.* **14,** R36 (2013).
52. Love, M. I., Huber, W. & Anders, S. Moderated estimation of fold change and dispersion for RNA-seq data with DESeq2. *Genome Biol.* **15,** 550 (2014).
53. Fulton, D. L. *et al.* TFCat: the curated catalog of mouse and human transcription factors. *Genome Biol.* **10,** R29 (2009).
54. Battke, F., Symons, S. & Nieselt, K. Mayday - integrative analytics for expression data. *BMC Bioinformatics* **11,** 121 (2010).
55. Theocharidis, A., van Dongen, S., Enright, A. J. & Freeman, T. C. Network visualization and analysis of gene expression data using BioLayout Express(3D). *Nat. Protoc.* **4,** 1535–50 (2009).
56. Maere, S., Heymans, K. & Kuiper, M. BiNGO: a Cytoscape plugin to assess overrepresentation of gene ontology categories in biological networks. *Bioinformatics* **21,** 3448–9 (2005).
57. Merico, D., Isserlin, R., Stueker, O., Emili, A. & Bader, G. D. Enrichment map: a network-based method for gene-set enrichment visualization and interpretation. *PLoS One* **5,** e13984 (2010).
58. Oesper, L., Merico, D., Isserlin, R. & Bader, G. D. WordCloud: a Cytoscape plugin to create a visual semantic summary of networks. *Source Code Biol. Med.* **6,** 7 (2011).
59. Scutari, M. Learning Bayesian Networks with thebnlearnRPackage. *J. Stat. Softw.* **35,** (2010).
60. Durinck, S., Spellman, P. T., Birney, E. & Huber, W. Mapping identifiers for the integration of genomic datasets with the R/Bioconductor package biomaRt. *Nat. Protoc.* **4,** 1184–1191 (2009).
61. Hänzelmann, S., Castelo, R. & Guinney, J. GSVA: gene set variation analysis for microarray and RNA-seq data. *BMC Bioinformatics* **14,** 7 (2013).
62. Budczies, J. *et al.* Cutoff Finder: a comprehensive and straightforward Web application enabling rapid biomarker cutoff optimization. *PLoS One* **7,** e51862 (2012).



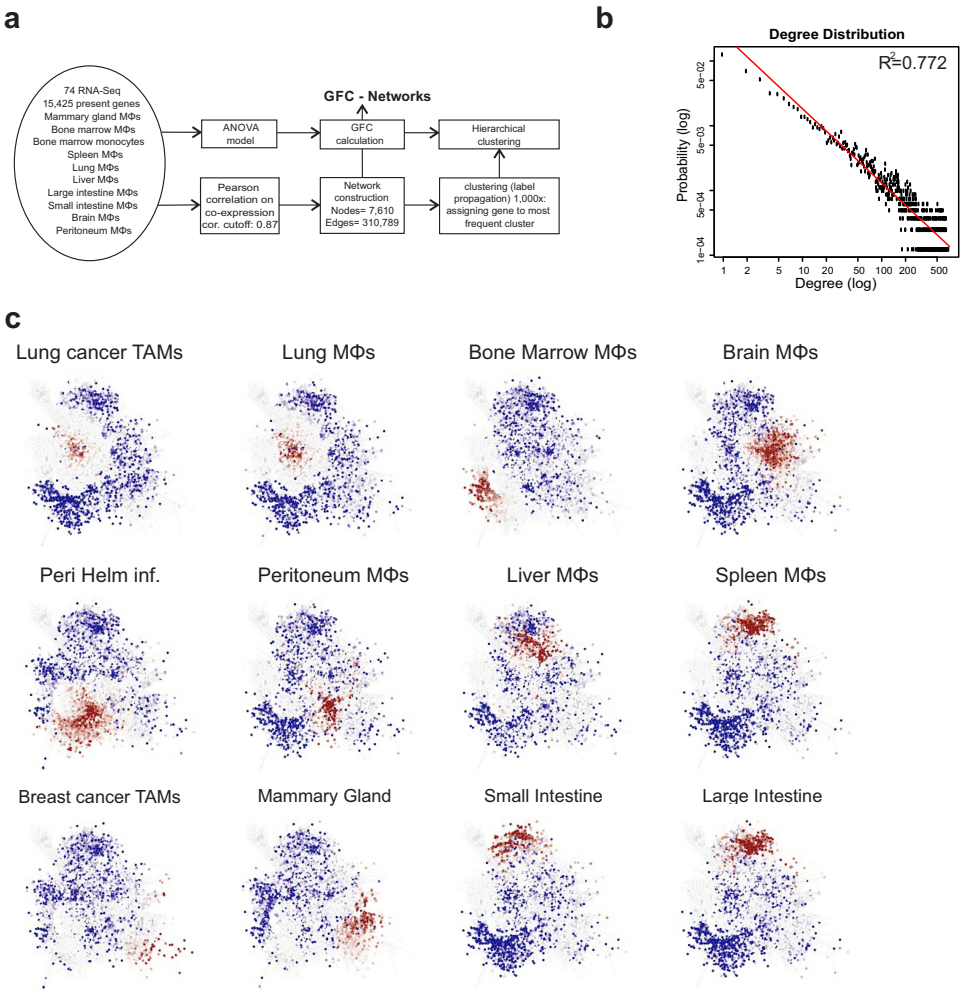
Supplementary Fig. 1 | Related to Fig. 1. TAMs in K14cre;Cdh1$^{F/F}$;Trp53$^{F/F}$ mammary tumors express low levels of CD206 and have a proliferative phenotype compared to TAMs from the MMTV-NeuT model. (a-b) Percentage of CD206^{+} macrophages in KEP tumors and WT FVB mammary glands (a) or NeuT tumors and WT Balb/c mammary glands (b) as determined by flow cytometry. Representative dot plots are shown. The gating was based on fluorescence-minus-one sample for CD206. (c-d) Percentage of MHC-II^{+} macrophages in KEP tumors and WT FVB mammary glands (c) or NeuT tumors and WT Balb/c mammary glands (d) as determined by flow cytometry. Representative dot plots are shown. (e-f) Percentage of Ki67^{+} macrophages in KEP tumors and WT FVB mammary glands (e) or in NeuT mammary tumor and WT Balb/c mammary glands (f) as determined by flow cytometry. Dot plots were gated on CD11b^{+}F4/80^{+} macrophages. Representative dot plots are shown. Data are mean values ± SEM from n=3 animals per group and were analyzed with Mann-Whitney test, *p < 0.05.



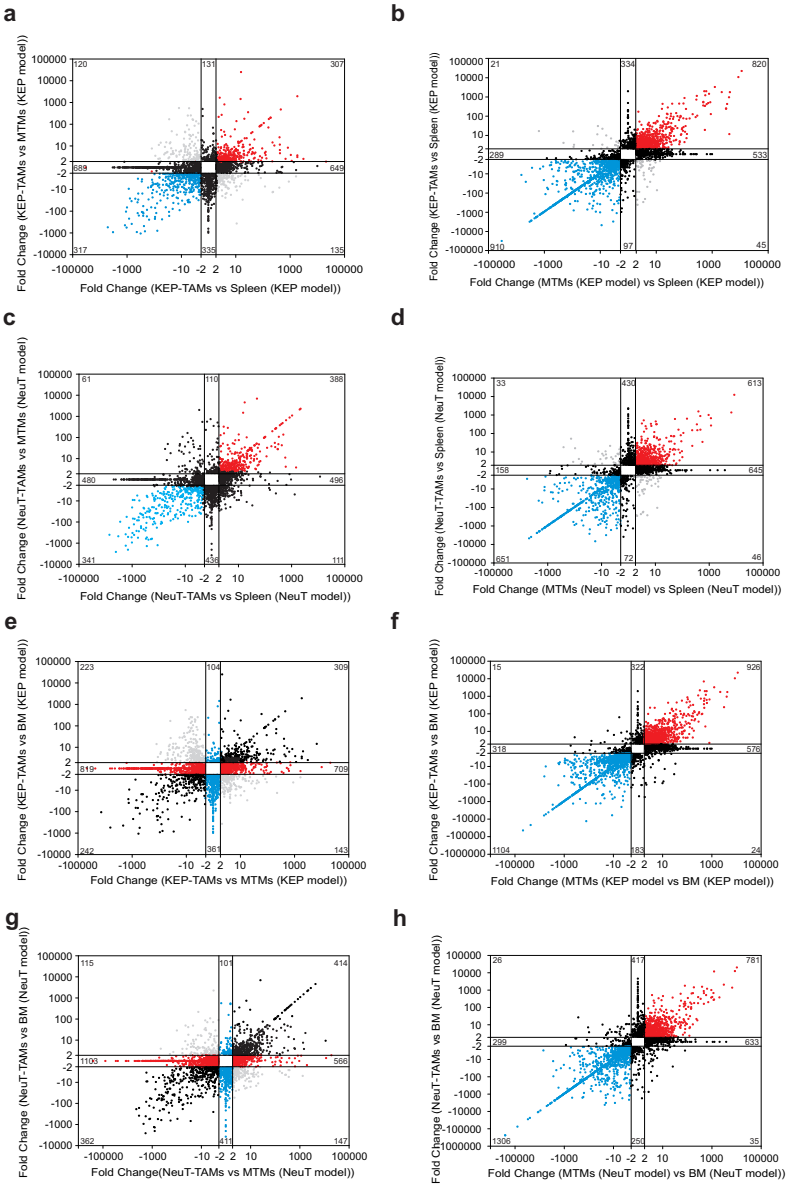
Supplementary Fig. 2 | Isolation procedure of CD11b$^+$F4/80$^+$ macrophages from mammary tumor, mammary gland, spleen and bone marrow by magnetic and fluorescence-activated cell sorting. (a-b) Representative dot plots of KEP (a) and NeuT (b) mammary tumors showing the CD11b$^+$F4/80$^+$ population before and after pre-enrichment by magnetic-activated cell sorting for CD11b$^+$ cells. (c-f) Representative dot plots illustrating the gating strategy for the isolation of CD11b$^+$F4/80$^+$ macrophages from KEP tumors (c), mammary gland (d), spleen (e) and bone marrow (f) by fluorescence-activated cell sorting after enrichment of CD11b$^+$ cells. (g) Dot plots showing the purity of the sorted macrophages in tumor, mammary gland, spleen and bone marrow of KEP mice. (h) Stacked bar plots showing the composition of KEP tumors in CD11b$^-$, CD11b$^+$F4/80$^-$ and CD11b$^+$F4/80$^+$ cells before and after macrophage sorting. Data are mean values ± SEM from 3 preps.



Supplementary Fig. 3 | Murine macrophages are distinguished from other immune cell populations by their transcriptome. (a) Schematic representation outlining bioinformatics workflow. (b) HC based on the 1,000 genes with the highest variance within the dataset. Macrophage transcriptomes derived from different organs (mammary gland, bone marrow, spleen, peritoneum, lung, brain, liver, large intestine and small intestine) and disease states (tumor, pre-lesion and helminth infection) were collectively named macrophages. (c) PCA using all present (15,782) genes with principle components (PC1-3) plotted in two-dimensional graphs.

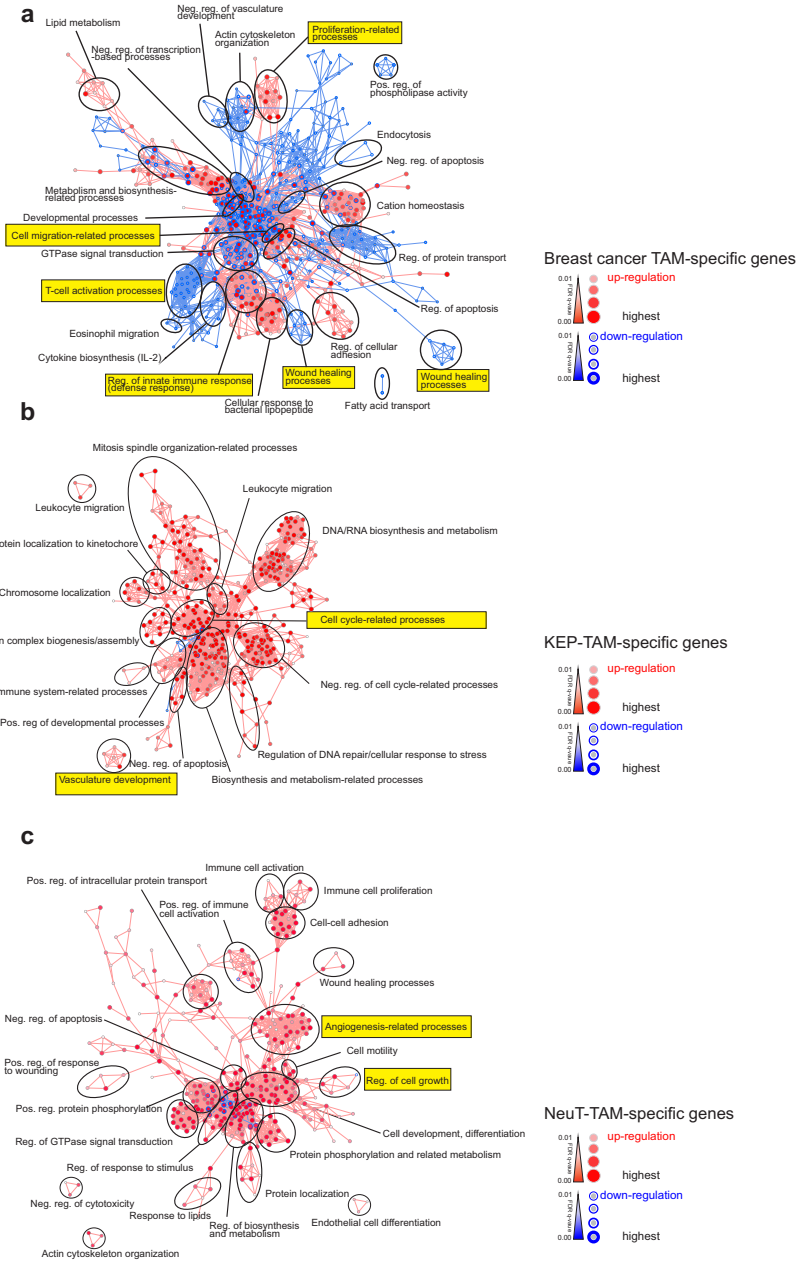


Supplementary Fig. 4 | Co-expression network analysis (CNA) of all present genes by CoCena². (a) Schematic representation depicting the bioinformatics workflow. (b) CoCena² logged network degree distribution with linear fitting. (c) Networks were colored according to Group Fold Changes (GFCs) for each condition, respectively (condition mean versus overall mean).

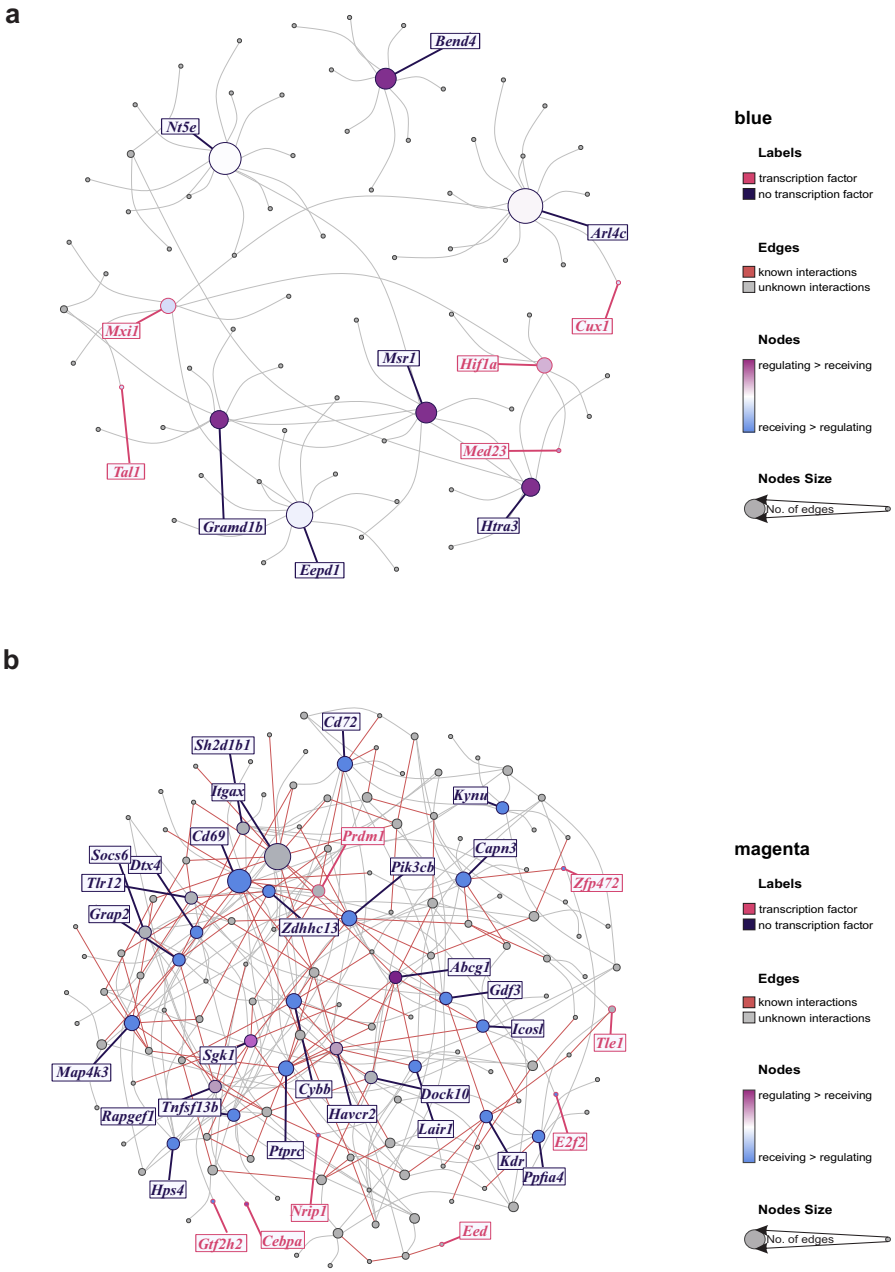


Supplementary Fig. 5 | Inter-tissue comparison leads to false interpretation of changes in TAMs. (a) FC/FC plot of the union of DE genes showing the fold change in expression of genes in KEP-TAMs compared to MTMs (KEP model) (y-axis) against KEP-TAMs compared to splenic macrophages (KEP model) (x-axis). (b) FC/FC plot of the union of DE genes showing the fold change in expression of genes in KEP-TAMs compared to splenic macrophages (KEP model) (y-axis) against MTMs (KEP model) compared to splenic macrophages (KEP model) (x-axis). (c) FC/FC plot of the union of DE genes showing the fold change in expression of genes in NeuT-TAMs compared to MTMs (NeuT model) (y-axis) against NeuT-TAMs compared to splenic macrophages (NeuT model) (x-axis). (d) FC/FC plot of the union of DE genes showing the fold change in expression of genes in NeuT-TAMs compared to splenic macrophages (NeuT model) (y-axis) against MTMs (NeuT model) compared to splenic macrophages (NeuT model) (x-axis). (e) FC/FC plot of the union of DE genes showing the fold change in expression of genes in

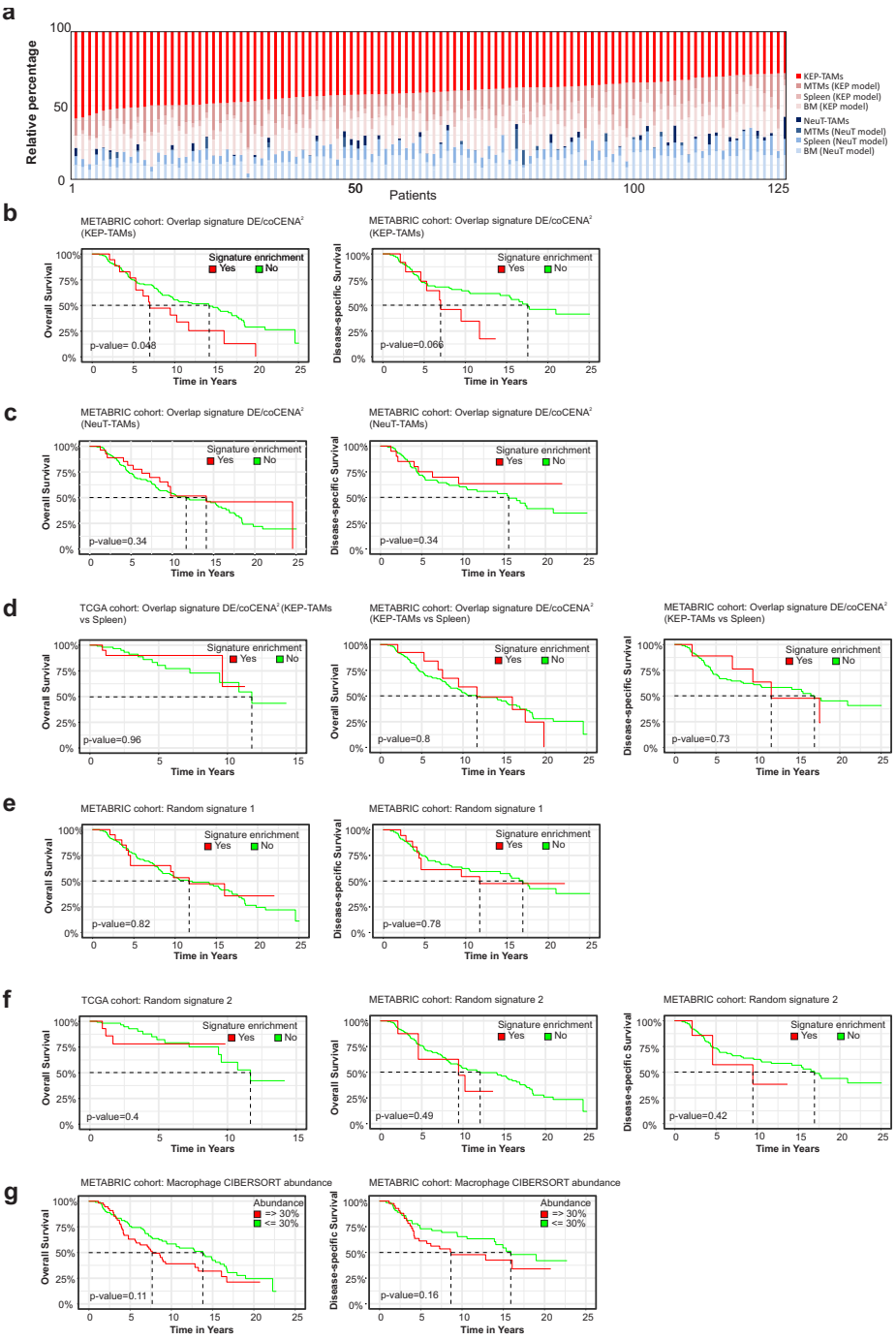
KEP-TAMs compared to bone marrow macrophages (KEP model) (y-axis) against KEP-TAMs compared to MTMs (KEP model) (x-axis). (f) FC/FC plot of the union of DE genes showing the fold change in expression of genes in KEP-TAMs compared to bone marrow macrophages (KEP model) (y-axis) against MTMs (KEP model) compared to bone marrow macrophages (KEP model) (x-axis). (g) FC/FC plot of the union of DE genes showing the fold change in expression of genes in NeuT-TAMs compared to bone marrow macrophages (NeuT model) (y-axis) against NeuT-TAMs compared to MTMs (NeuT model) (x-axis). (h) FC/FC plot of the union of DE genes showing the fold change in expression of genes in NeuT-TAMs compared to bone marrow macrophages (NeuT model) (y-axis) against MTMs (NeuT model) compared to bone marrow macrophages (NeuT model) (x-axis). Each dot represents one gene where red and blue dots indicate positive or negative fold change differences in both comparisons and grey dots correspond to opposite fold change differences across the axes.



Supplementary Fig. 6 | GOEA of breast cancer TAM-, KEP-TAM- and NeuT-TAM-specific genes. (a-c) Network visualization of GOEA using BiNGO and EnrichmentMap based on model-specific DE genes derived from (a) breast cancer TAM-, (b) KEP-TAM- and (c) NeuT-TAM-specific genes. Node size and color (positively enriched GO terms) and node border width (negatively enriched GO terms) represent corresponding FDR-adjusted enrichment p-values (p-value: ≤0.05). Enriched gene ontology terms mentioned in the text are highlighted in yellow boxes.



Supplementary Fig. 7 | I-GIN of KEP-TAM- and NeuT-TAM-specific genes. (a-b) I-GIN construction for KEP-TAM-specific (blue cluster) (a) and NeuT-specific (magenta cluster) (b) genes. Node coloring represents regulatory or receiving status obtained from a Bayesian approach and points out highly co-expressed genes and their known or proposed links to strongest correlated neighbors. Candidate genes mentioned in the text are highlighted in yellow boxes.



Supplementary Fig. 8 | Validation of Kaplan-Meier survival analysis of breast cancer model-specific signatures. (a) KEP-TAM, NeuT-TAM, splenic and bone marrow macrophage and MTM signatures from both models were computed using CIBERSORT and their relative abundance in the ILC specimens was calculated. (b) Kaplan-Meier overall (left) and disease-specific (right) survival analysis of METABRIC ILC patients (n=147). ILC specimens having a significant enrichment for KEP-TAMs signature are

visualized in red line and numbers. The rest ILC patients are visualized in green line and numbers. (c) Kaplan-Meier overall (left) and disease-specific (right) survival analysis of METABRIC ILC patients. ILC specimens having a significant enrichment for NeuT-TAMs signature are visualized in red line and numbers. The rest ILC patients are visualized in green line and numbers. (d) Kaplan-Meier overall (left and middle) and disease-specific (right) survival analysis of TCGA (left, n=125) and METABRIC (middle and right) ILC patients. ILC specimens having a significant enrichment for KEP-TAMs signature (using splenic macrophages from the KEP model as a control) are visualized in red line and numbers. The rest ILC patients are visualized in green line and numbers. (e) Kaplan-Meier overall (left) and disease-specific (right) survival analysis of METABRIC ILC patients. ILC specimens having a significant enrichment for a random signature are visualized in red line and numbers. The rest ILC patients are visualized in green line and numbers. (f) Kaplan-Meier overall (left and middle) and disease-specific (right) survival analysis of TCGA (left) and METABRIC (middle and right) ILC patients. ILC specimens having a significant enrichment for a random signature macrophage signature are visualized in red line and numbers. The rest ILC patients are visualized in green line and numbers. (g) Kaplan-Meier overall (left) and disease-specific (right) survival analysis of METABRIC ILC patients. ILC specimens having a significant enrichment for a CIBERSORT macrophage signature are visualized in red line and numbers. The rest ILC patients are visualized in green line and numbers. Z score above 2 marks significant enrichment of gene signatures.

CHAPTER 4

Exploiting the immunomodulatory properties of chemotherapeutic drugs to improve the success of cancer immunotherapy

Kelly Kersten[†], Camilla Salvagno[†] and Karin E. de Visser[*]

Division of Immunology, Netherlands Cancer Institute, Amsterdam, Netherlands

[†]These authors contributed equally to this work
[*]Correspondence:

Karin E. de Visser,
Division of Immunology, Netherlands
Cancer Institute, Plesmanlaan 121,
Amsterdam 1066 CX, Netherlands
k.d.visser@nki.nl

Front Immunol. 2015 Oct 7;6:516.

Abstract

Cancer immunotherapy is gaining momentum in the clinic. The current challenge is to understand why a proportion of cancer patients do not respond to cancer immunotherapy, and how this can be translated into the rational design of combinatorial cancer immunotherapy strategies aimed at maximizing success of immunotherapy. Here, we discuss how tumors orchestrate an immunosuppressive microenvironment, which contributes to their escape from immune attack. Relieving the immunosuppressive networks in cancer patients is an attractive strategy to extend the clinical success of cancer immunotherapy. Since the clinical availability of drugs specifically targeting immunosuppressive cells or mediators is still limited, an alternative strategy is to use conventional chemotherapy drugs with immunomodulatory properties to improve cancer immunotherapy. We summarize the preclinical and clinical studies that illustrate how the anti-tumor T cell response can be enhanced by chemotherapy-induced relief of immunosuppressive networks. Treatment strategies aimed at combining chemotherapy-induced relief of immunosuppression and T cell-boosting checkpoint inhibitors provide an attractive and clinically feasible approach to overcome intrinsic and acquired resistance to cancer immunotherapy, and to extend the clinical success of cancer immunotherapy.

Keywords

Cancer immunotherapy
Immune checkpoint blockade
Chemotherapy
Tumor microenvironment
Immunosuppression
Anti-tumor immunity

Introduction

Cancer immunotherapy – harnessing the patient's immune system against cancer – is currently gaining momentum in the clinic. Clinical trials with immune checkpoint inhibitors show remarkable success in patients with advanced metastatic melanoma, non-small cell lung cancer, renal cancer, bladder cancer, and Hodgkin's lymphoma (1–6). As a result, the journal *Science* proclaimed cancer immunotherapy as the breakthrough of 2013 (7). Furthermore, these encouraging results led to FDA approval of the immune checkpoint inhibitors ipilimumab (anti-CTLA-4), nivolumab, and pembrolizumab (anti-PD-1) in the past few years. Although cancer immunotherapy was proclaimed a breakthrough, a significant proportion of cancer patients do not show clinical benefit. There are various cancer cell-intrinsic and cancer cell-extrinsic processes that regulate intrinsic or acquired resistance to cancer immunotherapy. Cancer cell-intrinsic characteristics like the mutational load have been reported to affect responsiveness to immunotherapy (8, 9). In terms of cancer cell-extrinsic processes, tumors exploit different strategies to induce immune escape by hampering the recruitment and activation of effector T cells, and by creating a local immunosuppressive environment through recruitment of suppressive myeloid and regulatory T cells that dampen T cell effector functions. Which of these immune escape mechanisms are active in a certain tumor depends on the tumor type, tumor stage, and therapy history. A deeper understanding of the molecular mechanisms underlying these processes will contribute to the identification of biomarkers that can predict therapeutic efficacy of immunotherapy and to the design of combinatorial strategies aimed at maximizing the success of immunotherapy.

In this review, we discuss how tumor-induced immunosuppressive networks counteract efficacious anti-tumor immune responses, and how disruption of these networks can increase the anti-cancer efficacy of cancer immunotherapy with immune checkpoint inhibitors. Development and clinical testing of novel drugs specifically targeting immunosuppressive networks are ongoing and preliminary results are promising (10). An alternative strategy to relieve tumor-induced immunosuppressive states is to use conventional, and more easily accessible, anti-cancer treatment strategies with known immunomodulatory properties, such as chemotherapy, radiotherapy, and targeted therapy (11–15). Here, we focus on the immunomodulatory properties of conventional chemotherapy, and how these properties can be exploited to improve the anti-cancer efficacy of immune checkpoint inhibitors.

Cancer Immunotherapy: Opportunities and Challenges

Tumor-Induced Mechanisms of Immune Escape

Cancers do not merely consist of tumor cells, but comprise a variety of cell types that together form the tumor microenvironment (TME) (Figures 1 and 2). Infiltrating immune cells are of special interest because of their paradoxical role in cancer progression. While some immune cell populations have pro-tumorigenic properties, others counteract tumorigenesis (16–18). Many tumors are characterized by an

immunosuppressive TME, which makes it unfavorable for anti-tumor immunity. To mount effective anti-tumor immunity, tumor-associated antigens need to be sampled and processed by antigen-presenting cells (APCs). After receiving specific maturation signals, these APCs migrate to tumor-draining lymphoid organs where antigens are presented to T cells. Upon activation and proliferation, tumor antigen-specific T cells migrate to the tumor bed where they exert their cytotoxic function. At every step of this T cell priming and effector process, tumors employ strategies to hamper anti-cancer immunity.

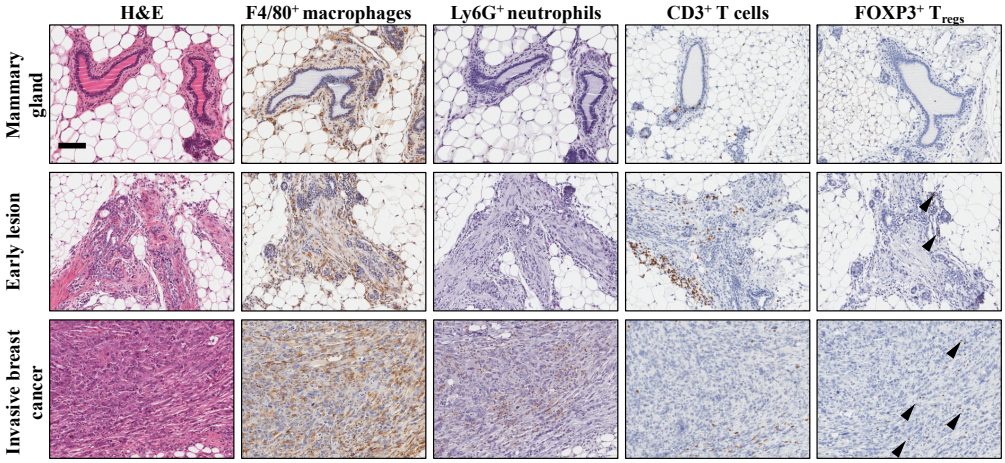


Fig. 1 | Establishment of the immune microenvironment during breast cancer progression in a conditional mouse model for mammary tumorigenesis. Female *K14Cre;Cdh1$^{F/F}$;Trp53$^{F/F}$* mice develop *de novo* invasive mammary tumors that closely resemble human invasive lobular carcinoma (19). Immunohistochemical staining on mammary tissue from *K14Cre;Cdh1$^{F/F}$;Trp53$^{F/F}$* mice obtained during different stages of mammary tumor progression. From top to bottom are represented wild-type mammary gland (top), early lesion (middle), established mammary tumor (bottom). From left to right, identification of different immune cell populations by H&E, F4/80 (macrophages), Ly6G (neutrophils), CD3 (total T cells), and FOXP3 (regulatory T cells) staining showing the dynamics of the tumor microenvironment. Arrowheads indicate FOXP3$^+$ nuclei. Scale bar 100 μm.

Tumors often show dysfunctional recruitment and activation of dendritic cells (DCs), which are the most potent APCs for initiating immune responses. Several studies show that tumor-infiltrating DCs display an immature phenotype (20, 21). Tumor-derived factors like IL10, IL6, CSF1, and VEGF interfere with DC maturation, causing failure to migrate to the tumor-draining lymphoid organs, and to provide the appropriate co-stimulatory signals required to stimulate T cells (21). Although a thorough analysis of the antigen-presenting myeloid immune cell compartment in the *MMTV-PyMT* mammary tumor model showed that intratumoral DCs are able to ingest and present tumor antigens to T cells, they fail to activate them (22). Nevertheless, even in these immunoevasive tumors, a rare population of IL12-expressing CD103$^+$ DCs exists that is able to prime tumor antigen-specific T cells (23). Besides hampered T cell priming, the recruitment of activated T cells and their access into the tumor bed is often disrupted by the disorganized tumor vasculature and impaired expression of adhesion molecules on endothelial cells (24, 25). Some

studies suggest that tumor-derived chemokines may cause selective trapping of T cells in the tumor stroma preventing access into the tumor bed (26). When tumor-specific T cells do succeed to reach the tumor, downregulation of MHC class I expression on tumor cells renders them invisible to T cell attack (27). Additionally, T cells face systemic and local tumor-induced immunosuppression, which limits their activation and function (28). Tumor-associated immunosuppression can be caused by tumor-infiltrating or systemically expanded myeloid cells or regulatory T cells (T_{regs}) that – directly or indirectly via secretion of soluble mediators – hamper T cell priming and effector function or even induce T cell death (28). These mechanisms will be discussed in more detail later.

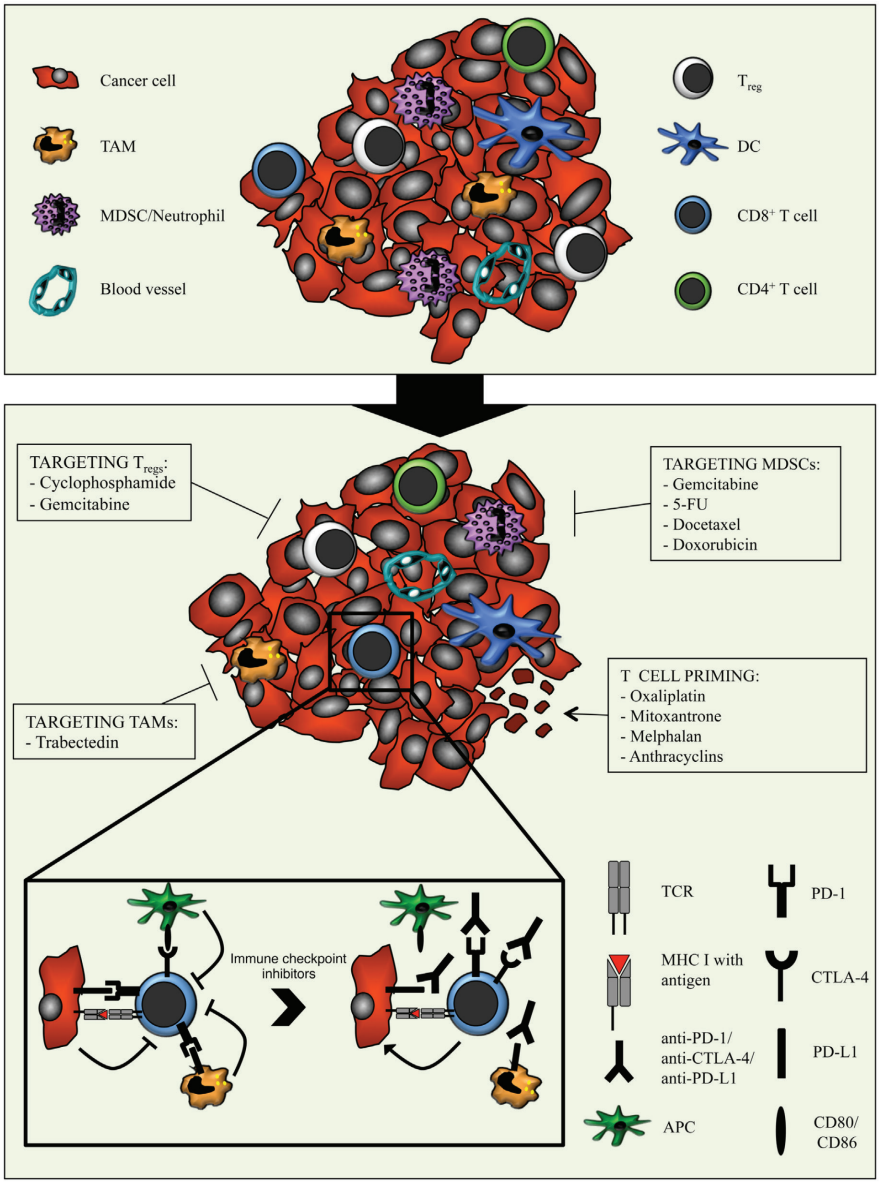


Fig. 2 | Combination strategies aimed at relieving the immunosuppressive tumor microenvironment with chemotherapy and potentiating cytotoxic T cells with immune checkpoint inhibitors. The tumor microenvironment is characterized by the presence of various immune cell types, including different subsets of adaptive immune cells and TAMs, MDSCs, and T_{regs}. The latter dampens the anti-cancer activity of T cells through several mechanisms. Moreover, cancer cells and myeloid cells express PD-L1/PD-L2 and APCs express CD80/CD86. Binding of these molecules to PD-1 and CTLA-4 respectively, expressed on T cells, results in inhibitory signals that counteract T cell activation and function. The immunomodulatory properties of different types of chemotherapeutic drugs can be exploited to enhance anti-tumor immunity. By optimally matching the immunomodulatory features of specific chemotherapeutic drugs with the T cell-boosting effect of immune checkpoint inhibitors, the efficacy of immunotherapy might be improved.

Enhancing Anti-Tumor Immunity by Immune Checkpoint Inhibitors

To improve anti-tumor T cell immunity, different types of cancer immunotherapy approaches exist. While passive immunotherapy is based on adoptive transfer of (genetically engineered) autologous T cells, active immunotherapy boosts the endogenous immune response via cancer vaccines or inhibitors of immune checkpoints. The therapeutic effect of the latter is aimed at inhibition of negative immune regulatory pathways including cytotoxic T-lymphocyte-associated protein-4 (CTLA-4) and the programed cell death protein-1 (PD-1) receptor and one of its ligands, PD-L1 (B7-H1; CD274) (29). CTLA-4 is a member of the CD28 immunoglobulin superfamily and is expressed mainly on the surface of activated $CD4^+$ T cells and T_{regs}, while absent on naïve T cells (30). CTLA-4 plays a central role in maintaining immune tolerance by competing with CD28 to bind the ligands CD80 and CD86 present on activated APCs to inhibit T cell co-stimulation. The PD-1/PD-L1 axis shows similarities to that of CTLA-4. PD-1 is mainly expressed on activated T cells upon T cell receptor (TCR) engagement and on T_{regs}, while naïve and memory T cells do not usually express this surface marker. Recent studies suggest that PD-1, rather than being a marker of activated T cells, identifies exhausted T cells (31). PD-L1 is expressed on multiple cell types, whereas expression of PD-L2 (B7-DC; CD273) seems to be restricted to APCs (32, 33). Like CTLA-4, binding of PD-L1/PD-L2 to its receptor results in an inhibitory signal that prevents T cell activation. While CTLA-4 blockade is hypothesized to act mainly in secondary lymphoid organs during the T cell priming phase, it is believed that blockade of PD-1 or PD-L1 targets the TME during the T cell effector phase (34). However, PD-1 can also play a role in the early T cell response as a regulator of $CD8^+$ T cell expansion upon antigen recognition (35). In addition to its role in T cell priming, CTLA-4 also regulates the suppressive function of tumor-infiltrating T_{regs} (36, 37). In line with this, blockade of CTLA-4 in the B16 melanoma model acts locally in the TME by inactivating T_{regs} in an Fc-dependent manner resulting in a favorable shift in the effector T cell/T_{reg} ratio (38). The exact mechanisms of action of anti-CTLA-4 and anti-PD-1/PD-L1 are not completely clear. Just recently, the combination of anti-CTLA-4 and anti-PD-1 was reported to significantly increase the fraction of melanoma patients responding to immunotherapy compared to anti-CTLA-4 monotherapy-treated patients (39), emphasizing the different modes of action of CTLA-4 and PD-1.

The rational of using CTLA-4 blockade in cancer therapy is to release the brake on pre-existing tumor-reactive T cells and to generate new T cell responses.

Ipilimumab (anti-CTLA-4) was the first immune checkpoint inhibitor that yielded a significant increase in survival of patients with metastatic melanoma, for which all conventional therapeutic options had failed (1). Interestingly, a broadening of the tumor-reactive T cell repertoire was reported upon ipilimumab treatment (40). In a second clinical study, ipilimumab was combined with dacarbazine in metastatic melanoma patients resulting in prolonged survival compared to dacarbazine alone (41). In both studies, a fraction of patients showed long-term durable responses (42). Similarly, clinical trials with anti-PD-1 have shown tumor regression in a substantial fraction of cancer patients (3). These initial results lead to an immense increase in clinical trials with drugs targeting the PD-1/PD-L1 axis in different cancer types, and many report anti-tumor efficacy (3–6, 43). Recent clinical observations show that the combination of anti-CTLA-4 and anti-PD-1 is more effective than either monotherapy (39). Although very successful and promising, a significant proportion of cancer patients do not show long-term benefit of immune checkpoint inhibitors. Therefore, it is of utmost importance to mechanistically understand intrinsic and acquired resistance to cancer immune checkpoint inhibitors, in order to identify biomarkers that can be used to pre-select those patients that will or will not benefit from cancer immunotherapy and to develop therapeutic strategies to overcome or bypass resistance mechanisms.

What are the Requirements for Therapeutic Response to Checkpoint Inhibitors?

To predict the response to immunotherapy per patient and tumor type, several variables should be taken into account. For successful activation of a T cell-mediated anti-tumor immune response, T cells need to "see" the cancer cells with their TCR. In general, there are three classes of tumor antigens that can potentially be recognized by T cells: viral antigens, self-antigens, and neo-antigens. Our T cell repertoire is basically built to recognize and respond to viral antigens because these antigens are perceived as foreign or non-self. However, only a subset of established human cancers expresses viral antigens. During the T cell maturation process, thymic selection eliminates maturing lymphocytes that display a high avidity for self-antigens. As a consequence, only low-avidity self-specific T cells can be found in the peripheral T cell repertoire, which may not be ideal for cancer immunotherapy. Non-synonymous somatic mutations can give rise to neo-antigens toward which no central T cell tolerance is present. Recently, neo-antigen-specific T cell responses have been reported in melanoma patients (44–46), indicating that these mutations can be recognized by T cells and induce tumor-specific T cell responses. In line with this, the number of predicted neo-antigens is linked with a metric for immune cytolytic activity based on gene expression in a large panel of cancer types (47). Thus, the extent of the mutational load of a certain tumor would serve – albeit at a low resolution – as a predictor of response to cancer immunotherapy. Indeed, a growing body of data supports this hypothesis (48). Whole-exome sequencing analyses revealed that melanoma and lung cancer – the two cancer types that show promising responses to immunotherapy – bear relatively high mutational loads compared to other types of cancer due to their exposure to DNA damaging insults like UV radiation and tobacco smoke, respectively (49). Recent studies uncovered that a high mutational load is associated with long-term clinical benefit to checkpoint inhibitors (8, 9). However, not all cancer patients with tumors bearing

a high mutational load respond to checkpoint inhibitors, and some patients bearing tumors with low mutational load do (8, 9). Together, these results suggest that the mutational load of tumors is correlated with response to immune checkpoint inhibitors, but it cannot solely be used to predict response.

A growing body of clinical observations suggests that the intratumoral presence of pre-existing T cells is required for clinical benefit of immunotherapy (50). PD-1 expression on tumor-infiltrating $CD8^+$ T cells has been suggested to identify the repertoire of clonally expanded tumor-reactive T cells (51). In addition, T cell infiltration correlates with PD-L1 expression in tumors and is associated with increased responsiveness to drugs targeting the PD-1/PD-L1 axis in melanoma patients (50, 52, 53). Expression of PD-L1 in tumors is one of the main characteristics pursued as a potential biomarker for response to PD-1/PD-L1 blockade. However, there are examples of tumors with high expression of PD-L1 that do not respond to PD-1 blockade, and PD-L1 negative tumors that do respond (53). Why certain tumors express PD-L1 and others do not remains to be elucidated.

Interestingly, expression of PD-L1 and responsiveness to immune checkpoint blockade is associated with genomic instability in different tumor types (54). Patients bearing mismatch-repair-deficient colorectal cancer (CRC) respond better to anti-PD-1 therapy than mismatch-repair-proficient CRC patients (54). In line with this, a microsatellite instable (MSI) subset of CRC patients shows high T cell influx (55). However, this is counterbalanced by simultaneous upregulation of checkpoint molecules including PD-1, PD-L1, and CTLA-4 leaving T cells dysfunctional (55). Moreover, in breast cancer, the expression of PD-L1 is correlated with TIL infiltration, and is mostly prevalent in basal-like, hormone-receptor-negative, and triple-negative tumors (56, 57). Furthermore, in glioma patients increased expression of PD-L1 in tumors was correlated with PTEN loss (58), suggesting that patients bearing genetically unstable cancer types might benefit from treatment with checkpoint inhibitors. Intriguingly, not only cancer cells, but also tumor-infiltrating myeloid cells express PD-L1, and counteract anti-tumor immunity in ovarian carcinoma and MSI-CRC (55, 59). Actually, PD-L1 expression on tumor-infiltrating immune cells has been suggested to be a better predictor of clinical response to anti-PD-L1 therapy than PD-L1 expression on cancer cells (52). It will be interesting to explore, which other cancer types are characterized by the influx of PD-L1-expressing myeloid cells.

In conclusion, to increase the efficacy of immunotherapy in different types of cancer, we could consider manipulating the many variables that determine intrinsic and acquired resistance. While altering cancer cell-intrinsic characteristics, such as mutational load or genomic instability, might be challenging, cancer cell-extrinsic characteristics, like an immunosuppressive TME, are easier to manipulate.

Evasion from Cancer Immunotherapy: Relieving Immunosuppression as an Attractive Strategy to Improve the Efficacy of Immune Checkpoint Blockade

Established tumors are characterized by an abundant influx of a variety of immune cells with immunosuppressive activity, including T_{regs}, myeloid-derived suppressor cells (MDSCs), and tumor-associated macrophages (TAMs) (Figures 1 and 2). There is accumulating evidence that interference with these immunosuppressive networks can improve anti-tumor immunity. Here, we discuss the different types of immunosuppressive immune cells present in the TME, and how blockade or reprograming of these cells or their downstream effects can enhance anti-tumor immunity and the efficacy of immune checkpoint blockade.

Regulatory T Cells

Regulatory T cells play an important role in maintaining homeostasis during infections and in preventing the development of autoimmune diseases by blocking proliferation and cytotoxic activity of effector T cells. The history of T_{regs} goes back to the 1970s, when it was discovered that a subpopulation of thymocytes induced tolerance to certain antigens in mice (60). A turning point in the research of these "suppressor cells" came in 1995. T_{regs}, phenotyped as $CD4^+CD25^+$ cells, were shown to be important for self-tolerance in mice, as inoculation of $CD4^+$ cells depleted of $CD4^+CD25^+$ cells resulted in autoimmunity in nude mice (61). Another big step forward in the characterization of T_{regs} was the identification of FOXP3, a member of the fork-head/winged-helix family of transcription factors and a key regulator of T_{reg} development and function (62). In the following years, the knowledge of T_{regs} expanded enormously. Two subpopulations of T_{regs} were identified: natural T_{regs} and induced T_{regs} (or adaptive T_{regs}), which are formed in the thymus and in the periphery, respectively. Regardless of their origin, both natural and induced T_{regs} inhibit effector T cells (63).

In 1980, it was hypothesized that a T cell population in tumors suppresses anti-tumor immune responses (64). Indeed, many experimental studies support the notion that tumor-associated T_{regs} contribute to immune escape via suppression of anti-tumor $CD8^+$ T cells. For example, elimination of T_{regs} in MO4 melanoma cell line-bearing mice results in T cell-dependent tumor rejection (65). Moreover, in a xenotransplant model for $HER2^+$ ovarian cancer, adoptive transfer of autologous $CD3^+CD25^-$ T cells and DCs loaded with $HER2^+$ antigen results in T cell-mediated tumor regression, whereas concomitant transfer of T_{regs} blocks this antigen-specific immune response (66). T_{regs} not only suppress $CD8^+$ T cells, but also $CD4^+$ T cells, NK, NKT, and B cells (67). T_{regs} exert their immunosuppressive function either by direct suppression of effector cells, or indirectly by affecting the activation state of APCs. Importantly, in order to exert their functions, T_{regs} need to be activated via their TCR, but once activated their suppressive function is non-specific (68, 69). The direct T cell-suppressive functions are mediated by release of cytokines, serine proteases and the expression of enzymes that catabolize ATP. For example, T_{regs} inhibit T cells via secretion of cytokines like TGFβ, IL10, and IL35 (70–72) or even induce T cell apoptosis by the release of granzyme B (GRZMB) or perforin (73–75). In addition, T_{regs}

express CD39 and CD73, two ectoenzymes that generate the immunosuppressive molecule adenosine from extracellular ATP (76). It has been shown that T_{regs} from CD39 knock-out mice fail to inhibit $CD4^+CD25^-$ cell proliferation (76). Finally, $CTLA\text{-}4^+$ T_{regs} can indirectly impair T cells by reducing the CD80/CD86 levels on APCs (36).

Supporting these data, increased numbers of intratumoral T_{regs} correlate with worse overall survival in patients with ovarian cancer, breast cancer, gastric cancer, and hepatocellular carcinoma (66, 77–81). Interestingly, this is not true for CRC in which a high number of $CD8^+$ cells and $FOXP3^+$ cells correlates with a good prognosis (82). This may be explained by the fact that T_{regs} in CRC attenuate inflammation against gut microbiota that would otherwise enhance tumor growth (82). These findings illustrate that the tumor context dictates the function of associated immune cells. Although strategies targeting CD25 (like the neutralizing monoclonal antibody daclizumab and the recombinant interleukin 2/diphtheria toxin conjugate Ontak) showed transient depletion of peripheral T_{regs} and increased activity of $CD8^+$ T cells, these approaches only result in a modest clinical benefit in cancer patients (83, 84). This might be explained by the fact that CD25 is also expressed on active effector T cells, so the lack of specificity for T_{regs} might complicate their clinical applicability. Therefore, a mechanistic understanding of the role of T_{regs} in different tumor contexts will be important for the design of therapeutic strategies aimed at suppressing the downstream effects of T_{regs}.

Myeloid-Derived Suppressor Cells

The first report describing the existence of MDSCs showed that bone marrow-derived cells were able to suppress the killing activity of splenocytes *in vitro* (85). These cells were called “natural suppressor cells” or “null cells” because they did not express markers of B, T, or NK cells or macrophages (86). Subsequently, these cells were found to expand in inflammatory conditions and in tumor-bearing hosts (85, 87). In tumor-bearing mice, tumor-derived growth factors trigger the accumulation of T cell suppressive myeloid cells in the bone marrow and spleen (87, 88). The identification of these cells was hampered by the lack of clear markers, which caused variation in terminology and ambiguity among researchers. In order to bring some clarity into the field, Gabrilovich and colleagues published a consensus paper in 2007 in which they coined the term “MDSC” to refer to a heterogeneous population of myeloid cells with the ability to suppress T cell activity (89). MDSCs consist of a group of immature and mature myeloid cells that are defined by their immunosuppressive function. Within the MDSC population, two subpopulations can be distinguished based on the expression of Ly6G and Ly6C: $Ly6C^{high}Ly6G^-$ monocytic-MDSC and $Ly6C^{low}Ly6G^+$ granulocytic-MDSC. In humans, MDSCs are defined as $CD11b^+CD33^+HLA\text{-}DR^-Lin^-$ cells with the addition of CD14 or CD15 to discriminate between monocytic- or granulocytic-MDSCs, respectively (90).

In patients with various cancer types, including melanoma, gastric, breast, and CRC, increased numbers of MDSCs in the circulation correlate with poor survival (91–93). Numerous cytokines have been implicated in the expansion of MDSCs during cancer progression, including G-CSF, GM-CSF, and stem-cell factor (SCF or KIT ligand) (94–96).

Myeloid-derived suppressor cells exert their immunosuppressive function by different mechanisms, one of which is the consumption of essential amino acids from the environment. MDSCs frequently express high levels of arginase I, which catabolizes arginine, thereby depriving T cells from arginine, which is essential for their metabolism and function (97, 98). L-Arginine is also the substrate of another enzyme highly expressed in MDSCs, called iNOS. The release of reactive oxygen species (ROS) and nitric oxide (NO) by iNOS can lead to the inhibition of MHC class II expression on APCs causing impaired antigen presentation to $CD4^+$ T cells (99). Moreover, NO can cause apoptosis of $CD8^+$ T cells (100). Another amino acid is tryptophan, whose breakdown by the enzyme IDO suppresses T cell proliferation. MDSCs isolated from human breast cancer tissues inhibit T cell proliferation and induce T cell apoptosis in an IDO-dependent manner (101). Moreover, IDO inhibitors enhance the therapeutic efficacy of anti-CTLA-4 treatment leading to intratumoral accumulation of T cells and improved survival in the B16 melanoma model (102). Additionally, the amino acid cysteine is also important for T cell activation and function. T cells depend on other cells (macrophages and DCs) for cysteine metabolism. MDSCs internalize cystine (formed of two cysteines linked via a disulfide bond), catabolize it to cysteine and, unlike macrophages and DCs, do not release it into the environment. Therefore, MDSCs limit the amount of cystine that macrophages and DCs can metabolize to activate T cells (103). Finally, MDSCs contribute to an immunosuppressive TME by inducing the development of T_{regs} in tumor-bearing mice, as adoptive transfer of MDSCs and $CD4^+$ T cells in MCA26 colon carcinoma cell line-bearing irradiated mice, induces expression of FOXP3 in transferred T cells (104). Thus, these data suggest that MDSCs play an important role in creating an immunosuppressive network in tumors, supporting the idea that reprograming or depletion of MDSCs could benefit immunotherapy strategies. Strategies to inhibit MDSCs include blocking their development or recruitment, targeting their immunosuppressive molecules or depleting them.

Tumor-Induced Neutrophils

In various cancer patients, a high neutrophil to T lymphocyte ratio in blood is associated with poor disease outcome (105, 106). Recent studies have reported that neutrophils also expand in experimental mouse tumor models, and that they exert immunosuppressive activity. A distinguishing feature of murine neutrophils is the expression of Ly6G, a surface marker shared with granulocytic-MDSC. When the T cell suppressive ability of neutrophils is confirmed, they can be categorized into the granulocytic-MDSC population (107). We recently showed in a mouse model for *de novo* breast cancer metastasis that neutrophils have a pro-metastatic phenotype and exert their function through suppression of $CD8^+$ T cells. While depletion of $Ly6G^+$ neutrophils results in decreased multi-organ metastasis, double depletion of neutrophils and $CD8^+$ T cells reverses this phenotype (108). In line with this, chemotherapy-induced neutropenia correlates with improved overall survival in breast cancer patients (109). The metastasis-promoting role of neutrophils has also been demonstrated in UV-induced melanoma and in tumor inoculation models (110, 111). It would be interesting to study whether – as in the experimental tumor models – T cells in neutropenic cancer patients are more active. Interestingly, in 4T1-tumor-bearing mice, neutrophils inhibit the seeding of metastatic cells in the

lung by the release of hydrogen peroxide (112). These data indicate a controversial role of neutrophils in metastasis that might be explained by the differences in tumor subtype or tumor model.

We and others have shown that T cell-suppressive neutrophils accumulate systemically during cancer progression in a G-CSF-dependent fashion (108, 113). In the transgenic *MMTV-PyMT* mammary tumor mouse model, tumor-derived G-CSF skews hematopoietic cell differentiation toward the granulocytic lineage in the bone marrow, resulting in increased numbers of immunosuppressive neutrophils in the circulation (113). In 4T1 mammary tumor-bearing mice, TGFβ polarizes mature neutrophils from cytotoxic anti-tumor activity toward pro-tumor immature immunosuppressive neutrophils (114). This is in line with previous findings identifying TGFβ as one of the drivers of pro-tumor polarized neutrophils (115). As such, it is tempting to speculate that for those tumors characterized by pro-metastatic neutrophils, inhibition of these cells – either by targeting upstream or downstream molecules – may be an interesting strategy for therapeutic intervention, in particular when combined with cancer immunotherapy.

Tumor-Associated Macrophages

Macrophages are frequently the most predominant immune cell type in tumors. In the past, macrophages were subdivided into classically activated macrophages (M1) exerting microbicidal and anti-tumor activity, or alternatively activated macrophages (M2) exerting pro-tumoral, immunosuppressive, and tissue repair functions (116, 117). TAMs are frequently classified as M2 macrophages. However, there is a growing realization that this black and white distinction of macrophage subsets is too simplistic and does not accurately reflect the heterogeneity, plasticity, and versatility of macrophages (118). Transcriptome and bioinformatic analyses of cultured macrophages exposed to different stimuli revealed a spectrum of activation programs for each stimulus that goes beyond the M1 and M2 model (119). Based on these data, it is to be expected that TAMs will also change their phenotype and function according to the cytokine milieu present in a specific tumor type. In the vast majority of cancers, high intratumoral macrophage density correlates with poor prognosis (120, 121). However, macrophages in CRC are associated with good prognosis, and in other types of cancers, like prostate and lung cancer, their role is still controversial (122). Depletion of macrophages by genetic ablation of CSF-1 in the *MMTV-PyMT* mammary tumor model reduces metastasis formation without affecting primary tumor growth (123). Likewise, several other experimental studies have reported a pro-metastatic role of macrophages (124, 125). TAMs produce a variety of factors that foster tumor growth and invasiveness, angiogenesis, and immunosuppression (120, 124, 126).

Tumor-associated macrophages exert their immunosuppressive activity in a similar fashion as that of MDSCs. TAMs can express various enzymes like arginase 1, IDO (127–129), and cytokines like IL10 (130). Another mechanism by which TAMs suppress T cells is the upregulation of PD-L1. In hepatocellular carcinoma, high density of peritumoral macrophages that express PD-L1 correlates with worse overall survival (131). Co-culture experiments showed that PD-L1^{+} macrophages suppress T cell activity unless anti-PD-L1 antibody is added in the culture (131).

Based on these immunosuppressive properties, it is tempting to speculate that interference with TAMs will unleash anti-tumor immunity. Indeed, this idea has recently been supported by experimental studies in mouse models for glioblastoma and pancreatic cancer showing that CSF-1/CSF-1R pathway blockade can shift TAM polarization toward an anti-tumor phenotype, resulting in enhanced $CD8^+$ T cell-mediated anti-tumor immunity (132, 133). Similarly, targeting the CCL2/CCR2 chemokine pathway – involved in recruitment of monocytes and macrophages – relieves the immunosuppressive phenotype of TAMs and enhances anti-tumor $CD8^+$ T cell responses (134, 135). Based on these encouraging results, clinical trials are ongoing in which compounds targeting TAMs are being tested in cancer patients. Preliminary results of a clinical trial with anti-CSF-1R in patients with various types of solid malignancies showed a decrease in TAMs and an increase in intratumoral CD8/CD4 ratio (10).

Blocking the Suppressors to Release Anti-Tumor T Cells

As discussed above, many immunosuppressive cells and mediators can be identified in the TME that dampen anti-tumor T cell responses and may contribute to immune escape upon cancer immunotherapy. The combination of compounds that relieve immunosuppression with T cell-boosting therapy seems attractive to overcome immune tolerance toward the tumor.

Regulatory T cells seem to be interesting targets, since, as discussed earlier in this review, these cells suppress the functionality of $CD4^+$ and $CD8^+$ effector cells. In line with this, in the transgenic TRAMP prostate cancer model – engineered to express prostate-specific antigen (PSA) – T_{reg}-depletion enhances IFNγ production by PSA-specific $CD8^+$ T cells (136). This augmented effect of anti-tumor immunity is further enhanced by CTLA-4 blockade, and results in delayed tumor growth. Interestingly, the same experiments performed in the parental TRAMP model show only a modest activation of PSA-specific T cells upon anti-CD25 and anti-CTLA-4, and no survival benefit, suggesting the requirement of a tumor-specific antigen for this anti-tumor response (136). In the ID8 ovarian cancer model, tumor-infiltrating T_{regs} – which express both CTLA-4 and PD-1 – are reduced upon CTLA-4 and PD-1 dual blockade coinciding with increased tumor-infiltrating $CD8^+$ T cells (137). However, additional depletion of T_{regs} does not further enhance this effect. In the same model, blockade of PD-L1, expressed on tumor cells and tumor-infiltrating immune cells, reduces the number of MDSCs and T_{regs} and enhances the frequency of effector T cells, resulting in prolonged survival (138). Furthermore, in a mouse model for rhabdomyosarcoma, PD-1 blockade increases the number of tumor-infiltrating $CD8^+$ T cells, but does not change their activation status. Upon interference with the chemokine receptor CXCR2, which prevents MDSC trafficking into the tumor, enhanced activation of $CD8^+$ T cells is observed (139). Blockade of CXCR2 improves the therapeutic efficacy of anti-PD-1 treatment resulting in a significant survival benefit (139). Moreover, in a mouse model of pancreatic ductal adenocarcinoma, blockade of CSF-1/CSF-1R signaling results in macrophage reprograming to support anti-tumor immune function and modestly delays tumor growth (133). TAMs obtained from anti-CSF1 treated mice are impaired in suppressing $CD8^+$ T cell proliferation compared to control TAMs. The induction of CTLA-4 expression on $CD8^+$ T cells and PD-L1

expression on tumor cells suggests the onset of acquired resistance to effective anti-tumor immune responses. Combining anti-CTLA-4 and anti-PD-1 with a CSF-1R inhibitor shows profound synergy with a significant reduction in tumor burden (133). Thus, together these results indicate that alleviation of immunosuppression reactivates anti-tumor immunity, which can be further enhanced by checkpoint inhibition.

Immunomodulatory Properties of Chemotherapeutic Drugs

Although various novel compounds targeting tumor-associated myeloid cells and their immunosuppressive mediators are being developed and tested, their clinical availability is still limited. An alternative and clinically available strategy is to relieve immunosuppression by exploiting the immunomodulatory effects of conventional anti-cancer strategies like chemotherapy (Figure 2). The impact of chemotherapeutic drugs on the proportion and phenotypic and functional characteristics of immune cells is to a great extent dictated by the type of drug and the dosing scheme: while high-dose chemotherapy usually results in lympho- or myelodepletion, low-dose (metronomic) treatment has more subtle anti-angiogenic and immunomodulatory effects (140, 141). In this section, we discuss the effects of chemotherapy on the immunosuppressive TME.

The Impact of Chemotherapy on T Cell Priming

Optimal T cell priming is dependent on antigen processing, presentation, and co-stimulation by properly matured and activated DCs. As discussed, impaired DC function and T cell priming are important mechanisms of immune escape by tumors. Certain chemotherapeutics induce anti-cancer immune responses by improving the recruitment and functionality of intratumoral DCs (142, 143). For example, low-dose cyclophosphamide promotes DC maturation (144). Besides the enhanced release of tumor antigens through induction of cancer cell death, chemotherapeutics, including oxaliplatin, doxorubicin, mitoxantrone, and melphalan, induce HMGB1 release and calreticulin translocation in cancer cells, facilitating antigen uptake by DCs and subsequent T cell stimulation (145–147). In addition, in the MCA205 fibrosarcoma model, anthracyclins induce the differentiation of myeloid cells in the tumor bed toward a DC-like phenotype in an ATP-dependent manner (142). In these relatively high immunogenic tumor models, the activated T cells subsequently enhance the anti-cancer efficacy of chemotherapy (142, 143, 145).

In less immunogenic models, such as *de novo* tumorigenesis models, an important role for T cells in chemotherapy efficacy is lacking (120, 148, 149). One possible explanation is that spontaneously arising tumors are characterized by local and systemic immunosuppression, which may overrule any chemotherapy-induced T cell responses. Indeed, in the *MMTV-PyMT* mammary tumor model, TAM-derived IL10 indirectly blocks anti-tumor $CD8^+$ T cell activity by suppressing IL12 expression by intratumoral DCs upon paclitaxel treatment (149). These results apply to human breast cancer patients since low $CD68^+$ macrophage over $CD8^+$ T cell ratio prior to neo-adjuvant chemotherapy correlates with a better pathologic response (120). Moreover, high levels of *IL12A* mRNA in human breast cancer samples correlates

with expression of DC-related transcription factors and *GRZMB*, *CD8A*, and *IFN*γ expression, suggesting an active anti-tumor T cell response (149). However, the role of TAMs and their potential suppressive function in cancer patients was not evaluated. Together, these results suggest that therapeutic targeting of TAMs could enhance the functionality of intratumoral DCs and anti-tumor T cell responses in chemotherapy treatment.

Impact of Chemotherapy on T_{regs}

With the knowledge that T_{regs} play an important role in suppressing effector T cell responses, a lot of effort has been put into the identification of chemotherapeutic drugs that target these cells. The best studied is cyclophosphamide, an alkylating agent, which crosslinks DNA, thus interfering with replication. Cyclophosphamide is known for its dose-dependent effect on the immune system. High doses of cyclophosphamide result in immunosuppression by reducing T cell proliferation and inducing apoptosis, thus making it useful for the prevention of graft-versus-host disease or rejection of transplanted organs (150, 151). In contrast, low doses selectively ablate T_{regs} and dampen their T cell suppressive ability (152). While the anti-tumor effect of high-dose cyclophosphamide is mainly due to its cytotoxic activity against cancer cells, the anti-tumor effect of low-dose cyclophosphamide depends on its immune-modulatory effects (153). Indeed, studies in T cell-deficient mice bearing inoculated tumors show loss of the anti-cancer activity of low-dose cyclophosphamide (153, 154). Moreover, reinfusion of $CD4^+CD25^+$ T cells in tumor-bearing mice, pre-treated with low-dose cyclophosphamide, abrogated the anti-tumor effect of the drug, emphasizing that T_{regs} counteract the therapeutic efficacy of the drug (153). In line with this, patients with different types of metastasized solid tumors receiving low-dose metronomic cyclophosphamide show a specific decrease of T_{regs} in the periphery with concomitant enhancement of NK lytic activity and T cell proliferation (155). In cancer patients receiving higher doses of metronomic cyclophosphamide, all lymphocyte populations were depleted, emphasizing the importance of accurate drug dosing to achieve selective T_{reg} depletion (155). It has been proposed that the increased sensitivity of T_{regs} for cyclophosphamide is linked to their low ATP levels. Low levels of ATP result in decreased synthesis of glutathione, which is important for cyclophosphamide detoxification (156).

Another chemotherapeutic drug affecting T_{regs} is gemcitabine, a nucleoside analog interfering with DNA replication. In an orthotopic pancreatic cancer model, gemcitabine reduces the percentage of T_{regs} in the tumor resulting in a small but significant survival benefit (157). Whether this also results in improved $CD8^+$ and $CD4^+$ T cell activity remains unknown. A study performed in cancer patients showed that the percentage of T_{regs} in blood was decreased after gemcitabine treatment (158). Among the $CD4^+$ cells, T_{regs} were identified as the most proliferative cells, which may explain the selectivity of gemcitabine for these cells. However, the effect of gemcitabine on other T cell populations was not assessed in this study (158). Also, other (combinations of) chemotherapy drugs have been reported to influence the presence or function of T_{regs} (159, 160).

Chemotherapeutics with Inhibitory Activity toward Tumor-Associated Myeloid Cells

Several chemotherapy drugs have been implicated in the selective reduction of MDSCs in the tumor and spleen of tumor-bearing mice (161, 162). In an EL4 inoculation tumor model, a set of chemotherapy drugs was tested for their influence on the number of splenic and intratumoral MDSCs (161). This study showed that high-dose gemcitabine and 5-fluorouracil (5-FU), two anti-metabolite drugs that interfere with DNA replication, reduce MDSC accumulation (161). Consequently, 5-FU-mediated MDSC depletion results in increased IFNγ-producing intratumoral $CD8^+$ T cells. This effect is reverted by adoptive transfer of MDSCs, suggesting that the effect of 5-FU is exerted through MDSCs (161). Similar results were obtained in the MCA203 cell line inoculation sarcoma model combined with cytotoxic T cell transfer (163), highlighting the critical role of MDSCs in dampening T cell activity upon 5-FU treatment. While the exact mechanisms underlying the selectivity of 5-FU for MDSCs are unknown, it has been proposed that 5-FU inhibits the enzyme thymidylate synthase and that the resistance to 5-FU is due to insufficient inhibition of this enzyme (164). Indeed, low levels of thymidylate synthase are found in MDSCs compared to splenocytes and EL4 tumor cells, suggesting that 5-FU selectivity for MDSCs could be due to this low enzymatic expression (161).

High-dose gemcitabine induces similar effects on MDSCs as 5-FU (162). *In vitro* analyses of splenocytes from TC-1 lung cancer-bearing mice showed the cytotoxic specificity of gemcitabine for MDSCs, while $CD4^+$, $CD8^+$ T cells, and B cells are unaffected (162). Although the exact mechanism underlying this specificity has not been identified, it has been hypothesized that gemcitabine induces apoptosis in MDSCs (162). Yet, a thorough mechanistic analysis of gemcitabine-induced apoptotic cell death in various immune cell populations has not been performed. In the 4T1 breast cancer mouse model, gemcitabine treatment also reduces splenic MDSC accumulation, which results in increased proliferation and IFNγ production by splenic lymphocytes upon antigen stimulation compared to untreated mice (165). However, no difference in anti-cancer efficacy of gemcitabine was observed between immunocompetent and nude mice, indicating a T cell-independent mechanism of 4T1 tumor control by gemcitabine (165). Perhaps, this observation might be explained by the presence of other immunosuppressive cells in the TME, like T_{regs} or macrophages.

The beneficial effect of chemotherapeutic drugs on the immunosuppressive TME is not only a direct result of reduced MDSC numbers, but also a result of a more favorable phenotype of the remaining MDSCs. For example, in the 4T1-Neu mammary tumor model, docetaxel reduces splenic granulocytic-MDSCs and enhances $CD8^+$ and $CD4^+$ cytotoxic activity (166). The remaining MDSCs exhibit a different phenotypic profile compared to MDSCs from untreated mice. In line with these *in vivo* findings, MDSCs pre-treated with docetaxel induce the proliferation of OVA-exposed OT-II $CD4^+$ T cells compared to untreated MDSCs *in vitro*, suggesting that docetaxel treatment induces a phenotypical switch to a more favorable state (166). Likewise, doxorubicin selectively decreases the proportion of MDSCs in the 4T1 breast tumor model via apoptosis and subdues the immunosuppressive

phenotype of the remaining MDSCs. The remaining MDSCs have a lower expression of immunosuppressive molecules like ROS, ARG-1, and IDO (167). This less suppressive environment caused by doxorubicin enhanced the activity of adoptively transferred T helper cells (167). Interestingly, some subpopulations of MDSCs may be more susceptible to chemotherapy than others. Whether chemotherapy selectively depletes pro-tumorigenic MDSCs or skews them toward an anti-tumor phenotype is unknown. Future studies using lineage tracing methodologies would provide more insight into this topic.

Besides the favorable immunomodulatory "off-target" effects of various chemotherapeutic drugs, these drugs can at the same time exert less desirable functions. For instance, in addition to its inhibitory effect on T_{regs}, cyclophosphamide increases the number of $CD11b^{+}Gr1^{+}$ MDSCs. In a transgenic mouse model for melanoma, a single injection of low-dose cyclophosphamide increases the accumulation of MDSCs in the tumor and spleen, stimulates their immunosuppressive ability by inducing NO and ROS production, and reduces splenocyte proliferation (168). In line with these findings, MDSCs accumulate in the blood of breast cancer patients after treatment with doxorubicin or cyclophosphamide (169). This may be due to IFNγ release by $CD4^{+}$ and $CD8^{+}$ T cells that promotes survival of MDSCs (170). Based on these data, a combination of cyclophosphamide and cancer immunotherapy might not work; however, additional studies in other tumor models should be performed to test this.

Another study underscoring the complex impact of chemotherapy on myeloid cells shows that in EL4-tumor-bearing mice 5-FU induces IL1β secretion in MDSCs in an Nlrp3 inflammasome-dependent manner (171). Using depletion experiments and knock-out mice, it was shown that the MDSC-derived IL1β triggers IL17 production by $CD4^{+}$ T cells, which limits the anti-cancer efficacy of 5-FU (171). These data highlight that the effect of certain chemotherapy drugs is not simply limited to depletion of immunosuppressive cells but these drugs also change the functionality of cells that may impair their efficacy. These results suggest that the combination of chemotherapeutic and immunomodulatory compounds must be chosen carefully to increase their anti-cancer efficacy (172).

While several chemotherapy drugs have been reported to target MDSCs, thus far only one drug seems to strongly affect TAMs. Trabectedin, a drug that binds DNA and affects transcription and DNA repair pathways, depletes macrophages, and suppresses the differentiation of monocytes in the tumor bed in the transplantable MN/MCA1 fibrosarcoma tumor model through a TRAIL-dependent mechanism (173). Importantly, this macrophage selectivity is also observed in sarcoma patients after trabectedin neo-adjuvant treatment (173). It would be interesting to assess whether the anti-cancer activity of trabectedin is $CD8^{+}$ T cell mediated. The macrophage-depleting effect of trabectedin makes it an interesting candidate for combination strategies with immunotherapy.

As discussed before, many studies illustrate the complexity of immunomodulation by conventional chemotherapeutics, which is highly context-dependent. The differential effect on specific immune cells of different types of chemotherapeutics

is to a large extent dependent on the timing and dosing schedule. While high-dose chemotherapy often depletes immune cell subsets, low-dose metronomic chemotherapy exerts a more subtle anti-angiogenic and immunomodulatory mode of action (140, 141). It will be interesting to perform a side-by-side comparison of various types of chemotherapies administered at high versus low (metronomic) dose and evaluate their immunomodulatory effects, followed by more mechanistic studies. Ideally, these types of experiments would be performed in clinically relevant mouse models that faithfully recapitulate human cancer (Box 1) to facilitate clinical translation.

Box 1. Experimental mouse models to study the anti-tumor immune response.
Understanding the complex crosstalk between innate and adaptive immune cells and (disseminated) cancer cells requires the use of preclinical mouse models that faithfully recapitulate human cancer. The most widely used experimental mouse models are carcinogen-induced cancer models and cell line inoculation models. The latter is based on inoculation of large numbers of (genetically modified) homogenous cancer cells grown in 2D conditions. Implantation of these cells often results in massive cell death, thereby priming an effective anti-tumor immune response. Shaping of the tumor immune microenvironment during cancer progression in these models can hardly take place in the short amount of time that it takes for transplanted tumors to grow to their maximum tolerated size. Of notice, when implanting human cancer cells, either patient-derived tumor material or established human cancer cell lines, immunocompromised mice are used, thereby excluding the important role of the adaptive immune system.

While cell line inoculation models proved useful to decipher some aspects of the anti-tumor immune response, we should keep in mind that these models do not reflect physiological processes as they occur in human patients. Genetically engineered mouse (GEM) models, which develop *de novo* cancers, generally mimic human cancer genetically – because of the introduction of specific driver mutations – and histopathologically (180). In addition, tumor progression occurs in a multi-step nature in their natural microenvironment shaping the local immune responses (Figure 1), therefore mimicking the human setting. In contrast to inoculation models expressing known tumor antigens, the anti-tumor immune response in GEM models can be considered a black box. Due to their cellular and genetic heterogeneity, GEM models induce a variety of T cell responses directed against multiple unknown tumor neo-antigens, which faithfully reflects human cancer. Interestingly, comparative studies have shown that inoculation models greatly differ from GEM models in terms of response to anti-cancer therapies and endogenous T cell responses (181, 182). The advantages and disadvantages of different experimental mouse models in studying responsiveness to anti-cancer therapy have been recently discussed (14, 183).

Future Perspectives: Exploiting the Immunomodulatory Properties of Chemotherapeutic Drugs to Improve Cancer Immunotherapy

Given their immunomodulatory properties, conventional chemotherapy drugs are interesting candidates to combine with T cell-boosting immunotherapy – a concept termed chemo-immunotherapy (174). Clinical trials report enhanced anti-tumor T cell responses in cancer patients treated with chemotherapy in combination with cancer vaccines (13). Moreover, clinical testing of chemotherapy combined with other immunotherapy approaches like adoptive transfer of (genetically engineered) autologous T cells or toll-like receptor (TLR) agonists are likely to be explored in

the near future. Indeed, various experimental studies support the concept that chemotherapy-induced relief of immunosuppression could improve cancer immunotherapy. In a passive immunotherapy setting, in the MC203 fibrosarcoma and TC-1 lung cancer cell line inoculation models, low-dose gemcitabine and 5-FU reduced the splenic population of $CD11b^+Gr1^+$ MDSCs, resulting in enhanced anti-tumor activity of adoptively transferred tumor-specific CTL (163).

The results obtained in preclinical models combining chemotherapeutics with immune checkpoint inhibitors are promising. The immunomodulatory effects of melphalan – administered in a subtherapeutic dose – synergizes with CTLA-4 blockade in a plasmacytoma model (175). *In vitro* assays revealed that splenocytes obtained from melphalan-treated mice co-cultured with anti-CTLA-4 induced tumor cell cytotoxicity, while splenocytes from non-treated mice – irrespective of CTLA-4 blockade – did not (175). Furthermore, in the poorly immunogenic AB-1 malignant mesothelioma and Lewis lung cancer (LLC) inoculation tumor models, a combination therapy of gemcitabine and CTLA-4 blockade synergizes, inducing potent anti-tumor immune responses and subsequent regression of tumors in a CD4- and CD8-dependent manner (176). In addition, in a subcutaneous murine mesothelioma model, synergy is observed between cisplatin and CTLA-4 blockade, resulting in a profound anti-tumor effect that is characterized by increased influx and activation of $CD4^+$ and $CD8^+$ T cells in the tumor (177). Moreover, preclinical studies in mice show that doxorubicin, cisplatin, and paclitaxel in addition to their immunomodulatory role, can sensitize tumor cells for CTL attack in a direct manner (178). Here, chemotherapy causes increased permeability of tumor cell membranes to GRZMB, which sensitizes cancer cells to the cytotoxic effects of T cells and improved different cancer immunotherapy strategies (178). Together, these preclinical studies – albeit limited numbers – show the potential to exploit immunomodulatory chemotherapeutic drugs to improve the efficacy of checkpoint blockade.

Clinical trials that evaluate the combination of chemotherapeutic drugs and checkpoint inhibitors in cancer patients are still limited. Some studies in melanoma and lung cancer have used chemotherapeutics in combination with checkpoint blockade resulting in improved survival compared to chemotherapy alone (41, 179). However, the rational of these studies was not to evaluate the effect of treatment on the immunosuppressive microenvironment. Moreover, the design of clinical trials makes it impossible to perform a structural comparison in patients to study the effect of the immunosuppressive microenvironment on immunotherapy efficacy and whether this efficacy can be enhanced by adding chemotherapeutics to the treatment regimen. Therefore, we need to rely on preclinical research in mouse tumor models that faithfully recapitulate human cancer in terms of the genetic composition, anti-tumor immunity, and the immunosuppressive TME (Box 1). Results obtained in mouse models that mimic human cancer might shape the design of clinical trials and guide toward interesting treatment strategies. There are still various important questions that need to be addressed to maximally exploit the therapeutic efficacy of chemotherapy and immunotherapy combinations, like the determination of the most optimal combinations. Based on preclinical findings,

different cancer types will likely require different combinations of therapy. In addition, despite the devastating effects of metastatic disease, mechanistic insights into the site-specific therapeutic response profiles and resistance mechanisms of cancer immunotherapy are completely lacking. Moreover, it is critical to gain insights into the mechanisms underlying intrinsic and acquired resistance to cancer immunotherapy. To answer these questions within the next decade, it is critical that basic researchers and clinicians intensify their efforts to join forces, so that results from preclinical research can guide the design of clinical trials, and the results from clinical trials, in turn, can guide mechanistic studies in mouse models. Together, these efforts will improve treatment strategies using chemotherapeutics to alleviate immunosuppression and enhance cancer immunotherapy.

Author Contributions

KK, CS, and KV reviewed relevant literature and drafted the manuscript. KV revised the manuscript and supervised KK and CS. All authors read and approved the final manuscript.

Conflict of Interest Statement

The authors declare that the research was conducted in the absence of any commercial or financial relationships that could be construed as a potential conflict of interest.

Acknowledgments

We thank Seth Coffelt for insightful comments on the manuscript. Work in the lab is supported by grants from the European Union (FP7 MCA-ITN 317445 TIMCC), the European Research Council (ERC consolidator award INFLAMET 615300), the Beug Foundation for Metastasis Research, the Dutch Cancer Society (2011-5004), and the Netherlands Organization for Scientific Research (NWO VIDI 917.96.307).

References

1. Hodi FS, O'Day SJ, McDermott DF, Weber RW, Sosman JA, Haanen JB, et al. Improved survival with ipilimumab in patients with metastatic melanoma. *N Engl J Med* (2010) **363**(8):711–23. doi:10.1056/NEJMoa1003466
2. Powles T, Eder JP, Fine GD, Braiteh FS, Loriot Y, Cruz C, et al. MPDL3280A (anti-PD-L1) treatment leads to clinical activity in metastatic bladder cancer. *Nature* (2014) **515**(7528):558–62. doi:10.1038/nature13904
3. Topalian SL, Hodi FS, Brahmer JR, Gettinger SN, Smith DC, McDermott DF, et al. Safety, activity, and immune correlates of anti-PD-1 antibody in cancer. *N Engl J Med* (2012) **366**(26):2443–54. doi:10.1056/NEJMoa1200690
4. Wolchok JD, Kluger H, Callahan MK, Postow MA, Rizvi NA, Lesokhin AM, et al. Nivolumab plus ipilimumab in advanced melanoma. *N Engl J Med* (2013) **369**(2):122–33. doi:10.1056/NEJMoa1302369
5. Ansell SM, Lesokhin AM, Borrello I, Halwani A, Scott EC, Gutierrez M, et al. PD-1 blockade with nivolumab in relapsed or refractory Hodgkin's lymphoma. *N Engl J Med* (2015) **372**(4):311–9. doi:10.1056/NEJMoa1411087
6. Motzer RJ, Rini BI, McDermott DF, Redman BG, Kuzel TM, Harrison MR, et al. Nivolumab for metastatic renal cell carcinoma: results of a randomized phase II trial. *J Clin Oncol* (2015) **33**(13):1430–7. doi:10.1200/JCO.2014.59.0703
7. Couzin-Frankel J. Cancer immunotherapy. *Science* (2013) **342**(6165):1432–3. doi:10.1126/science.342.6165.1432
8. Snyder A, Makarov V, Merghoub T, Yuan J, Zaretsky JM, Desrichard A, et al. Genetic basis for clinical response to CTLA-4 blockade in melanoma. *N Engl J Med* (2014) **371**(23):2189–99. doi:10.1056/NEJMoa1406498
9. Rizvi NA, Hellmann MD, Snyder A, Kvistborg P, Makarov V, Havel JJ, et al. Cancer immunology. Mutational landscape determines sensitivity to PD-1 blockade in non-small cell lung cancer. *Science* (2015) **348**(6230):124–8. doi:10.1126/science.aaa1348
10. Ries CH, Cannarile MA, Hoves S, Benz J, Wartha K, Runza V, et al. Targeting tumor-associated macrophages with anti-CSF-1R antibody reveals a strategy for cancer therapy. *Cancer Cell* (2014) **25**(6):846–59. doi:10.1016/j.ccr.2014.05.016
11. Vanneman M, Dranoff G. Combining immunotherapy and targeted therapies in cancer treatment. *Nat Rev Cancer* (2012) **12**(4):237–51. doi:10.1038/nrc3237
12. Verbrugge I, Hagekyriakou J, Sharp LL, Galli M, West A, McLaughlin NM, et al. Radiotherapy increases the permissiveness of established mammary tumors to rejection by immunomodulatory antibodies. *Cancer Res* (2012) **72**(13):3163–74. doi:10.1158/0008-5472.CAN-12-0210
13. Chen G, Emens LA. Chemoimmunotherapy: reengineering tumor immunity. *Cancer Immunol Immunother* (2013) **62**(2):203–16. doi:10.1007/s00262-012-1388-0
14. Coffelt SB, de Visser KE. Immune-mediated mechanisms influencing the efficacy of anticancer therapies. *Trends Immunol* (2015) **36**(4):198–216. doi:10.1016/j.it.2015.02.006
15. Wargo JA, Reuben A, Cooper ZA, Oh KS, Sullivan RJ. Immune effects of chemotherapy, radiation, and targeted therapy and opportunities for combination with immunotherapy. *Semin Oncol* (2015) **42**(4):601–16. doi:10.1053/j.seminoncol.2015.05.007
16. DeNardo DG, Coussens LM. Inflammation and breast cancer. Balancing immune response: crosstalk between adaptive and innate immune cells during breast cancer progression. *Breast Cancer Res* (2007) **9**(4):212. doi:10.1186/bcr1746
17. Hanahan D, Coussens LM. Accessories to the crime: functions of cells recruited to the tumor microenvironment. *Cancer Cell* (2012) **21**(3):309–22. doi:10.1016/j.ccr.2012.02.022
18. de Visser KE, Eichten A, Coussens LM. Paradoxical roles of the immune system during cancer development. *Nat Rev Cancer* (2006) **6**(1):24–37. doi:10.1038/nrc1782
19. Derksen PW, Liu X, Saridin F, van der Gulden H, Zevenhoven J, Evers B, et al. Somatic inactivation of E-Cadherin and p53 in mice leads to metastatic lobular mammary carcinoma through

induction of anoikis resistance and angiogenesis. *Cancer Cell* (2006) **10**(5):437–49. doi:10.1016/j.ccr.2006.09.013
20. Bell D, Chomarat P, Broyles D, Netto G, Harb GM, Lebecque S, et al. In breast carcinoma tissue, immature dendritic cells reside within the tumor, whereas mature dendritic cells are located in peritumoral areas. *J Exp Med* (1999) **190**(10):1417–26. doi:10.1084/jem.190.10.1417
21. Pinzon-Charry A, Maxwell T, López JA. Dendritic cell dysfunction in cancer: a mechanism for immunosuppression. *Immunol Cell Biol* (2005) **83**(5):451–61. doi:10.1111/j.1440-1711.2005.01371.x
22. Engelhardt JJ, Boldajipour B, Beemiller P, Pandurangi P, Sorensen C, Werb Z. Marginating dendritic cells of the tumor microenvironment cross-present tumor antigens and stably engage tumor-specific T cells. *Cancer Cell* (2012) **21**(3):402–17. doi:10.1016/j.ccr.2012.01.008
23. Broz ML, Binnewies M, Boldajipour B, Nelson AE, Pollack JL, Erle DJ, et al. Dissecting the tumor myeloid compartment reveals rare activating antigen-presenting cells critical for T Cell immunity. *Cancer Cell* (2014) **26**(5):638–52. doi:10.1016/j.ccell.2014.09.007
24. Shrimali RK, Yu Z, Theoret MR, Chinnasamy D, Restifo NP, Rosenberg SA. Antiangiogenic agents can increase lymphocyte infiltration into tumor and enhance the effectiveness of adoptive immunotherapy of cancer. *Cancer Res* (2010) **70**(15):6171–80. doi:10.1158/0008-5472.CAN-10-0153
25. Buckanovich RJ, Facciabene A, Kim S, Benencia F, Sasaroli D, Balint K. Endothelin B receptor mediates the endothelial barrier to T cell homing to tumors and disables immune therapy. *Nat Med* (2008) **14**(1):28–36. doi:10.1038/nm1699
26. Molon B, Ugel S, Del Pozzo F, Soldani C, Zilio S, Avella D, et al. Chemokine nitration prevents intratumoral infiltration of antigen-specific T cells. *J Exp Med* (2011) **208**(10):1949–62. doi:10.1084/jem.20101956
27. Pardoll DM. The blockade of immune checkpoints in cancer immunotherapy. *Nat Rev Cancer* (2012) **12**(4):252–64. doi:10.1038/nrc3239
28. Joyce JA, Fearon DT. T cell exclusion, immune privilege, and the tumor microenvironment. *Science* (2015) **348**(6230):74–80. doi:10.1126/science.aaa6204
29. Sharma P, Allison JP. The future of immune checkpoint therapy. *Science* (2015) **348**(6230):56–61. doi:10.1126/science.aaa8172
30. Walunas TL, Lenschow DJ, Bakker CY, Linsley PS, Freeman GJ, Green JM, et al. CTLA-4 can function as a negative regulator of T cell activation. *Immunity* (1994) **1**(5):405–13. doi:10.1016/1074-7613(94)90071-X
31. Barber DL, Wherry EJ, Masopust D, Zhu B, Allison JP, Sharpe AH, et al. Restoring function in exhausted cd8 t cells during chronic viral infection. *Nature* (2006) **439**(7077):682–7. doi:10.1038/nature04444
32. Okazaki T, Honjo T. PD-1 and PD-1 ligands: from discovery to clinical application. *Int Immunol* (2007) **19**(7):813–24. doi:10.1093/intimm/dxm057
33. Shin DS, Ribas A. The evolution of checkpoint blockade as a cancer therapy: what's here, what's next? *Curr Opin Immunol* (2015) **33**(April):23–35. doi:10.1016/j.coi.2015.01.006
34. Topalian SL, Drake CG, Pardoll DM. Immune checkpoint blockade: a common denominator approach to cancer therapy. *Cancer Cell* (2015) **27**(4):450–61. doi:10.1016/j.ccell.2015.03.001
35. Goldberg MV, Maris CH, Hipkiss EL, Flies AS, Zhen L, Tuder RM, et al. Role of PD-1 and its ligand, B7-H1, in early fate decisions of CD8 T cells. *Blood* (2007) **110**(1):186–92. doi:10.1182/blood-2006-12-062422
36. Wing K, Onishi Y, Prieto-Martin P, Yamaguchi T, Miyara M, Fehervari Z, et al. CTLA-4 control over Foxp3+ regulatory T cell function. *Science* (2008) **322**(5899):271–5. doi:10.1126/science.1160062
37. Peggs KS, Quezada SA, Chambers CA, Korman AJ, Allison JP. Blockade of CTLA-4 on both effector and regulatory T cell compartments contributes to the antitumor activity of anti-CTLA-4

antibodies. *J Exp Med* (2009) **206**(8):1717–25. doi:10.1084/jem.20082492
38. Simpson TR, Li F, Montalvo-Ortiz W, Sepulveda MA, Bergerhoff K, Arce F, et al. Fc-dependent depletion of tumor-infiltrating regulatory T cells Co-defines the efficacy of anti-CTLA-4 therapy against melanoma. *J Exp Med* (2013) **210**(9):1695–710. doi:10.1084/jem.20130579
39. Postow MA, Chesney J, Pavlick AC, Robert C, Grossmann K, McDermott D, et al. Nivolumab and ipilimumab versus ipilimumab in untreated melanoma. *N Engl J Med* (2015) **372**(21):2006–17. doi:10.1056/NEJMoa1414428
40. Kvistborg P, Philips D, Kelderman S, Hageman L, Ottensmeier C, Joseph-Pietras D, et al. Anti-CTLA-4 therapy broadens the melanoma-reactive CD8+ T cell response. *Sci Transl Med* (2014) **6**(254):254ra128. doi:10.1126/scitranslmed.3008918
41. Robert C, Thomas L, Bondarenko I, O'Day S, Weber J, Garbe C, et al. Ipilimumab plus dacarbazine for previously untreated metastatic melanoma. *N Engl J Med* (2011) **364**(26):2517–26. doi:10.1056/NEJMoa1104621
42. Schadendorf D, Hodi FS, Robert C, Weber JS, Margolin K, Hamid O, et al. Pooled analysis of long-term survival data from phase II and phase III trials of ipilimumab in unresectable or metastatic melanoma. *J Clin Oncol* (2015) **33**(17):1889–94. doi:10.1200/JCO.2014.56.2736
43. Brahmer JR, Tykodi SS, Chow LQ, Hwu WJ, Topalian SL, Hwu P, et al. Safety and activity of anti-PD-L1 antibody in patients with advanced cancer. *N Engl J Med* (2012) **366**(26):2455–65. doi:10.1056/NEJMoa1200694
44. Gubin MM, Zhang X, Schuster H, Caron E, Ward JP, Noguchi T, et al. Checkpoint blockade cancer immunotherapy targets tumour-specific mutant antigens. *Nature* (2014) **515**(7528):577–81. doi:10.1038/nature13988
45. Linnemann C, van Buuren MM, Bies L, Verdegaal EM, Schotte R, Calis JJ, et al. High-throughput epitope discovery reveals frequent recognition of neo-antigens by CD4+ T cells in human melanoma. *Nat Med* (2015) **21**(1):81–5. doi:10.1038/nm.3773
46. van Rooij N, van Buuren MM, Philips D, Velds A, Toebes M, Heemskerk B, et al. Tumor exome analysis reveals neoantigen-specific T-cell reactivity in an ipilimumab-responsive melanoma. *J Clin Oncol* (2013) **31**(32):e439–42. doi:10.1200/JCO.2012.47.7521
47. Rooney MS, Shukla SA, Wu CJ, Getz G, Hacohen N. Molecular and genetic properties of tumors associated with local immune cytolytic activity. *Cell* (2015) **160**(1–2):48–61. doi:10.1016/j.cell.2014.12.033
48. Schumacher TN, Schreiber RD. Neoantigens in cancer immunotherapy. *Science* (2015) **348**(6230):69–74. doi:10.1126/science.aaa4971
49. Alexandrov LB, Nik-Zainal S, Wedge DC, Aparicio SA, Behjati S, Biankin AV, et al. Signatures of mutational processes in human cancer. *Nature* (2013) **500**(7463):415–21. doi:10.1038/nature12477
50. Tumeh PC, Harview CL, Yearley JH, Shintaku IP, Taylor EJ, Robert L, et al. PD-1 blockade induces responses by inhibiting adaptive immune resistance. *Nature* (2014) **515**(7528):568–71. doi:10.1038/nature13954
51. Gros A, Robbins PF, Yao X, Li YF, Turcotte S, Tran E, et al. PD-1 identifies the patient-specific $CD8^+$ tumor-reactive repertoire infiltrating human tumors. *J Clin Invest* (2014) **124**(5):2246–59. doi:10.1172/JCI73639
52. Herbst RS, Soria JC, Kowanetz M, Fine GD, Hamid O, Gordon MS, et al. Predictive correlates of response to the anti-PD-L1 antibody MPDL3280A in cancer patients. *Nature* (2014) **515**(7528):563–7. doi:10.1038/nature14011
53. Taube JM, Klein A, Brahmer JR, Xu H, Pan X, Kim JH, et al. Association of PD-1, PD-1 ligands, and other features of the tumor immune microenvironment with response to anti-PD-1 therapy. *Clin Cancer Res* (2014) **20**(19):5064–74. doi:10.1158/1078-0432.CCR-13-3271
54. Le DT, Uram JN, Wang H, Bartlett BR, Kemberling H, Eyring AD, et al. PD-1 blockade in tumors with mismatch-repair deficiency. *N Engl J Med* (2015) **372**(26):2509–20. doi:10.1056/NEJMoa1500596

55. Llosa NJ, Cruise M, Tam A, Wicks EC, Hechenbleikner EM, Taube JM, et al. The vigorous immune microenvironment of microsatellite instable colon cancer is balanced by multiple counter-inhibitory checkpoints. *Cancer Discov* (2015) **5**(1):43–51. doi:10.1158/2159-8290.CD-14-0863
56. Wimberly H, Brown JR, Schalper K, Haack H, Silver MR, Nixon C, et al. PD-L1 expression correlates with tumor-infiltrating lymphocytes and response to neoadjuvant chemotherapy in breast cancer. *Cancer Immunol Res* (2015) **3**(4):326–32. doi:10.1158/2326-6066.CIR-14-0133
57. Ali HR, Glont S-E, Blows FM, Provenzano E, Dawson S-J, Liu B, et al. PD-L1 protein Expression in breast cancer is rare, enriched in basal-like tumours and associated with infiltrating lymphocytes. *Ann Oncol* (2015) **26**(7):1488–93. doi:10.1093/annonc/mdv192
58. Parsa AT, Waldron JS, Panner A, Crane CA, Parney IF, Barry JJ, et al. Loss of tumor suppressor PTEN function increases B7-H1 expression and immunoresistance in glioma. *Nat Med* (2007) **13**(1):84–8. doi:10.1038/nm1517
59. Curiel TJ, Wei S, Dong H, Alvarez X, Cheng P, Mottram P, et al. Blockade of B7-H1 improves myeloid dendritic cell-mediated antitumor immunity. *Nat Med* (2003) **9**(5):562–7. doi:10.1038/nm863
60. Gershon RK, Kondo K. Cell interactions in the induction of tolerance: the role of thymic lymphocytes. *Immunology* (1970) **18**(5):723–37.
61. Sakaguchi S, Sakaguchi N, Asano M, Itoh M, Toda M. Immunologic self-tolerance maintained by activated T cells expressing IL-2 receptor alpha-chains (CD25). Breakdown of a single mechanism of self-tolerance causes various autoimmune diseases. *J Immunol* (1995) **155**(3):1151–64.
62. Fontenot JD, Gavin MA, Rudensky AY. Foxp3 programs the development and function of CD4+CD25+ regulatory T cells. *Nat Immunol* (2003) **4**(4):330–6. doi:10.1038/ni904
63. Adeegbe DO, Nishikawa H. Natural and induced T regulatory cells in cancer. *Front Immunol* (2013) **4**:190. doi:10.3389/fimmu.2013.00190
64. Berendt MJ, North RJ. T-cell-mediated suppression of anti-tumor immunity. An explanation for progressive growth of an immunogenic tumor. *J Exp Med* (1980) **151**(1):69–80. doi:10.1084/jem.151.1.69
65. Li X, Kostareli E, Suffner J, Garbi N, Hämmerling GJ. Efficient Treg depletion induces T-cell infiltration and rejection of large tumors. *Eur J Immunol* (2010) **40**(12):3325–35. doi:10.1002/eji.201041093
66. Curiel TJ, Coukos G, Zou L, Alvarez X, Cheng P, Mottram P, et al. Specific recruitment of regulatory T cells in ovarian carcinoma fosters immune privilege and predicts reduced survival. *Nat Med* (2004) **10**(9):942–9. doi:10.1038/nm1093
67. Shevach EM. Mechanisms of foxp3+ T regulatory cell-mediated suppression. *Immunity* (2009) **30**(5):636–45. doi:10.1016/j.immuni.2009.04.010
68. Thornton AM, Shevach EM. Suppressor effector function of CD4+CD25+ immunoregulatory T cells is antigen nonspecific. *J Immunol* (2000) **164**(1):183–90. doi:10.4049/jimmunol.164.1.183
69. Thornton AM, Shevach EM. CD4+CD25+ immunoregulatory T cells suppress polyclonal T cell activation in vitro by inhibiting interleukin 2 production. *J Exp Med* (1998) **188**(2):287–96. doi:10.1084/jem.188.2.287
70. Chen W, Jin W, Hardegen N, Lei KJ, Li L, Marinos N, et al. Conversion of peripheral CD4+CD25- naive T cells to CD4+CD25+ regulatory T cells by TGF-beta induction of transcription factor Foxp3. *J Exp Med* (2003) **198**(12):1875–86. doi:10.1084/jem.20030152
71. Groux H, O'Garra A, Bigler M, Rouleau M, Antonenko S, de Vries JE, et al. A CD4+ T-cell subset inhibits antigen-specific T-cell responses and prevents colitis. *Nature* (1997) **389**(6652):737–42. doi:10.1038/39614
72. Collison LW, Workman CJ, Kuo TT, Boyd K, Wang Y, Vignali KM. The inhibitory cytokine IL-35 contributes to regulatory T-cell function. *Nature* (2007) **450**(7169):566–9. doi:10.1038/nature06306
73. Cao X, Cai SF, Fehniger TA, Song J, Collins LI, Piwnica-Worms DR. Granzyme B and perforin are important for regulatory T cell-mediated suppression of tumor clearance. *Immunity* (2007)

27(4):635–46. doi:10.1016/j.immuni.2007.08.014
74. Grossman WJ, Verbsky JW, Barchet W, Colonna M, Atkinson JP, Ley TJ. Human T regulatory cells can use the perforin pathway to cause autologous target cell death. *Immunity* (2004) **21**(4):589–601. doi:10.1016/j.immuni.2004.09.002
75. Gondek DC, Lu LF, Quezada SA, Sakaguchi S, Noelle RJ. Cutting edge: contact-mediated suppression by CD4+CD25+ regulatory cells involves a granzyme B-dependent, perforin-independent mechanism. *J Immunol* (2005) **174**(4):1783–6. doi:10.4049/jimmunol.174.4.1783
76. Deaglio S, Dwyer KM, Gao W, Friedman D, Usheva A, Erat A, et al. Adenosine generation catalyzed by CD39 and CD73 expressed on regulatory T cells mediates immune suppression. *J Exp Med* (2007) **204**(6):1257–65. doi:10.1084/jem.20062512
77. Bates GJ, Fox SB, Han C, Leek RD, Garcia JF, Harris AL, et al. Quantification of regulatory T cells enables the identification of high-risk breast cancer patients and those at risk of late relapse. *J Clin Oncol* (2006) **24**(34):5373–80. doi:10.1200/JCO.2006.05.9584
78. Sasada T, Kimura M, Yoshida Y, Kanai M, Takabayashi A. CD4+CD25+ regulatory T cells in patients with gastrointestinal malignancies: possible involvement of regulatory T cells in disease progression. *Cancer* (2003) **98**(5):1089–99. doi:10.1002/cncr.11618
79. Gao Q, Qiu SJ, Fan J, Zhou J, Wang XY, Xiao YS. Intratumoral balance of regulatory and cytotoxic T cells is associated with prognosis of hepatocellular carcinoma after resection. *J Clin Oncol* (2007) **25**(18):2586–93. doi:10.1200/JCO.2006.09.4565
80. Li YQ, Liu FF, Zhang XM, Guo XJ, Ren MJ, Fu L. Tumor secretion of CCL22 activates intratumoral Treg infiltration and is independent prognostic predictor of breast cancer. *PLoS One* (2013) **8**(10):e76379. doi:10.1371/journal.pone.0076379
81. Huang Y, Liao H, Zhang Y, Yuan R, Wang F, Gao Y, et al. Prognostic value of tumor-infiltrating FoxP3+ T cells in gastrointestinal cancers: a meta analysis. *PLoS One* (2014) **9**(5):e94376. doi:10.1371/journal.pone.0094376
82. Ladoire S, Martin F, Ghiringhelli F. Prognostic role of FOXP3+ regulatory T cells infiltrating human carcinomas: the paradox of colorectal cancer. *Cancer Immunol Immunother* (2011) **60**(7):909–18. doi:10.1007/s00262-011-1046-y
83. Rasku MA, Clem AL, Telang S, Taft B, Gettings K, Gragg H, et al. Transient T cell depletion causes regression of melanoma metastases. *J Transl Med* (2008) **6**:12. doi:10.1186/1479-5876-6-12
84. Rech AJ, Mick R, Martin S, Recio A, Aqui NA, Powell DJ Jr, et al. CD25 blockade depletes and selectively reprograms regulatory T cells in concert with immunotherapy in cancer patients. *Sci Transl Med* (2012) **4**(134):134ra62. doi:10.1126/scitranslmed.3003330
85. Bennett JA, Rao VS, Mitchell MS. Systemic Bacillus Calmette-Guérin (BCG) activates natural suppressor cells. *Proc Natl Acad Sci U S A* (1978) **75**(10):5142–4. doi:10.1073/pnas.75.10.5142
86. Oseroff A, Okada S, Strober S. Natural suppressor (NS) cells found in the spleen of neonatal mice and adult mice given total lymphoid irradiation (TLI) express the null surface phenotype. *J Immunol* (1984) **132**(1):101–10.
87. Tsuchiya Y, Igarashi M, Suzuki R, Kumagai K. Production of colony-stimulating factor by tumor cells and the factor-mediated induction of suppressor cells. *J Immunol* (1988) **141**(2):699–708.
88. Lee MY, Rosse C. Depletion of lymphocyte subpopulations in primary and secondary lymphoid organs of mice by a transplanted granulocytosis-inducing mammary carcinoma. *Cancer Res* (1982) **42**(4):1255–60.
89. Gabrilovich DI, Bronte V, Chen SH, Colombo MP, Ochoa A, Ostrand-Rosenberg S. The terminology issue for myeloid-derived suppressor cells. *Cancer Res* (2007) **67**(1):425. doi:10.1158/0008-5472.CAN-06-3037
90. Dumitru CA, Moses K, Trellakis S, Lang S, Brandau S. Neutrophils and granulocytic myeloid-derived suppressor cells: immunophenotyping, cell biology and clinical relevance in human oncology. *Cancer Immunol Immunother* (2012) **61**(8):1155–67. doi:10.1007/s00262-012-1294-5
91. Chevolet I, Speeckaert R, Schreuer M, Neyns B, Krysko O, Bachert C. Clinical significance of plasmacytoid dendritic cells and myeloid-derived suppressor cells in melanoma. *J Transl Med*

(2015) **13**(1):9. doi:10.1186/s12967-014-0376-x
92. Wang L, Chang EW, Wong SC, Ong SM, Chong DQ, Ling KL. Increased myeloid-derived suppressor cells in gastric cancer correlate with cancer stage and plasma S100A8/A9 proinflammatory proteins. *J Immunol* (2013) **190**(2):794–804. doi:10.4049/jimmunol.1202088
93. Solito S, Falisi E, Diaz-Montero CM, Doni A, Pinton L, Rosato A, et al. A human promyelocytic-like population is responsible for the immune suppression mediated by myeloid-derived suppressor cells. *Blood* (2011) **118**(8):2254–65. doi:10.1182/blood-2010-12-325753
94. Waight JD, Hu Q, Miller A, Liu S, Abrams SI. Tumor-derived G-CSF facilitates neoplastic growth through a granulocytic myeloid-derived suppressor cell-dependent mechanism. *PLoS One* (2011) **6**(11):e27690. doi:10.1371/journal.pone.0027690
95. Serafini P, Carbley R, Noonan KA, Tan G, Bronte V, Borrello I. High-dose granulocyte-macrophage colony-stimulating factor-producing vaccines impair the immune response through the recruitment of myeloid suppressor cells. *Cancer Res* (2004) **64**(17):6337–43. doi:10.1158/0008-5472.CAN-04-0757
96. Pan PY, Wang GX, Yin B, Ozao J, Ku T, Divino CM, et al. Reversion of immune tolerance in advanced malignancy: modulation of myeloid-derived suppressor cell development by blockade of stem-cell factor function. *Blood* (2008) **111**(1):219–28. doi:10.1182/blood-2007-04-086835
97. Rodriguez PC, Hernandez CP, Quiceno D, Dubinett SM, Zabaleta J, Ochoa JB, et al. Arginase I in myeloid suppressor cells is induced by COX-2 in lung carcinoma. *J Exp Med* (2005) **202**(7):931–9. doi:10.1084/jem.20050715
98. Rodriguez PC, Ernstoff MS, Hernandez C, Atkins M, Zabaleta J, Sierra R, et al. Arginase I-producing myeloid-derived suppressor cells in renal cell carcinoma are a subpopulation of activated granulocytes. *Cancer Res* (2009) **69**(4):1553–60. doi:10.1158/0008-5472.CAN-08-1921
99. Harari O, Liao JK. Inhibition of MHC II gene transcription by nitric oxide and antioxidants. *Curr Pharm Des* (2004) **10**(8):893–8. doi:10.2174/1381612043452893
100. Saio M, Radoja S, Marino M, Frey AB. Tumor-infiltrating macrophages induce apoptosis in activated CD8(+) T cells by a mechanism requiring cell contact and mediated by both the cell-associated form of TNF and nitric oxide. *J Immunol* (2001) **167**(10):5583–93. doi:10.4049/jimmunol.167.10.5583
101. Yu J, Du W, Yan F, Wang Y, Li H, Cao S, et al. Myeloid-derived suppressor cells suppress antitumor immune responses through IDO expression and correlate with lymph node metastasis in patients with breast cancer. *J Immunol* (2013) **190**(7):3783–97. doi:10.4049/jimmunol.1201449
102. Holmgaard RB, Zamarin D, Munn DH, Wolchok JD, Allison JP. Indoleamine 2,3-dioxygenase is a critical resistance mechanism in antitumor T cell immunotherapy targeting CTLA-4. *J Exp Med* (2013) **210**(7):1389–402. doi:10.1084/jem.20130066
103. Srivastava MK, Sinha P, Clements VK, Rodriguez P, Ostrand-Rosenberg S. Myeloid-derived suppressor cells inhibit T-cell activation by depleting cystine and cysteine. *Cancer Res* (2010) **70**(1):68–77. doi:10.1158/0008-5472.CAN-09-2587
104. Huang B, Pan PY, Li Q, Sato AI, Levy DE, Bromberg J, et al. Gr-1+CD115+ immature myeloid suppressor cells mediate the development of tumor-induced T regulatory cells and T-cell anergy in tumor-bearing host. *Cancer Res* (2006) **66**(2):1123–31. doi:10.1158/0008-5472.CAN-05-1299
105. Noh H, Eomm M, Han A. Usefulness of pretreatment neutrophil to lymphocyte ratio in predicting disease-specific survival in breast cancer patients. *J Breast Cancer* (2013) **16**(1):55–9. doi:10.4048/jbc.2013.16.1.55
106. Tomita M, Shimizu T, Ayabe T, Yonei A, Onitsuka T. Preoperative neutrophil to lymphocyte ratio as a prognostic predictor after curative resection for non-small cell lung cancer. *Anticancer Res* (2011) **31**(9):2995–8.
107. Pillay J, Tak T, Kamp VM, Koenderman L. Immune suppression by neutrophils and granulocytic myeloid-derived suppressor cells: similarities and differences. *Cell Mol Life Sci* (2013) **70**(20):3813–27. doi:10.1007/s00018-013-1286-4
108. Coffelt SB, Kersten K, Doornebal CW, Weiden J, Vrijland K, Hau CS, et al. IL-17-producing γδ T cells

and neutrophils conspire to promote breast cancer metastasis. *Nature* (2015) **522**(7556):345–8. doi:10.1038/nature14282
109. Han Y, Yu Z, Wen S, Zhang B, Cao X, Wang X. Prognostic value of chemotherapy-induced neutropenia in early-stage breast cancer. *Breast Cancer Res Treat* (2012) **131**(2):483–90. doi:10.1007/s10549-011-1799-1
110. Bald T, Quast T, Landsberg J, Rogava M, Glodde N, Lopez-Ramos D, et al. Ultraviolet-radiation-induced inflammation promotes angiotropism and metastasis in melanoma. *Nature* (2014) **507**(7490):109–13. doi:10.1038/nature13111
111. Kowanetz M, Wu X, Lee J, Tan M, Hagenbeek T, Qu X, et al. Granulocyte-colony stimulating factor promotes lung metastasis through mobilization of Ly6G+Ly6C+ granulocytes. *Proc Natl Acad Sci U S A* (2010) **107**(50):21248–55. doi:10.1073/pnas.1015855107
112. Granot Z, Henke E, Comen EA, King TA, Norton L, Benezra R. Tumor entrained neutrophils inhibit seeding in the premetastatic lung. *Cancer Cell* (2011) **20**(3):300–14. doi:10.1016/j.ccr.2011.08.012
113. Casbon AJ, Reynaud D, Park C, Khuc E, Gan DD, Schepers K. Invasive breast cancer reprograms early myeloid differentiation in the bone marrow to generate immunosuppressive neutrophils. *Proc Natl Acad Sci U S A* (2015) **112**(6):E566–75. doi:10.1073/pnas.1424927112
114. Sagiv JY, Michaeli J, Assi S, Mishalian I, Kisos H, Levy L, et al. Phenotypic diversity and plasticity in circulating neutrophil subpopulations in cancer. *Cell Rep* (2015) **10**(4):562–73. doi:10.1016/j.celrep.2014.12.039
115. Fridlender ZG, Sun J, Kim S, Kapoor V, Cheng G, Ling L. Polarization of tumor-associated neutrophil phenotype by TGF-beta: 'N1' versus 'N2' TAN. *Cancer Cell* (2009) **16**(3):183–94. doi:10.1016/j.ccr.2009.06.017
116. Mantovani A, Sica A, Sozzani S, Allavena P, Vecchi A, Locati M. The chemokine system in diverse forms of macrophage activation and polarization. *Trends Immunol* (2004) **25**(12):677–86. doi:10.1016/j.it.2004.09.015
117. Murray PJ, Allen JE, Biswas SK, Fisher EA, Gilroy DW, Goerdt S, et al. Macrophage activation and polarization: nomenclature and experimental guidelines. *Immunity* (2014) **41**(1):14–20. doi:10.1016/j.immuni.2014.06.008
118. Schultze JL. Transcriptional programming of human macrophages: on the way to systems immunology. *J Mol Med (Berl)* (2015) **93**(6):589–97. doi:10.1007/s00109-015-1286-y
119. Xue J, Schmidt SV, Sander J, Draffehn A, Krebs W, Quester I, et al. Transcriptome-based network analysis reveals a spectrum model of human macrophage activation. *Immunity* (2014) **40**(2):274–88. doi:10.1016/j.immuni.2014.01.006
120. DeNardo DG, Brennan DJ, Rexhepaj E, Ruffell B, Shiao SL, Madden SF, et al. Leukocyte complexity predicts breast cancer survival and functionally regulates response to chemotherapy. *Cancer Discov* (2011) **1**:54–67. doi:10.1158/2159-8274.CD-10-0028
121. Leek RD, Lewis CE, Whitehouse R, Greenall M, Clarke J, Harris AL. Association of macrophage infiltration with angiogenesis and prognosis in invasive breast carcinoma. *Cancer Res* (1996) **56**(20):4625–9.
122. Ruffell B, Coussens LM. Macrophages and therapeutic resistance in cancer. *Cancer Cell* (2015) **27**(4):462–72. doi:10.1016/j.ccell.2015.02.015
123. Lin EY, Nguyen AV, Russell RG, Pollard JW. Colony-stimulating factor 1 promotes progression of mammary tumors to malignancy. *J Exp Med* (2001) **193**(6):727–40. doi:10.1084/jem.193.6.727
124. DeNardo DG, Barreto JB, Andreu P, Vasquez L, Tawfik D, Kolhatkar N. CD4(+) T cells regulate pulmonary metastasis of mammary carcinomas by enhancing protumor properties of macrophages. *Cancer Cell* (2009) **16**(2):91–102. doi:10.1016/j.ccr.2009.06.018
125. Qian BZ, Li J, Zhang H, Kitamura T, Zhang J, Campion LR, et al. CCL2 recruits inflammatory monocytes to facilitate breast-tumour metastasis. *Nature* (2011) **475**(7355):222–5. doi:10.1038/nature10138
126. Lin EY, Li JF, Gnatovskiy L, Deng Y, Zhu L, Grzesik DA, et al. Macrophages regulate the angiogenic switch in a mouse model of breast cancer. *Cancer Res* (2006) **66**(23):11238–46. doi:10.1158/0008-

5472.CAN-06-1278
127. Sharda DR, Yu S, Ray M, Squadrito ML, De Palma M, Wynn TA, et al. Regulation of macrophage arginase expression and tumor growth by the ron receptor tyrosine kinase. *J Immunol* (2011) **187**(5):2181–92. doi:10.4049/jimmunol.1003460
128. Rodriguez PC, Zea AH, DeSalvo J, Culotta KS, Zabaleta J, Quiceno DG, et al. L-arginine consumption by macrophages modulates the expression of CD3 zeta chain in T lymphocytes. *J Immunol* (2003) **171**(3):1232–9. doi:10.4049/jimmunol.171.3.1232
129. Munn DH, Shafizadeh E, Attwood JT, Bondarev I, Pashine A, Mellor AL. Inhibition of T cell proliferation by macrophage tryptophan catabolism. *J Exp Med* (1999) **189**(9):1363–72. doi:10.1084/jem.189.9.1363
130. Sica A, Saccani A, Bottazzi B, Polentarutti N, Vecchi A, van Damme J, et al. Autocrine production of IL-10 mediates defective IL-12 production and NF-kappa B activation in tumor-associated macrophages. *J Immunol* (2000) **164**(2):762–7. doi:10.4049/jimmunol.164.2.762
131. Kuang DM, Zhao Q, Peng C, Xu J, Zhang JP, Wu C, et al. Activated monocytes in peritumoral stroma of hepatocellular carcinoma foster immune privilege and disease progression through PD-L1. *J Exp Med* (2009) **206**(6):1327–37. doi:10.1084/jem.20082173
132. Pyonteck SM, Akkari L, Schuhmacher AJ, Bowman RL, Sevenich L, Quail DF, et al. CSF-1R inhibition alters macrophage polarization and blocks glioma progression. *Nat Med* (2013) **19**(10):1264–72. doi:10.1038/nm.3337
133. Zhu Y, Knolhoff BL, Meyer MA, Nywening TM, West BL, Luo J, et al. CSF1/CSF1R blockade reprograms tumor-infiltrating macrophages and improves response to T-cell checkpoint immunotherapy in pancreatic cancer models. *Cancer Res* (2014) **74**(18):5057–69. doi:10.1158/0008-5472.CAN-13-3723
134. Fridlender ZG, Buchlis G, Kapoor V, Cheng G, Sun J, Singhal S, et al. CCL2 blockade augments cancer immunotherapy. *Cancer Res* (2010) **70**(1):109–18. doi:10.1158/0008-5472.CAN-09-2326
135. Fridlender ZG, Kapoor V, Buchlis G, Cheng G, Sun J, Wang LC. Monocyte chemoattractant protein-1 blockade inhibits lung cancer tumor growth by altering macrophage phenotype and activating CD8+ cells. *Am J Respir Cell Mol Biol* (2011) **44**(2):230–7. doi:10.1165/rcmb.2010-0080OC
136. Klyushnenkova EN, Riabov VB, Kouiavskaia DV, Wietsma A, Zhan M, Alexander RB. Breaking immune tolerance by targeting CD25+ regulatory T cells is essential for the anti-tumor effect of the CTLA-4 blockade in an HLA-DR transgenic mouse model of prostate cancer. *Prostate* (2014) **74**(14):1423–32. doi:10.1002/pros.22858
137. Duraiswamy J, Kaluza KM, Freeman GJ, Coukos G. Dual blockade of PD-1 and CTLA-4 combined with tumor vaccine effectively restores T-cell rejection function in tumors. *Cancer Res* (2013) **73**(12):3591–603. doi:10.1158/0008-5472.CAN-12-4100
138. Duraiswamy J, Freeman GJ, Coukos G. Therapeutic PD-1 pathway blockade augments with other modalities of immunotherapy T-cell function to prevent immune decline in ovarian cancer. *Cancer Res* (2013) **73**(23):6900–12. doi:10.1158/0008-5472.CAN-13-1550
139. Highfill SL, Cui Y, Giles AJ, Smith JP, Zhang H, Morse E, et al. Disruption of CXCR2-mediated MDSC tumor trafficking enhances anti-PD1 efficacy. *Sci Transl Med* (2014) **6**(237):237ra67. doi:10.1126/scitranslmed.3007974
140. Nars MS, Kaneno R. Immunomodulatory effects of low dose chemotherapy and perspectives of its combination with immunotherapy. *Int J Cancer* (2013) **132**(11):2471–8. doi:10.1002/ijc.27801
141. Kerbel RS, Kamen BA. The anti-angiogenic basis of metronomic chemotherapy. *Nat Rev Cancer* (2004) **4**(6):423–36. doi:10.1038/nrc1369
142. Ma Y, Adjemian S, Mattarollo SR, Yamazaki T, Aymeric L, Yang H, et al. Anticancer chemotherapy-induced intratumoral recruitment and differentiation of antigen-presenting cells. *Immunity* (2013) **38**(4):729–41. doi:10.1016/j.immuni.2013.03.003
143. Ghiringhelli F, Apetoh L, Tesniere A, Aymeric L, Ma Y, Ortiz C, et al. Activation of the NLRP3 inflammasome in dendritic cells induces IL-1beta-dependent adaptive immunity against tumors. *Nat Med* (2009) **15**(10):1170–8. doi:10.1038/nm.2028

144. Wada S, Yoshimura K, Hipkiss EL, Harris TJ, Yen HR, Goldberg MV, et al. Cyclophosphamide augments antitumor immunity: studies in an autochthonous prostate cancer model. *Cancer Res* (2009) **69**(10):4309–18. doi:10.1158/0008-5472.CAN-08-4102
145. Apetoh L, Ghiringhelli F, Tesniere A, Obeid M, Ortiz C, Criollo A, et al. Toll-like receptor 4-dependent contribution of the immune system to anticancer chemotherapy and radiotherapy. *Nat Med* (2007) **13**(9):1050–9. doi:10.1038/nm1622
146. Obeid M, Tesniere A, Ghiringhelli F, Fimia GM, Apetoh L, Perfettini JL, et al. Calreticulin exposure dictates the immunogenicity of cancer cell death. *Nat Med* (2007) **13**(1):54–61. doi:10.1038/nm1523
147. Bezu L, Gomes-de-Silva LC, Dewitte H, Breckpot K, Fucikova J, Spisek R. Combinatorial strategies for the induction of immunogenic cell death. *Front Immunol* (2015) **6**:187. doi:10.3389/fimmu.2015.00187
148. Ciampricotti M, Hau CS, Doornebal CW, Jonkers J, de Visser KE. Chemotherapy response of spontaneous mammary tumors is independent of the adaptive immune system. *Nat Med* (2012) **18**(3):344–6. doi:10.1038/nm.2652
149. Ruffell B, Chang-Strachan D, Chan V, Rosenbusch A, Ho CM, Pryer N, et al. Macrophage IL-10 blocks CD8+ T cell-dependent responses to chemotherapy by suppressing IL-12 expression in intratumoral dendritic cells. *Cancer Cell* (2014) **26**(5):623–37. doi:10.1016/j.ccell.2014.09.006
150. Luznik L, Jones RJ, Fuchs EJ. High-dose cyclophosphamide for graft-versus-host disease prevention. *Curr Opin Hematol* (2010) **17**(6):493–9. doi:10.1097/MOH.0b013e32833eaf1b
151. Luznik L, O'Donnell PV, Symons HJ, Chen AR, Leffell MS, Zahurak M, et al. HLA-haploidentical bone marrow transplantation for hematologic malignancies using nonmyeloablative conditioning and high-dose, posttransplantation cyclophosphamide. *Biol Blood Marrow Transplant* (2008) **14**(6):641–50. doi:10.1016/j.bbmt.2008.03.005
152. Lutsiak ME, Semnani RT, De Pascalis R, Kashmiri SV, Schlom J, Sabzevari H. Inhibition of CD4(+)25+ T regulatory cell function implicated in enhanced immune response by low-dose cyclophosphamide. *Blood* (2005) **105**(7):2862–8. doi:10.1182/blood-2004-06-2410
153. Motoyoshi Y, Kaminoda K, Saitoh O, Hamasaki K, Nakao K, Ishii N, et al. Different mechanisms for anti-tumor effects of low- and high-dose cyclophosphamide. *Oncol Rep* (2006) **16**(1):141–6. doi:10.3892/or.16.1.141
154. Ghiringhelli F, Larmonier N, Schmitt E, Parcellier A, Cathelin D, Garrido C. CD4+CD25+ regulatory T cells suppress tumor immunity but are sensitive to cyclophosphamide which allows immunotherapy of established tumors to be curative. *Eur J Immunol* (2004) **34**(2):336–44. doi:10.1002/eji.200324181
155. Ghiringhelli F, Menard C, Puig PE, Ladoire S, Roux S, Martin F, et al. Metronomic cyclophosphamide regimen selectively depletes CD4+CD25+ regulatory T cells and restores T and NK effector functions in end stage cancer patients. *Cancer Immunol Immunother* (2007) **56**(5):641–8. doi:10.1007/s00262-006-0225-8
156. Zhao J, Cao Y, Lei Z, Yang Z, Zhang B, Huang B. Selective depletion of CD4+CD25+Foxp3+ regulatory T cells by low-dose cyclophosphamide is explained by reduced intracellular ATP levels. *Cancer Res* (2010) **70**(12):4850–8. doi:10.1158/0008-5472.CAN-10-0283
157. Shevchenko I, Karakhanova S, Soltek S, Link J, Bayry J, Werner J, et al. Low-dose gemcitabine depletes regulatory T cells and improves survival in the orthotopic panc02 model of pancreatic cancer. *Int J Cancer* (2013) **133**(1):98–107. doi:10.1002/ijc.27990
158. Rettig L, Seidenberg S, Parvanova I, Samaras P, Curioni A, Knuth A, et al. Gemcitabine depletes regulatory T-cells in human and mice and enhances triggering of vaccine-specific cytotoxic T-cells. *Int J Cancer* (2011) **129**(4):832–8. doi:10.1002/ijc.25756
159. Beyer M, Kochanek M, Darabi K, Popov A, Jensen M, Endl E, et al. Reduced frequencies and suppressive function of CD4+CD25hi regulatory T cells in patients with chronic lymphocytic leukemia after therapy with fludarabine. *Blood* (2005) **106**(6):2018–25. doi:10.1182/blood-2005-02-0642

160. Chen C, Chen Z, Chen D, Zhang B, Wang Z, Le H. Suppressive effects of gemcitabine plus cisplatin chemotherapy on regulatory T cells in nonsmall-cell lung cancer. *J Int Med Res* (2015) **43**(2):180–7. doi:10.1177/0300060514561504
161. Vincent J, Mignot G, Chalmin F, Ladoire S, Bruchard M, Chevriaux A, et al. 5-fluorouracil selectively kills tumor-associated myeloid-derived suppressor cells resulting in enhanced T cell-dependent antitumor immunity. *Cancer Res* (2010) **70**(8):3052–61. doi:10.1158/0008-5472.CAN-09-3690
162. Suzuki E, Kapoor V, Jassar AS, Kaiser LR, Albelda SM. Gemcitabine selectively eliminates splenic Gr-1+/CD11b+ myeloid suppressor cells in tumor-bearing animals and enhances antitumor immune activity. *Clin Cancer Res* (2005) **11**(18):6713–21. doi:10.1158/1078-0432.CCR-05-0883
163. Ugel S, Peranzoni E, Desantis G, Chioda M, Walter S, Weinschenk T, et al. Immune tolerance to tumor antigens occurs in a specialized environment of the spleen. *Cell Rep* (2012) **2**(3):628–39. doi:10.1016/j.celrep.2012.08.006
164. Peters GJ, van der Wilt CL, van Triest B, Codacci-Pisanelli G, Johnston PG, van Groeningen CJ, et al. Thymidylate synthase and drug resistance. *Eur J Cancer* (1995) **31A**(7–8):1299–305. doi:10.1016/0959-8049(95)00172-F
165. Le HK, Graham L, Cha E, Morales JK, Manjili MH, Bear HD. Gemcitabine directly inhibits myeloid derived suppressor cells in BALB/c mice bearing 4T1 mammary carcinoma and augments expansion of T cells from tumor-bearing mice. *Int Immunopharmacol* (2009) **9**(7–8):900–9. doi:10.1016/j.intimp.2009.03.015
166. Kodumudi KN, Woan K, Gilvary DL, Sahakian E, Wei S, Djeu JY. A novel chemoimmunomodulating property of docetaxel: suppression of myeloid-derived suppressor cells in tumor bearers. *Clin Cancer Res* (2010) **16**(18):4583–94. doi:10.1158/1078-0432.CCR-10-0733
167. Alizadeh D, Trad M, Hanke NT, Larmonier CB, Janikashvili N, Bonnotte B. Doxorubicin eliminates myeloid-derived suppressor cells and enhances the efficacy of adoptive T-cell transfer in breast cancer. *Cancer Res* (2014) **74**(1):104–18. doi:10.1158/0008-5472.CAN-13-1545
168. Sevko A, Sade-Feldman M, Kanterman J, Michels T, Falk CS, Umansky L, et al. Cyclophosphamide promotes chronic inflammation-dependent immunosuppression and prevents antitumor response in melanoma. *J Invest Dermatol* (2013) **133**(6):1610–9. doi:10.1038/jid.2012.444
169. Diaz-Montero CM, Salem ML, Nishimura MI, Garrett-Mayer E, Cole DJ, Montero AJ. Increased circulating myeloid-derived suppressor cells correlate with clinical cancer stage, metastatic tumor burden, and doxorubicin–cyclophosphamide chemotherapy. *Cancer Immunol Immunother* (2009) **58**(1):49–59. doi:10.1007/s00262-008-0523-4
170. Guo Q, Lv Z, Fu Q, Jiang C, Liu Y, Lai L, et al. IFN-γ producing T cells contribute to the increase of myeloid derived suppressor cells in tumor-bearing mice after cyclophosphamide treatment. *Int Immunopharmacol* (2012) **12**(2):425–32. doi:10.1016/j.intimp.2011.12.016
171. Bruchard M, Mignot G, Derangère V, Chalmin F, Chevriaux A, Végran F, et al. Chemotherapy-triggered cathepsin B release in myeloid-derived suppressor cells activates the Nlrp3 inflammasome and promotes tumor growth. *Nat Med* (2013) **19**(1):57–64. doi:10.1038/nm.2999
172. Shurin MR. Dual role of immunomodulation by anticancer chemotherapy. *Nat Med* (2013) **19**(1):20–2. doi:10.1038/nm.3045
173. Germano G, Frapolli R, Belgiovine C, Anselmo A, Pesce S, Liguori M, et al. Role of macrophage targeting in the antitumor activity of trabectedin. *Cancer Cell* (2013) **23**(2):249–62. doi:10.1016/j.ccr.2013.01.008
174. Lake RA, Robinson BW. Immunotherapy and chemotherapy – a practical partnership. *Nat Rev Cancer* (2005) **5**(5):397–405. doi:10.1038/nrc1613
175. Mokyr MB, Kalinichenko T, Gorelik L, Bluestone JA. Realization of the therapeutic potential of CTLA-4 blockade in low-dose chemotherapy-treated tumor-bearing mice. *Cancer Res* (1998) **58**(23):5301–4.
176. Lesterhuis WJ, Salmons J, Nowak AK, Rozali EN, Khong A, Dick IM, et al. Synergistic effect of CTLA-4 blockade and cancer chemotherapy in the induction of anti-tumor immunity. *PLoS One* (2013) **8**(4):e61895. doi:10.1371/journal.pone.0061895

177. Wu L, Yun Z, Tagawa T, Rey-McIntyre K, de Perrot M. CTLA-4 blockade expands infiltrating T cells and inhibits cancer cell repopulation during the intervals of chemotherapy in murine mesothelioma. *Mol Cancer Ther* (2012) **11**(8):1809–19. doi:10.1158/1535-7163.MCT-11-1014
178. Ramakrishnan R, Assudani D, Nagaraj S, Hunter T, Cho HI, Antonia S, et al. Chemotherapy enhances tumor cell susceptibility to CTL-mediated killing during cancer immunotherapy in mice. *J Clin Invest* (2010) **120**(4):1111–24. doi:10.1172/JCI40269
179. Lynch TJ, Bondarenko I, Luft A, Serwatowski P, Barlesi F, Chacko R, et al. Ipilimumab in combination with paclitaxel and carboplatin as first-line treatment in stage IIIB/IV non-small-cell lung cancer: results from a randomized, double-blind, multicenter phase II study. *J Clin Oncol* (2012) **30**(17):2046–54. doi:10.1200/JCO.2011.38.4032
180. Singh M, Murriel CL, Johnson L. Genetically engineered mouse models: closing the gap between preclinical data and trial outcomes. *Cancer Res* (2012) **72**(11):2695–700. doi:10.1158/0008-5472.CAN-11-2786
181. DuPage M, Cheung AF, Mazumdar C, Winslow MM, Bronson R, Schmidt LM, et al. Endogenous T cell responses to antigens expressed in lung adenocarcinomas delay malignant tumor progression. *Cancer Cell* (2011) **19**(1):72–85. doi:10.1016/j.ccr.2010.11.011
182. Olive KP, Jacobetz MA, Davidson CJ, Gopinathan A, McIntyre D, Honess D, et al. Inhibition of hedgehog signaling enhances delivery of chemotherapy in a mouse model of pancreatic cancer. *Science* (2009) **324**(5933):1457–61. doi:10.1126/science.1171362
183. DuPage M, Jacks T. Genetically engineered mouse models of cancer reveal new insights about the antitumor immune response. *Curr Opin Immunol* (2013) **25**(2):192–9. doi:10.1016/j.coi.2013.02.005

CHAPTER 5

Therapeutic targeting of macrophages enhances chemotherapy efficacy by unleashing type I interferon response

Camilla Salvagno[1], Metamia Ciampricotti[1,9,12], Sander Tuit[2,10,12], Cheei-Sing Hau[1], Antoinette van Weverwijk[1], Seth B. Coffelt [1,11], Kelly Kersten[1], Kim Vrijland[1], Kevin Kos[1], Thomas Ulas[2], Ji-Ying Song[3], Chia-Huey Ooi[4], Dominik Rüttinger[5], Philippe A. Cassier[6], Jos Jonkers[7], Joachim L. Schultze[2,8], Carola H. Ries[5] and Karin E. de Visser[1*]

1 Division of Tumor Biology & Immunology, Oncode Institute, Netherlands Cancer Institute, Amsterdam, The Netherlands.
2 Genomics and Immunoregulation, LIMES-Institute, University of Bonn, Bonn, Germany.
3 Division of Experimental Animal Pathology, Netherlands Cancer Institute, Amsterdam, The Netherlands.
4 Roche Innovation Center Basel, Roche Pharma Research and Early Development, Basel, Switzerland.
5 Roche Innovation Center Munich, Roche Pharma Research and Early Development, Penzberg, Germany.
6 Department of Medicine, Centre Léon Bérard, Lyon, France.
7 Division of Molecular Pathology, Oncode Institute, Netherlands Cancer Institute, Amsterdam, The Netherlands.
8 Platform for Single Cell Genomics and Epigenomics (PRECISE) at the German Center for Neurodegenerative Diseases and the University of Bonn, Bonn, Germany.
9 Present address: Molecular Pharmacology Program and Department of Medicine, Memorial Sloan Kettering Cancer Center, New York, NY, USA.
10 Present address: Department of Anatomy and Embryology, Leiden University Medical Center, Leiden, The Netherlands.
11 Present address: Cancer Research UK Beatson Institute and Institute of Cancer Sciences, University of Glasgow, Glasgow, UK.
12 These authors contributed equally: Metamia Ciampricotti, Sander Tuit.
* e-mail: k.d.visser@nki.nl

Nat Cell Biol. 2019 Apr;21(4):511-521

Abstract

Recent studies have revealed a role for macrophages and neutrophils in limiting chemotherapy efficacy; however, the mechanisms underlying the therapeutic benefit of myeloid-targeting agents in combination with chemotherapy are incompletely understood. Here, we show that targeting tumour-associated macrophages by colony-stimulating factor-1 receptor (CSF-1R) blockade in the *K14cre;Cdh1*$^{F/F}$*;Trp53*$^{F/F}$ transgenic mouse model for breast cancer stimulates intratumoural type I interferon (IFN) signalling, which enhances the anticancer efficacy of platinum-based chemotherapeutics. Notably, anti-CSF-1R treatment also increased intratumoural expression of type I IFN-stimulated genes in patients with cancer, confirming that CSF-1R blockade is a powerful strategy to trigger an intratumoural type I IFN response. By inducing an inflamed, type I IFN-enriched tumour microenvironment and by further targeting immunosuppressive neutrophils during cisplatin therapy, antitumour immunity was activated in this poorly immunogenic breast cancer mouse model. These data illustrate the importance of breaching multiple layers of immunosuppression during cytotoxic therapy to successfully engage antitumour immunity in breast cancer.

Main

Poor chemotherapy response is a major obstacle to successful cancer treatment. There is a growing appreciation for the influential role of the immune system on the success of cytotoxic anticancer therapy[1]. Although the adaptive immune system contributes to the therapeutic benefit of certain chemotherapeutic drugs in immunogenic tumour models[2], it frequently fails to be unleashed by these same agents in less immunogenic transgenic mouse tumour models[3,4,5], suggesting the involvement of immunosuppressive mechanisms. Indeed, macrophages and neutrophils are frequently the most abundant immune cells in tumours, and clinical studies have reported a correlation between these myeloid cells and poor chemotherapy efficacy[4,6,7,8,9,10]. Experimental animal studies confirm a causal relationship between tumour-associated myeloid cells and poor chemotherapy response[4,5,11,12,13,14,15,16,17,18,19,20]. For example, inhibition of macrophages in mammary tumour-bearing MMTV-PyMT mice increases paclitaxel efficacy via activation of antitumour immunity[4,5]. Notably, macrophage-targeting and neutrophil-targeting agents are currently under clinical evaluation[21,22,23]. Although promising, the aforementioned preclinical studies only show a transient therapeutic effect of combined myeloid cell targeting and chemotherapy. A deeper understanding of the mechanisms of action is needed to facilitate the rational design of therapeutic combination strategies that convert 'cold' non-T cell-inflamed tumours into 'hot' inflamed tumours, thus engaging durable antitumour immunity in otherwise poorly immunogenic tumours.

By combining in vivo intervention experiments and mechanistic studies in the *K14cre;Cdh1$^{F/F}$;Trp53$^{F/F}$* (KEP) mouse model for spontaneous mammary tumorigenesis[24] with validation studies in tumour biopsies of patients treated with anti-colony-stimulating factor-1 receptor (anti-CSF-1R), here, we demonstrate that CSF-1R inhibition synergizes with platinum-based chemotherapy by unleashing an intratumoural type I interferon (IFN) response. Besides this anti-CSF-1R-mediated conversion of the tumour microenvironment (TME) into a type I IFN-enriched milieu, it takes breaching of an additional layer of immunosuppression to engage antitumour immunity during cytotoxic therapy.

Results

CSF-1R blockade does not affect mammary tumour growth or metastasis in KEP mice

We set out to assess the role of CSF-1–CSF-1R signalling, which is vital for macrophages[25], in tumour progression in the KEP model, which spontaneously develops mammary tumours resembling human invasive lobular carcinomas (ILCs) at 6–8 months of age[24]. Similar to human ILCs, KEP tumours are strongly infiltrated by macrophages (Supplementary Fig. 1a,b). Whereas in the MMTV-PyMT breast cancer model it has been reported that two distinct macrophage populations reside within the TME: CD11b^{hi}MHCII^{hi}CD206^{hi} mammary tissue macrophages and CD11b^{lo}MHCII^{hi}CD206^{lo} tumour-associated macrophages (TAMs)[26], in mammary tumours of KEP mice, all F4/80^{+} macrophages express high levels of CD11b, low levels

of CD206 and only a proportion of these cells expresses major histocompatibility complex class II (MHCII) (Supplementary Fig. 1c). These differences in intratumoural macrophage phenotypes between mouse tumour models underscore the complexity of macrophage plasticity in different tumour contexts. In line with the macrophage influx, CSF-1 protein levels are increased in KEP tumours versus healthy mammary glands of age-matched wild-type littermates (Fig. 1a). Both cancer cells and host cells in KEP tumours express *Csf1* mRNA, whereas *Csf1* mRNA is barely detectable in healthy mammary glands (Fig. 1b). CSF-1R is highly expressed on TAMs and to a lesser extent on infiltrating monocytes and neutrophils (Supplementary Fig. 1d), but not on other tumour-associated immune cells or $CD45^-$ cells (Supplementary Fig. 1d).

To determine whether intratumoural macrophage accumulation depends on CSF-1–CSF-1R signalling and whether macrophages influence tumour outgrowth and dissemination, we treated tumour-bearing KEP mice with a chimeric mouse IgG1 antagonistic antibody (2G2) that binds to mouse CSF-1R with high affinity (dissociation constant (K_d) = 0.2 nM) or with a control antibody[21]. CSF-1R blockade strongly reduced the TAM population (Fig. 1c,d) and, as a result, also the total $CD45^+$ population (Supplementary Fig. 1e). Treatment with anti-CSF-1R alone did not influence tumour-specific survival (Fig. 1f) or spontaneous metastasis formation (Supplementary Fig. 1f). We also investigated the therapeutic activity of anti-CSF-1R in the KEP-based model of spontaneous breast cancer metastasis[27]. In this model, after orthotopic transplantation of a KEP-derived tumour piece followed by surgical removal of the outgrown tumour, mice develop overt multi-organ metastatic disease. Anti-CSF-1R was started either after a palpable mammary tumour had developed (continuous setting) or after mastectomy (adjuvant setting) and continued until the development of metastatic disease (Supplementary Fig. 1g). Regardless of the treatment schedule, metastasis-specific survival and metastatic burden in the lungs were similar between control and anti-CSF-1R groups (Supplementary Fig. 1h,i). Thus, anti-CSF-1R monotherapy fails to affect outgrowth and dissemination of KEP mammary tumours.

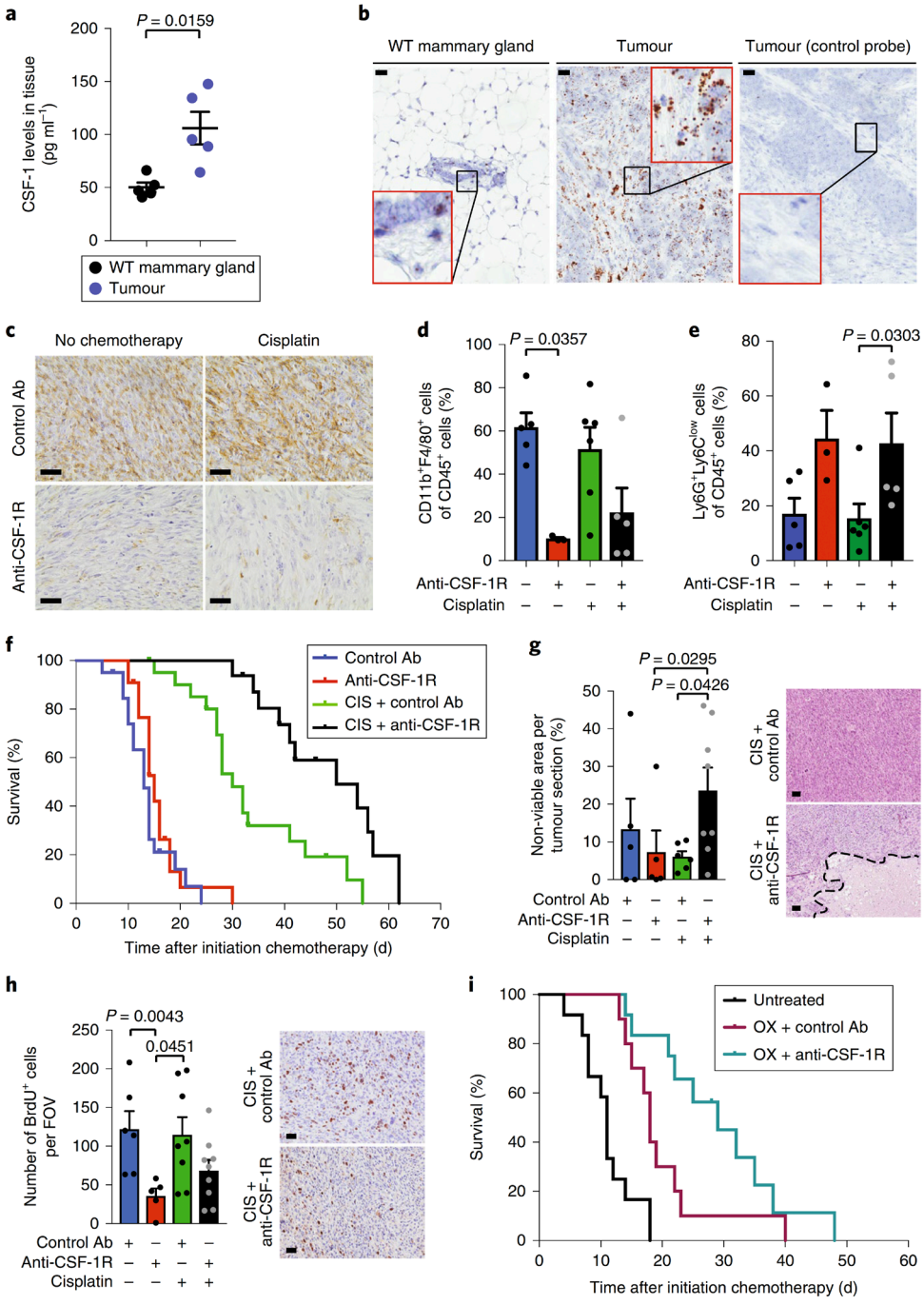


Fig. 1 | CSF-1R blockade improves the anticancer efficacy of platinum-based chemotherapeutic drugs in the KEP mouse model for de novo mammary tumorigenesis.

a, CSF-1 protein levels in end-stage mammary tumours of KEP mice and mammary glands of age-matched wild-type (WT) mice ($n = 5$ animals per group) measured by Luminex cytokine array. **b**,

Representative images of RNA in situ hybridization of *Csf1* (brown signal) in end-stage KEP tumours and normal mammary glands of age-matched WT mice. Data are representative of three animals per group. Scale bars, 25 µm. **c**, Representative immunohistochemistry images of F4/80$^+$ macrophages in tumours of time-point-sacrificed KEP mice treated as indicated. Data are representative of five animals per group. Scale bars, 25 µm. **d**,**e**, Proportion of CD11b$^+$F4/80$^+$ macrophages (**d**) and Ly6G$^+$Ly6C^{low} neutrophils (**e**) gated on CD45$^+$ cells, as determined by flow cytometry in tumours of end-stage KEP mice treated as indicated (untreated: $n = 5$ animals; anti-CSF-1R: $n = 3$ animals; cisplatin: $n = 6$ animals; cisplatin + anti-CSF-1R: $n = 5$ animals). **f**, Kaplan–Meier tumour-specific survival curves of KEP mice treated with control antibody (Ab) ($n = 20$ animals), anti-CSF-1R ($n = 22$ animals), cisplatin (CIS) + control Ab ($n = 21$ animals) or cisplatin + anti-CSF-1R ($n = 16$ animals). Cisplatin + control Ab versus control Ab: $P = 0.0001$; cisplatin + control Ab versus anti-CSF-1R: $P = 0.0001$; cisplatin + anti-CSF-1R versus cisplatin + control Ab: $P = 0.0011$ (two-tailed log-rank test). **g**, Percentage of non-viable area per tumour section of time-point-sacrificed KEP mice quantified by digital area analysis of H&E-stained sections (control Ab: $n = 5$ animals; anti-CSF-1R: $n = 5$ animals; cisplatin + control Ab: $n = 6$ animals; cisplatin + anti-CSF-1R: $n = 8$ animals). Representative H&E sections are shown, and the dashed line separates the viable from the non-viable area. Scale bars, 50 µm. **h**, Quantification of BrdU$^+$ cells in viable areas of mammary tumours of time-point-sacrificed KEP mice (control Ab: $n = 6$ animals, anti-CSF-1R: $n = 5$ animals, cisplatin + control Ab: $n = 8$ animals, cisplatin + anti-CSF-1R: $n = 9$ animals). The values represent the average number of BrdU$^+$ cells per field of view (FOV) quantified by counting five high-power microscopic fields per tumour. Representative BrdU immunohistochemistry stainings are shown. Scale bars, 25 µm. **i**, Kaplan–Meier tumour-specific survival curves of untreated KEP mice ($n = 12$ animals) or mice treated with oxaliplatin (OX) + control Ab ($n = 10$ animals) and oxaliplatin + anti-CSF-1R ($n = 12$ animals). Oxaliplatin + control Ab versus no treatment: $P = 0.0015$; oxaliplatin + control Ab versus oxaliplatin + anti-CSF-1R: $P = 0.0507$ (two-tailed log-rank test). Data presented in **a**, **d**, **e**, **g** and **h** are mean ± s.e.m., and statistical analysis was performed using the two-tailed Mann–Whitney test.

CSF-1R blockade in tumour-bearing KEP mice enhances the anticancer efficacy of platinum-based chemotherapy

We next tested the anticancer efficacy of anti-CSF-1R in combination with two conventional chemotherapeutics with a different mode of action: cisplatin, a platinum-based anticancer drug that crosslinks DNA and induces apoptosis, and docetaxel, an antimitotic agent that interferes with cell division through stabilization of microtubules. Successful blockade of the CSF-1R pathway during treatment of tumour-bearing KEP mice with chemotherapy and anti-CSF-1R was confirmed by the reduction in the number of TAMs (Fig. 1c,d and Supplementary Fig. 2a,b). Interestingly, anti-CSF-1R synergized with cisplatin, resulting in prolonged survival compared to cisplatin + control antibody-treated mice (Fig. 1f). By contrast, no therapeutic synergy was observed in docetaxel + anti-CSF-1R-treated mice (Supplementary Fig. 2c). The therapeutic synergy observed upon cisplatin + anti-CSF-1R was associated with more necrosis in KEP tumours (Fig. 1g) but not with more cleaved caspase 3$^+$ apoptotic cells (Supplementary Fig. 2d). Perhaps other mechanisms of cell death are involved or the timing of our analysis was suboptimal for this parameter. Furthermore, anti-CSF-1R monotherapy—and to a lesser extent, the combination with cisplatin—decreased the number of BrdU$^+$-proliferating cells (Fig. 1h). No significant changes in the number and pericyte coverage of CD31$^+$ microvessels, the amount of intratumoural DNA double-strand breaks and intratumoural cisplatin-adduct formation were observed at the time-point analysed (Supplementary Fig. 2e–h). As expected, none of these parameters was changed in the docetaxel setting (Supplementary Fig. 2i–m).

To assess whether the anti-CSF-1R-mediated therapeutic synergy was unique to cisplatin or could be extended to drugs with a similar mechanism of action, we tested another platinum-containing drug, oxaliplatin, and also found that the survival benefit of oxaliplatin was improved by combined CSF-1R blockade (Fig. 1i and Supplementary Fig. 2n). These data demonstrate that anti-CSF-1R acts synergistically with platinum-based chemotherapeutic drugs to extend the survival of mammary tumour-bearing KEP mice.

CSF-1R inhibition alters the innate immune landscape of KEP tumours

Macrophages are key orchestrators of the inflammatory TME[28]. Thus, we set out to assess the effect of anti-CSF-1R on the innate immune landscape of KEP tumours. Despite the strong reduction of $CD11b^+F4/80^+$ TAMs on anti-CSF-1R, up to 20% of the intratumoural $CD45^+$ immune cells still expresses the macrophage marker F4/80 (Fig. 1d). Detailed analysis of this surviving $CD11b^+F4/80^+$ population revealed that an increased proportion of these cells expresses the inflammatory monocyte marker Ly6C compared to $CD11b^+F4/80^+$ cells in control antibody-treated tumours (Fig. 2a and Supplementary Fig. 3a). Moreover, the surviving $CD11b^+F4/80^+$ cells in cisplatin + anti-CSF-1R-treated tumours express elevated levels of the co-stimulatory molecules CD80 and CD86, slightly elevated MHCII levels, decreased levels of the chemokine receptors C-C chemokine receptor type 2 (CCR2) and CX3C chemokine receptor 1 (CX3CR1), and increased levels of programmed cell death 1 ligand 1 (PD-L1) compared to intratumoural $CD11b^+F4/80^+$ cells in cisplatin + control antibody-treated mice (Fig. 2b–g). Furthermore, in the independent orthotopically transplanted *K14cre;Trp53$^{F/F}$* (KP) mammary tumour model, intratumoural $CD11b^+F4/80^+$ myeloid cells remaining after CSF-1R inhibition display an altered phenotype corresponding to that in anti-CSF-1R-treated KEP tumours (Fig. 2h–m). Thus, anti-CSF-1R depletes the majority of $CD11b^+F4/80^+$ TAMs, whereas a small population of $CD11b^+F4/80^+$ cells with a distinct phenotype survives. To explore whether these surviving cells could derive from circulating monocytes, we transferred $tdTomato^+$ monocytes into control antibody or anti-CSF-1R-treated tumour-bearing KEP mice. After 4 d, the transferred monocytes that infiltrated tumours of anti-CSF-1R-treated, and not control antibody-treated, animals partially acquired the phenotype of the surviving intratumoural $CD11b^+F4/80^+$ cell population (that is, loss of CX3CR1 and elevated PD-L1 expression) (Supplementary Fig. 3b–d). These findings suggest that the surviving $CD11b^+F4/80^+$ cells in anti-CSF-1R-treated tumours may derive from newly recruited circulating monocytes, although other mechanisms cannot be excluded.

Whereas in treatment-naive KEP tumours the macrophage/neutrophil ratio is approximately 3/1, in anti-CSF-1R-treated tumours, either in the presence or absence of cisplatin, this ratio is reversed (Fig. 1d,e). However, the absolute number of intratumoural neutrophils was not increased upon CSF-1R inhibition (Supplementary Fig. 3e). Anti-CSF-1R treatment induced an increase in the number of monocytes and a modest, but not significant, and very variable increase in the number of intratumoural eosinophils and mast cells (Supplementary Fig. 3f–h). Together, these data show that cisplatin + anti-CSF-1R synergy is accompanied by changes in the myeloid immune landscape of tumours. Most notably, anti-CSF-1R treatment resulted in a surviving population of $CD11b^+F4/80^+$ cells with an altered

phenotype.

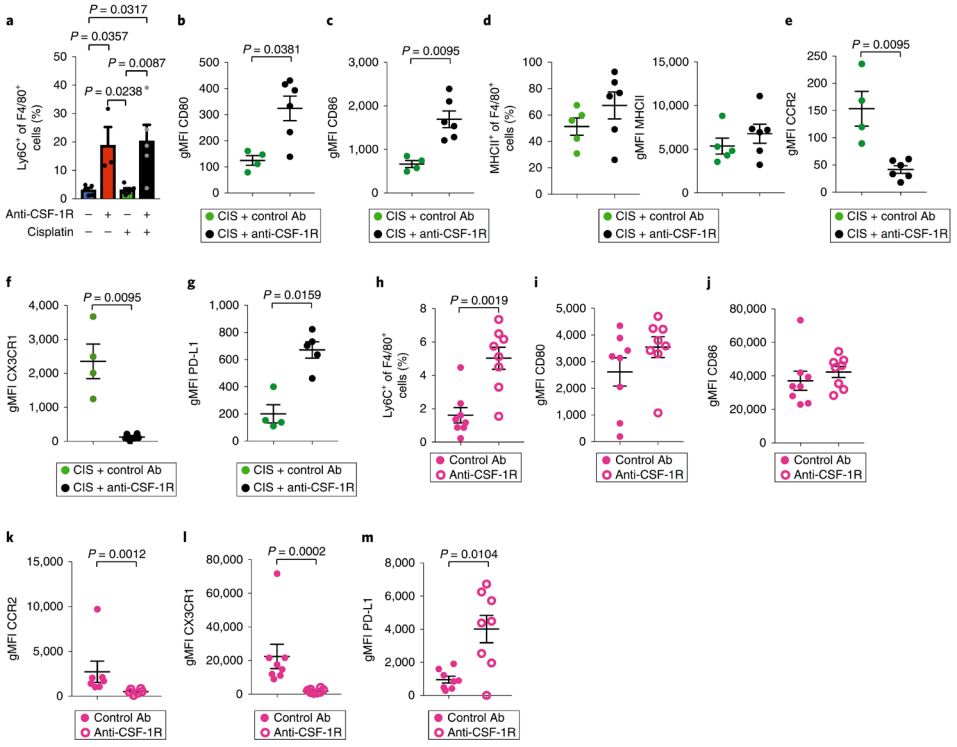


Fig. 2| Characterization of F4/80⁺ cells by flow cytometry in spontaneous KEP tumours and in orthotopically transplanted KP tumours after anti-CSF-1R treatment. a, Percentage of CD11b⁺F4/80⁺ immune cells expressing Ly6C in end-stage KEP tumours (untreated: *n* = 5 animals; anti-CSF-1R: *n* = 3 animals; cisplatin: *n* = 6 animals; cisplatin + anti-CSF-1R: *n* = 5 animals). **b**,**c**, Geometric mean fluorescence intensity (gMFI) of CD80 (**b**) and CD86 (**c**) expression on F4/80⁺Siglec F⁻ cells in KEP tumours (cisplatin + control Ab: *n* = 4 animals; cisplatin + anti-CSF-1R: *n* = 6 animals). **d**, Percentage of MHCII-expressing F4/80⁺Siglec F⁻ cells (left) and gMFI (right) of MHCII on F4/80⁺Siglec F⁻ in the KEP tumours (cisplatin + control Ab: *n* = 5 animals; cisplatin + anti-CSF-1R: *n* = 6 animals). gMFI was calculated by subtracting the gMFI of the MHCII-negative population from the gMFI of the MHCII-positive population. **e**–**g**, gMFI of CCR2 (**e**), CX3CR1 (**f**) and PD-L1 (**g**) expression on F4/80⁺Siglec F⁻ cells in KEP tumours (CCR2 and CX3CR1: cisplatin + control Ab: *n* = 4 animals; cisplatin + anti-CSF-1R: *n* = 6 animals; PD-L1: cisplatin + control Ab: *n* = 4 animals; cisplatin + anti-CSF-1R: *n* = 5 animals). **h**–**m**, KP tumour pieces were orthotopically transplanted in the mammary fat pad of FVB/N mice. The percentage of CD11b⁺F4/80⁺Siglec F⁻ immune cells expressing Ly6C in time-point-sacrificed KP tumours (**h**). gMFI of CD80 (**i**), CD86 (**j**), CCR2 (**k**), CX3CR1 (**l**) and PD-L1 (**m**) expression on F4/80⁺Siglec F⁻ cells in time-point-sacrificed KP tumours (*n* = 8 animals per group, except CCR2: control Ab: *n* = 7 animals, anti-CSF-1R: *n* = 6 animals). The gMFI values presented in **b**, **c**, **e**–**g** and **i**–**m** were determined by subtracting the gMFIs of the fluorescence minus one staining from the gMFI of the full staining. Data presented in **a**–**m** are mean ± s.e.m., and statistical analysis was performed using the two-tailed Mann–Whitney test.

Macrophage blockade enhances cisplatin response by unleashing intratumoural type I IFN signalling

To better characterize the phenotype of the anti-CSF-1R-surviving intratumoural $CD11b^+F4/80^+$ cells, next-generation RNA sequencing (RNA-seq) analysis was performed on $CD11b^+F4/80^+$ cells sorted from cisplatin + control antibody-treated or cisplatin + anti-CSF-1R-treated tumours. Hierarchical clustering of the top 400 variable genes revealed that $CD11b^+F4/80^+$ cells from cisplatin + anti-CSF-1R-treated tumours displayed a different transcriptome profile, mainly characterized by a strong enrichment of genes involved in type I IFN signalling and type I IFN production, whereas cell-cycle-associated genes were reduced (Fig. 3a,b). Interestingly, CSF-1R expression levels were lower in the remaining $CD11b^+F4/80^+$ cells from cisplatin + anti-CSF-1R-treated tumours (fold change: −2,04; $P = 3.63 \times 10^{-5}$), perhaps explaining why these cells resisted anti-CSF-1R therapy. In parallel, we also performed RNA-seq on flow-sorted $Ly6G^+Ly6C^{low}$ neutrophils isolated from tumours of cisplatin + control antibody-treated and cisplatin + anti-CSF-1R-treated KEP mice. Hierarchical clustering of the top 400 variable genes within this data set revealed that anti-CSF-1R treatment also had a significant effect on the transcriptome profile of tumour-associated neutrophils (Supplementary Fig. 4a). To ensure that these transcriptome alterations in neutrophils are not a direct effect of anti-CSF-1R on neutrophils, but rather an indirect consequence of macrophage targeting, we performed gene set enrichment analysis (GSEA) of target genes of early growth receptor 2 (EGR2), a transcription factor downstream of CSF-1R signalling[29]. No differences were observed in the expression of EGR2 target genes between neutrophils isolated from anti-CSF-1R-treated and control antibody-treated tumours (Supplementary Fig. 4b), suggesting that neutrophils are not directly influenced by anti-CSF-1R. Interestingly, BiNGO analysis of the top 100 upregulated and downregulated genes and Ingenuity pathway analysis of the differentially expressed genes revealed an enrichment in genes involved in type I IFN signalling in neutrophils isolated from cisplatin + anti-CSF-1R-treated tumours versus cisplatin + control antibody-treated tumours (Supplementary Fig. 4c,d and Supplementary Table 3). These data indicate that the therapeutic benefit of cisplatin + anti-CSF-1R is accompanied by induction of type I IFN-stimulated genes (ISGs) in both intratumoural $CD11b^+F4/80^+$ cells and neutrophils.

We hypothesized that the enrichment of ISGs in these intratumoural immune populations was a consequence of increased levels of type I IFNs in KEP tumours upon CSF-1R blockade. Indeed, by using primers hybridizing to all *Ifna* genes, mRNA expression of *Ifna*, but not *Ifnb*, was increased in tumours of cisplatin + anti-CSF-1R-treated KEP mice compared to cisplatin + control antibody-treated mice (Fig. 3c). In line with this, the mRNA levels of various intracellular pattern recognition receptors, such as *Tlr3*, *Rig1* and *Ifih1*, whose signals induce type I IFN production, were upregulated in cisplatin + anti-CSF-1R-treated tumours compared to cisplatin + control antibody treatment (Fig. 3d). Notably, the increase in type I IFN expression upon anti-CSF-1R was independent of chemotherapy treatment, as a similar intratumoural increase in *Ifna* expression was observed upon anti-CSF-1R alone (Fig. 3e) or with docetaxel + anti-CSF-1R (Supplementary Fig. 5a). We also confirmed the increased expression of *Ifna*—and of two ISGs, *Isg15* and *Oas1a*—

upon anti-CSF-1R treatment in the independent KP-based tumour transplantation model and in inoculated MC38 colorectal adenocarcinoma tumours[21] (Fig. 3f,g and Supplementary Fig. 5b,c). Together, these data demonstrate that anti-CSF-1R induces type I IFN in the TME.

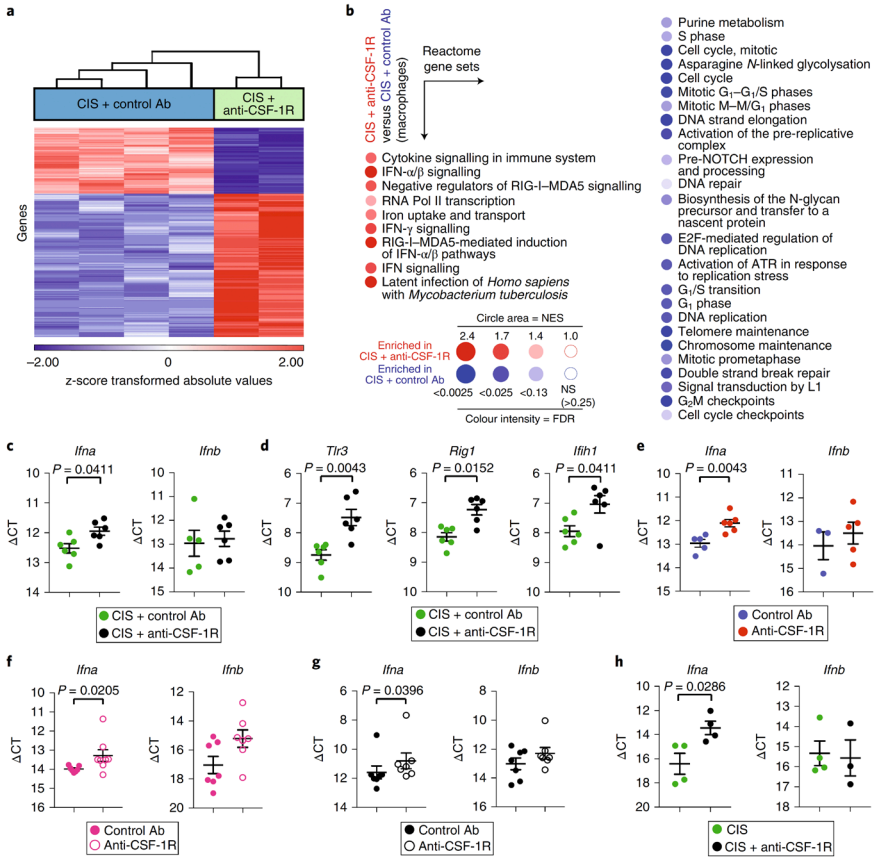


Fig. 3 | CSF-1R inhibition alters TAM phenotype and induces type I IFN signalling in the TME. a, Hierarchical clustering of the top 400 variable genes between CD11b$^+$F4/80$^+$ cells isolated from KEP tumours treated with cisplatin + control Ab (n = 4 animals) and cisplatin + anti-CSF-1R (n = 2 biologically independent samples, a pool of five mice each). Fold change ≥ 1.5; P value with FDR correction ≤ 0.05. Statistical analysis was performed using two-way ANOVA. **b**, BubbleGUM visualization of GSEA using reactome gene sets comparing CD11b$^+$F4/80$^+$ cells from cisplatin + anti-CSF-1R-treated tumours versus macrophages from cisplatin + control Ab-treated tumours. Same mice as in **a**. Normalized enrichment score (NES) ≥ 1, FDR value: ≤0.25. The enrichment score was calculated using a weighted Kolmogorov–Smirnov-like statistic. MDA5, melanoma differentiation-associated protein 5 (encoded by *Ifih1*); Pol, polymerase; RIG-I, retinoic acid inducible gene I; ATR, ATM and Rad3-related; NS, not significant. **c**, Transcripts of *Ifna* (n = 6 animals per group) and *Ifnb* (n = 5 animals in cisplatin + control Ab; n = 6 animals in cisplatin + anti-CSF-1R). **d**, *Tlr3*, *Rig1* and *Ifih1* in KEP mammary tumours isolated 1 d after the second cisplatin injection were determined by quantitative PCR and normalized to β-actin (n = 6 animals per group). **e**–**g**, Transcripts of *Ifna* and *Ifnb* in KEP mammary tumours (*Ifna*: n = 5 animals in control Ab, n = 6 animals in anti-CSF-1R; *Ifnb:* n = 3 animals in control Ab, n = 5 animals in anti-CSF-1R) (**e**), orthotopically transplanted KP mammary tumour (*Ifna:* n = 7 animals in control Ab, n = 8 animals in anti-CSF-1R; *Ifnb:* n = 7 animals per group) (**f**) and subcutaneously inoculated MC38 tumours (n = 7 animals per group) (**g**) treated with control Ab and anti-CSF-1R were determined by quantitative PCR

and normalized to β-actin. Mice were analysed at a tumour size of 100 mm^2 (KP) or after 12 d from the start of the treatment (MC38). **h**, Transcripts of *Ifna* (*n* = 4 animals per group) and *Ifnb* (*n* = 4 animals in cisplatin, *n* = 3 animals in cisplatin + anti-CSF-1R) in $CD11b^+F4/80^+$ cells isolated from end-stage KEP tumours were determined by quantitative PCR and normalized to β-actin. Graphs in **c–h** show the mean ± s.e.m. in ΔCT values, and statistical analysis was performed using the two-tailed Mann–Whitney test.

To pursue the cellular source of type I IFN, we flow-sorted different cell populations from cisplatin and cisplatin + anti-CSF-1R-treated KEP tumours (Supplementary Fig. 5d) and compared *Ifna* and *Ifnb* transcript levels. Plasmacytoid dendritic cells are known for their ability to produce type I IFN; however, as very few plasmacytoid dendritic cells—less than 0.1% of the total intratumoural immune population—are present in KEP tumours (Supplementary Fig. 5e,f), we could not recover RNA of sufficient quality. Likewise, we did not obtain RNA of sufficient quality from sorted $CD31^+$ endothelial cells. Only the $CD11b^+F4/80^+$ immune cell population displayed elevated *Ifna* expression levels upon CSF-1R blockade (Fig. 3h and Supplementary Fig. 5g,h). In line with these in vivo findings, in vitro treatment of bone marrow-derived macrophages (BMDMs) with anti-CSF-1R modestly induces *Ifna* levels after 24 h of culture (Supplementary Fig. 5i). These analyses suggest that the surviving population of intratumoural $CD11b^+F4/80^+$ cells is an important source of IFN-α in cisplatin + anti-CSF-1R-treated KEP tumours.

To dissect the functional significance of type I IFN signalling in the therapeutic benefit of cisplatin + anti-CSF-1R therapy, we blocked the IFN-α/β receptor subunit 1 (IFNAR1) in KEP mice. Whereas blockade of type I IFN signalling did not influence the anticancer efficacy of cisplatin, anti-IFNAR1 treatment completely abrogated the synergistic effect of cisplatin + anti-CSF-1R treatment (Fig. 4a). These findings reveal that therapeutic targeting of macrophages with anti-CSF-1R in tumour-bearing KEP mice unleashes intratumoural type I IFN signalling, which enhances the therapeutic efficacy of cisplatin.

Emactuzumab treatment induces intratumoural type I ISGs in patients with cancer
To validate our preclinical findings that CSF-1R blockade unleashes intratumoural type I IFN signalling in patients, we compared ISG expression levels in pre-treatment and on-treatment tumour biopsies from patients with advanced solid tumours treated with emactuzumab (RG7155), a humanized anti-human CSF-1R monoclonal antibody (NCT01494688)21,30. Gene expression profiling was performed on tumour biopsies taken before the start of treatment and after 4 weeks of emactuzumab therapy. We assessed the expression level of a set of 28 ISGs that was selected based on the RNA-seq results from our KEP mouse model (Fig. 3a, Supplementary Fig. 4a,c,d and Supplementary Table 3). The intratumoural expression of all 28 selected ISGs was increased in emactuzumab on-treatment biopsies versus pre-treatment biopsies, of which 11 ISGs were significantly upregulated (Fig. 4b,c). Thus, in line with our preclinical studies, these clinical findings indicate that CSF-1R blockade is a powerful strategy to augment intratumoural type I IFN signalling.

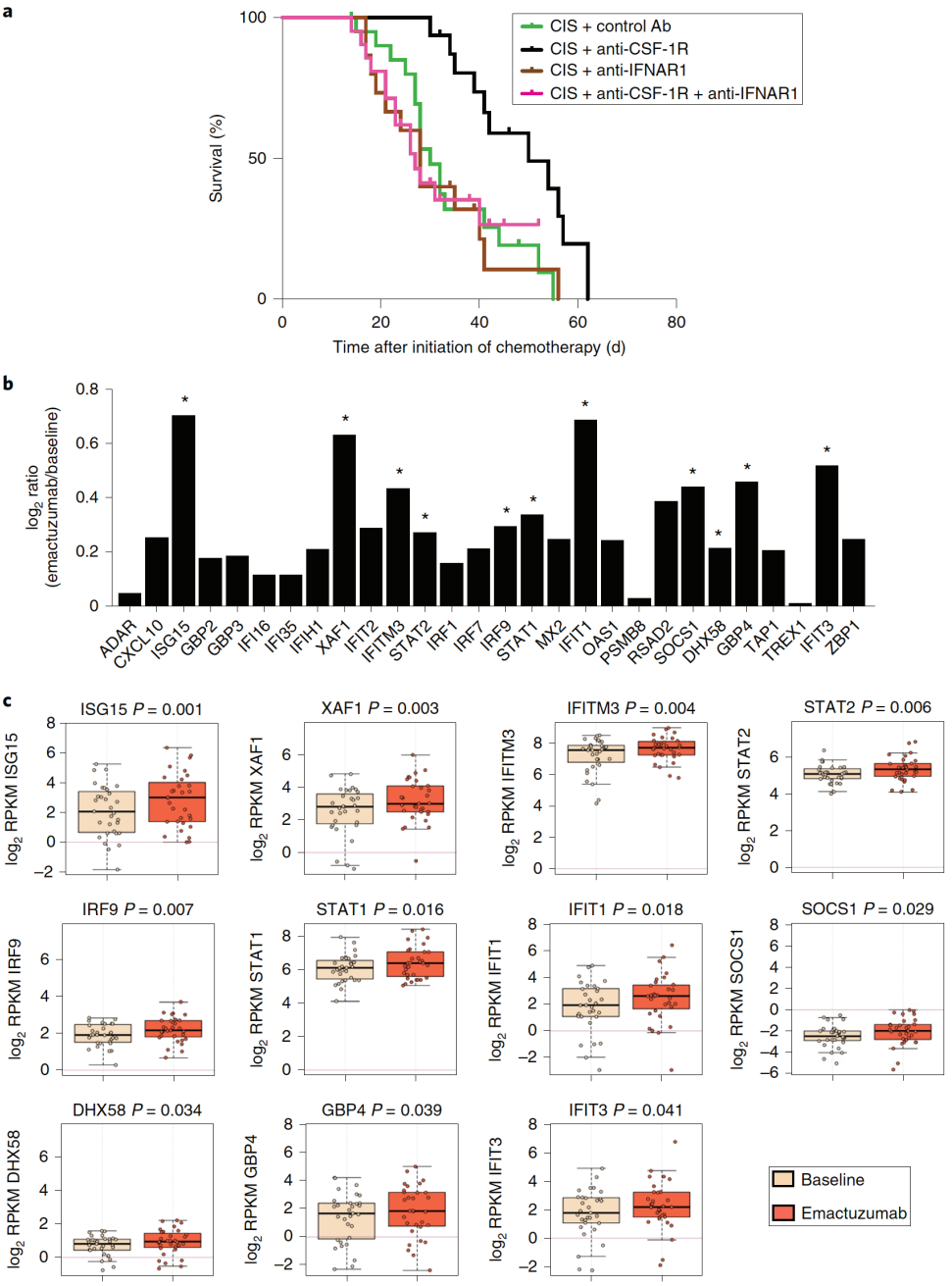


Fig. 4 | CSF-1R blockade increases the expression of intratumoural type I IFN signalling in patients with cancer treated with emactuzumab and is essential for the therapeutic synergy of cisplatin + anti-CSF-1R in the KEP mouse model. a, Kaplan–Meier tumour-specific survival curves of KEP mice treated with cisplatin + control Ab, cisplatin + anti-CSF-1R (same groups as in Fig. 1f), cisplatin + anti-IFNAR1 ($n = 15$ animals) or cisplatin + anti-CSF-1R + anti-IFNAR1 ($n = 21$ animals). Cisplatin + anti-CSF-1R versus cisplatin + anti-CSF-1R + anti-IFNAR1: $P = 0.0064$ (two-tailed log-rank test). **b**, $\log_2$ ratio of

intratumoural expression levels of 28 type I ISGs in emactuzumab (anti-CSF-1R)-treated patients (n = 31 patients) normalized against the pre-treatment expression levels. **c**, Box plots of the expression level of the 11 statistically significant upregulated type I ISGs in tumours of emactuzumab-treated patients (data from **b**, indicated by asterisks). Expression levels in the pre-treatment (baseline) tumour biopsies are compared to on-treatment (emactuzumab) biopsies. The top-most line is the maximum, the top of the box is the third quartile, the centre line is the median, the bottom of the box is the first quartile and the bottom-most line is the minimum. RPKM, reads per kilobase of exon per million mapped reads. The P values were determined by a two-tailed Student's t-test.

Combined CSF-1R inhibition and neutrophil depletion engages antitumour immunity that further improves the therapeutic benefit of cisplatin

Type I IFNs are emerging as key regulators of cancer growth and therapy response[31,32]. Type I IFNs can affect cancer biology via different mechanisms, including the induction of anti-proliferative and pro-apoptotic effects on IFNAR$^+$ cancer cells[33,34]. Indeed, exposure of a cell line derived from a spontaneous KEP mammary tumour to recombinant IFN-α1 results in a dose-dependent decrease in colony-forming ability, also in combination with cisplatin, suggesting that type I IFNs have a direct inhibitory effect on KEP cancer cells (Fig. 5). Because type I IFNs are also key orchestrators of antitumour immunity[33,34,35], we hypothesized that the anti-CSF-1R-induced type I IFN-enriched TME may foster antitumour CD8$^+$ T cell activity. However, we observed fewer numbers of tumour-infiltrating CD4$^+$ or CD8$^+$ T cells in cisplatin + anti-CSF-1R-treated tumours than in cisplatin + control antibody-treated tumours (Supplementary Fig. 6a–c), and the CD8/regulatory T cell ratio was not affected (Fig. 6a). More natural killer (NK) cells were infiltrating the cisplatin + anti-CSF-1R-treated KEP tumours; however, the number of granzyme B$^+$ cells was not affected compared to cisplatin + control antibody treatment (Fig. 6b,c and Supplementary Fig. 6d). We previously reported that cisplatin efficacy is independent of the adaptive immune system[3], and, in line with the lack of more intratumoural granzyme B$^+$ cells and T cells, here, we also show that antibody-mediated depletion of CD8$^+$ T cells does not reduce the therapeutic efficacy of cisplatin + anti-CSF-1R therapy (Fig. 6d). In addition, genetic ablation of the entire adaptive immune system by crossing KEP mice with *Rag1*$^{-/-}$ mice did not affect therapeutic synergy (Fig. 6g). These data indicate that the anti-CSF-1R-mediated conversion of the TME into a type I IFN-enriched milieu in cisplatin-treated mice is not sufficient to successfully engage an endogenous antitumour T cell response.

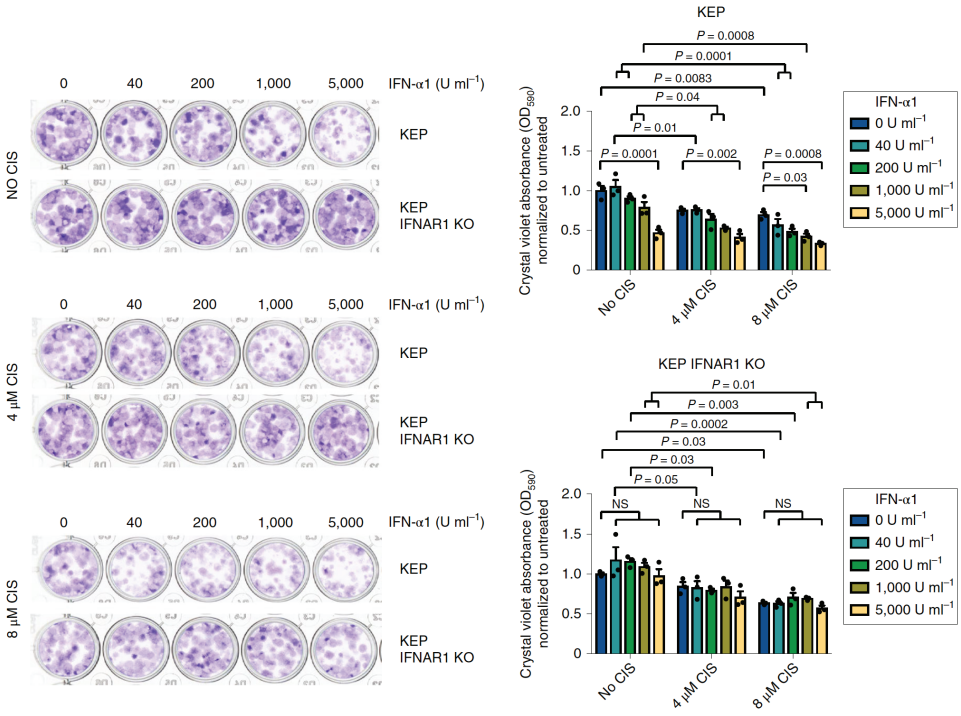


Fig. 5 | Direct inhibitory effect of IFN-α1 on a KEP-derived cancer cell line. Representative images of a colony-forming assay with KEP-derived cancer cells and IFNAR1 KO KEP cancer cells treated with increasing concentrations of IFN-α1 and cisplatin. After 7 d, crystal violet was dissolved and absorbance was measured at 590 nm. Data are representative of three independent experiments. Data are mean ± s.e.m. The *P* value was determined by two-way ANOVA with Tukey's multiple comparison test.

We next hypothesized that it may be necessary to breach an additional layer of immunosuppression before antitumour immunity can be unleashed. The most abundant immune cell population in cisplatin + anti-CSF-1R-treated KEP tumours is neutrophils (Fig. 1e) and we have previously reported that KEP tumour-educated neutrophils are very immunosuppressive[36]. To address whether neutrophils impede antitumour immunity in cisplatin + anti-CSF-1R-treated mice, we treated tumour-bearing KEP mice with the neutrophil-specific anti-Ly6G antibody (clone 1A8). Immunohistochemistry for S100A9 confirmed a reduction in the number of neutrophils in the lungs and to a lesser extent in the tumour (Supplementary Fig. 6e,f). Cisplatin + anti-CSF-1R + anti-Ly6G treatment significantly improved tumour control and prolonged the survival of KEP mice compared to cisplatin + anti-CSF-1R therapy (Fig. 6e). Whereas cisplatin + anti-CSF-1R temporarily stabilizes tumour outgrowth, we observed tumour shrinkage in six out of ten mice treated with cisplatin + anti-CSF-1R + anti-Ly6G, and the mammary tumours of two of these mice regressed completely during treatment (Supplementary Fig. 6g,h). Anti-Ly6G treatment alone failed to influence primary tumour growth in KEP mice

as previously shown[36], neither did the combination of anti-CSF-1R + anti-Ly6G (Supplementary Fig. 6i) nor did anti-Ly6G alter the efficacy of cisplatin (Fig. 6e). Further characterization of cisplatin + anti-CSF-1R + anti-Ly6G-treated KEP tumours showed a significant reduction in the number of $BrdU^+$-proliferating cells and γ-$H2AX^+$ DNA-damaged cells (Supplementary Fig. 6j,k). No statistically significant differences were observed in the number of apoptotic cells, $CD31^+$ vessels and cisplatin adducts (Supplementary Fig. 6l–n). Interestingly, the CD8/regulatory T cell ratio, the absolute number of NK cells and the absolute and relative number of granzyme B^+ immune cells were increased in cisplatin + anti-CSF-1R + anti-Ly6G-treated tumours compared to cisplatin + control antibody therapy (Fig. 6a–c and Supplementary Fig. 6d). Importantly, the additional therapeutic benefit obtained by anti-Ly6G treatment was partially lost after antibody-mediated depletion of $CD8^+$ T cells or NK cells (Fig. 6e,f) and was completely abrogated when the same treatment was performed in KEP;*Rag1*$^{-/-}$ mice (Fig. 6g). Collectively, these data indicate that the combined anti-CSF-1R-mediated conversion of the tumour milieu into a type I IFN-enriched environment and the relieve of neutrophil-dependent immunosuppression fosters engagement of antitumour immunity in the anticancer effect of cisplatin in this poorly immunogenic mouse tumour model.

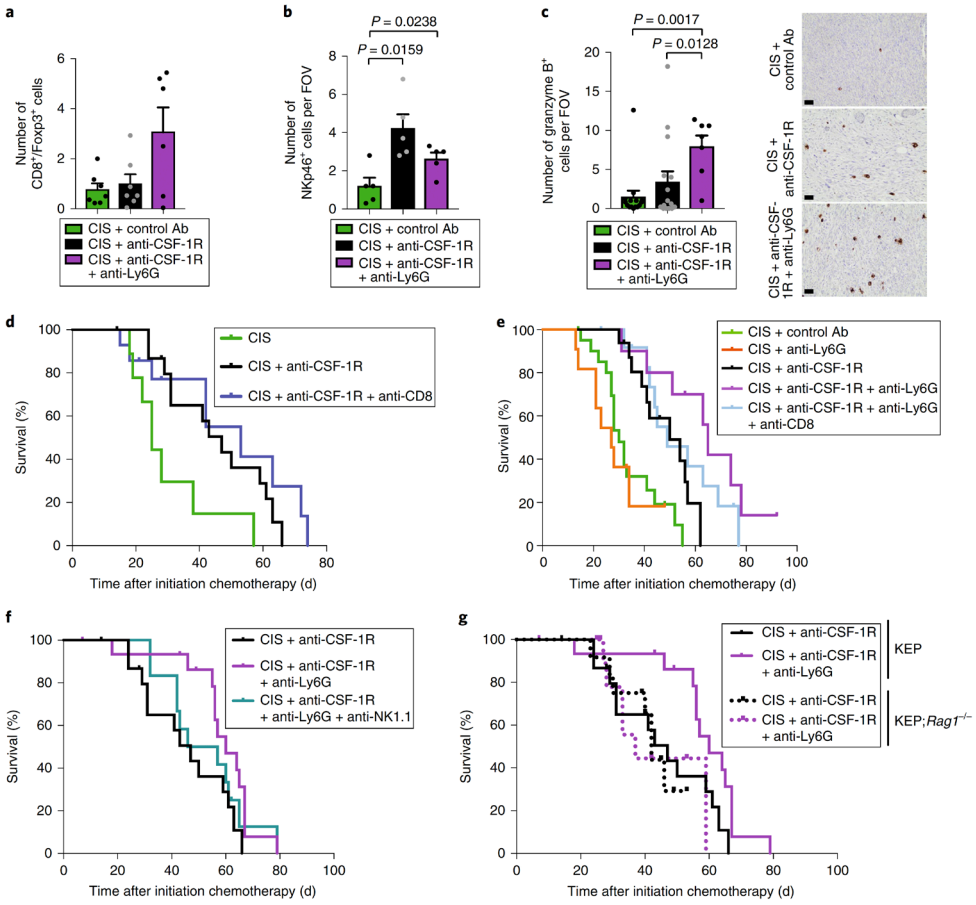


Fig. 6 | Neutrophil inhibition engages antitumour immunity and further improves cisplatin + anti-CSF-1R efficacy. a, $CD8^+$ T cell/$Foxp3^+$ T cell ratio based on immunohistochemistry staining in the tumour of time-point-sacrificed KEP mice (cisplatin + control Ab and cisplatin + anti-CSF-1R: $n = 7$ animals; cisplatin + anti-CSF-1R + anti-Ly6G: $n = 6$ animals). **b**,**c**, Quantification of $NKp46^+$ cells (**b**) and granzyme B^+ cells (**c**) in viable areas of mammary tumours of time-point-sacrificed KEP mice treated with cisplatin + control Ab (NKp46: $n = 5$ animals; granzyme B: $n = 15$ animals), cisplatin + anti-CSF-1R (NKp46: $n = 5$ animals; granzyme B: $n = 15$ animals) and cisplatin + anti-CSF-1R + anti-Ly6G (NKp46: $n = 5$ animals; granzyme B: $n = 7$ animals). The values represent the average number of positive cells per FOV quantified by counting five high-power microscopic fields per tumour. Representative granzyme B immunohistochemistry stainings are shown (**c**). Scale bars, 50 µm. **d**, Kaplan–Meier tumour-specific survival curves of KEP mice treated with cisplatin + control Ab ($n = 6$ animals), cisplatin + anti-CSF-1R ($n = 16$ animals) and cisplatin + anti-CSF-1R + anti-CD8 ($n = 14$ animals). Cisplatin + anti-CSF-1R + anti-CD8-treated mice versus cisplatin + anti-CSF-1R-treated mice: $P = 0.3728$ (two-tailed log-rank test). **e**, Kaplan–Meier tumour-specific survival curves of KEP mice treated with cisplatin + control Ab, cisplatin + anti-CSF-1R (same groups as in Fig. 1f), cisplatin + anti-Ly6G ($n = 11$ animals), cisplatin + anti-CSF-1R + anti-Ly6G ($n = 10$ animals) or cisplatin + anti-CSF-1R + anti-Ly6G + anti-CD8 ($n = 13$ animals). Cisplatin + anti-CSF-1R-treated mice versus cisplatin + anti-CSF-1R + anti-Ly6G-treated mice: $P = 0.0085$; cisplatin + anti-CSF-1R-treated mice versus cisplatin + anti-CSF-1R + anti-Ly6G + anti-CD8-treated mice: $P = 0.1104$ (two-tailed log-rank test). **f**, Kaplan–Meier tumour-specific survival curves of KEP mice treated with cisplatin + anti-CSF-1R ($n = 16$ animals, same curve as in **d**), cisplatin + anti-CSF-1R + anti-Ly6G ($n = 17$ animals of which 4 mice were treated with cisplatin + anti-CSF-1R + anti-Ly6G + IgG2a; no differences were observed between cisplatin + anti-CSF-1R + anti-Ly6G

and cisplatin + anti-CSF-1R + anti-Ly6G + IgG2a), or cisplatin + anti-CSF-1R + anti-Ly6G + anti-NK1.1 (n = 12 animals). Cisplatin + anti-CSF-1R-treated mice versus cisplatin + anti-CSF-1R + anti-Ly6G-treated mice: P = 0.0226; cisplatin + anti-CSF-1R-treated mice versus cisplatin + anti-CSF-1R + anti-Ly6G + anti-NK1.1-treated mice: P = 0.4073 (two-tailed log-rank test). **g**, Kaplan–Meier tumour-specific survival curves comparing cisplatin + anti-CSF-1R and cisplatin + anti-CSF-1R + anti-Ly6G treatment in KEP (same as in **f**) and KEP;*Rag1*$^{-/-}$ mice. Cisplatin + anti-CSF-1R in KEP;*Rag1*$^{-/-}$ (n = 12 animals) and cisplatin + anti-CSF-1R + anti-Ly6G in KEP;*Rag1*$^{-/-}$ (n = 11 animals). Cisplatin + anti-CSF-1R + anti-Ly6G-treated KEP;*Rag1*$^{-/-}$ mice versus cisplatin + anti-CSF-1R-treated KEP;*Rag1*$^{-/-}$ mice: P = 0.9597 (two-tailed log-rank test). Data presented in **a**–**c** are mean ± s.e.m., and statistical analysis was performed using the two-tailed Mann–Whitney test.

Discussion

There is a growing realization that immune-mediated mechanisms influence the responsiveness of tumours to chemotherapy[1]. Notably, macrophages actively interfere with the therapeutic efficacy of chemotherapy via several mechanisms in mouse tumour models, including suppression of antitumour immunity through IL-10 secretion[5], secretion of chemoprotective proteases such as cathepsins[12] or secretion of lysophospholipids[15] that interfere with the DNA damage response. These macrophage-mediated chemotherapy resistance mechanisms are dependent on the production of soluble mediators from TAMs. Our study reveals a conceptually different mechanism of how therapeutic targeting of macrophages improves chemotherapy efficacy. Through in vivo mechanistic studies in the KEP transgenic mouse model for breast cancer, we demonstrate that macrophage inhibition with anti-CSF-1R induces intratumoural type I IFN signalling, which acts synergistically with cisplatin to inhibit tumour outgrowth and extend survival.

There is a growing interest in the effect of type I IFNs on cancer behaviour and response to immune checkpoint inhibitors, radiotherapy and chemotherapy[32,37,38,39]. Besides being associated with an improved prognosis[40,41,42], an intratumoural IFN signature in patients with breast cancer has been correlated with improved chemotherapy response[37], and preclinical studies reported that type I IFN enhanced chemotherapy efficacy[37,43]. However, IFN-related gene signatures have also been correlated with chemotherapy resistance[44], consistent with a pleomorphic and still poorly understood role of type I IFN signalling in the tumour context. Importantly, impaired type I IFN signalling is a prominent feature of immune dysfunction in patients with cancer[45]. Our study reveals that anti-CSF-1R represents a powerful approach to induce intratumoural IFN signalling and to sensitize tumours to cisplatin. Notably, we find that anti-CSF-1R treatment in patients with cancer also results in increased intratumoural expression of ISGs, confirming our findings that anti-CSF-1R unleashes type I IFN response in tumours.

Our study shows that anti-CSF-1R depletes the majority of F4/80$^+$ TAMs; however, a small intratumoural CD11b$^+$F4/80$^+$ population with a distinct phenotype survives. Interestingly, these surviving cells express lower levels of *Csf1r* and significantly higher *Ifna* mRNA levels than the CD11b$^+$F4/80$^+$ cells in untreated tumours, probably accounting for the increased *Ifna* levels in the tumours. A shift in

macrophage phenotype was also observed in pancreatic cancer and glioblastoma models upon interference with the CSF-1–CSF-1R pathway[46,47,48,49]. Similar to our model, targeting CSF-1 in the pancreatic cancer models on the one hand depleted TAMs and on the other hand reprogrammed the remaining macrophages to an antitumour phenotype. Interestingly, type I IFN was also found to be increased in these macrophages[49]; however, its effect was not functionally pursued in this study. These data, combined with our observation that IFN-α is also upregulated in anti-CSF-1R-treated MC38 colon adenocarcinoma tumours, indicate that anti-CSF-1R-mediated induction of type I IFNs is not limited to breast cancer, but extends to other cancer types.

Type I IFNs can directly affect cancer cells by inducing apoptosis or blocking proliferation, or indirectly by stimulating antitumour immune responses or inhibiting angiogenesis[33]. In line with the observed in vivo reduction of proliferating tumour cells upon anti-CSF-1R therapy, our in vitro studies indicate that IFN-α1 can directly suppress KEP cancer cells. We did not observe an effect of CSF-1R inhibition on the number of intratumoural blood vessels or their pericyte coverage, excluding an angiogenesis effect. Despite a key role for type I IFNs in dictating antitumour immunity[31,32], the increase in the number of intratumoural type I IFNs was not sufficient to induce effective antitumour T cell responses. In line with the immunosuppressive phenotype of tumour-educated neutrophils in KEP mice[36] and in other models[50], the additional ablation of neutrophils stimulated antitumour immunity. It may be surprising that we observed a therapeutic benefit of depletion of neutrophils with an IFN gene signature in cisplatin + anti-CSF-1R-treated KEP mice, whereas some studies have suggested that type I IFNs can induce antitumour properties in neutrophils[51]. However, in line with our data, a type I IFN transcriptional signature in neutrophils in malaria-infected hosts and in patients with active tuberculosis correlated with tissue damage and disease pathogenesis[52,53], suggesting that, in these settings, type I IFN signalling in neutrophils may contribute to their harmful actions. In addition, although type I IFNs are often considered to exert antitumour functions, several studies on chronic viral infections show negative-feedback mechanisms when persistently present in the environment by, for example, generating an immunosuppressive milieu[34,54,55]. Perhaps in our study a similar mechanism is involved, explaining why the cytotoxic activity of platinum-based chemotherapy is enhanced by type I IFNs, but at the same time, this therapeutic synergy is limited by an immunosuppressive programme. Although T cell activation was implicated in controlling tumour growth upon combined macrophage and neutrophil depletion in a mouse model for pancreatic cancer[20], the full mechanism in the context of chemotherapy was not completely resolved. Our in vivo data demonstrate that, although the release of type I IFN is necessary for cisplatin + anti-CSF-1R therapeutic synergy, it takes further depletion of neutrophils to engage an antitumour immune response during cisplatin treatment.

Interestingly, the platinum-based drugs cisplatin and oxaliplatin synergized with anti-CSF-1R treatment, whereas docetaxel did not, despite the induction of IFN-α in the docetaxel setting. It will be important to mechanistically understand how the type of chemotherapy dictates its ability to act in synergy with type I IFN signalling. These

insights will facilitate the development of optimal combination therapies of CSF-1R-targeting drugs or other type I IFN-inducing agents, including STING (stimulator of IFN genes) agonists[56], with chemotherapeutic agents. To maximize the therapeutic benefit of cytotoxic therapy in poorly immunogenic tumour types, it will be critical to simultaneously target neutrophil-dependent immunosuppression.

Methods

Mice

The generation and characterization of KEP mice have been previously described[24] and are commercially available via Taconic Biosciences. KEP mice were back-crossed onto the FVB/N background, and genotyping was performed by PCR analysis on tail-tip DNA as described[24,36]. KEP mice were crossed with *Rag1*$^{-/-}$ mice (FVB/N, a gift from L. Coussens, Oregon Health & Science University, Portland) to generate KEP;*Rag1*$^{-/-}$ mice[3]. Female KEP and KEP;*Rag1*$^{-/-}$ mice were monitored twice weekly for the spontaneous onset of mammary tumour formation by palpation starting at 4 months of age. Donor tumours from KEP and KP[24] mice were collected in ice-cold PBS, cut into small pieces and resuspended in DMEM F12 containing 30% FCS and 10% dimethyl sulfoxide and stored at −150 °C. The perpendicular tumour diameters of mammary tumours were measured twice a week using a caliper. Age-matched wild-type littermates were used as controls. Female FVB/N mice (10–12 weeks of age) were obtained from Charles River. mTmG mice[57] (back-crossed to the FVB/N background) express tdTomato ubiquitously and were used for the isolation of bone marrow monocytes. Mice were kept in individually ventilated cages at the animal laboratory facility of the Netherlands Cancer Institute (NKI; Amsterdam, the Netherlands). Food and water were provided ad libitum. Animal experiments were approved by the Animal Ethics Committee of the NKI and performed in accordance with institutional, national and European guidelines for animal care and use. The study is compliant with all relevant ethical regulations regarding animal research.

In vivo intervention studies

KEP mice bearing spontaneous mammary tumours were randomized over the treatment groups before initiation of the treatment. Mice were injected intraperitoneally with the chimeric (hamster/mouse) anti-CSF-1R antibody (clone 2G2, Roche Innovation Center Munich; single loading dose of 60 mg per kg followed by 30 mg per kg once a week); control antibody (IgG1, MOPC21, Roche Innovation Center Munich; single loading dose of 60 mg per kg followed by 30 mg per kg once a week); anti-Ly6G antibody (1A8, BioXCell; single loading dose of 400 μg followed by 100 μg three times a week); anti-IFNAR1 (MAR1-5A3, BioXCell; 100 μg three times a week); anti-CD8 (2.43, BioXCell; single loading dose of 400 μg followed by 100 μg three times a week); anti-NK1.1 (PK136, BioXCell; single loading dose of 400 μg followed by 100 μg three times a week); and IgG2a (C1.18.4, BioXCell; single loading dose of 400 μg followed by 100 μg three times a week). The maximum tolerated dose (MTD) dose of cisplatin (5 mg per kg; Accord Healthcare Limited) was administered intravenously every other week for a total of four cycles. The MTD dose of docetaxel (15 mg per kg; Accord Healthcare Limited) was administered

intravenously every week for a total of four cycles. The MTD dose of oxaliplatin (6 mg per kg diluted in NaCl; Fresenius Kabi) was administered intravenously every 10 days for three cycles.

Anti-CSF-1R, control antibodies, anti-Ly6G, anti-CD8 and anti-NK1.1 treatment started when mammary tumours reached a size of 25 mm^2; and anti-IFNAR1, cisplatin, docetaxel and oxaliplatin treatment started when mammary tumours reached a size of 50 mm^2. For survival curve experiments and end-stage analyses, antibody treatment continued until the tumour or the cumulative tumour burden reached a size of 225 mm^2. For survival curve experiments, an event is defined as an animal with a cumulative tumour size of 225 mm^2. The main cause of death of censored mice was ulcerated tumours or cisplatin-induced renal toxicity for cisplatin-treated mice.

For time-point analyses, mice were killed 1 d after the second chemotherapy injection (therapy-responsive phase) or at a tumour size of 100 mm^2 in chemotherapy-naive mice. To assess tumour cell proliferation, BrdU (50 mg per kg) was injected intraperitoneally into mice 90 min before being sacrificed.

KP tumour pieces were orthotopically transplanted into the mammary fat pad of 10–12-week-old FVB/N female mice. Before initiation of the treatment, mice were randomized over the experimental groups and treated either with control antibody or anti-CSF-1R as described above. Treatment started at a tumour size of 25 mm^2 and continued until the tumour reached a size of 100 mm^2 when the mice were sacrificed.

MC38 tumours were provided by Roche Innovation Center Munich. MC38 cells were subcutaneously injected into C57Bl6/N mice and, when the tumour volume reached 100 mm^3, treated with either control antibody or anti-CSF-1R as described above. Mice were sacrificed 5 d after the second treatment[21].

Intervention studies in the KEP-based spontaneous metastasis model

The orthotopic KEP-based spontaneous metastasis model was described previously in detail[27]. Briefly, KEP tumour pieces (1 × 1 mm) were orthotopically transplanted into 10–12-week-old FVB/N female mice. Mammary tumours were surgically removed once they reached a tumour size of 225 mm^2, after which mice were monitored and sacrificed when they reached the humane end point due to clinically overt metastatic disease. Tumour-bearing recipient mice were treated either with control antibody or with anti-CSF-1R once the mammary tumours reached 5 mm^2 (continuous setting) or 3 d after mastectomy (adjuvant setting). Antibody treatment continued until recipient mice developed clinical signs of distress caused by metastatic disease (for example, respiratory distress).

Histology, immunohistochemistry, immunofluorescence and RNA in situ hybridization

All histochemical and immunohistochemical analyses, except NKp46 immunohistochemistry, were performed by the Animal Pathology facility at the NKI. NKp46 immunohistochemistry was performed at the Histology core facility within the Cancer Research UK Beatson Institute (Glasgow, UK). For histochemical analysis, formalin-fixed tissues were processed, sectioned and stained as described[27]. Briefly, tissues were fixed for 24 h in 10% neutral-buffered formalin, embedded in paraffin, sectioned at 4 µm and stained with haematoxylin and eosin (H&E) for histopathological evaluation. H&E slides were digitally processed using the Aperio ScanScope (Aperio). For the quantitative assessment of areas in the tumour that had lost viability, slides were analysed with ImageJ by quantifying the percentage of non-viable areas (defined as areas that lost cellularity) over the total tumour area. Histochemistry for mast cells was performed with Toluidine blue.

For immunohistochemical analysis, paraffin sections were cut and deparaffinized. Antibodies and antigen retrieval methods are described in Supplementary Table 1. Cisplatin adduct staining was performed on frozen tissues embedded in OCT. Quantification of positive cells was performed manually by counting five high-power (40×) fields of view (FOVs) per tumour by two independent operators in a blinded manner. Samples were visualized with a BX43 upright microscope (Olympus) and images were acquired in bright field using cellSens Entry software (Olympus).

The percentages of metastasis-bearing spontaneous KEP mice were calculated based on the microscopic presence or absence of metastatic nodules in lungs and lymph nodes. In the metastasis model, the number of metastatic nodules in the lungs was based on cytokeratin 8 expression. Mice that developed overt metastatic disease were included in the analysis, and mice that were sacrificed because of local recurrence of the primary tumour were excluded.

Immunohistochemistry analysis for CD68 expression (1:2,000, clone KP1, Dako) was performed by the NKI-AvL Core Facility Molecular Pathology and Biobanking on formalin-fixed paraffin-embedded material of ILC breast cancer patients from the RATHER cohort[58,59] enrolled at the NKI. Anonymized archival tissue was used according to national guidelines regarding the use of archival material and with approval of the NKI-AVL translational research board.

Immunofluorescence analysis was performed on formalin-fixed paraffin-embedded material. The list of primary and secondary antibodies is provided in Supplementary Table 1. Sections were counterstained with DAPI (4,6-diamidino-2-phenylindole) and visualized with a Leica SP5 confocal microscope. Images were taken with LAS AF software (Leica) and values were obtained by counting α-SMA$^+$CD31$^+$ cells and total CD31$^+$ cells in six fields per tumour by two independent researches.

I

n situ detection of *Csf1* mRNA was performed using the RNAscope 2.0 FFPE Assay (Advanced Cell Diagnostics) and performed according to the manufacturer's recommendations[60].

Flow cytometry
KEP tumours were collected in ice-cold PBS and processed as described[61]. Briefly, samples were mechanically chopped using the McIlwain tissue chopper (Mickle Laboratory Engineering) and enzymatically digested with 3 mg ml^{-1} collagenase type A (Roche) and 25 µg ml^{-1} DNase I (Sigma) in serum-free medium for 1 h at 37°C in a shaking water bath. After washing, cells were stained with fluorochrome-conjugated antibodies (Supplementary Table 1). For intracellular staining of granzyme B, single-cell suspensions were stimulated in IMDM containing 8% FCS, 100 IU ml^{-1} penicillin, 100 µg ml^{-1} streptomycin, 0.5% β-mercaptoethanol, 50 ng ml^{-1} PMA, 1 µM ionomycin and Golgi-Plug (1:1,000; BD Biosciences) for 3 h at 37 °C. Following surface antigen staining, samples were fixed and permeabilized (BD Biosciences) and stained for intracellular proteins. Data acquisition was performed on BD LSRII or BD LSRFortessa flow cytometer using DIVA software (BD Biosciences) and data analysis was performed using FlowJo software version 9.9.6.

Isolation of intratumoural cell populations
Primary mammary tumours were harvested from KEP mice 1 d after two cycles of chemotherapy (±100 mm^2) or at end-stage (±225 mm^2), and single-cell suspensions were generated as described above. Enrichment of $CD11b^+$ cells was performed using magnetic columns (Miltenyi Biotec), as described previously[61]. Briefly, single-cell suspensions were stained with anti-CD11b-APC (1:200; clone M1/70, eBioscience) for 20 min and incubated with magnetic anti-APC MicroBeads according to the manufacturer's instructions (Miltenyi Biotec). $CD11b^+$ cells were isolated with LS columns (Miltenyi Biotec) according to the manufacturer's instructions. For the isolation of macrophages and neutrophils from tumours at the therapy-responsive phase, the enriched $CD11b^+$ fraction was stained with antibodies against Ly6G-FITC (1:200; clone 1A8, BD Biosciences), F4/80-PE (1:200; clone BM8, eBioscience) and Ly6C-ef450 (1:400; clone hk1.4, eBioscience). LIVE/DEAD fixable aqua dead cell stain (Thermo Fisher Scientific) was added 1:100 in PBS to exclude dead cells. $CD11b^+F4/80^+$ macrophages and $F4/80^-Ly6G^+Ly6C^{low}$ neutrophils were isolated with the BD FACSARIA II sorter with DIVA software (BD Biosciences).

For the isolation of cell populations from end-stage tumours, we separated intratumoural $CD11b^+$ and $CD11b^-$ cells by magnetic cell sorting as described above. The $CD11b^-$ and $CD11b^+$ fractions were stained as described in Supplementary Table 1. $CD11b^+F4/80^+$ macrophages, $CD11b^+F4/80^-Ly6G^-Ly6C^+$ monocytes, $CD11b^+F4/80^-Ly6G^+Ly6C^{low}$ neutrophils, $CD11b^-CD45^+CD11c^-$ lymphocytes and $CD11b^-CD45^-CD31^-$ tumour cells were isolated with BD FACSARIA FUSION sorter with DIVA software (BD Biosciences).

Adoptive transfer of monocytes
Front legs, hind legs and hips were collected from female mTmG mice and the bone marrow was flushed out. Bone marrow cells were incubated with Fc Block (1:50; CD16/CD32, BD Biosciences), stained with anti-Ly6G-APC (1:200; clone 1A8, BioLegend) and, consequently, negative selection for neutrophils was performed using magnetic columns (Miltenyi Biotec) as described previously[61]. The $Ly6G^-$ fraction was then stained with fluorochrome-conjugated antibodies (Supplementary

Table 1). After gating out Lineage$^+$ cells (CD3, CD8, CD4, NKp46 and Ter119) and Siglec F$^+$, Sca1$^+$ and cKIT$^+$ cells, tdTomato$^+$CD11b^{int}Ly6G$^-$Ly6C$^+$ monocytes were isolated with BD FACSARIA FUSION sorter with DIVA software (BD Biosciences). Between 1.5 and 2 × 10^6 tdTomato$^+$ monocytes were adoptively transfer into the tail vein of a tumour-bearing KEP mouse treated with control antibody or anti-CSF-1R. Antibody treatments started at a tumour size of 25 mm^2, and 1 d after the second antibody injection (1 week apart), monocytes were transferred. KEP mice were sacrificed 4 d later and tumours were isolated for flow cytometry analysis. Antibodies are listed in Supplementary Table 1.

CRISPR–Cas9-mediated gene disruption and colony-forming assay

IFNAR1 was knocked out (KO) from a cell line derived from a spontaneous KEP mammary tumour by transient transfection with a lentiCRISPRv2 (ref. [62]) containing IFNAR1-specific single guide RNA targeting exon 1 (sgRNA1: 5′-GCTCGCTGTCGTGGGCGCGG-3′). Twenty-four hours after transfection, cells were exposed to puromycin for 48 h. Cells were stained with IFNAR1-PE (1:200; clone MAR1-5A3, eBioscience) and IFNAR1-negative cells were sorted with BD FACSARIA FUSION sorter with DIVA software (BD Biosciences).

KEP and IFNAR1 KO KEP cells (250 cells per well) were seeded in triplicate in a 24-well plate, and the next day, cells were treated with an increasing concentration of recombinant IFN-α1 (BioLegend) for 7 d. On day 5, 4 μM or 8 μM cisplatin were added. At day 7, cells were washed, fixed in ice-cold methanol and incubated with 0.05% crystal violet. For quantification, crystal violet was dissolved in 10% acetic acid for 20 min and the absorbance was measured at 590 nm.

BMDMs

To generate BMDMs, bone marrow cells were harvested from the hind legs of wild-type mice and cultured for 7 days in RPMI medium containing 8% FCS, 100 IU ml^{-1} penicillin, 100 mg ml^{-1} streptomycin and 20 ng ml^{-1} recombinant M-CSF (Peprotech). After differentiation, BMDMs were harvested and seeded in a 24-well plate (400,000 BMDMs per well) and cultured overnight. The next morning, BMDMs were exposed to conditioned medium from a KEP cancer cell line in the presence of 8μg ml^{-1} of either control antibody or anti-CSF-1R for 24 h. Conditioned medium was obtained by culturing KEP cancer cells (80–90% confluency) for 24 h in RPMI containing 8% FCS, 100 IU ml^{-1} penicillin and 100 mg ml^{-1} streptomycin. The RNA of BMDMs was isolated with the Isolate II RNA Mini Kit (Bioline), and quantitative RT–PCR for *Ifna* was performed as described below.

RNA isolation and quantitative RT–PCR

RNA from sorted cells and tumours of KEP mice was isolated using TRIzol (Invitrogen). Samples were treated with DNase I (Invitrogen) followed by RNA cleanup with the Qiagen RNeasy Mini Kit according to the manufacturer's recommendation. Isolated RNA was quantified with Nanodrop (Thermo Scientific). Transformation of RNA into cDNA was performed with the Cloned AMV First-Strand cDNA Synthesis Kit (Invitrogen) using oligo(dT) primers. cDNA (20 ng per well) was analysed by SYBR green real-time PCR with 500 nM primers (Supplementary Table 2) using a

LightCycler 480 thermocycler (Roche). Samples were run in duplicate and were only further considered if the difference between the CT values of the duplo was less than one cycle. β-Actin was used as a reference gene.

Luminex cytokine array

Tumours and mammary glands were prepared with Bio-Rad cell lysis buffer, and the protein concentration of lysates was determined using the Pierce BCA Protein Assay Kit (Thermo Fischer Scientific) according to the manufacturer's recommendations. CSF-1 concentration in protein lysates was determined using the Bio-Plex Pro Cytokine 23-Plex Kits (Bio-Rad) and measured according to the manufacturer's instruction. Data acquisition and analysis were performed on a Bio-Plex 200 reader, using Bio-Plex Manager 6.0 software (Bio-Rad).

RNA-seq and data analysis

RNA isolation, library construction and deep sequencing

$CD11b^{+}F4/80^{+}$ and $CD11b^{+}F4/80^{-}Ly6G^{+}Ly6C^{low}$ immune cell populations were isolated as described above from KEP tumours treated with either control antibody, anti-CSF-1R, cisplatin + control antibody or cisplatin + anti-CSF-1R at the therapy-responsive phase (tumour size ± 100 mm^2). Some of the biological replicates consisted of pools of cells from two to six different mice. Total RNA was extracted using the RNeasy Mini and Microkits (Qiagen). According to the Ovation RNA-seq system V2 and Encore Rapid library systems protocols (NuGen), 10 ng RNA was converted into cDNA libraries, subsequently sequenced on a HiSeq 1500 system and demultiplexed using CASAVA v1.8 (Illumina).

Preprocessing of sequenced data

Using default parameters, all reads were aligned against the murine mm10 reference genome by TopHat2 v2.0.11 (ref. [63]). The data were imported into Partek Genomics Suite v6.6 (PGS), and the gene and transcript information was deducted before conducting normalization utilizing statistical software R (v3.3.1) and the DESeq2 package (https://doi.org/10.1101/002832). Normalized read counts were floored to a value of at least one thereafter and the data set was trimmed by defining a gene as expressed if the maximum value over all group means was higher than ten.

Identification of differentially expressed genes

Using PGS, a two-way analysis of variance (ANOVA) was performed to compute the top variable genes (treatment versus control) within the data set, as well as differentially expressed genes present in cisplatin + anti-CSF-1R neutrophils (versus cisplatin + control antibody neutrophils). Genes were defined to be differentially expressed when having a fold change of ≥1.5 and an unadjusted $P \leq 0.05$. Based on the ANOVA model, hierarchical clustering was performed on the top 400 variable genes within the data set (neutrophils and macrophages, cisplatin + anti-CSF-1R versus cisplatin + control antibody) using default settings in PGS.

Gene Ontology enrichment analysis, Gene Ontology network visualization, Ingenuity pathway analysis and GSEA

To link transcriptome information to previous knowledge, we applied Gene Ontology enrichment analysis on the 100 most upregulated and 100 most downregulated genes (fold change ≥ 1.5, unadjusted $P \leq 0.05$) extracted from neutrophils exposed to cisplatin + anti-CSF-1R treatment (versus cisplatin + control antibody-exposed neutrophils). Subsequently, the data were visualized using BiNGO[64], EnrichmentMap[65] and Word Clouding[66] plug-ins in Cytoscape. In addition, all differentially expressed genes found in neutrophils were analysed with Ingenuity pathway analysis (Qiagen).

GSEA was performed utilizing the BubbleGUM GSEA tool[67] to find enriched pathways in macrophages from cisplatin + anti-CSF-1R-treated tumours (versus cisplatin + control antibody macrophages). Pathways interrogated were derived from the reactome gene sets, and all pathways demonstrating a significant enrichment (false discovery rate (FDR) ≤ 0.25) in one condition were shown. Specifically addressing enrichment of EGR2 target genes in neutrophils from anti-CSF-1R-treated tumours versus neutrophils from control antibody-treated tumours, GSEA was employed on transcription factor target gene sets using the GSEA tool previously published[68]. The reactome and transcription factor target gene sets were obtained via the online available Molecular Signatures Database (MSigDB) of the Broad Institute (http://software.broadinstitute.org/gsea/msigdb/index.jsp).
No custom codes were used in the manuscript.

Evaluation of expression of ISGs in patient biopsies

The selection of type I ISGs was based on the RNA-seq results from our KEP mouse model upon cisplatin + anti-CSF-1R. The genes belong to the biological processes listed in Supplementary Table 3. We assessed the effect of anti-CSF-1R on these selected genes in human tumours by analysing RNA-seq data of paired baseline and on-treatment tumour biopsies of patients enrolled in a clinical phase I trial with emactuzumab (RG7155), a humanized anti-human CSF-1R monoclonal antibody. Biopsies were taken from a multicentre, open-label study (ClinicalTrials.gov identifier NCT01494688). Patients received emactuzumab every 2 weeks as intravenous infusion. Tumour biopsies of 31 patients with a broad range of different solid malignancies treated with either emactuzumab alone or in combination with paclitaxel (with an overrepresentation of breast cancer (n = 13) and ovarian cancer (n = 7) samples) were collected. The study was conducted in accordance with the Declaration of Helsinki, current International Conference on Harmonisation of Technical Requirements for Registration of Pharmaceuticals for Human Use guidelines and all applicable regulatory and ethical requirements. The study is compliant with all relevant ethical regulations regarding research involving human participants. All patients provided written informed consent before study-related procedures were performed. RNA extraction, RNA-seq and data analysis were performed as previously described[69].

Statistics and reproducibility
Information on study design, sample size, number of biological replicates, number of independent experiments and statistical analysis is reported in the main text and figure legends. The survival curves of cisplatin + control antibody (or cisplatin only)-treated, cisplatin + anti-CSF-1R-treated and cisplatin + anti-CSF-1R + anti-Ly6G-treated mice were repeated and confirmed in a separate animal facility (Figs. 1f and 6d–f); other in vivo interventions were performed once. In vitro experiments were repeated independently with similar results. Statistical analyses were performed using GraphPad Prism 7 and 8 (GraphPad Software Inc.). The two-tailed Mann–Whitney test was used for immunohistochemistry and flow cytometry analysis. Two-way ANOVA with Tukey's multiple comparison test was used for the quantification of crystal violet absorbance. Two-tailed log-rank tests were used for Kaplan–Meier survival curves. Fisher's exact test (two-sided) was used for metastasis analysis. $P < 0.05$ was considered statistically significant.

Reporting Summary
Further information on research design is available in the Nature Research Reporting Summary linked to this article.

Data availability

The RNA-seq data derived from mouse samples that support the findings of this study have been deposited in the Gene Expression Omnibus (GEO) repository under accession number GSE101881. Source data for Figs. 1a,d–i, 2, 3c–h, 4, 5 and 6 and Supplementary Figs. 1a,b,e,f,h,i, 2, 3e–h, 5a–c,f–i and 6a–f,i–n have been provided as Supplementary Table 4. All other data supporting the findings of this study are available from the corresponding author on reasonable request.

Additional information

Publisher's note: Springer Nature remains neutral with regard to jurisdictional claims in published maps and institutional affiliations.

Acknowledgements

This work was supported by the European Union (FP7 MCA-ITN 317445 TIMCC), the Dutch Cancer Society (NKI10623), the European Research Council (ERC consolidator award INFLAMET 615300), Worldwide Cancer Research (AICR 11-0677), the Netherlands Organization for Scientific Research NWO VIDI (917.96.307) and Oncode. K. Kos is supported by an OOA/NWO Diamond grant. K.E.d.V. is an EMBO Young Investigator. J.L.S. is a member of the Excellence Cluster ImmunoSensation and is in part supported by the DFG (SFB704, Excellence Cluster ImmunoSensation). We thank M. D. Wellenstein, H. Garner, S. Bissinger, J. Borst and T. Schumacher for useful discussions. We thank M. Hauptmann for advice on statistical analyses on the mouse survival curves. We thank the clinical investigators J.-Y. Blay, C. Gomez-Roca, J.-P. Delord, M. Toulmond, C. le Tourneau and A. Italiano for running clinical trials

with emactuzumab, and M. Cannarile, B. Quackenbush and A. Jegg for translational medicine support at Roche. We thank the histology core facility within the Cancer Research UK Beatson Institute for performing NKp46 immunohistochemistry on mouse tumour tissue. We thank K. Wartha, S. Klarenbeek and I. Peters Rit for technical assistance and the researchers involved in the RATHER project for generously providing tissue sections of human ILCs. We thank the flow cytometry facility, the animal facility, the animal pathology facility and the Core Facility Molecular Pathology and Biobanking at the NKI.

Contributions

C.S., M.C., C.H.R., J.J. and K.E.d.V. conceived the ideas and designed the experiments. C.S., M.C., C.-S.H., S.B.C., K. Kersten, A.v.W., K.V., K. Kos and K.E.d.V. performed the experiments and analysed the data. C.H.R. provided the anti-CSF-1R antibody and control antibody. S.T., T.U. and J.L.S. prepared the samples and conducted the RNA-seq and bioinformatics analyses on murine cells. J.-Y.S. performed the metastasis scoring. C.-H.O., D.R. and P.A.C. were involved in the collection of patient samples and bioinformatic analysis of the human data. C.S. and K.E.d.V. wrote the paper.

Competing interests

C.H.R., C.-H.O. and D.R. are employees of F. Hoffman La Roche. C.H.R. is an inventor of granted and pending patent applications relating to emactuzumab and a stockholder in F. Hoffman La Roche. F. Hoffman La Roche provided financial research support for the experiments with anti-CSF-1R. P.A.C. received funding from Roche for the described clinical trial and other Roche-sponsored studies.

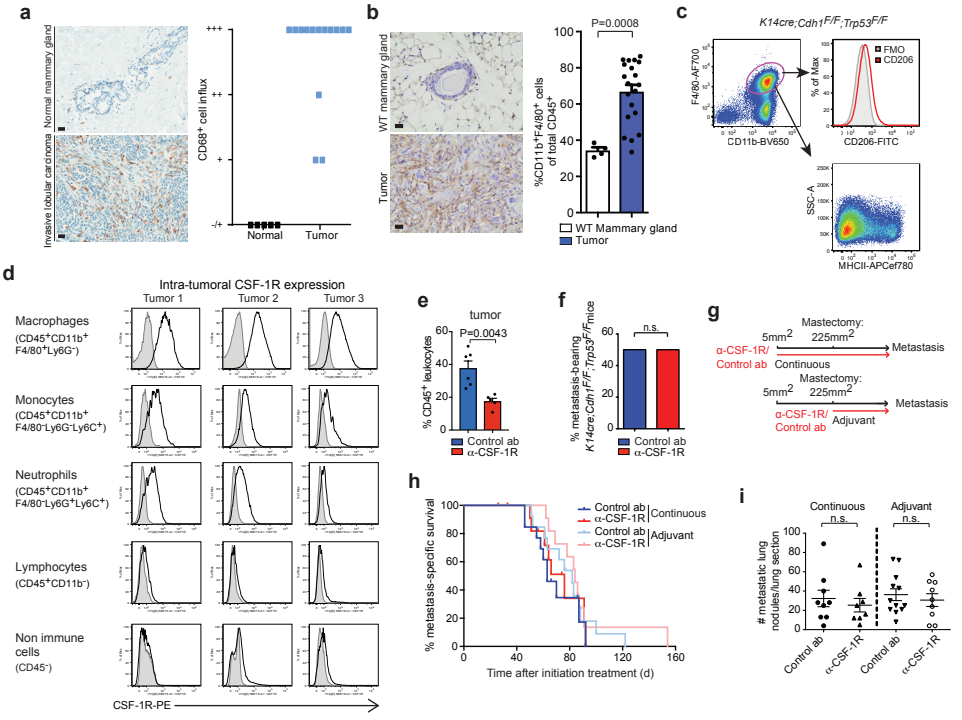
References

1. Coffelt, S. B. & de Visser, K. E. Immune-mediated mechanisms influencing the efficacy of anticancer therapies. *Trends Immunol.* **36**, 198–216 (2015).
2. Galluzzi, L., Buque, A., Kepp, O., Zitvogel, L. & Kroemer, G. Immunogenic cell death in cancer and infectious disease. *Nat. Rev. Immunol.* **17**, 97–111 (2017).
3. Ciampricotti, M., Hau, C. S., Doornebal, C. W., Jonkers, J. & de Visser, K. E. Chemotherapy response of spontaneous mammary tumors is independent of the adaptive immune system. *Nat. Med.* **18**, 344–346 (2012).
4. DeNardo, D. G. et al. Leukocyte complexity predicts breast cancer survival and functionally regulates response to chemotherapy. *Cancer Discov.* **1**, 54–67 (2011).
5. Ruffell, B. et al. Macrophage IL-10 blocks $CD8^+$ T cell-dependent responses to chemotherapy by suppressing IL-12 expression in intratumoral dendritic cells. *Cancer Cell* **26**, 623–637 (2014).
6. Campbell, M. J. et al. The prognostic implications of macrophages expressing proliferating cell nuclear antigen in breast cancer depend on immune context. *PLoS One* **8**, e79114 (2013).
7. Chua, W., Charles, K. A., Baracos, V. E. & Clarke, S. J. Neutrophil/lymphocyte ratio predicts chemotherapy outcomes in patients with advanced colorectal cancer. *Br. J. Cancer* **104**, 1288–1295 (2011).
8. Kishi, Y. et al. Blood neutrophil-to-lymphocyte ratio predicts survival in patients with colorectal liver metastases treated with systemic chemotherapy. *Ann. Surg. Oncol.* **16**, 614–622 (2009).
9. Miao, Y., Yan, Q., Li, S., Li, B. & Feng, Y. Neutrophil to lymphocyte ratio and platelet to lymphocyte ratio are predictive of chemotherapeutic response and prognosis in epithelial ovarian cancer patients treated with platinum-based chemotherapy. *Cancer Biomark.* **17**, 33–40 (2016).
10. Pistelli, M. et al. Pre-treatment neutrophil to lymphocyte ratio may be a useful tool in predicting survival in early triple negative breast cancer patients. *BMC Cancer* **15**, 195 (2015).
11. Paulus, P., Stanley, E. R., Schafer, R., Abraham, D. & Aharinejad, S. Colony-stimulating factor-1 antibody reverses chemoresistance in human MCF-7 breast cancer xenografts. *Cancer Res.* **66**, 4349–4356 (2006).
12. Shree, T. et al. Macrophages and cathepsin proteases blunt chemotherapeutic response in breast cancer. *Genes Dev.* **25**, 2465–2479 (2011).
13. Mitchem, J. B. et al. Targeting tumor-infiltrating macrophages decreases tumor-initiating cells, relieves immunosuppression, and improves chemotherapeutic responses. *Cancer Res.* **73**, 1128–1141 (2013).
14. Di Mitri, D. et al. Tumour-infiltrating Gr-1^+ myeloid cells antagonize senescence in cancer. *Nature* **515**, 134–137 (2014).
15. Houthuijzen, J. M. et al. Lysophospholipids secreted by splenic macrophages induce chemotherapy resistance via interference with the DNA damage response. *Nat. Commun.* **5**, 5275 (2014).
16. Acharyya, S. et al. A CXCL1 paracrine network links cancer chemoresistance and metastasis. *Cell* **150**, 165–178 (2012).
17. Olson, O. C., Kim, H., Quail, D. F., Foley, E. A. & Joyce, J. A. Tumor-associated macrophages suppress the cytotoxic activity of antimitotic agents. *Cell Rep.* **19**, 101–113 (2017).
18. Weizman, N. et al. Macrophages mediate gemcitabine resistance of pancreatic adenocarcinoma by upregulating cytidine deaminase. *Oncogene* **33**, 3812–3819 (2014).
19. Nakasone, E. S. et al. Imaging tumor–stroma interactions during chemotherapy reveals contributions of the microenvironment to resistance. *Cancer Cell* **21**, 488–503 (2012).
20. Nywening, T. M. et al. Targeting both tumour-associated $CXCR2^+$ neutrophils and $CCR2^+$ macrophages disrupts myeloid recruitment and improves chemotherapeutic responses in pancreatic ductal adenocarcinoma. *Gut* **67**, 1112–1123 (2018).
21. Ries, C. H. et al. Targeting tumor-associated macrophages with anti-CSF-1R antibody reveals a strategy for cancer therapy. *Cancer Cell* **25**, 846–859 (2014).
22. Quail, D. F. & Joyce, J. A. Molecular pathways: deciphering mechanisms of resistance to

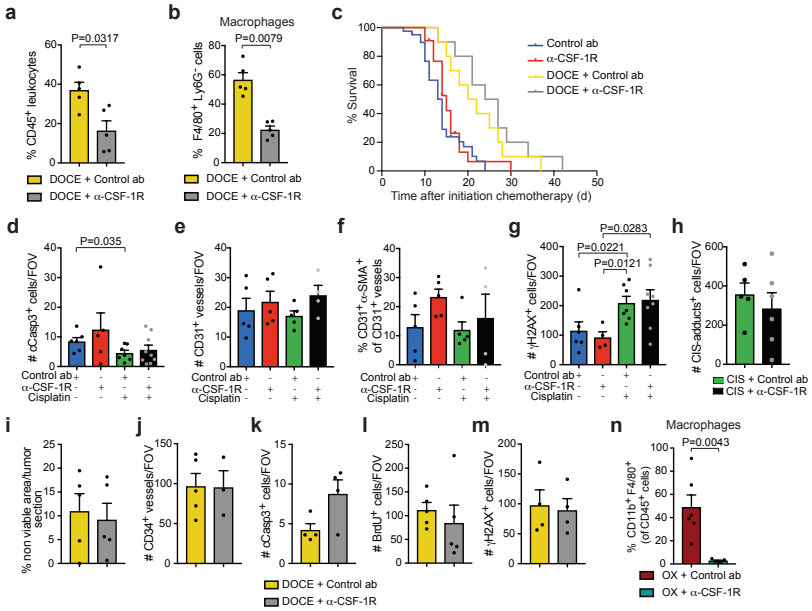
macrophage-targeted therapies. *Clin. Cancer Res.* **23**, 876–884 (2017).
23. Crusz, S. M. & Balkwill, F. R. Inflammation and cancer: advances and new agents. *Nat. Rev. Clin. Oncol.* **12**, 584–596 (2015).
24. Derksen, P. W. et al. Somatic inactivation of E-cadherin and p53 in mice leads to metastatic lobular mammary carcinoma through induction of anoikis resistance and angiogenesis. *Cancer Cell* **10**, 437–449 (2006).
25. Hume, D. A. & MacDonald, K. P. Therapeutic applications of macrophage colony-stimulating factor-1 (CSF-1) and antagonists of CSF-1 receptor (CSF-1R) signaling. *Blood* **119**, 1810–1820 (2012).
26. Franklin, R. A. et al. The cellular and molecular origin of tumor-associated macrophages. *Science* **344**, 921–925 (2014).
27. Doornebal, C. W. et al. A preclinical mouse model of invasive lobular breast cancer metastasis. *Cancer Res.* **73**, 353–363 (2013).
28. Noy, R. & Pollard, J. W. Tumor-associated macrophages: from mechanisms to therapy. *Immunity* **41**, 49–61 (2014).
29. Bradley, E. W., Ruan, M. M. & Oursler, M. J. Novel pro-survival functions of the Kruppel-like transcription factor Egr2 in promotion of macrophage colony-stimulating factor-mediated osteoclast survival downstream of the MEK/ERK pathway. *J. Biol. Chem.* **283**, 8055–8064 (2008).
30. Gomez-Roca, C. A. et al. Phase I study of RG7155, a novel anti-CSF1R antibody, in patients with advanced/metastatic solid tumors. *J. Clin. Oncol.* **33**, 3005 (2015).
31. Zitvogel, L., Galluzzi, L., Kepp, O., Smyth, M. J. & Kroemer, G. Type I interferons in anticancer immunity. *Nat. Rev. Immunol.* **15**, 405–414 (2015).
32. Vacchelli, E. et al. Autocrine signaling of type 1 interferons in successful anticancer chemotherapy. *Oncoimmunology* **4**, e988042 (2015).
33. Parker, B. S., Rautela, J. & Hertzog, P. J. Antitumour actions of interferons: implications for cancer therapy. *Nat. Rev. Cancer* **16**, 131–144 (2016).
34. Snell, L. M., McGaha, T. L. & Brooks, D. G. Type I interferon in chronic virus infection and cancer. *Trends Immunol.* **38**, 542–557 (2017).
35. Fuertes, M. B. et al. Host type I IFN signals are required for antitumor $CD8^+$ T cell responses through $CD8\alpha^+$ dendritic cells. *J. Exp. Med.* **208**, 2005–2016 (2011).
36. Coffelt, S. B. et al. IL-17-producing γδ T cells and neutrophils conspire to promote breast cancer metastasis. *Nature* **522**, 345–348 (2015).
37. Sistigu, A. et al. Cancer cell-autonomous contribution of type I interferon signaling to the efficacy of chemotherapy. *Nat. Med.* **20**, 1301–1309 (2014).
38. Burnette, B. C. et al. The efficacy of radiotherapy relies upon induction of type I interferon-dependent innate and adaptive immunity. *Cancer Res.* **71**, 2488–2496 (2011).
39. Deng, L. et al. STING-dependent cytosolic DNA sensing promotes radiation-induced type I interferon-dependent antitumor immunity in immunogenic tumors. *Immunity* **41**, 843–852 (2014).
40. Bidwell, B. N. et al. Silencing of Irf7 pathways in breast cancer cells promotes bone metastasis through immune escape. *Nat. Med.* **18**, 1224–1231 (2012).
41. Callari, M. et al. Subtype-dependent prognostic relevance of an interferon-induced pathway metagene in node-negative breast cancer. *Mol. Oncol.* **8**, 1278–1289 (2014).
42. Snijders, A. M. et al. An interferon signature identified by RNA-sequencing of mammary tissues varies across the estrous cycle and is predictive of metastasis-free survival. *Oncotarget* **5**, 4011–4025 (2014).
43. Schiavoni, G. et al. Cyclophosphamide synergizes with type I interferons through systemic dendritic cell reactivation and induction of immunogenic tumor apoptosis. *Cancer Res.* **71**, 768–778 (2011).
44. Weichselbaum, R. R. et al. An interferon-related gene signature for DNA damage resistance is a predictive marker for chemotherapy and radiation for breast cancer. *Proc. Natl Acad. Sci. USA* **105**, 18490–18495 (2008).

45. Critchley-Thorne, R. J. et al. Impaired interferon signaling is a common immune defect in human cancer. *Proc. Natl Acad. Sci. USA* **106**, 9010–9015 (2009).
46. Pyonteck, S. M. et al. CSF-1R inhibition alters macrophage polarization and blocks glioma progression. *Nat. Med.* **19**, 1264–1272 (2013).
47. Quail, D. F. et al. The tumor microenvironment underlies acquired resistance to CSF-1R inhibition in gliomas. *Science* **352**, aad3018 (2016).
48. Yan, D. et al. Inhibition of colony stimulating factor-1 receptor abrogates microenvironment-mediated therapeutic resistance in gliomas. *Oncogene* **36**, 6049–6058 (2017).
49. Zhu, Y. et al. CSF1/CSF1R blockade reprograms tumor-infiltrating macrophages and improves response to T-cell checkpoint immunotherapy in pancreatic cancer models. *Cancer Res.* **74**, 5057–5069 (2014).
50. Coffelt, S. B., Wellenstein, M. D. & de Visser, K. E. Neutrophils in cancer: neutral no more. *Nat. Rev. Cancer* **16**, 431–446 (2016).
51. Pylaeva, E., Lang, S. & Jablonska, J. The essential role of type I interferons in differentiation and activation of tumor-associated neutrophils. *Front. Immunol.* **7**, 629 (2016).
52. Berry, M. P. et al. An interferon-inducible neutrophil-driven blood transcriptional signature in human tuberculosis. *Nature* **466**, 973–977 (2010).
53. Rocha, B. C. et al. Type I interferon transcriptional signature in neutrophils and low-density granulocytes are associated with tissue damage in malaria. *Cell Rep.* **13**, 2829–2841 (2015).
54. Teijaro, J. R. et al. Persistent LCMV infection is controlled by blockade of type I interferon signaling. *Science* **340**, 207–211 (2013).
55. Cunningham, C. R. et al. Type I and type II interferon coordinately regulate suppressive dendritic cell fate and function during viral persistence. *PLoS Pathog.* **12**, e1005356 (2016).
56. Corrales, L. et al. Direct activation of STING in the tumor microenvironment leads to potent and systemic tumor regression and immunity. *Cell Rep.* **11**, 1018–1030 (2015).
57. Muzumdar, M. D., Tasic, B., Miyamichi, K., Li, L. & Luo, L. A global double-fluorescent Cre reporter mouse. *Genesis* **45**, 593–605 (2007).
58. Michaut, M. et al. Integration of genomic, transcriptomic and proteomic data identifies two biologically distinct subtypes of invasive lobular breast cancer. *Sci. Rep.* **6**, 18517 (2016).
59. Schouten, P. C. et al. Robust BRCA1-like classification of copy number profiles of samples repeated across different datasets and platforms. *Mol. Oncol.* **9**, 1274–1286 (2015).
60. Wang, F. et al. RNAscope: a novel in situ RNA analysis platform for formalin-fixed, paraffin-embedded tissues. *J. Mol. Diagn.* **14**, 22–29 (2012).
61. Salvagno, C. & de Visser, K. E. Purification of immune cell populations from freshly isolated murine tumors and organs by consecutive magnetic cell sorting and multi-parameter flow cytometry-based sorting. *Methods Mol. Biol.* **1458**, 125–135 (2016).
62. Sanjana, N. E., Shalem, O. & Zhang, F. Improved vectors and genome-wide libraries for CRISPR screening. *Nat. Methods* **11**, 783–784 (2014).
63. Kim, D. et al. TopHat2: accurate alignment of transcriptomes in the presence of insertions, deletions and gene fusions. *Genome Biol.* **14**, R36 (2013).
64. Maere, S., Heymans, K. & Kuiper, M. BiNGO: a Cytoscape plugin to assess overrepresentation of gene ontology categories in biological networks. *Bioinformatics* **21**, 3448–3449 (2005).
65. Merico, D., Isserlin, R., Stueker, O., Emili, A. & Bader, G. D. Enrichment map: a network-based method for gene-set enrichment visualization and interpretation. *PLoS One* **5**, e13984 (2010).
66. Oesper, L., Merico, D., Isserlin, R. & Bader, G. D. WordCloud: a Cytoscape plugin to create a visual semantic summary of networks. *Source Code Biol. Med.* **6**, 7 (2011).
67. Spinelli, L., Carpentier, S., Montanana Sanchis, F., Dalod, M. & Vu Manh, T. P. BubbleGUM: automatic extraction of phenotype molecular signatures and comprehensive visualization of multiple gene set enrichment analyses. *BMC Genomics* **16**, 814 (2015).
68. Subramanian, A. et al. Gene set enrichment analysis: a knowledge-based approach for interpreting genome-wide expression profiles. *Proc. Natl Acad. Sci. USA* **102**, 15545–15550 (2005).

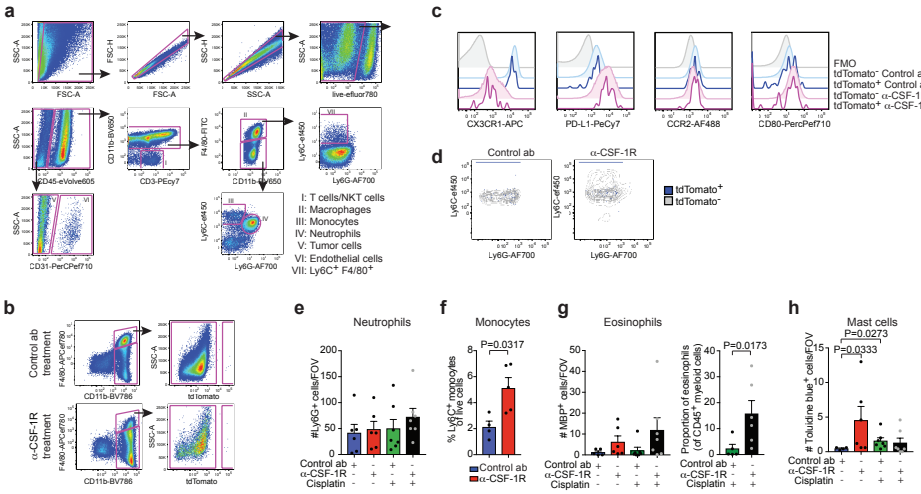
69. Pradel, L. P. et al. Macrophage susceptibility to emactuzumab (RG7155) treatment. *Mol. Cancer Ther.* **15**, 3077–3086 (2016).



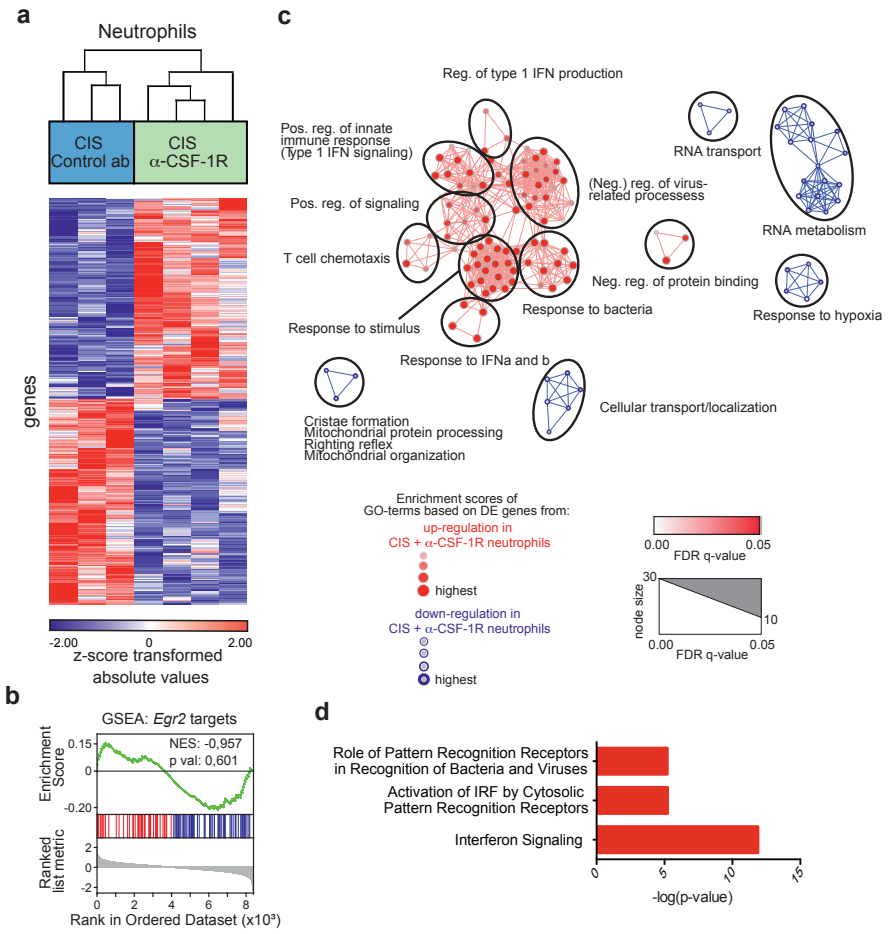
Supplementary Fig. 1 | CSF-1R blockade does not influence spontaneous metastasis formation. **(a)** Presence of CD68$^+$ macrophages in untreated human invasive lobular carcinomas and in adjacent normal breast tissue. Influx of CD68$^+$ macrophages was scored based on immunohistochemistry (normal breast tissue, n=5 patients; invasive lobular carcinomas, n=14 patients). Representative images are shown. Scale bar=25µm. **(b)** Representative IHC staining of F4/80$^+$ macrophages in a mammary tumor of a KEP mouse and in a normal mammary gland of an age-matched WT mouse. Scale bar=20µm. Percentage of CD11b$^+$F4/80$^+$ macrophages gated on CD45$^+$ cells in KEP mammary tumors (n=20 animals) and in normal mammary glands of age-matched WT mice (n=4 animals). **(c)** Representative flow cytometry histogram and plot showing CD206 and MHCII expression, respectively, on F4/80$^+$ macrophages in a KEP mammary tumor. Data are representative of 5 independent KEP mammary tumors. **(d)** Flow cytometry histograms showing CSF-1R expression levels (white) and Fluorescence minus one (FMO) control (grey) in 3 independent KEP mammary tumors. **(e)** Proportion of CD45$^+$ immune cells of total live cells in tumors of time point-sacrificed KEP mice treated with control ab (n=6 animals) or anti-CSF-1R (n=5 animals) as determined by flow cytometry. **(f)** Organs collected from KEP mice bearing end-stage mammary tumors treated with control ab (n=20 animals) or anti-CSF-1R (n=22 animals) were microscopically analyzed for the presence of metastases. Percentage of tumor-bearing KEP mice with metastases is displayed. p=0.1 by Fisher's exact test (Two-sided). **(g)** Schematic overview of continuous and adjuvant antibody treatment in the KEP-based spontaneous metastasis model as described in Methods. **(h)** Kaplan-Meier metastasis-specific survival curves of recipient mice orthotopically transplanted with tumor fragments from KEP mice and treated either continuously (control ab n=13 animals, anti-CSF-1R n=14 animals) or in an adjuvant setting (control ab n=13 animals, anti-CSF-1R n=11 animals). An event is defined as an animal that was sacrificed because of clinical signs of metastatic disease. **(i)** Quantification of the number of spontaneous pulmonary metastases in mice treated either continuously (control ab n=9 animals; anti-CSF-1R n=8 animals) or in an adjuvant setting (Control ab n=12 animals; anti-CSF-1R n=9 animals). Data presented in **b, e** and **i** are mean ± SEM and statistical analysis was performed using two-tailed Mann–Whitney test.



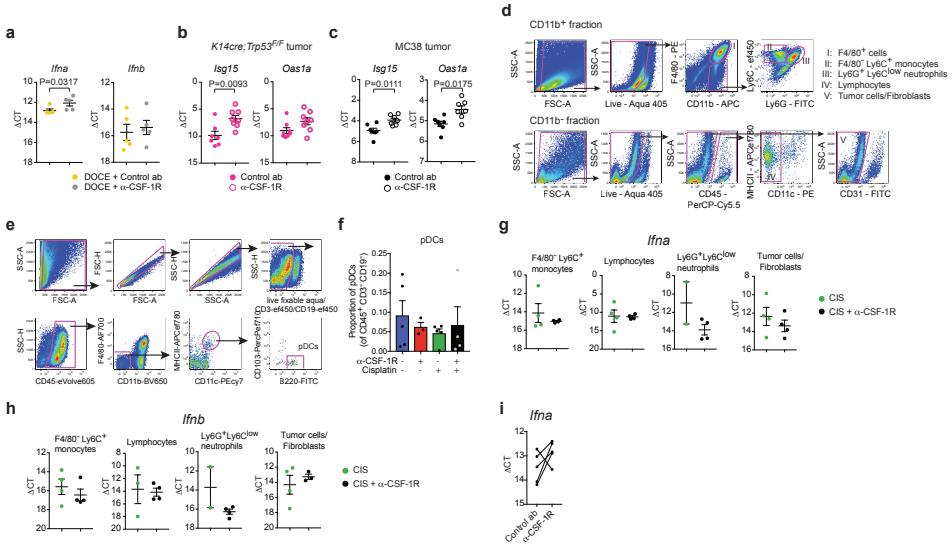
Supplementary Fig. 2 | CSF-1R blockade synergizes with platinum-based chemotherapy drugs, and not with docetaxel. (a-b) Proportion of CD45$^+$ immune cells gated on live cells **(a)** and F4/80$^+$Ly6G$^-$ macrophages gated on CD11b$^+$ cells **(b)** determined by flow cytometry in tumors of time point-sacrificed KEP mice treated as indicated (n=5 animals/group). **(c)** Kaplan Meier tumor-specific survival curves of KEP mice treated with control ab, anti-CSF-1R (same groups as Fig. 1f), docetaxel/control ab (n=10 animals) or docetaxel/anti-CSF-1R (n=10 animals). Docetaxel/control ab versus Control ab, p=0.0021; Docetaxel/control ab versus docetaxel/anti-CSF-1R, p=0.329 (two-tailed log-rank test). **(d)** Quantification of cleaved caspase 3$^+$ cells in viable areas of mammary tumors of time point-sacrificed KEP mice treated with control ab (n=6 animals), anti-CSF-1R (n=5 animals), cisplatin/control ab (n=7 animals) and cisplatin/anti-CSF-1R (n=9 animals) as determined by IHC. **(e)** Quantification of CD31$^+$ vessels in viable areas of mammary tumors of time point-sacrificed KEP mice treated with control ab (n=5 animals), anti-CSF-1R (n=5 animals), cisplatin/control ab (n=5 animals) and cisplatin/anti-CSF-1R (n=4 animals) as determined by immunofluorescence. Values represent average number of positive cells per FOV quantified by counting six fields per tumor. **(f)** Percentage of vessels covered by alpha-SMA$^+$ pericytes in viable areas of mammary tumors as determined by immunofluorescence. Same mice as **e**. Percentage was determined by counting alpha-SMA$^+$CD31$^+$ cells and total CD31$^+$ cells in six high-power microscopic fields per tumor. **(g-h)** Quantification of γH2AX$^+$ cells **(g)** and cisplatin adducts$^+$ cells **(h)** in viable areas of mammary tumors of time point-sacrificed KEP mice treated as indicated (γH2AX: control ab n=6 animals, anti-CSF-1R n=4 animals, cisplatin/control ab n=7 animals, cisplatin/anti-CSF-1R n=8 animals; CIS-adducts: cisplatin/control ab n=5 animals, cisplatin/anti-CSF-1R n=6 animals). **(i)** Percentage of non-viable area per tumor section of time point-sacrificed KEP mice quantified by digital area analysis of H&E stained sections (n=5 animals/group). **(j-m)** Quantification of CD34$^+$ cells **(j)**, cleaved caspase 3$^+$ cells **(k)**, BrdU$^+$ cells **(l)**, γH2AX$^+$ cells **(m)** in viable areas of mammary tumors of time point-sacrificed KEP mice treated as indicated (CD34: docetaxel/control ab n=5 animals, docetaxel/anti-CSF-1R n=3 animals; cCasp3: n=4 animals/group; BrdU: n=5 animals/group; γH2AX: n=4 animals/group). **(n)** Proportion of CD11b$^+$F4/80$^+$ macrophages gated on CD45$^+$ cells as determined by flow cytometry in tumors of end-stage KEP mice treated as indicated (oxaliplatin/Control ab treatment n=6 animals; oxaliplatin/anti-CSF-1R treatment n=5 animals). Data presented in **d, g-h, j-m** show average number of positive cells per field of view (FOV) quantified by counting five high-power microscopic fields per tumor. Data presented in **a-b** and **d-n** are mean values ± SEM and statistical analysis was performed using two-tailed Mann–Whitney test. DOCE, docetaxel, CIS, cisplatin, OX, oxaliplatin.



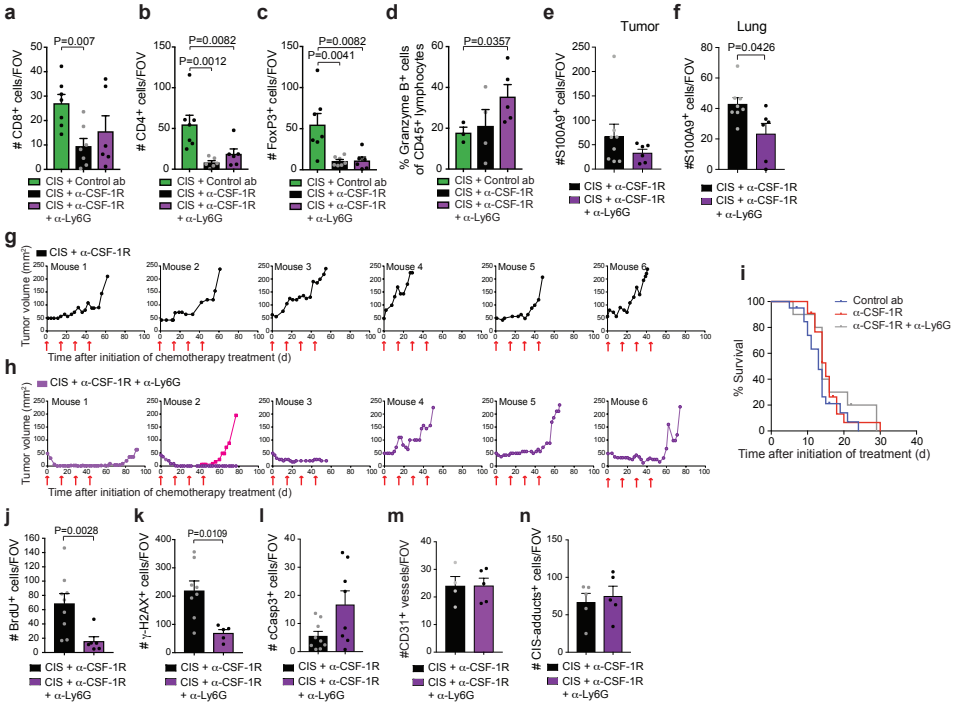
Supplementary Fig. 3 | Impact of CSF-1R inhibition on the intratumoral presence of diverse myeloid immune cell types. (a) Representative dot plots of a KEP mammary tumor illustrating the gating strategy for the identification of cell populations. Antibody panel used: "tumor panel I" (see supplementary Table 1). Arrows indicate directionality of sub-gates. **(b-d)** tdTomato$^+$ (Lineage$^-$ SiglecF$^-$cKIT$^-$CD11b^{int}Ly6G$^-$Ly6C$^+$) monocytes were isolated from the bone marrow of mTmG mice and adoptively transferred into tumor-bearing KEP mice that had previously received either control ab or anti-CSF-1R. 4 days after the monocyte transfer, the presence and phenotype of tdTomato$^+$ cells in tumors were analyzed. **(b)** Gating strategy showing intratumoral tdTomato$^+$ cells that express F4/80 in control ab- or anti-CSF-1R-treated recipient KEP mice. **(c)** Representative flow cytometry histograms showing CX3CR1, PD-L1, CCR2 and CD80 expression in tdTomato$^+$ and tdTomato$^-$ macrophages in KEP tumors. **(d)** Overlay of representative dot plots showing Ly6C expression in tdTomato$^+$ and tdTomato$^-$ macrophages in control ab- and anti-CSF-1R-treated KEP mice. Data presented in **b-d** are representative of 2 (control ab treatment) and 3 (anti-CSF-1R treatment) independent experiments. **(e)** Quantification of Ly6G$^+$ neutrophils in viable areas of mammary tumors of time point-sacrificed KEP mice treated with control ab (n=6 animals), anti-CSF-1R (n=6 animals), cisplatin/control ab (n=7 animals) or cisplatin/anti-CSF-1R (n=7 animals). **(f)** Proportion of Ly6C$^+$Ly6G$^-$ monocytes determined by flow cytometry in KEP mammary tumors treated with control ab (n=4 animals) or anti-CSF-1R (n=5 animals). **(g)** Quantification of Major Basic Protein (MBP)$^+$ cells in viable areas of mammary tumors of time point-sacrificed KEP mice as determined by IHC (control ab n=5 animals, anti-CSF-1R n=6 animals, cisplatin/control ab n=7 animals, cisplatin/anti-CSF-1R n=7 animals) and proportion of Siglec F$^+$ eosinophils gated on intratumoral CD45$^+$ cells of time point-sacrificed KEP mice as determined by flow cytometry (cisplatin/control ab n=5 animals, cisplatin/anti-CSF-1R n=6 animals). **(h)** Quantification of Toluidine Blue$^+$ mast cells in viable areas of mammary tumors of time point-sacrificed KEP mice (control ab n=4 animals, anti-CSF-1R n=6 animals, cisplatin/control ab n=7 animals, cisplatin/anti-CSF-1R n=7 animals) as determined by histochemistry. Values in **e**, **g** and **h** represent average number of positive cells per field of view (FOV) quantified by counting five high-power microscopic fields per tumor. Data presented in **e-h** are mean values ± SEM. Statistical analysis was performed using two-tailed Mann–Whitney test.



Supplementary Fig. 4 | Intratumoral neutrophils show elevated expression levels of type I IFN-stimulated genes upon CSF-1R blockade. (a) Hierarchical clustering of the top 400 variable genes between neutrophils isolated from tumors of KEP mice treated with cisplatin/control ab (n=3 biologically independent samples) and cisplatin/anti-CSF-1R (n=4 biologically independent samples). Mice were sacrificed one day after second cisplatin injection. FC: ≥ 1,5; unadjusted p-value: ≤ 0,05. Statistical analysis was performed using two-way ANOVA. **(b)** Gene set enrichment analysis (GSEA) of Egr2 target genes obtained from RNA-Seq data in tumor-infiltrating neutrophils of anti-CSF-1R-treated KEP mice compared to control ab-treated KEP mice (n=4 animals/group). Enrichment scores were calculated using a weighted Kolmogorov–Smirnov-like statistic. **(c)** Network visualization of GOEA of the top 100 up-regulated and top 100 down-regulated genes (cisplatin/anti-CSF-1R vs. cisplatin/control ab neutrophils; FC: 1,5, unadjusted p-value: ≤ 0.05) using BiNGO and EnrichmentMap. Red and blue nodes represent the positively and negatively enriched GO-terms, respectively. Node size represents corresponding enrichment p-values (FDR corrected p-value: ≤ 0.05). The genes used as input for the BiNGO analysis are derived from the 2-way ANOVA model. The enrichment score was calculated with a hypergeometric statistical test, multiple testing correction was performed with the Benjamin & Hochberg FDR correction. **(d)** Top three canonical pathways identified using ingenuity pathway analysis (IPA) enriched in neutrophils isolated from cisplatin/anti-CSF-1R-treated tumors (n=4 biologically independent samples) compared to neutrophils from cisplatin/control ab-treated tumors (n=3 biologically independent samples). Statistical analysis was performed with standard IPA software statistics.



Supplementary Fig. 5 | CSF-1R blockade increases intratumoral *Ifna* expression. (a) Transcripts of *Ifna* and *Ifnb* in KEP mammary tumors were determined by qPCR and normalized to β-actin (n=5 animals/group). Mice were analyzed one day after the second docetaxel injection. Graphs show the mean ± SEM in ΔCt values. **(b-c)** Transcripts of *Isg15* and *Oas1a* in orthotopically transplanted *K14cre;Trp53$^{F/F}$* (KP) tumors (*Isg15*: control ab n=7 animals, anti-CSF-1R n=8 animals; *Oas1a*: n=8 animals/group) **(b)** and subcutaneous MC38 tumors (n=8 animals/group) **(c)** treated as indicated were determined by qPCR and normalized to β-actin. Mice were analysed at a tumor size of 100mm^2 (KP) or after 12 days from the start of the treatment (MC38). Graphs show the mean ± SEM in ΔCt values. **(d)** Representative dot plots of a KEP tumor illustrating the gating strategy for cell sorting by flow cytometry. After cell separation based on CD11b expression by magnetic columns, the CD11b$^+$ and CD11b$^-$ fractions were stained as described in Methods followed by flow cytometry-based sorting of intratumoral cell populations. **(e)** Representative dot plots of a KEP tumor illustrating the gating strategy for the identification of pDCs. Antibody panel "tumor panel II" was used. Arrows indicate directionality of sub-gates. **(f)** Proportion of plasmacytoid dendritic cells (pDCs) in mammary tumors of end-stage KEP mice as determined by flow cytometry (control ab n=5 animals, anti-CSF-1R n=3 animals, cisplatin/control ab n=5 animals, cisplatin/anti-CSF-1R n=4 animals). **(g-h)** Transcripts of *Ifna* and *Ifnb* in CD11b$^+$F4/80$^-$Ly6G$^-$Ly6C$^+$ monocytes (*Ifna* and *Ifnb*: n=4 animals/group), CD45$^+$CD11b$^-$CD11c$^-$ lymphocytes (*Ifna*: n=4 animals/group; *Ifnb*: cisplatin/control ab n=3 animals, cisplatin/anti-CSF-1R n=4 animals), CD11b$^+$F4/80$^-$Ly6G$^+$Ly6C^{low} neutrophils (*Ifna* and *Ifnb*: cisplatin/control ab n=2 animals, cisplatin/anti-CSF-1R n=4 animals) and CD45$^-$CD11b$^-$CD31$^-$ tumor cells/fibroblasts (*Ifna*: n=4 animals/group; *Ifnb*: cisplatin/control ab n=4 animals, cisplatin/anti-CSF-1R n=3 animals) isolated from end-stage KEP tumors were determined by qPCR and normalized to β-actin. **(i)** Transcript of *Ifna* in cultured bone marrow-derived macrophages treated for 24h with either control antibody or anti-CSF-1R in the presence of KEP cancer cell line-derived conditioned medium. Data are representative of 4 independent experiments. Data presented in **a-c** and **f-h** are mean values ± SEM and statistical analysis was performed using two-tailed Mann–Whitney test. CIS, cisplatin; DOCE, docetaxel.



Supplementary Fig. 6 | Neutrophil inhibition enhances intratumoral granzyme B expression and improves the synergistic anti-cancer effect of cisplatin/anti-CSF-1R in *K14cre;Cdh1$^{F/F}$;Trp53$^{F/F}$* mice. **(a-c)** Quantification of CD8$^+$ T cells **(a)**, CD4$^+$ T cells **(b)** and FoxP3$^+$ regulatory T cells **(c)** in viable areas of mammary tumors of time point-sacrificed KEP mice (CD8: cisplatin/control ab n=7 animals, cisplatin/anti-CSF-1R n=7 animals, cisplatin/anti-CSF-1R/anti-Ly6G n=7 animals; CD4: cisplatin/control ab n=7 animals, cisplatin/anti-CSF-1R n=6 animals, cisplatin/anti-CSF-1R/anti-Ly6G n=6 animals; FoxP3: cisplatin/control ab n=7 animals, cisplatin/anti-CSF-1R n=7 animals, cisplatin/anti-CSF-1R/anti-Ly6G n=6 animals). **(d)** Proportion of granzyme B$^+$ CD45$^+$ lymphocytes (lymphocyte gate was based on SSC and FSC) determined by flow cytometry in the tumor of time point-sacrificed KEP mice treated as indicated (cisplatin/control ab n=3 animals, cisplatin/anti-CSF-1R n=4 animals, cisplatin/anti-CSF-1R/anti-Ly6G n=5 animals). **(e-f)** Quantification of S100A9$^+$ cells in viable areas of mammary tumors **(e)** and lung **(f)** of end-stage KEP mice treated with cisplatin/anti-CSF-1R (n=8 animals) or cisplatin/anti-CSF-1R/anti-Ly6G (n=6 animals). **(g-h)** Representative tumor growth graphs of six individual KEP mice treated with cisplatin/anti-CSF-1R **(g)** and cisplatin/anti-CSF-1R/anti-Ly6G **(h)**. Data are representative of 16 cisplatin/anti-CSF-1R-treated mice and 10 cisplatin/anti-CSF-1R/anti-Ly6G-treated mice. Red arrows indicate cisplatin injections. In pink, growth curve of a secondary tumor that developed in another mammary gland during the treatment. **(i)** Kaplan-Meier tumor-specific survival curves of KEP mice treated with control ab, anti-CSF-1R (same groups as Fig. 1f) or anti-CSF-1R/anti-Ly6G (n=10 animals). **(j-n)** Quantification of BrdU$^+$ **(j)** γH2AX$^+$ cells **(k)**, cleaved caspase 3$^+$ cells **(l)**, CD31$^+$ vessels **(m)** and cisplatin adducts$^+$ cells **(n)** in viable areas of mammary tumors of time point-sacrificed KEP mice treated with cisplatin/anti-CSF-1R (same as Fig. 1h and Supplementary Fig. 2) and cisplatin/anti-CSF-1R/anti-Ly6G (BrdU n=6 animals; γH2AX n=5 animals; cCasp3 n=8 animals; CD31 n=5 animals; CIS adducts n=5 animals). Values presented in **a-c**, **e-f, j-l** and **n** represent average number of positive cells per field of view (FOV) as determined by IHC quantified by counting five high-power microscopic fields per tumor. Values presented in **m** represent average number of positive cells per FOV as determined by immunofluorescence by counting six field per tumor. Data presented in **a-f** and **j-n** are mean values ± SEM. Statistical analysis was performed using two-tailed Mann–Whitney test. CIS, cisplatin.

Supplementary Table 1: List of antibodies used

Immunohistochemistry

Antibody	Antigen retrieval	Clone	Vendor	Dilution	Catalog number
BrdU	TRIS/EDTA pH 9.0	Bu20a	DakoCytomation	1:100	M 0744
CD3	TRIS/EDTA pH 9.0	SP7	Thermo Scientific	1:600	RM-9107
CD4	TRIS/EDTA pH 9.0	4SM95	eBioscience	1:1000	14-9766-80
CD8	TRIS/EDTA pH 9.0	4SM15	eBioscience	1:2000	14-0808
FoxP3	Citrate buffer	FJK-16s	eBioscience	1:400	14-5773
F4/80	Proteinase K 20µg/ml	Cl:A3-1	AbD Serotec	1:400	MCA497
Granzyme B	Citrate buffer	-	Novus Biologicals	1:200	NB100-684
Ly6G	Proteinase K 20µg/ml	1A8	BD Biosciences	1:150	551459
Cleaved Caspase 3	TRIS/EDTA pH 9.0	-	Cell Signaling	1:400	#9661
CD34	TRIS/EDTA pH 9.0	MEC 14.7	Abcam	1:500	ab8158
γH2AX (Ser139)	Citrate buffer	-	Cell Signaling	1:50	#2577
S100A9	TRIS/EDTA pH 9.0	HPA004193	Atlas Antibodies	1:1000	HPA 004193
NKp46	PT module buffer 1 (Thermo, TA-250-PM1X)	-	R&D systems	1:100	AF2225
MBP	Pepsin solution	-	Lee Laboratory, Mayo Clinic	1:500	-
cytokeratin 8	Citrate buffer	Troma 1	Developmental Studies Hybridoma Bank, University of Iowa	1:600	Troma I

Cisplatin adducts	-	-	NKI-A59	1:100	-

Immunofluorescence

Antibody	Antigen retrieval	Clone	Vendor	Dilution	Catalog number
actin a-Smooth muscle-Cy3	Citrate Buffer	1A4	Sigma-Aldrich	1:200	C6198
CD31	Citrate Buffer	-	Abcam	1:200	ab28364
Donkey anti-rabbit AF647	-	-	Invitrogen, ThermoFisher Scientific,	1:500	A-31573

Flow cytometry

CSF-1R expression panel:

Antibody	Fluorophore	Clone	Vendor	Dilution	Catalog number
CD45	eVolve605	30-F11	eBioscience	1:100	83-0451-42
CD11b	BV650	M1/70	Biolegend	1:400	101239
F4/80	APCef780	BM8	eBioscience	1:200	47-4801-82
Ly6C	ef450	hk1.4	eBioscience	1:400	48-5932-82
Ly6G	AF700	1A8	Biolegend	1:200	127622
CD115 (CSF-1R)	PE	AFS98	eBioscience	1:200	12-1152-82
7AAD			eBioscience	1:20	00-6993-50

Intratumoral macrophage panel:

Antibody	Fluorophore	Clone	Vendor	Dilution	Catalog number
CD16/CD32	-	2.4G2	BD Biosciences	1:50	553141
CD45	BUV395	30-F11	BD Biosciences	1:200	564279
CD11b	BV650	M1/70	Biolegend	1:400	101239
F4/80	AF700	BM8	Biolegend	1:200	123130
MHCII	APCef780	M5/114.15.2	eBioscience	1:200	47-5321-82
CD206	AF488	MR5D3	AbD serotec	1:100	MCA2235
7AAD			eBioscience	1:20	00-6993-50

Tumor panel I:

Antibody	Fluorophore	Clone	Vendor	Dilution	Catalog number
CD45	eVolve605	30-F11	eBioscience	1:100	83-0451-42
CD11b	BV650	M1/70	Biolegend	1:400	101239
Ly6C	ef450	hk1.4	eBioscience	1:400	48-5932-82
Ly6G	AF700	1A8	Biolegend	1:200	127622
F4/80	FITC	BM8	eBioscience	1:200	11-4801-82
CD3	PE-cy7	145-2c11	eBioscience	1:200	17-0031-82
CD31	PercPef710	390	eBioscience	1:200	46-0311-82
Fixable Viability Dye eFluor® 780			eBioscience	1:1000	65-0865-14

Tumor panel II:

Antibody	Fluorophore	Clone	Vendor	Dilution	Catalog number
CD45	eVolve605	30-F11	eBioscience	1:100	83-0451-42
CD11b	BV650	M1/70	Biolegend	1:400	101239
F4/80	AF700	BM8	Biolegend	1:200	123130
CD103	PercPef710	2E7	eBioscience	1:200	46-1031-82
B220	FITC	RA3-6B2	eBioscience	1:200	11-0452-82
MHCII	APCef780	M5/114.15.2	eBioscience	1:200	47-5321-82
CD11c	PE-cy7	HL3	BD Biosciences	1:200	558079
CD3 (dump)	ef450	145-2c11	eBioscience	1:200	48-0031-82
CD19 (dump)	ef450	ebio1D3	eBioscience	1:200	48-0193-82
LIVE/ DEAD® Fixable Aqua Dead Cell Stain, for 405 nm excitation			ThermoFisher Scientific	1:100	L34957

tumor panel III (oxaliplatin-treated mice):

Antibody	Fluorophore	Clone	Vendor	Dilution	Catalog number
CD16/CD32	-	2.4G2	BD Biosciences	1:50	553141
CD45	APCef780	30-F11	eBioscience	1:200	47-0451-82
CD11b	BV786	M1/70	BD Biosciences	1:400	740861
Ly6C	BV605	hk1.4	Biolegend	1:400	128035
Ly6G	AF700	1A8	Biolegend	1:200	127622
F4/80	Ef450	BM8	eBioscience	1:200	48-4801-82
7AAD				1:20	00-6993-50

Lymphocyte panel:

Antibody	Fluorophore	Clone	Vendor	Dilution	Catalog number
CD45	eVolve605	30-F11	eBioscience	1:100	83-0451-42
CD3	PE-cy7	145-2c11	eBioscience	1:200	17-0031-82
CD8	PerCPef710	53-6.7	eBioscience	1:200	46-0081-82
CD4	PE-cy5	H129.19	BD Biosciences	1:200	553654
Granzyme B	PE	GB-11	Pelicluster Sanquin	1:100	M2289
F4/80 (dump)	APCef780	BM8	eBioscience	1:200	47-4801-82
CD11b (dump)	APCef780	M1/70	eBioscience	1:200	47-0112-82
CD19 (dump)	APCef780	ebio1D3	eBioscience	1:200	47-0193-82
Fixable Viability Dye eFluor® 780			eBioscience	1:1000	65-0865-14

Macrophage characterization panel 1:

Antibody	Fluorophore	Clone	Vendor	Dilution	Catalog number
CD16/ CD32	-	2.4G2	BD Biosciences	1:50	553141
CD45	BUV395	30-F11	BD Biosciences	1:200	564279
CD11b	BV650	M1/70	Biolegend	1:400	101239
F4/80	FITC	BM8	eBioscience	1:200	11-4801-82
Ly6C	PE/Dazzle	hk1.4	Biolegend	1:400	128044
MHCII	APCef780	M5/114.15.2	eBioscience	1:200	47-5321-82
CD11c	PE-cy7	HL3	BD Biosciences	1:200	558079
CD80	PerCPef710	16-10A1	eBioscience	1:200	46-0801-82
CD86	PE	GL1	eBioscience	1:400	12-0862-82
Siglec F	BV605	E50-2440	BD Biosciences	1:200	740388
Ly6G	AF700	1A8	Biolegend	1:200	127622
CD3 (dump)	ef450	145-2c11	eBioscience	1:200	48-0031-82
CD19 (dump)	ef450	ebio1D3	eBioscience	1:200	48-0193-82
CD49b (dump)	ef450	DX5	eBioscience	1:200	48-5971-82
DAPI			Sigma-Aldrich	1:20	D9542

Macrophage characterization panel 2:

Antibody	Fluorophore	Clone	Vendor	Dilution	Catalog number
CD16/ CD32	-	2.4G2	BD Biosciences	1:50	553141
CD45	BUV395	30-F11	BD Biosciences	1:200	564279
CD11b	BV650	M1/70	Biolegend	1:400	101239
F4/80	AF700	BM8	Biolegend	1:200	123130
Ly6C	PE/Dazzle	hk1.4	Biolegend	1:400	128044
MHCII	APCef780	M5/114.15.2	eBioscience	1:200	47-5321-82
CD274	PerCPef710	MIH5	eBioscience	1:200	46-5982-82
Siglec F	BV605	E50-2440	BD Biosciences	1:200	740388
Ly6G (dump)	ef450	1A8	eBioscience	1:400	48-9668-82
CD3 (dump)	ef450	145-2c11	eBioscience	1:200	48-0031-82
CD19 (dump)	ef450	ebio1D3	eBioscience	1:200	48-0193-82
CD49b (dump)	ef450	DX5	eBioscience	1:200	48-5971-82
DAPI			Sigma-Aldrich	1:20	D9542

Macrophage characterization panel 3:

Antibody	Fluorophore	Clone	Vendor	Dilution	Catalog number
CD16/ CD32	-	2.4G2	BD Biosciences	1:50	553141
CD45	BUV395	30-F11	BD Biosciences	1:200	564279
CD11b	BV650	M1/70	Biolegend	1:400	101239
F4/80	FITC	BM8	eBioscience	1:200	11-4801-82
Ly6C	PE/Dazzle	hk1.4	Biolegend	1:400	128044
MHCII	APCef780	M5/114.15.2	eBioscience	1:200	47-5321-82
CCR2	PE	475301	R&D systems	1:100	FAB5538P-025
CX3CR1	APC	SA011F11	Biolegend	1:400	149008
Siglec F	BV605	E50-2440	BD Biosciences	1:200	740388
Ly6G (dump)	ef450	1A8	eBioscience	1:400	48-9668-82
CD3 (dump)	ef450	145-2c11	eBioscience	1:200	48-0031-82
CD19 (dump)	ef450	ebio1D3	eBioscience	1:200	48-0193-82
CD49b (dump)	ef450	DX5	eBioscience	1:200	48-5971-82
DAPI			Sigma-Aldrich	1:20	D9542

Macrophage characterization in K14cre;Trp53$^{F/F}$ tumor panel 1:

Antibody	Fluorophore	Clone	Vendor	Dilution	Catalog number
CD16/CD32	-	2.4G2	BD Biosciences	1:50	553141
CD45	BUV395	30-F11	BD Biosciences	1:200	564279
CD11b	BV786	M1/70	BD Biosciences	1:400	740861
F4/80	APCef780	BM8	eBioscience	1:200	47-4801-82
Ly6C	ef450	hk1.4	eBioscience	1:400	48-5932-82
Ly6G	FITC	1A8	BD Biosciences	1:200	551460
Siglec F	BV605	E50-2440	BD Biosciences	1:200	740388
CD86	PE	GL1	eBioscience	1:400	12-0862-82
CX3CR1	APC	SA011F11	Biolegend	1:400	149008
CD80	PercPef710	16-10A1	eBioscience	1:200	46-0801-82
CD274	PEcy7	MIH5	eBioscience	1:200	25-5982-82
7AAD				1:20	00-6993-50

Macrophage characterization in K14cre;Trp53$^{F/F}$ tumor panel 2:

Antibody	Fluorophore	Clone	Vendor	Dilution	Catalog number
CD16/CD32	-	2.4G2	BD Biosciences	1:50	553141
CD45	BUV395	30-F11	BD Biosciences	1:200	564279
CD11b	BV786	M1/70	BD Biosciences	1:400	740861
F4/80	APCef780	BM8	eBioscience	1:200	47-4801-82
Ly6C	ef450	hk1.4	eBioscience	1:400	48-5932-82
Ly6G	AF700	1A8	Biolegend	1:200	127622
Siglec F	BV605	E50-2440	BD Biosciences	1:200	740388
CCR2	PE	475301	R&D systems	1:200	FAB5538P-025
7AAD				1:20	00-6993-50

tdTomato⁺ monocyte panel:

Antibody	Fluorophore	Clone	Vendor	Dilution	Catalog number
CD16/ CD32	-	2.4G2	BD Biosciences	1:50	553141
CD45	BUV395	30-F11	BD Biosciences	1:200	564279
CD11b	BV786	M1/70	BD Biosciences	1:400	740861
F4/80	APCef780	BM8	eBioscience	1:200	47-4801-82
Ly6C	ef450	hk1.4	eBioscience	1:400	48-5932-82
Ly6G	AF700	1A8	Biolegend	1:200	127622
Siglec F	BV605	E50-2440	BD Biosciences	1:200	740388
CCR2	AF488	475301	R&D systems	1:200	FAB55381RG-100UG
CX3CR1	APC	SA011F11	Biolegend	1:400	149008
CD80	PercPef710	16-10A1	eBioscience	1:200	46-0801-82
CD274	PEcy7	MIH5	eBioscience	1:200	25-5982-82
7AAD				1:20	00-6993-50

Isolation of mTmG monocytes from bone marrow:

Antibody	Fluorophore	Clone	Vendor	Dilution	Catalog number
CD11b	BV786	M1/70	BD Biosciences	1:400	740861
Ly6C	Ef450	hk1.4	eBioscience	1:400	48-5932-82
Siglec F	BV605	E50-2440	BD Biosciences	1:200	740388
cKIT	BV605	2B8	BD Biosciences	1:200	563146
Sca1	BV605	D7	Biolegend	1:200	108133
CD3	FITC	145-2C11	eBioscience	1:200	11-0031-63
CD8	FITC	53-6.7	eBioscience	1:400	11-0081-82
CD4	FITC	GK1.5	eBioscience	1:400	11-0041-82
NKp46	FITC	29A1.4	eBioscience	1:200	11-3351-82
Ter119	FITC	TER-119	Biolegend	1:200	116205
F4/80	APCef780	BM8	eBioscience	1:200	47-4801-82
7AAD			eBioscience	1:20	00-6993-50

Isolation of cells populations from intratumoral CD11b$^+$ fraction:

Antibody	Fluorophore	Clone	Vendor	Dilution	Catalog number
Ly6G	FITC	1A8	BD Biosciences	1:200	551460
F4/80	PE	BM8	eBioscience	1:200	12-4801-82
Ly6C	Ef450	hk1.4	eBioscience	1:400	48-5932-82

Isolation of cells populations from intratumoral CD11b^{-} fraction:

Antibody	Fluorophore	Clone	Vendor	Dilution	Catalog number
CD45	PercPcy5.5	30-F-11	eBioscience	1:200	45-0451-82
B220	PE-Cy7	RA3-6B2	eBioscience	1:200	25-0452-82
CD31	FITC	390	eBioscience	1:200	11-0311-82
CD11c	PE	N418	eBioscience	1:200	12-0114-82
MHCII	APCef780	M5/114.15.2	eBioscience	1:200	47-5321-82
CD19	Ef450	eBio1D3	eBioscience	1:200	48-0193-82
LIVE/ DEAD® Fixable Aqua Dead Cell Stain, for 405 nm excitation			ThermoFisher Scientific	1:100	L34957

Supplementary Table 2: List of primer sequences used for RT-PCR.

Gene	Primer Forward (5'-3')	Primer Reverse (5'-3')
IFNα (all genes)	TCTGATGCAGCAGGTGGG	AGGGCTCTCCAGACTTCTGCTCTG
IFNβ	GCACTGGGTGGAATGAGACT	AGTGGAGAGCAGTTGAGGACA
TLR3	GTGAGATACAACGTAGCTGACTG	TCCTGCATCCAAGATAGCAAGT
RIG-1	CCACCTACATCCTCAGCTACATGA	TGGGCCCTTGTTGTTCTTCT
IFIH1	GTGATGACGAGGCCAGCAGTTG	ATTCATCCGTTTCGTCCAGTTTCA
ISG15	GGTGTCCGTGACTAACTCCAT	TGGAAAGGGTAAGACCGTCCT
OAS1A	GCCTGATCCCAGAATCTATGC	GAGCAACTCTAGGGCGTACTG
β-actin	CCTCATGAAGATCCTGACCGA	TTTGATGTCACGCACGATTTC

Supplementary Table 3: List of type I IFN-related pathways and genes

List of type I IFN-related pathways and corresponding genes selected from BiNGO and Ingenuity Pathway Analysis (IPA) that are differentially expressed in neutrophils from cisplatin/anti-CSF-1R-treated tumors (n=4 biological independent samples) compared to neutrophils from cisplatin/control ab-treated tumors (n=3 biological independent samples). Statistical analysis was performed using two-way ANOVA

Biological processes by BiNGO Analysis	Genes	Fold change	p-value
POSITIVE REGULATION OF RESPONSE TO CYTOKINE STIMULUS	ZBP1	3.91	0.0027
	IRF7	3.17	0.0014
	NLRC5	2.84	0.0065
REGULATION OF RESPONSE TO CYTOKINE STIMULUS	ZBP1	3.91	0.0027
	IRF7	3.17	0.0014
	NLRC5	2.84	0.0065
REGULATION OF CYTOKINE-MEDIATED SIGNALING PATHWAY	ZBP1	3.91	0.0027
	IRF7	3.17	0.0014
	NLRC5	2.84	0.0065
REGULATION OF INNATE IMMUNE RESPONSE	ZBP1	3.91	0.0027
	IRF7	3.17	0.0014
	NLRC5	2.84	0.0065
	TAP1	2.8	0.0052
	DHX58	3.32	0.0006
REGULATION OF TYPE I INTERFERON-MEDIATED SIGNALING PATHWAY	ZBP1	3.91	0.0027
	IRF7	3.17	0.0014
	NLRC5	2.84	0.0065

POSITIVE REGULATION OF TYPE I INTERFERON-MEDIATED SIGNALING PATHWAY	ZBP1	3.91	0.0027
	IRF7	3.17	0.0014
	NLRC5	2.84	0.0065
POSITIVE REGULATION OF CYTOKINE-MEDIATED SIGNALING PATHWAY	ZBP1	3.91	0.0027
	IRF7	3.17	0.0014
	NLRC5	2.84	0.0065
NEGATIVE REGULATION OF TYPE I INTERFERON PRODUCTION	GBP4	11	0.002
	DHX58	3.32	0.0006
REGULATION OF TYPE I INTERFERON PRODUCTION	IRF7	3.17	0.0014
	GBP4	11	0.002
	DHX58	3.32	0.0006
REGULATION OF INTERFERON-ALPHA PRODUCTION	IRF7	3.17	0.0014
	GBP4	11	0.002
CELLULAR RESPONSE TO INTERFERON-BETA	IFI205	4.68	0.0073
	GBP2B	3.79	8.40E-05
	TREX1	2.86	6.10E-05
	GBP2	2.78	0.0043
	IFI202B	2.94	0.011
	IFIT1	2.89	0.0002
	IFIT3	3.58	0.0001

RESPONSE TO INTERFERON-BETA	IFI205	4.68	0.0073
	GBP2B	3.79	8.40E-05
	TREX1	2.86	6.10E-05
	GBP2	2.78	0.0043
	XAF1	3.89	0.0029
	IFI202B	2.94	0.011
	IFIT1	2.89	0.0002
	IFIT3	3.58	0.0001
RESPONSE TO INTERFERON-ALPHA	IFIT1	2.89	0.0002
	IFIT3	3.58	0.0001
	IFIT2	3.42	0.0003
CELLULAR RESPONSE TO INTERFERON-ALPHA	IFIT1	2.89	0.0002
	IFIT3	3.58	0.0001
	IFIT2	3.42	0.0003
DEFENSE RESPONSE TO VIRUS	ZBP1	3.91	0.0027
	GBP2B	3.79	8.40E-05
	RSAD2	3.14	0.0063
	MX2	3.02	0.001
	IFIT1	2.89	0.0002
	IFIT3	3.58	0.0001
	IFIT2	3.42	0.0003
	CXCL10	2.75	0.0005
	DHX58	3.32	0.0006
Biological processes by IPA	**Genes**	**Fold change**	**p-value**

INTERFERON SIGNALING	IFI35	2.02	0.0066
	IFIT1	2.89	0.0002
	IFIT3	3.58	0.0001
	IFITM3	2.42	0.002
	IRF1	2.25	0.0006
	IRF9	2.12	0.0015
	MX2	3.02	0.001
	OAS1a	2.37	0.0023
	OAS1g	4.21	0.0008
	PSMB8	1.97	0.0465
	SOCS1	2.59	0.0176
	STAT1	2.24	0.0029
	STAT2	2.46	0.0002
	TAP1	2.8	0.0052
ACTIVATION OF IRF BY CYTOSOLIC PATTERN RECOGNITION RECEPTORS	ADAR	1.67	0.0463
	DHX58	3.32	0.0006
	IFIH1	2.38	0.0009
	IFIT2	3.42	0.0003
	IRF7	3.17	0.0014
	IRF9	2.12	0.0015
	ISG15	2.46	0.0022
	STAT1	2.24	0.0029
	STAT2	2.46	0.0002
	ZBP1	3.91	0.0027

CHAPTER 6

hMRP8-ATTAC mice: a new model for conditional and reversible neutrophil ablation

Camilla Salvagno[1], Lisanne Raeven [1], Kim Vrijland[1], Marjolein C. Stip[1,2], Cheei-Sing Hau[1], Colin Pritchard[3], Linda Henneman[3], Rahmen Bin Ali[3], Ivo Huijbers[3], Karin E. de Visser[1,*]

[1] Division of Tumor Biology & Immunology, Oncode Institute, the Netherlands Cancer Institute, Plesmanlaan 121, 1066 CX Amsterdam, The Netherlands
[2] Current address: Immunotherapy Laboratory, Laboratory for Translational Immunology, University Medical Center Utrecht, Utrecht, Netherlands.
[3] Mouse clinic – Transgenic core facility the Netherlands Cancer Institute, Plesmanlaan 121, 1066 CX Amsterdam, The Netherlands
* Corresponding Author: Karin E. de Visser, Division of Tumor Biology & Immunology, The Netherlands Cancer Institute, Plesmanlaan 121, 1066 CX Amsterdam, The Netherlands. Phone: +31-20-5126104. Fax: +31-20-5122057. E-mail: k.d.visser@nki.nl

Unpublished

Abstract

Neutrophils are not only crucial immune cells for the neutralization of pathogens during infections, but they are also key players during tumor initiation, tumor growth and metastasis formation. Several methods are available to investigate the in vivo role of neutrophils in these conditions, including depletion of neutrophils with neutralizing antibodies against Ly6G, or blockade of neutrophil recruitment with CXCR2 inhibitors. A limited number of transgenic mouse models has been generated that rely on the disruption of genes important for neutrophil development or on the injection of diphtheria toxin to induce neutrophil ablation. However, these methods have various limitations, including lack of neutrophil specificity, lack of long-term efficacy, or lack of the ability to conditionally deplete neutrophils. Therefore, we generated a transgenic mouse model for the inducible and reversible ablation of neutrophils using the ATTAC (Apoptosis Through Targeted Activation of Caspase 8) approach. With the ATTAC strategy, which relies on the expression of caspase 8-FKBP fusion protein, apoptosis is induced upon administration of a chemical dimerizer (FK506 analogue) leading to the dimerization and activation of caspase 8. In order to achieve specific neutrophil depletion, we cloned the ATTAC construct under the human migration inhibitory factor-related protein 8 (hMRP8) promotor. The newly generated hMRP8-ATTAC mice express high levels of the transgene in neutrophils and, as a consequence, dimerizer injection induces an efficient neutrophil reduction in all the organs analyzed. In contrast, no efficient neutrophil depletion was achieved in mammary tumor-bearing hMRP8-ATTAC mice, suggesting that tumor-induced neutrophil expansion prevails over dimerizer-mediated apoptosis. In conclusion, we here describe the generation and characterization of a new transgenic model for neutrophil ablation and highlight the need to improve the ATTAC strategy for the depletion of large numbers of rapidly generated short-lived cells, such as neutrophils.

Introduction

Neutrophils are polymorphonucleated cells that have a major role in infection. Known to be the first cells to arrive at a site of inflammation, neutrophils can clear pathogens by means of several mechanisms, like phagocytosis, release of bactericidal molecules from their granules and neutrophil extracellular traps (NETosis)[1]. On top of their well-established role in infection, neutrophils are also a critical component of tumor initiation, tumor growth and metastasis formation, and both tumor-promoting and tumor-suppressing effects have been described[2]. Several cancer types, including breast cancer, are often associated with elevated numbers of circulating neutrophils and a high neutrophil-to-lymphocyte ratio (NLR) in blood predicts a worse survival[3,4]. In addition, also intratumoral neutrophils are predictive of adverse prognosis[5]. Neutrophils are constantly produced in the bone marrow under the control of granulocyte colony stimulating factor (G-CSF) and released in the circulation as terminally differentiated and mature cells[2]. The retention and the release of neutrophils in and from the bone marrow is strictly controlled by the expression of the chemokine receptors CXCR4 and CXCR2, respectively. Chemokines secreted by endothelial cells and megakariocytes like CXCL1, CXCL2 and CXCL5 are essential for the mobilization of $CXCR2^{+}$ neutrophils from the bone marrow into the circulation[2]. In cancer, both tumor and host cells can produce G-CSF which results in a strong pressure on the bone marrow to release new neutrophils, a proportion of which have an immature nuclear morphology and retain the expression of the progenitor marker cKIT[6-9]. In addition, cancer cells can express CXCR2 ligands to recruit neutrophils in the tumor microenvironment[10].

Current *in vivo* methods to study neutrophils involve either depletion of the cells or blockade of their recruitment. Neutrophils, defined as myeloid cells expressing $Ly6G^{high}Ly6C^{int}$, can be depleted using anti-Gr-1 antibodies, which recognize a shared epitope between Ly6C and Ly6G surface markers[11,12]. However, because inflammatory monocytes express high level of Ly6C, this strategy does not target only neutrophils[11]. A more specific approach is to deplete neutrophils with the anti-Ly6G antibody (clone 1A8)[11]. However, the depletion efficiency of this antibody is strongly reduced after 2 weeks of treatment, likely due to a neutralizing antibody response against the rat IgG2a antibody. Furthermore, the 1A8 antibody provides poor neutrophil depletion in C57BL/6J mice[13]. Another strategy to study the role of neutrophils in tumors is by impairing neutrophil trafficking using CXCR2-deficient mice or CXCR2 antagonists[10,14]. However, it should be considered that CXCR2 expression is not exclusive to neutrophils, but it is also expressed by other cells, including some cancer cells[15]. Recently a mouse model for the selective and inducible neutrophil depletion was developed by intercrossing $ROSA\text{-}iDTR^{KI}$ mice, which bear a Cre-inducible simian diphtheria toxin receptor (DTR), with human migration inhibitory factor-related protein 8 (hMRP8)-Cre mice, which express Cre recombinase under the control of the promoter of the neutrophil-associated S100 Calcium Binding Protein A8 (S100A8). As a result, DTR is expressed mainly in neutrophils (*hMRP8cre;ROSA-iDTR*^{KI})[16]. It is known, however, that DTR systems are not ideal for long term experiments because prolonged DT injection induces an immune response against DT, annihilating its effect[17,18]. In order to overcome immunogenicity issues, we generated a novel transgenic mouse model for the

conditional and reversible ablation of neutrophils using the ATTAC (Apoptosis Through Targeted Activation of Caspase 8) approach developed by Pajvani *et al*.[19]. The ATTAC construct strategy was previously used to successfully and over prolonged periods ablate adipocytes, podocytes, pancreatic β–cells and $p16^{Ink4a}$-positive senescent cell by inducing apoptosis in these cells[19-22]. We have used the hMRP8 promotor to drive expression of the ATTAC transgene, and we here describe and characterize the hMRP8-ATTAC mouse in a non-tumor and tumor setting.

Results

Generation of the hMRP8-ATTAC mouse model

In order to set up a system allowing genetic depletion of neutrophils *in vivo*, we utilized the ATTAC approach in which a mutated FK506-binding-protein (FKBP) domain is fused to caspase 8[19] and expressed under control of the hMRP8 promoter. Injection of the dimerizer AP20187 induces dimerization of two FKBP domains, leading to activation of membrane-bound myristoylated caspase 8 resulting in apoptosis. An IRES-EGFP fragment was cloned after the ATTAC construct (Fig. 1A) to allow detection of transgene positive cells. The purified transgene fragment was injected in the pronucleus of FVB/N zygotes and progeny was screened for the presence of GFP. A total of 9 transgenic founders carrying the transgene were obtained, of which 3 founders showed GFP expression in circulating neutrophils with varying intensity (Fig. 1B-C). Because founder 19 had the highest GFP expression in neutrophils, we generated the hMRP8-ATTAC line from this founder mouse. Southern blot analysis of founder 19 and heterozygous progeny showed that the construct integrated in the genome in one locus as a concatemer of multiple copies (Supp. Fig. 1). Mice were bred to obtain heterozygous (HET) and homozygous (HOM) progeny. Flow cytometry analyses of several organs of HET and HOM mice showed no differences in immune cell proportion compared to wild-type (WT) mice (Supp. Fig. 2A-F, Supp. Fig. 3-5 and data not shown), indicating that the construct does not interfere with immune cell development.

Neutrophils in hMRP8-ATTAC mice express GFP

Because S100A8 is not only expressed in neutrophils, but also in monocytes and other granulocytes[23], we set out to assess the transgenic GFP expression pattern in immune cells in hMRP8-ATTAC mice by flow cytometry analysis. Neutrophils showed GFP expression in all the organs analyzed, *i.e.* blood, spleen, lung, liver and lymph node, of HET hMRP8-ATTAC mice (Fig. 2A-E). In line with the double number of transgene copies, neutrophils in HOM mice displayed a more intense GFP expression (Fig. 2A-E). Further analyses of other myeloid cell populations showed a minimal expression of GFP in eosinophils and monocytes of HOM hMRP8-ATTAC mice compared to WT mice (Supp. Fig. 6A-E). These levels were much lower than the GFP levels of neutrophils (Fig. 2F). Dendritic cells and resident macrophages, like red pulp macrophages in the spleen, Kupffer cells in the liver, alveolar macrophages in the lung and the $CD169^+$ macrophages in the lymph node, were GFP negative (Supp. Fig. 6A-E). As expected, also $CD3^+$ T cells did not express GFP (Supp. Fig. 6A-D).

We next set out to investigate at which stage of hematopoietic differentiation

(Fig. 3A) the ATTAC construct was expressed. By flow cytometry analysis of bone marrow cells from HET and HOM hMRP8-ATTAC mice, we observed that Lineage$^-$ Sca1$^+$cKIT$^-$ (LSK), common myeloid progenitors (CMP) and megakaryocyte erythroid progenitor (MEP) were GFP negative (Fig. 3B and Supp. Fig. 7A). Along the line of neutrophil differentiation, we observed a modest increase in GFP expression, albeit not significant, in granulocyte monocyte progenitor (GMP), which intensified in promyelocytes and even more in neutrophils (Fig. 3B and Supp. Fig. 7A). A small increment in GFP expression was also seen in monocyte dendritic cell progenitor (MDP) and monocytes (Fig. 3B and Supp. Fig. 7A), in line with previous data showing modest GFP expression in monocytes in several organs (Supp. Fig. 6A-E). Altogether, these data indicate that the hMRP8 promoter becomes active in the promyelocytes and MDP populations, inducing transgene expression in these cells and in the following differentiated populations.

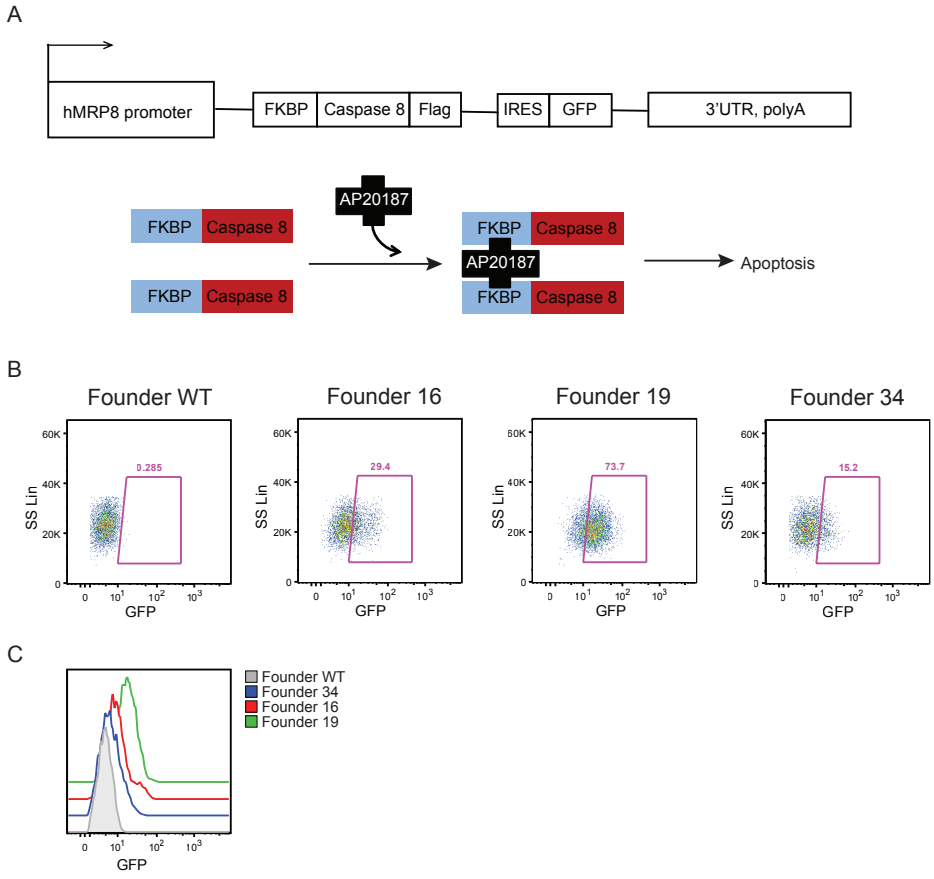


Fig. 1 | Generation of hMRP8-ATTAC mice. (A) Schematic representation of the ATTAC construct and the mechanism of apoptosis induced by the dimerizer AP20187. (B-C) Dot plots and histograms showing GFP expression in circulating neutrophils of four hMRP8-ATTAC founders as determined by flow cytometry. One of the founders does not carry the transgene as detected by PCR (Founder WT), the other three carry the transgene and express GFP at different levels (Founders 16, 19, 34).

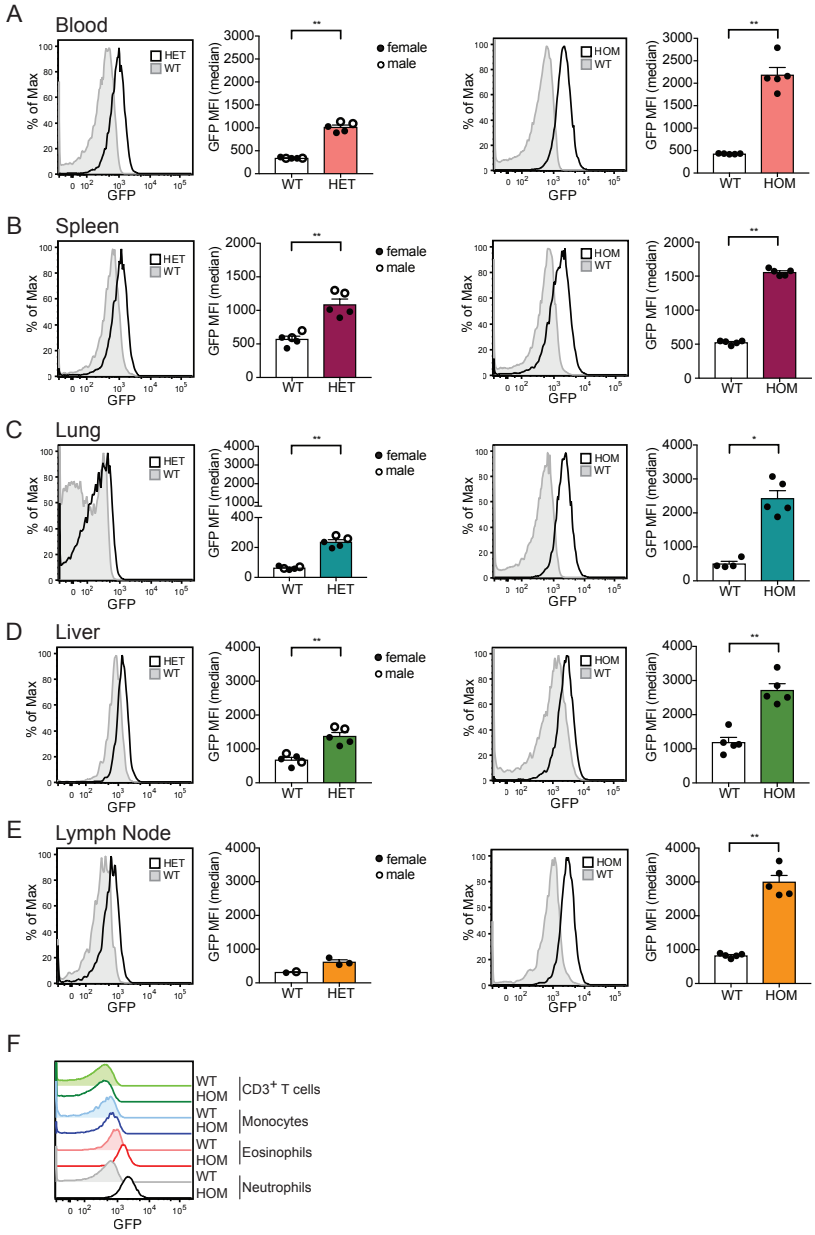


Fig. 2 | Neutrophils in the hMRP8-ATTAC mouse model express the transgene. (A-E) Representative histograms of GFP expression and quantification of the Median Fluorescence Intensity (MFI) of GFP in neutrophils from blood, (A), spleen (B), lung (C), liver (D) and lymph node (E) of heterozygous (left) and homozygous (right) hMRP8-ATTAC mice (n=3-5) compared to WT littermates (n=2-5), as determined by flow cytometry. Open circles represent male hMRP8-ATTAC mice and closed circles represent female hMRP8-ATTAC mice. (F) Representative histogram comparing GFP expression levels in circulating neutrophils, eosinophils, monocytes and $CD3^+$ T cells of homozygous hMRP8-ATTAC mice and WT littermates. WT, wild type; HET, heterozygous; HOM, homozygous. Data presented in A-E are mean values ± SEM. *$p < 0.05$, **$p<0.01$ by Mann–Whitney test.

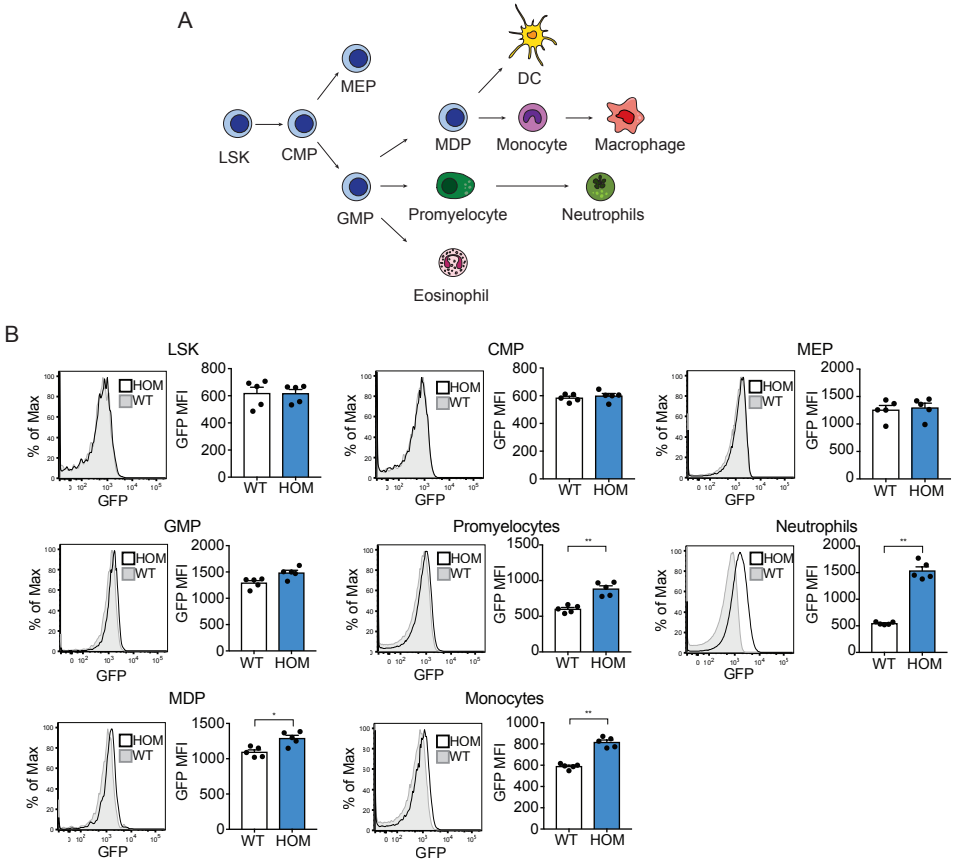


Fig. 3 | The ATTAC transgene starts to be expressed at the GMP level in the bone marrow. (A) Schematic representation of the hematopoietic tree. (B) Representative histograms of GFP expression and quantification of the Median Fluorescence Intensity (MFI) of GFP in different hematopoietic cell populations depicted in (A) in the bone marrow of homozygous female hMRP8-ATTAC mice and WT littermates (n=5/group), as determined by flow cytometry. WT, wild type; HOM, homozygous. LSK, Lineage$^-$SCA1$^+$Kit$^-$; CMP, common myeloid progenitor; MEP, megakaryocyte-erythroid progenitor; GMP, granulocyte-macrophage progenitor; MDP, monocyte/macrophage-dendritic cell progenitor. Data presented in B are mean values ± SEM. *p < 0.05, **p<0.01 by Mann–Whitney test.

Depletion of neutrophils in the hMRP8-ATTAC mouse model upon dimerizer injection

Because HOM hMRP8-ATTAC mice showed a stronger transgene expression, we continued to evaluate the functional activity of the construct in these mice. In order to test the depletion specifically of transgene-expressing cells, we injected hMRP8-ATTAC and non-transgene-carrying control WT mice with the dimerizer AP20187 every day for a week (Fig. 4A). Two days of dimerizer treatment resulted in a reduction of circulating neutrophils in hMRP8-ATTAC mice and not WT mice, while monocytes and eosinophils were not affected (Fig. 4B-C and Supp. Fig. 8A). Interestingly, a slight decrease in neutrophils was observed in the control groups (vehicle-treated hMRP8-ATTAC and vehicle/dimerizer-treated WT mice) compared to pre-treatment samples (Fig. 4B-C and Supp. Fig. 8A), probably due to fluctuation in experimental conditions between time points. After a week of dimerizer treatment, neutrophils were strongly reduced in blood and lungs and modestly in spleen and bone marrow of hMRP8-ATTAC mice with a concomitant small, but significant, relative increase in monocytes in all the organs (Fig. 4D-E). The frequency of eosinophils was not influenced by the dimerizer treatment, except for a reduction in pulmonary eosinophils (Fig. 4F). Tissue resident macrophages in the spleen and lung were not affected (Fig. 4G). We observed a small increase in circulating neutrophils and monocytes, but not in eosinophils and resident macrophages, in WT mice after dimerizer injection, probably due to a modest inflammatory response against the compound (Supp. Fig. 8B-E). Overall, these data illustrate that, in line with the GFP expression profile, neutrophils are most efficiently depleted in all analyzed organs and circulation upon dimerizer inoculation. Other immune cell populations are minimally affected.

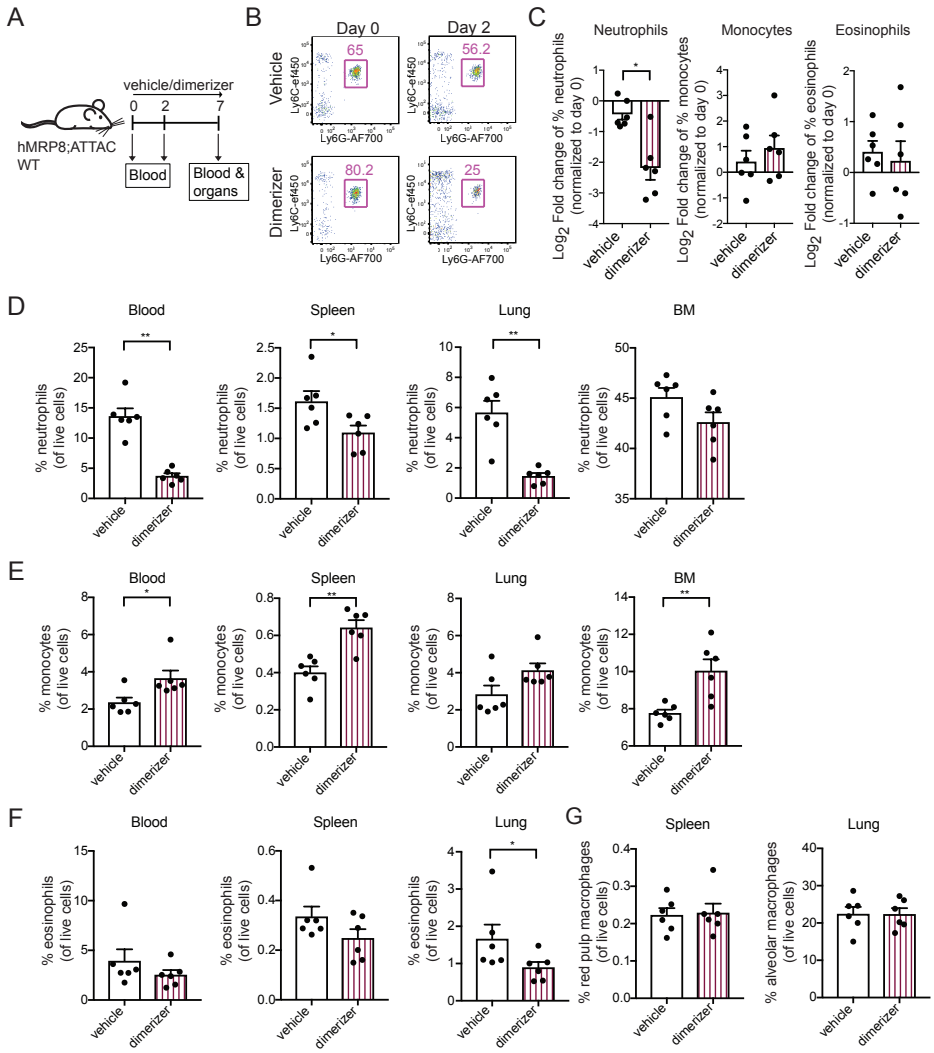


Fig. 4 | Dimerizer treatment reduces neutrophil frequency in hMRP8-ATTAC mice. (A) Schematic representation of the experimental design. Homozygous hMRP8-ATTAC or age-matched WT female mice were treated daily with vehicle or dimerizer for 7 consecutive days. Blood was analyzed by flow cytometry before the start of the treatment and two days after the start of the treatment. At the seventh day, mice were sacrificed and tissues were processed and analyzed by flow cytometry. (B) Representative dot plots showing percentages of neutrophils (of $CD11b^{+}Siglec\ F^{-}$ cells) in the blood of either vehicle- or dimerizer-treated hMRP8-ATTAC mice before and after two days of treatment. (C) Log_2 fold change of circulating neutrophils, monocytes and eosinophils defined as % of live two days after treatment compared to day 0 in hMRP8-ATTAC mice (n=6/group). Fold change was calculated by dividing the frequency of neutrophil at day 2 by the frequency of neutrophils at day 0. (D-G) Frequencies of neutrophils (D), monocytes (E), eosinophils (F) and resident macrophages (G) in blood, spleen, lung and bone marrow of hMRP8-ATTAC mice (n=6/group) treated with vehicle or dimerizer for seven consecutive days. Data presented in C-G are mean values ± SEM. *p < 0.05, **p<0.01 by Mann-Whitney test.

Dimerizer treatment does not reduce neutrophils in tumor-bearing hMRP8-ATTAC mice

We and others have reported previously that neutrophils accumulate in several organs of tumor-bearing mice and that their expansion is related to primary tumor size[2,6,7]. In order to investigate the depletion efficacy of neutrophils in the hMRP8;ATTAC model in a tumor setting, we transplanted mammary tumor pieces, derived from the transgenic *K14cre;Cdh1$^{F/F}$;Trp53$^{F/F}$* (KEP) mouse mammary tumor model[24,25], in the mammary fat pad of syngeneic mice. Vehicle or dimerizer treatment started at a tumor size of 25mm^2 and continued until the tumor size reached the humane end-point (225mm^2) (Fig. 5A). As a positive control, we treated a group of hMRP8-ATTAC mice with the neutralizing antibody against Ly6G (clone 1A8) that was previously used in our studies to deplete neutrophils[7]. In line with the finding that neutrophils do not have an impact on primary KEP tumor outgrowth[7], treatment of tumor-bearing hMRP8-ATTAC mice with either anti-Ly6G or dimerizer did not influence the tumor-specific survival compared to vehicle-treated mice (Supp. Fig. 9A). The frequency of circulating neutrophils was increased at a tumor size of 100mm^2 in vehicle-treated mice when compared to baseline levels at a tumor size of 25mm^2 (Fig. 5B). As expected, neutrophil levels were reduced in anti-Ly6G-treated tumor-bearing mice (Fig. 5B). In contrast, dimerizer treatment did not reduce neutrophils in the circulation at the same tumor size (Fig. 5B). Circulating monocytes expanded with tumor growth in anti-Ly6G- and dimerizer-treated mice while the frequency of eosinophils modestly increased in anti-Ly6G-treated mice compared to vehicle-treated mice at a tumor size of 100 mm^2 (Fig. 5C-D). Prolonged dimerizer treatment did not reduce neutrophil levels in the blood and in the other organs, including the tumor, when mice were analyzed at end-stage (Fig. 5E-H; Supp. Fig. 10). As anticipated, while short-term anti-Ly6G treatment reduced circulating neutrophils (Fig. 5B), this effect was lost over time as no differences were observed in the proportion of neutrophils in the blood of end-stage mice (Fig. 5E); yet, a significant increase in neutrophil accumulation was observed in the spleen, possibly because of the appearance of emergency granulopoiesis, triggered by neutrophil depletion, in this organ (Fig. 5E). Monocyte levels were increased in all tissues analyzed after dimerizer treatment, while the proportion of eosinophils did not change, except for a slight decrease in the blood of dimerizer-treated mice (Supp. Fig. 9B-C and Supp. Fig. 10). A modest reduction in CD3$^+$ T cells was also observed in lungs after dimerizer treatment (Supp. Fig. 9D). In addition, spleen and lung resident macrophages and tumor-associated macrophages (TAMs) were not affected by the treatment (Supp. Fig. 9E). Because inflammation can induce S100A8 upregulation in endothelial cells[26], we counted the number of CD31$^+$ vessels in the tumor of dimerizer-treated hMRP8-ATTAC mice. No difference in vessel density was observed upon dimerizer administration, suggesting that KEP tumors do not activate the hMRP8 promotor in endothelial cells (Fig. 9F).

These data show that, although dimerizer treatment was effective in reducing neutrophils in a homeostatic situation (Fig. 4), it was not successful in a cancer setting, probably due to the high cancer-induced pressure for neutrophil production on the bone marrow.

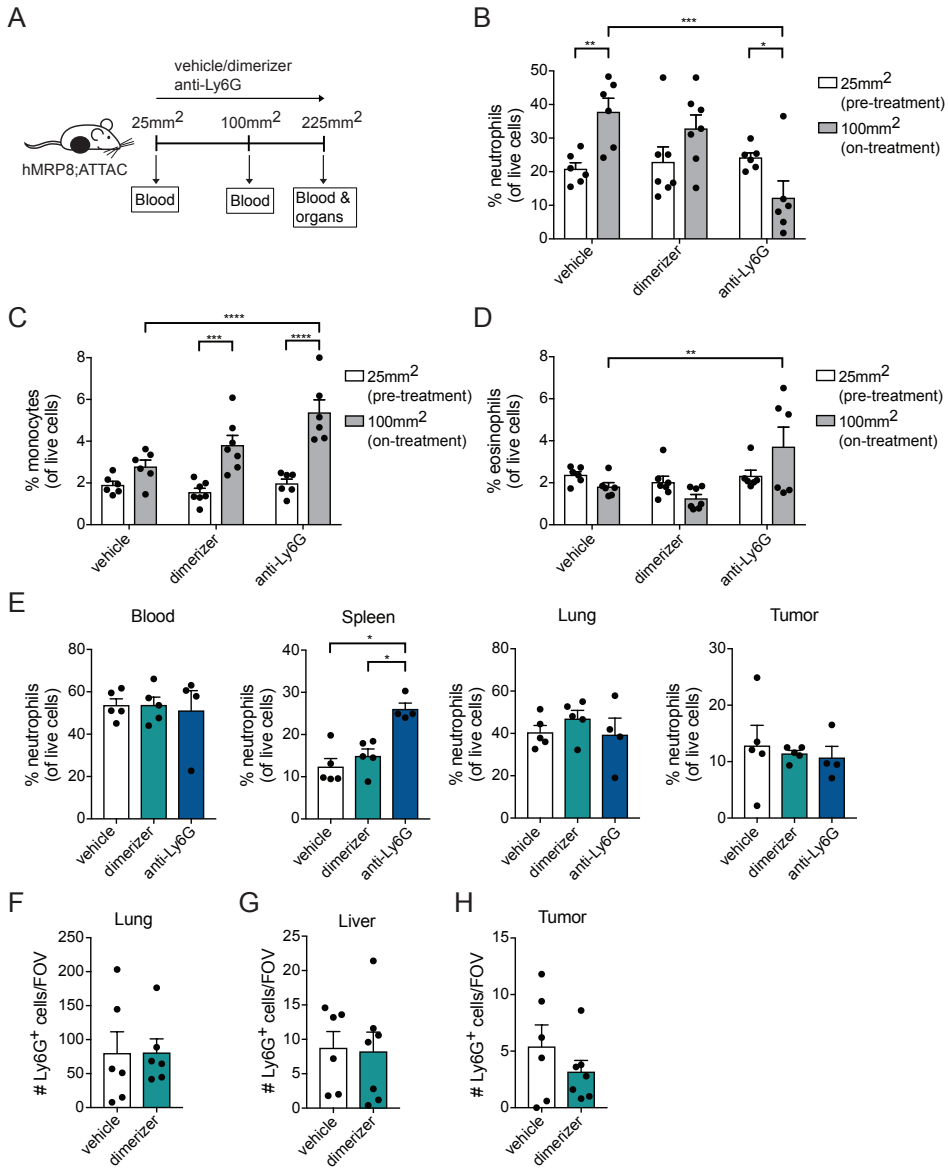


Fig. 5 | Dimerizer treatment does not reduce neutrophil frequency in tumor-bearing hMRP8-ATTAC mice. (A) Schematic representation of the experimental design. Female homozygous hMRP8-ATTAC mice were orthotopically transplanted in the mammary fat pad with *K14cre;Cdh1*$^{F/F}$*,Trp53*$^{F/F}$ tumor fragments. Mice were treated with either vehicle, dimerizer or anti-Ly6G until they were sacrificed when the tumor size reached 225mm^2. Blood was collected before the start of the treatment (25mm^2) and at a tumor size of 100mm^2. (B-D) Frequency of neutrophils (B), monocytes (C) and eosinophils (D) in the blood of hMRP8-ATTAC mice treated as indicated (vehicle and anti-Ly6G treatments, n=6/tumor size; dimerizer treatment, n=7/tumor size) at a tumor size of 25mm^2 and 100mm^2, as determined by flow cytometry. (E) Frequency of neutrophils in blood, spleen, lung and tumor of end-stage hMRP8-

ATTAC mice (n=4-5) as determined by flow cytometry. (F-H) Quantification of Ly6G$^+$ cells in viable areas of lung (F), liver (G) and tumor (H) of end-stage hMRP8-ATTAC mice (n=6-7) as determined by IHC. Values represent average number of positive cells per field of view (FOV) quantified by counting five high-power microscopic fields per tumor. Data presented in B-D are mean values ± SEM. *p < 0.05, **p<0.01, ***p<0.001, ***p<0.0001 by two-way ANOVA with Sidak's multiple comparisons test. Data presented in E-H are mean values ± SEM. *p < 0.05 by Mann–Whitney test.

Discussion

As one of the first immune cells that arrive into an inflamed area, neutrophils represent an indispensable component to fight infections. Recent studies have also shown that they are not only important against pathogens, but they also play a critical role in tumor progression and metastasis formation, with both pro- and anti-tumoral functions being discovered[2]. In order to investigate the functional contribution of neutrophils to specific inflammatory stimuli, infections or cancer, it is desirable to deplete or inhibit these cells and monitor the consequences. Thus far, the most commonly used *in vivo* strategies to ablate neutrophils are treatment with the depleting anti-Ly6G and anti-Gr1 antibodies and the use of CXCR2 antagonists to interfere with neutrophil trafficking. However, the short-term efficacy of anti-Ly6G, its inefficiency at depleting neutrophils in C57BL/6J mice and the non-specificity of anti-Gr1 and CXCR2 antagonists are the main concerns[11,13,15]. In addition, several genetic models have been generated. For example, the *LysMcre;Mcl-1$^{F/F}$* model is deficient in the anti-apoptotic molecule Mcl-1, a Bcl-2 family member, in neutrophil and monocyte/macrophage populations[27]. This mouse model shows decreased numbers of neutrophils, while macrophage levels were not influenced because of a compensatory upregulation of other Bcl-2 family members[27]. Others have used mice bearing point mutations in or full knock-out of the growth factor independence 1 (Gfi1), which is important for neutrophil and T cell development[28,29]. In addition, since G-CSF is the main growth factor for neutrophil development, G-CSF$^{-/-}$ mice display neutropenia and deficiency in granulocyte and macrophage progenitors[30]. Although these models are characterized by a decrease in neutrophil levels, they do not allow to conditionally induce or revert neutrophil depletion. Furthermore, other concerns of the aforementioned genetic models are that they may have unknown developmental defects, or may have developed compensatory mechanisms to cope with the absence of neutrophils or, since neutrophils are critical for immune defense, may have a different composition of the host microbiome. Recently another mouse model for neutrophil ablation was developed by intercrossing ROSA-iDTR^{KI} mice, which bear a Cre-inducible simian diphtheria toxin receptor (DTR), with hMRP8-Cre mice to induce DTR expression (*hMRP8cre;ROSA-iDTR^{KI}*) in S100A8-expressing cells[16]. It is known, however, that long-term treatment with DT induces an immune reaction against the compound itself, blocking its effect[17,18]. There is a clear need for genetic models that allow for long-term efficient and specific conditional and reversible neutrophil depletion. We here describe a novel transgenic mouse model for neutrophil depletion that relies on the activation of caspase 8-FKBP fusion protein upon injection with a chemical dimerizer. The hMRP8-ATTAC mouse model shows a striking hMRP8 promotor activity in neutrophils and a much lower activity in monocytes and eosinophils, as defined by GFP expression in these cells. In the

bone marrow, the transgene is expressed at very low levels at the GMP stage and is upregulated during differentiation along the monocytic and granulocytic lineages. Importantly, because S100A8 expression is downregulated during differentiation into macrophages and DCs[31,32], we did not observe GFP expression in these cells. As expected, because of their high transgene expression, neutrophils in the hMRP8-ATTAC model are very sensitive to the effects of the dimerizer, resulting in a decreased frequency of these cells in blood, lung and spleen, and to a lesser extent in the bone marrow. Future experiments will evaluate if neutrophil depletion is also achieved after long-term treatment with the dimerizer. Although the dimerizer treatment reduces neutrophil levels in this mouse model, it fails to do so in tumor-bearing hMRP8-ATTAC mice. Several reasons might be responsible for the lack of neutrophil depletion in tumor-bearing hMRP8-ATTAC mice. First, it is well established that tumors stimulate granulopoiesis in the bone marrow and release immature and mature neutrophils into the circulations[2,6-8]. Thus, in chronic inflammatory conditions, like in tumor-bearing hosts, neutrophils are constantly produced in excessive amounts, thus perhaps exceeding the activity of the dimerizer. Secondly, the half-life of the dimerizer is approximately 5 hours (Takara Bio Inc.) and because we injected it only once a day, it is probably not frequent enough to suppress the continuous tumor-induced neutrophil expansion. Thirdly, neutrophils are quickly replenished after they die[2,33]. Indeed, previous studies using the ATTAC system aimed at depleting adipocytes, podocytes, pancreatic β–cells and $p16^{Ink4a}$-positive senescent cells showed a pronounced and long-lasting depletion of these cells[19-22,34]. Although these studies used even a lower concentration of the dimerizer per injection compared to our study, these cells are not renewed at the same rate as neutrophils, likely explaining the more stable depletion. Frequent dimerizer injections for the tumor-bearing hMRP8-ATTAC model might be a solution, or future studies should aim at increasing dimerizer half-life or at developing a formulation of the dimerizer that remains stable in the animals' chow. As for the DT in the *hMRP8cre;ROSA-iDTR^{KI}* mouse, the dimerizer might be immunogenic and trigger a neutralizing antibody-mediated response. However, others have performed long dimerizer treatment for 4 weeks[19] and even for 4 months[34] in immunoproficient mice resulting in efficacious cell depletion, suggesting that the dimerizer does not elicit an immune response.

Importantly, in a cancer setting, inflammation can induce S100A8 upregulation. For example, tumor-derived VEGF-A, TGFβ and TNFα may induce S100A8 expression in macrophages and endothelial cells[26] or monocyte/macrophage-derived factors may stimulate its expression in cancer cells[35]. However, in tumor-bearing hMRP8-ATTAC mice, we did not observe loss of TAMs or endothelial cells upon dimerizer treatment, suggesting that in this context these cells do not upregulate the transgene. Moreover, because in this tumor model we transplanted a *K14cre;Cdh1$^{F/F}$;Trp53$^{F/F}$* tumor fragment that does not carry the ATTAC transgene, the dimerizer could not affect directly cancer cells.

Interestingly, differently from the *hMRP8cre;ROSA-iDTR^{KI}* mice, monocyte proportions modestly increase in several tissues of non-tumor-bearing hMRP8-ATTAC and WT mice and tumor-bearing hMRP8-ATTAC upon dimerizer injection. Most likely, this is just a relative increase in monocytes due to neutrophil reduction or an increment in their absolute number due to dimerizer-mediated stimulation of

myelopoiesis. Indeed, we observed a higher proportion of monocytes in the bone marrow of dimerizer-treated hMRP8-ATTAC mice. Interestingly, a similar increase in monocytes was also observed in the Gfi1 mutated and knock-out models[28,29]. Future experiments should aim at evaluating the absolute number of myeloid cells upon dimerizer injection.
In conclusion, we here describe the generation and characterization of a new mouse model for the conditional ablation of neutrophils. Although successful conditional induction of apoptosis in neutrophils through the activation of caspase 8 is achieved in hMRP8-ATTAC mice, future studies should focus on improving the model in order to sustain neutrophil depletion in a chronically inflamed context.

Acknowledgments

This work was supported by the European Research Council (ERC consolidator award INFLAMET 615300), European Union (FP7 MCA-ITN 317445 TIMCC) and Oncode. We thank the mouse clinic – transgenic core facility, flow cytometry facility, the animal facility and the animal pathology facility at the Netherlands Cancer Institute. We thank Philipp Scherer (the University of Texas Southwestern Medical Center, Dallas) and Massimiliano Mazzone (VIB-KU, Belgium) for providing us with reagents.

Author contributions

C.S. and K.E.dV conceived the ideas and designed the experiments. C.P., R.B.A., L.H. and I.H generated the hMRP8-ATTAC mice. C.S., L.R., K.V., M.C.S., and C-S.H. performed the experiments and analyzed the data. C.S. and K.E.dV wrote the paper.

Competing financial interests

The authors declare no competing financial interests.

Methods

Generation of hMRP8-ATTAC transgenic mice
hMRP8-ATTAC mice were generated in the animal laboratory facility of the Netherlands Cancer Institute by the Mouse clinic – Transgenic core facility. The hMRP8-ATTAC transgenic construct was designed as follows. The FKBP-Caspase8 fragment was subcloned from the POD-ATTAC construct[21] (kindly provided by P. Scherer, the University of Texas Southwestern Medical Center, Dallas) and inserted into a pRRL2 vector containing the humanMRP8 (hMRP8) promoter and hMRP8 3' untranslated region[36] (a gift from M. Mazzone, VIB-KU, Belgium). An IRES-EGFP fragment was inserted at 3' of the ATTAC construct. The fragment containing the hMRP8 promoter, FKBP-Caspase8 fusion protein, and the 3' untranslated region was released by ClaI and PspXI digestion, purified from agarose gel by electroelution and microinjected in the pronucleus of FVB/N zygotes. Progenies were screened for GFP by PCR on toe clip-derived genomic DNA (forward: 5'– CTGGACGGCGACGTAAACGGC

– 3'; reverse: 5'– TCCTTGAAGAAGATGGTGCG – 3'). A total of 9 founders were obtained carrying the transgene, and 3 of them showed GFP expression in circulating neutrophils as assessed by flow cytometry.
Heterozygous hMRP8-ATTAC mice were maintained in breeding with FVB/N mice, obtained from Janvier, (HET x FVB/N) to obtain HET and WT mice. Offspring was genotyped by lysing toe clips from the mice in Direct PCR tail (Viagen) containing 1% proteinase K (Sigma Aldrich) and subsequent PCR for the hMRP8 promoter (forward: 5'– CACCACAGTCTTCAAGGTTG – 3'; reverse: 5'– GGCCATACATCCCTGAAACTGA – 3'). After crossing two heterozygous mice to obtain homozygous mice, the colony was maintained by breeding two homozygous mice (HOM x HOM). Genotyping was performed by quantitative RT-PCR for the *Egfp* gene on toe clip lysate. The TaqMan Copy Number Reference Assay for the mouse *Tfrc* gene (Thermo Fisher) was used as the endogenous reference gene. This reference, DNA (5ng/µl), GFP-specific primers (forward: 5' - GAAGCGCGATCACATGGT - 3'; reverse: 5' - CCATGCCGAGAGTGATCC - 3') (Invitrogen) and GFP probe (UPL 67, Roche) were added to TaqMan Universal Mastermix (Thermo Fischer) and the RT-PCR was run on a StepOnePLus PCR system. The copy number of the construct in the mice was calculated using the comparative threshold cycle (CT) method, using a sample containing a single GFP copy as a reference.

Materials and animals
The chemical dimerizer AP20187 was diluted in ethanol according to manufacturer's recommendation (Takara Bio Inc.) before injection. Dimerizer or vehicle (ethanol) was diluted in water containing 2% Tween and 10% PEG-400 (Sigma Aldrich) and was injected i.p. every day for a week at a dose of 0,5µg/g body weight in homozygous female hMRP8-ATTAC mice (age 17-19 weeks-old) and age-matched female FVB/N mice. Blood was collected before the start of the treatment and after two days by tail vein puncture.
For tumor transplantation experiments, donor tumors from KEP mice[24] were collected in ice-cold PBS, cut in small pieces and resuspended in Dulbecco's Modified Eagle's Medium F12 containing 30% fetal calf serum and 10% dimethyl sulfoxide and stored at −150 °C. At the day of transplantation, KEP tumor pieces were thawed and tumor pieces (1x1 mm) were orthotopically transplanted into the mammary fat pad of 8-13 weeks-old hMRP8-ATTAC female mice. Mice were palpated three times a week and the perpendicular tumor diameters of mammary tumors were measured twice a week using a caliper. Treatment with vehicle, dimerizer or anti-Ly6G (single loading dose of 400 µg followed by 100 µg three times a week, clone 1A8, BioXCell) started at a tumor size of 25mm^2 and continued until the tumor reached 100mm^2 when the mice were sacrificed. Blood was collected before the start of the treatment and at a tumor size of 100mm^2 by tail vein puncture.
Mice were kept in individually ventilated cages at the animal laboratory facility of the Netherlands Cancer Institute. Food and water were provided ad libitum. Animal experiments were approved by the Animal Ethics Committee of the Netherlands Cancer Institute and performed in accordance with institutional, national and European guidelines for Animal Care and Use.

Southern Blot
Genomic DNA was isolated from tissue by proteinase K lysis and organic extraction with phenol-chloroform. Southern blot analysis was performed using 10 µg genomic DNA, digested with EcoRV to determine the status of transgene integration. Blotting and hybridization was performed as described previously[37]. Primers for amplification of the GFP probe are the following: forward primer 5'-CCA TGG TGA GCA AGG GCG AGG AGC TG-3'; and reverse primer 5'-CCT TGT ACA GCT CGT CCA TGC CGA GA-3'. The GFP probe was radioactively labeled using Random primers DNA labeling kit (Thermo Fisher Scientific). Hybridization of the GFP probe to EcoRV-digested DNA resulted in a concatemer band of 6114 kb.

Flow cytometry
Tumor, spleen, liver, lung, lymph nodes and bones were collected in ice-cold PBS, while blood was collected in heparine or in EDTA-coated tubes (for tail vein puncture). Tumors were mechanically chopped using the McIlwain Tissue Chopper (Mickle Laboratory Engineering) as described[38], while spleen, liver and lungs were minced using a scalpel. Subsequently, tumor, spleen and liver were digested in serum-free DMEM containing 3mg/mL Collagenase A (Roche) and 25µg/mL DNAse (Sigma Aldrich), while lungs were digested in serum-free DMEM containing 100µg/mL TM Liberase (Roche) and 25µg/mL DNAse. After 30min for spleen, lung and liver and 1hour for tumors, digestion was inactivated by adding DMEM containing 8% FCS and P/S. Samples were then filtered through a 100µm cell strainer. Lymph nodes were cut manually, digested in serum-free RPMI containing 100µg/mL TL Liberase (Roche) and 25µg/mL DNAse for 30 min, inactivated in RPMI containing 8% FCS, P/S and β-mercaptoethanol and filtered through a 100µm cell strainer. Bone marrow cells were flushed out from humeri and tibiae and filtered through a 100µm cell strainer. Erythrocytes were lysed using a NH4Cl buffer (155mM NH4Cl, 10mM KHCO3, 0.1mM EDTA) on the lungs, spleen, liver, blood and bone marrow. Cells were then washed using FACS buffer (PBS containing 0.5% BSA and 2mM EDTA) and counted with TC20 Automated Cell Counter (Bio-rad).
$3*10^6$ cells of the single cell suspensions were seeded in a 96-well plat and stained with antibodies for flow cytometry analysis. Briefly, all cells except BM cells, were incubated in Fc block (BD, clone 2.4G2) diluted 1:50 in FACS buffer for 5min. Cells were then stained with fluorochrome-conjugated antibodies (Supplementary Table 1) for 20 min at 4°C in the dark in FACS buffer. 7AAD (1:20; eBioscience) was added to exclude dead cells. Acquisition was performed on a BD LSRII flow cytometer using Diva Software (BD Biosciences) and data analysis was performed using FlowJo software version 9.9.6.
To determine the reduction of neutrophils after dimerizer treatment, the % of circulating neutrophils (of live cells) at day 2 was divided by the % of circulating neutrophils at day 0. Log_2 was consequently calculated.

Immunohistochemistry
All immunohistochemical analyses were performed by the Animal Pathology facility at the NKI, Amsterdam. Tissues were fixed for 24 h in 10% neutral buffered formalin and embedded in paraffin. 5 µm thick paraffin sections were cut, deparaffinized and antigen retrieval was performed with Proteinase K. Samples were then stained with

anti-Ly6G antibody (clone 1A8, BD Biosciences, 1:150) or CD31 (polyclonal, Abcam, 1:200). Quantification of positive cells was performed manually by counting five high-power (40x) fields of view (FOV) per tumor. Samples were visualized with a BX43 upright microscope (Olympus) and images were acquired in bright field using cellSens Entry software (Olympus).

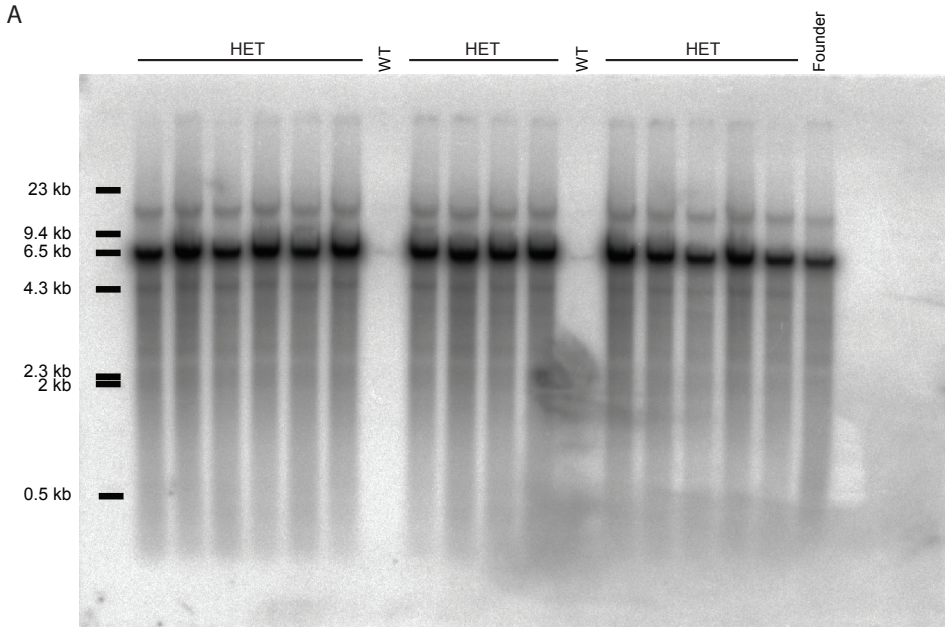
Statistical analysis

Statistical analyses were performed using GraphPad Prism 7 (GraphPad Software Inc., La Jolla, CA). The two-tailed Mann-Whitney test was used for immunohistochemistry and flow cytometry analysis. Where indicated, two-way ANOVA with Sidak's multiple comparison test was used. P values < 0.05 were considered statistically significant.

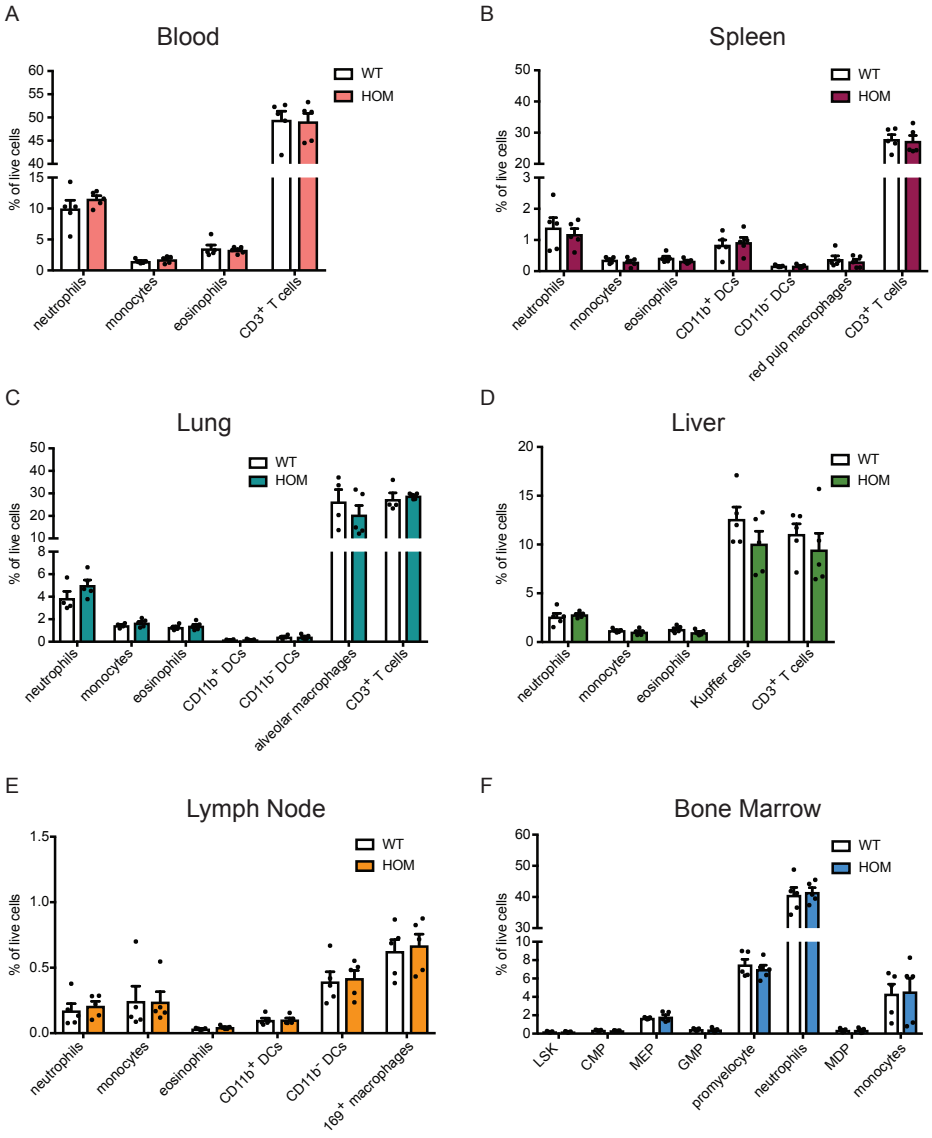
References

1. Nathan, C. Neutrophils and immunity: challenges and opportunities. *Nat Rev Immunol* **6**, 173-182 (2006).
2. Coffelt, S.B., Wellenstein, M.D. & de Visser, K.E. Neutrophils in cancer: neutral no more. *Nat Rev Cancer* **16**, 431-446 (2016).
3. Templeton, A.J.*, et al.* Prognostic role of neutrophil-to-lymphocyte ratio in solid tumors: a systematic review and meta-analysis. *J Natl Cancer Inst* **106**, dju124 (2014).
4. Wei, B.*, et al.* The neutrophil lymphocyte ratio is associated with breast cancer prognosis: an updated systematic review and meta-analysis. *Onco Targets Ther* **9**, 5567-5575 (2016).
5. Gentles, A.J.*, et al.* The prognostic landscape of genes and infiltrating immune cells across human cancers. *Nat Med* **21**, 938-945 (2015).
6. Casbon, A.J.*, et al.* Invasive breast cancer reprograms early myeloid differentiation in the bone marrow to generate immunosuppressive neutrophils. *Proc Natl Acad Sci U S A* **112**, E566-575 (2015).
7. Coffelt, S.B.*, et al.* IL-17-producing gammadelta T cells and neutrophils conspire to promote breast cancer metastasis. *Nature* **522**, 345-348 (2015).
8. Sagiv, J.Y.*, et al.* Phenotypic diversity and plasticity in circulating neutrophil subpopulations in cancer. *Cell Rep* **10**, 562-573 (2015).
9. Yang, X.D.*, et al.* Histamine deficiency promotes inflammation-associated carcinogenesis through reduced myeloid maturation and accumulation of CD11b+Ly6G+ immature myeloid cells. *Nat Med* **17**, 87-95 (2011).
10. Chao, T., Furth, E.E. & Vonderheide, R.H. CXCR2-Dependent Accumulation of Tumor-Associated Neutrophils Regulates T-cell Immunity in Pancreatic Ductal Adenocarcinoma. *Cancer Immunol Res* **4**, 968-982 (2016).
11. Daley, J.M., Thomay, A.A., Connolly, M.D., Reichner, J.S. & Albina, J.E. Use of Ly6G-specific monoclonal antibody to deplete neutrophils in mice. *J Leukoc Biol* **83**, 64-70 (2008).
12. Fleming, T.J., Fleming, M.L. & Malek, T.R. Selective expression of Ly-6G on myeloid lineage cells in mouse bone marrow. RB6-8C5 mAb to granulocyte-differentiation antigen (Gr-1) detects members of the Ly-6 family. *J Immunol* **151**, 2399-2408 (1993).
13. Faget, J.*, et al.* Efficient and specific Ly6G+ cell depletion: A change in the current practices toward more relevant functional analyses of neutrophils. *biorxiv*, 498881 (2018).
14. Steele, C.W.*, et al.* CXCR2 Inhibition Profoundly Suppresses Metastases and Augments Immunotherapy in Pancreatic Ductal Adenocarcinoma. *Cancer Cell* **29**, 832-845 (2016).
15. Saintigny, P.*, et al.* CXCR2 expression in tumor cells is a poor prognostic factor and promotes invasion and metastasis in lung adenocarcinoma. *Cancer Res* **73**, 571-582 (2013).
16. Reber, L.L.*, et al.* Neutrophil myeloperoxidase diminishes the toxic effects and mortality induced by lipopolysaccharide. *J Exp Med* **214**, 1249-1258 (2017).
17. Rombouts, M.*, et al.* Long-Term Depletion of Conventional Dendritic Cells Cannot Be Maintained in an Atherosclerotic Zbtb46-DTR Mouse Model. *PLoS One* **12**, e0169608 (2017).
18. Wang, J., Siffert, M., Spiliotis, M. & Gottstein, B. Repeated Long-Term DT Application in the DEREG Mouse Induces a Neutralizing Anti-DT Antibody Response. *J Immunol Res* **2016**, 1450398 (2016).
19. Pajvani, U.B.*, et al.* Fat apoptosis through targeted activation of caspase 8: a new mouse model of inducible and reversible lipoatrophy. *Nat Med* **11**, 797-803 (2005).
20. Baker, D.J.*, et al.* Clearance of p16Ink4a-positive senescent cells delays ageing-associated disorders. *Nature* **479**, 232-236 (2011).
21. Rutkowski, J.M.*, et al.* Adiponectin promotes functional recovery after podocyte ablation. *J Am Soc Nephrol* **24**, 268-282 (2013).
22. Wang, Z.V.*, et al.* PANIC-ATTAC: a mouse model for inducible and reversible beta-cell ablation. *Diabetes* **57**, 2137-2148 (2008).
23. Srikrishna, G. S100A8 and S100A9: new insights into their roles in malignancy. *J Innate Immun* **4**,

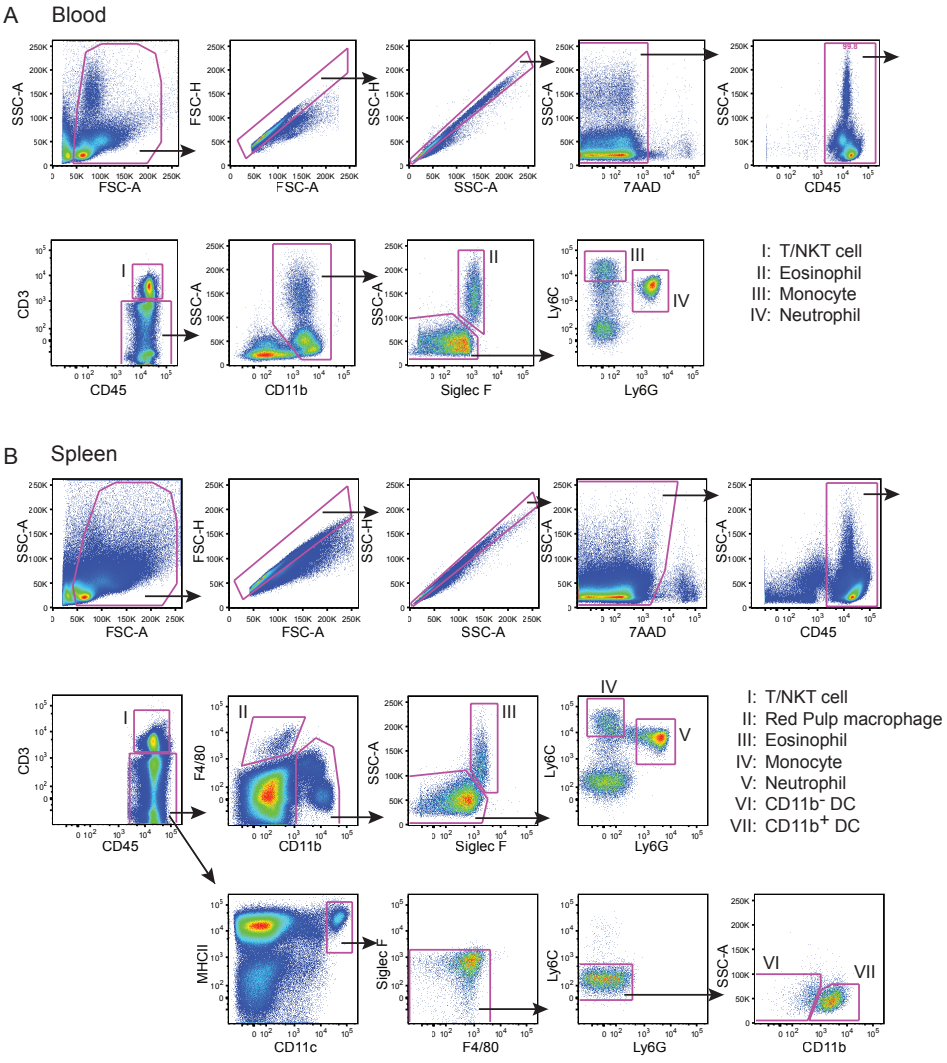
31-40 (2012).
24. Derksen, P.W*., et al.* Somatic inactivation of E-cadherin and p53 in mice leads to metastatic lobular mammary carcinoma through induction of anoikis resistance and angiogenesis. *Cancer Cell* **10**, 437-449 (2006).
25. Doornebal, C.W*., et al.* A preclinical mouse model of invasive lobular breast cancer metastasis. *Cancer Res* **73**, 353-363 (2013).
26. Hiratsuka, S., Watanabe, A., Aburatani, H. & Maru, Y. Tumour-mediated upregulation of chemoattractants and recruitment of myeloid cells predetermines lung metastasis. *Nat Cell Biol* **8**, 1369-1375 (2006).
27. Dzhagalov, I., St John, A. & He, Y.W. The antiapoptotic protein Mcl-1 is essential for the survival of neutrophils but not macrophages. *Blood* **109**, 1620-1626 (2007).
28. Karsunky, H*., et al.* Inflammatory reactions and severe neutropenia in mice lacking the transcriptional repressor Gfi1. *Nat Genet* **30**, 295-300 (2002).
29. Ordonez-Rueda, D*., et al.* A hypomorphic mutation in the Gfi1 transcriptional repressor results in a novel form of neutropenia. *Eur J Immunol* **42**, 2395-2408 (2012).
30. Lieschke, G.J*., et al.* Mice lacking granulocyte colony-stimulating factor have chronic neutropenia, granulocyte and macrophage progenitor cell deficiency, and impaired neutrophil mobilization. *Blood* **84**, 1737-1746 (1994).
31. Cheng, P*., et al.* Inhibition of dendritic cell differentiation and accumulation of myeloid-derived suppressor cells in cancer is regulated by S100A9 protein. *J Exp Med* **205**, 2235-2249 (2008).
32. Lagasse, E. & Clerc, R.G. Cloning and expression of two human genes encoding calcium-binding proteins that are regulated during myeloid differentiation. *Mol Cell Biol* **8**, 2402-2410 (1988).
33. Dancey, J.T., Deubelbeiss, K.A., Harker, L.A. & Finch, C.A. Neutrophil kinetics in man. *J Clin Invest* **58**, 705-715 (1976).
34. Yuan, H*., et al.* MMTV-NeuT/ATTAC mice: a new model for studying the stromal tumor microenvironment. *Oncotarget* **9**, 8042-8053 (2018).
35. Lim, S.Y., Yuzhalin, A.E., Gordon-Weeks, A.N. & Muschel, R.J. Tumor-infiltrating monocytes/macrophages promote tumor invasion and migration by upregulating S100A8 and S100A9 expression in cancer cells. *Oncogene* **35**, 5735-5745 (2016).
36. Finisguerra, V*., et al.* MET is required for the recruitment of anti-tumoural neutrophils. *Nature* **522**, 349-353 (2015).
37. Huijbers, I.J*., et al.* Using the GEMM-ESC strategy to study gene function in mouse models. *Nat Protoc* **10**, 1755-1785 (2015).
38. Salvagno, C. & de Visser, K.E. Purification of Immune Cell Populations from Freshly Isolated Murine Tumors and Organs by Consecutive Magnetic Cell Sorting and Multi-parameter Flow Cytometry-Based Sorting. *Methods Mol Biol* **1458**, 125-135 (2016).



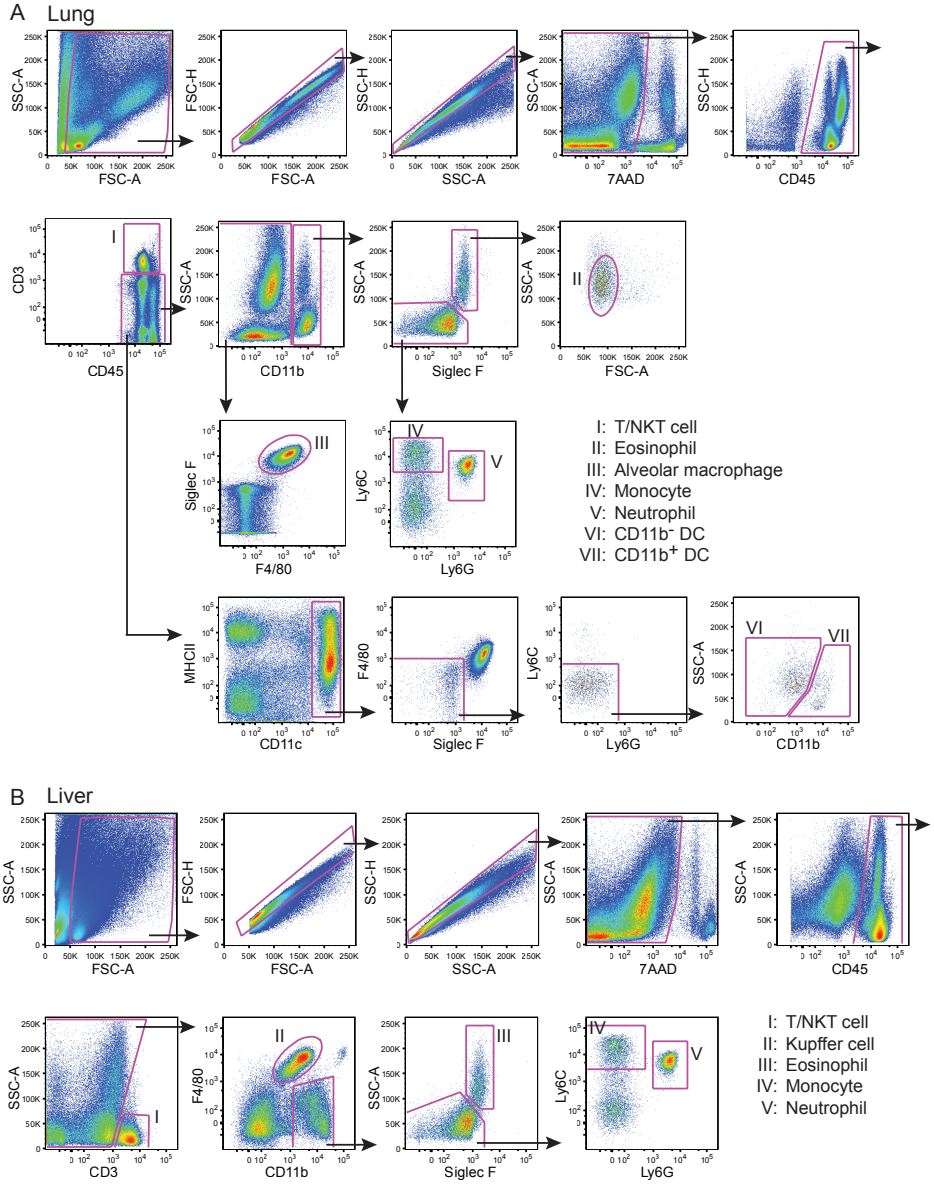
Supplementary Fig. 1 | The hMRP8-ATTAC construct is integrated in one site in multiple copies. (A) Southern Blot analysis of toe-derived genomic DNA of Founder 19, and heterozygous and WT F1 progeny. The transgene is identified by the hybridization of the GFP probe (concatamer band of 6114kb). HET, heterozygous. WT, wild-type



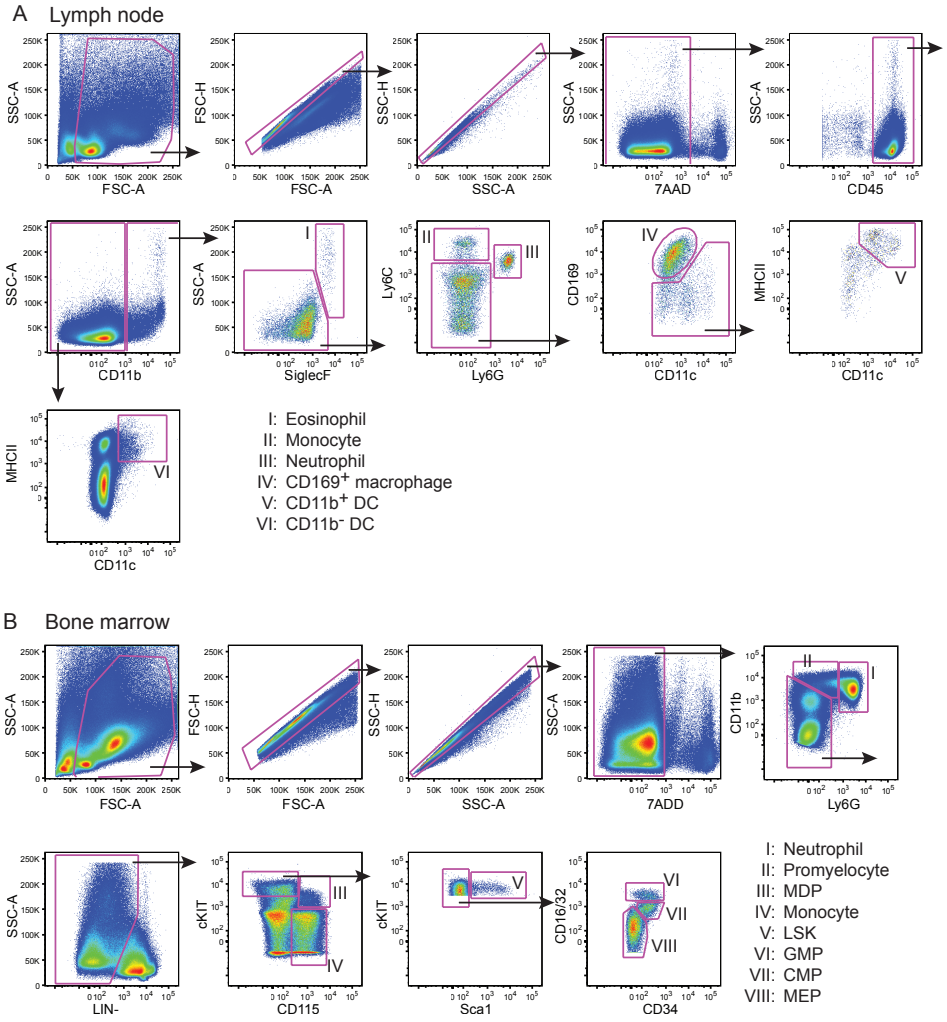
Supplementary Fig. 2 | No changes in the immune cell composition in hMRP8-ATTAC mice. (A-F) Immune cell proportion in the blood (A), spleen (B), lung (C), liver (D), lymph node (E) and bone marrow (F) of hMRP8-ATTAC mice and WT littermates (n=4-5). HOM, homozygous. Data are mean values ± SEM.



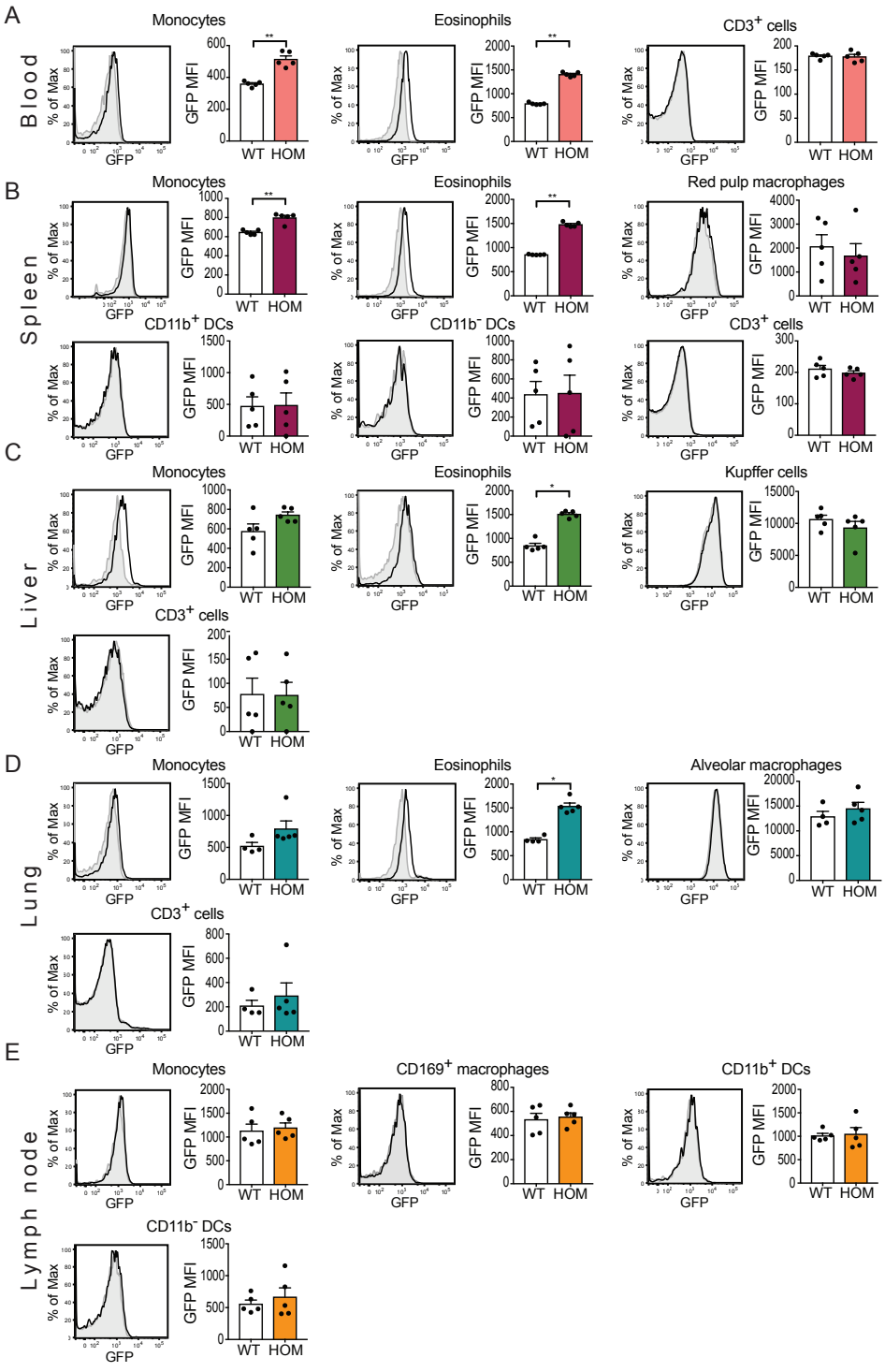
Supplementary Fig. 3 | Flow cytometry gating strategy for blood and spleen samples. (A-B) Representative dot plots of blood (A) and spleen (B) of a homozygous hMRP8-ATTAC mouse illustrating the gating strategy for the identification of cell populations. Antibody panel used: "Panel 1". Arrows indicate directionality of sub-gates.



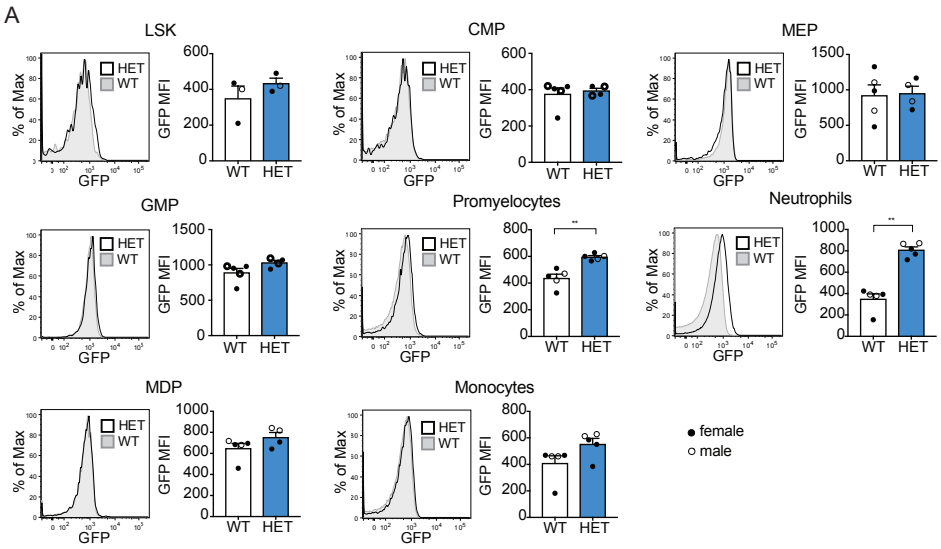
Supplementary Fig. 4 | Flow cytometry gating strategy for lung and liver samples. (A-B) Representative dot plots of lung (A) and liver (B) of a homozygous hMRP8-ATTAC mouse illustrating the gating strategy for the identification of cell populations. Antibody panel used: "Panel 1". Arrows indicate directionality of sub-gates.



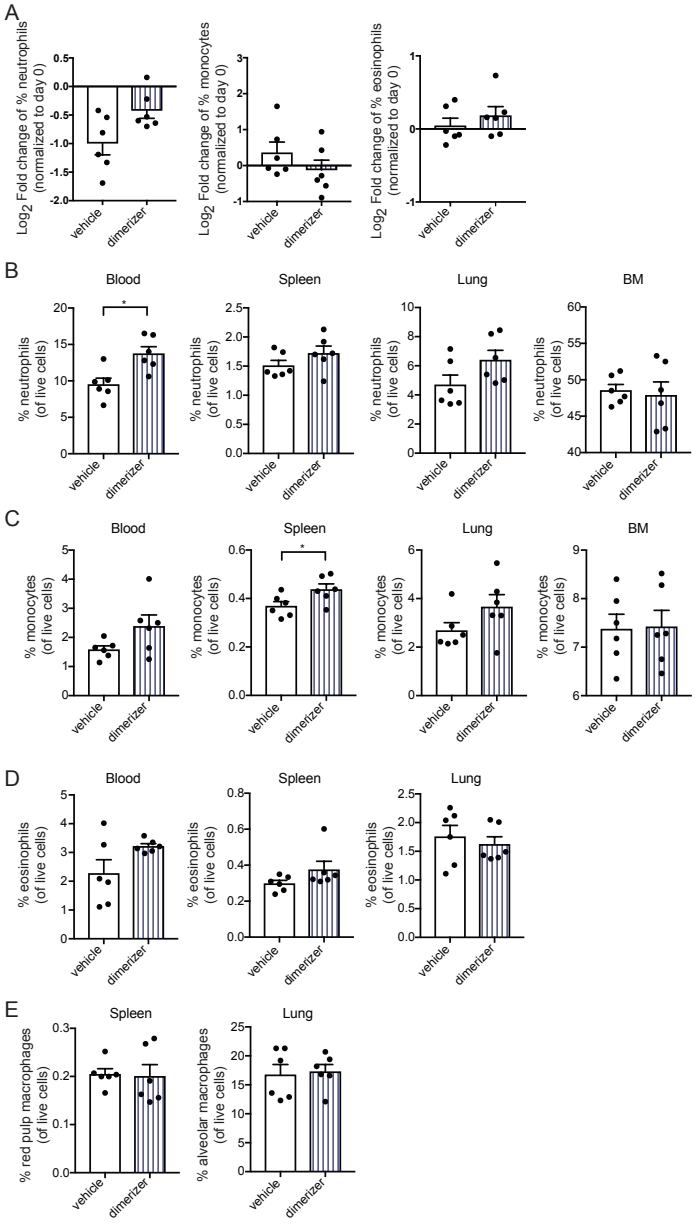
Supplementary Fig. 5| Flow cytometry gating strategy for lymph node and bone marrow samples. (A-B) Representative dot plots of lymph node (A) and bone marrow (B) of a homozygous hMRP8-ATTAC mouse illustrating the gating strategy for the identification of cell populations. Antibody panel used: "Panel 2" for lymph node and "Panel 3" for bone marrow. Arrows indicate directionality of sub-gates.


A
Blood
Monocytes
Eosinophils
CD3+ cells
B
Spleen
Monocytes
Eosinophils
Red pulp macrophages
CD11b+ DCs
CD11b- DCs
CD3+ cells
C
Liver
Monocytes
Eosinophils
Kupffer cells
CD3+ cells
D
Lung
Monocytes
Eosinophils
Alveolar macrophages
CD3+ cells
E
Lymph node
Monocytes
CD169+ macrophages
CD11b+ DCs
CD11b- DCs
% of Max
GFP
GFP MFI
WT HOM

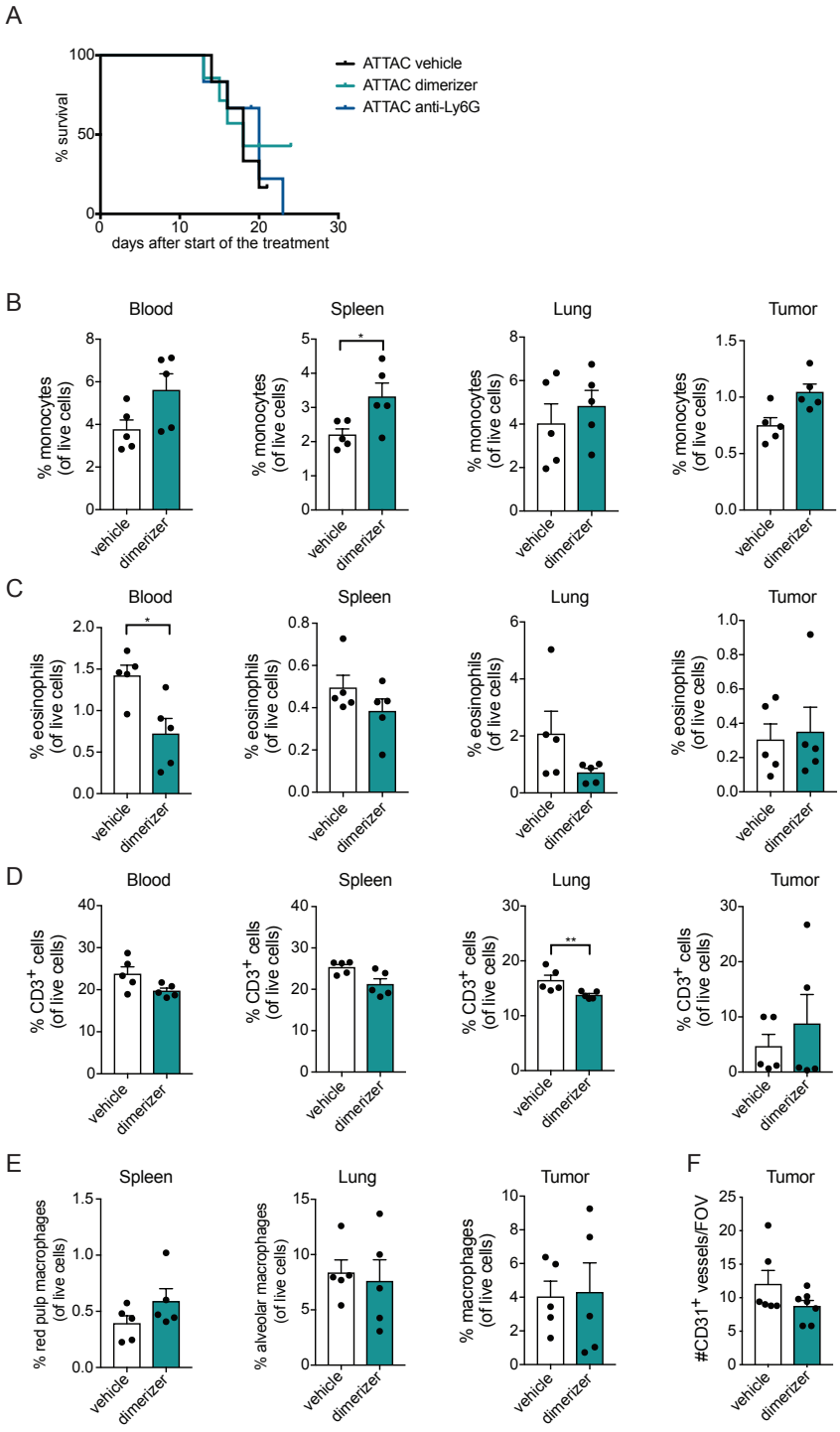
Supplementary Fig. 6 | Monocytes and eosinophils in the hMRP8-ATTAC model express low levels of the transgene. (A-E) Representative histograms of GFP expression and quantification of the Median Fluorescence Intensity (MFI) of GFP in several immune cells from blood (A), spleen (B), liver (C), lung (D) and lymph node (E) of homozygous female hMRP8-ATTAC mice (n=5) compared to WT littermates (n=4-5), as determined by flow cytometry. WT, wild type; HOM, homozygous. Data are mean values ± SEM. *$p < 0.05$, **$p<0.01$ by Mann–Whitney test.



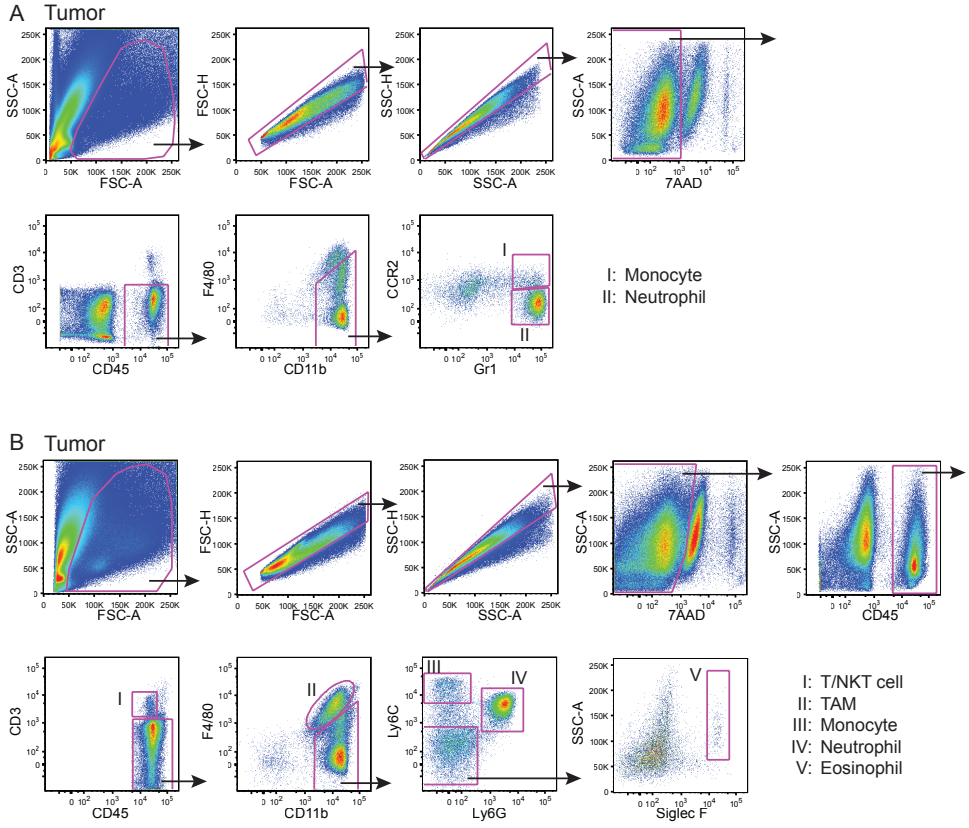
Supplementary Fig. 7 | GFP expression in the bone marrow of heterozygous hMRP8-ATTAC mice. (A) Representative histograms of GFP expression and quantification of the Median Fluorescence Intensity (MFI) of GFP in different hematopoietic cell populations depicted in Fig. 3A in the bone marrow of heterozygous hMRP8-ATTAC mice (n=3-5) and WT littermates (n=3-5), as determined by flow cytometry. Open circles represent male hMRP8-ATTAC mice and full circles represent female hMRP8-ATTAC mice. WT, wild type; HET, heterozygous. LSK, Lineage-SCA1+Kit-; CMP, common myeloid progenitor; MEP, megakaryocyte-erythroid progenitor; GMP, granulocyte-macrophage progenitor; MDP, monocyte/macrophage-dendritic cell progenitor. Data presented are mean values ± SEM. **p<0.01 by Mann–Whitney test.



Supplementary Fig. 8 | Dimerizer treatment has modest effects on neutrophils in WT mice. (A) Log2 fold change of circulating neutrophils, monocytes and eosinophils defined as % of live two days after treatment compared to day 0 in WT female mice (n=6/group). Fold change was calculated by dividing the frequency of neutrophil at day 2 by the frequency of neutrophils at day 0. (B-E) Frequencies of neutrophils (B), monocytes (C), eosinophils (D) and resident macrophages (E) in blood, spleen, lung and bone marrow of WT mice treated with vehicle or dimerizer for seven consecutive days, as determined by flow cytometry (n=6/group, same mice as in A). Data are mean values ± SEM. *$p < 0.05$ by Mann–Whitney test.


A
% survival
days after start of the treatment
ATTAC vehicle
ATTAC dimerizer
ATTAC anti-Ly6G
B
Blood
Spleen
Lung
Tumor
% monocytes (of live cells)
C
% eosinophils (of live cells)
D
% CD3+ cells (of live cells)
E
% red pulp macrophages (of live cells)
% alveolar macrophages (of live cells)
% macrophages (of live cells)
F
#CD31+ vessels/FOV
vehicle
dimerizer

Supplementary Fig. 9 | Dimerizer treatment slightly increases monocyte frequency and reduces circulating eosinophils in tumor-bearing hMRP8-ATTAC mice. (A) Kaplan-Meier tumor-specific survival curves of hMRP8-ATTAC mice treated with vehicle (n=6), dimerizer (n=7) or anti-Ly6G (n=6). An event is defined as an animal with a tumor size of 225mm^2. (B-E) Frequency of monocytes (B), eosinophils (C), CD3$^+$ T cells (D) and macrophages (E) in the blood, spleen, lung and tumor of end-stage tumor-bearing hMRP8-ATTAC mice (n=5/group), as determined by flow cytometry. (F) Quantification of CD31$^+$ vessels in viable areas of mammary tumors in hMRP8-ATTAC mice treated as indicated (n=6-7). Data are mean values ± SEM. *$p < 0.05$, **<0.01 by Mann–Whitney test.



Supplementary Fig. 10 | Flow cytometry gating strategy for tumor samples. (A-B) Representative dot plots of tumor samples of a homozygous hMRP8-ATTAC mouse orthotopically transplanted with *K14cre;Cdh1$^{F/F}$;Trp53$^{F/F}$* mammary tumor piece illustrating two gating strategies for the identification of cell populations. Antibody panel used: "Panel 4" in (A) and "Panel 5" in (B). Arrows indicate directionality of sub-gates. (A) was used in Fig. 5E to identify neutrophils.

Supplementary Table 1: List of antibodies used for flow cytometry analyses.

Panel 1. Blood, spleen, lung and liver

Antibody	Fluorophore	Clone	Vendor	Dilution
CD45	BUV395	30-F11	BD Biosciences	1:200
CD3	PE-cy7	145-2c11	eBioscience	1:200
Siglec F	BV605	E50-2440	BD Biosciences	1:200
CD11b	BV786	M1/70	BD Biosciences	1:400
CD11c	PE	N418	eBioscience	1:200
Ly6G	AF700	1A8	Biolegend	1:200
Ly6C	Ef450	HK1.4	eBioscience	1:400
F4/80	APC	BM8	eBioscience	1:200
MHC class II	APCef780	M5/114.15.2	eBioscience	1:200

Panel 2. Lymph node

Antibody	Fluorophore	Clone	Vendor	Dilution
CD45	BUV395	30-F11	BD Biosciences	1:200
Siglec F	BV605	E50-2440	BD Biosciences	1:200
CD11b	BV786	M1/70	BD Biosciences	1:400
CD11c	BV421	HL3	BD Biosciences	1:200
Ly6G	AF700	1A8	Biolegend	1:200
Ly6C	PEcy7	HK1.4	Biolegend	1:400
F4/80	APC	BM8	eBioscience	1:200
MHC class II	APCef780	M5/114.15.2	eBioscience	1:200
CD169	PE	3D6.112	Biolegend	1:200

Panel 3. Bone marrow

Antibody	Fluorophore	Clone	Vendor	Dilution
CD11b	APCef780	M1/70	eBioscience	1:400
CD115	BV711	AFS98	Biolegend	1:200
Ly6G	AF700	1A8	Biolegend	1:200
Ter119	PE	TER-119	Biolegend	1:400
CD3	PE	145-2C11	Biolegend	1:400
CD4	PE	H129.19	Biolegend	1:400
CD8	PE	53-6.7	eBioscience	1:400
CD19	PE	eBio1D3	eBioscience	1:400
Sca1	BV421	D7	Biolegend	1:400
CD117	BV605	2B8	BD Biosciences	1:200
CD16/32	BUV395	2.4G2	BD Biosciences	1:200
CD34	AF647	RAM34	BD Biosciences	1:100

Panel 4. Dimerizer treatment in tumor-bearing hMRP8;ATTAC mice: blood, spleen, lung and tumor

Antibody	Fluorophore	Clone	Vendor	Dilution
CD45	BUV395	30-F11	BD Biosciences	1:200
CD3	PE-cy7	145-2c11	eBioscience	1:200
CD11b	BV786	M1/70	BD Biosciences	1:400
CCR2	PE	475301	R&D systems	1:100
Gr1	BV421	RB6-8C5	Biolegend	1:200
F4/80	APC	BM8	eBioscience	1:200

Panel 5. Dimerizer treatment in tumor-bearing hMRP8;ATTAC mice: blood, spleen, lung and tumor

Antibody	Fluorophore	Clone	Vendor	Dilution
CD45	BUV395	30-F11	BD Biosciences	1:200
CD3	PE-cy7	145-2c11	eBioscience	1:200
Siglec F	PE	E50-2440	BD Biosciences	1:200
CD11b	BV786	M1/70	BD Biosciences	1:400
CD11c	BUV737	HL3	BD Biosciences	1:100
CD117	BV605	2B8	BD Biosciences	1:100
Ly6G	AF700	1A8	Biolegend	1:200
Ly6C	Ef450	HK1.4	eBioscience	1:400
F4/80	APC	BM8	eBioscience	1:200
MHC class II	APCef780	M5/114.15.2	eBioscience	1:200

CHAPTER 7

Discussion

Myeloid cells represent an important component of the tumor microenvironment (TME) as they have been shown to contribute to tumor progression and impact therapy response. As a result, immunomodulatory agents targeting myeloid cells are currently being evaluated in clinical trials. To maximize the success of these compounds and to develop new therapeutic approaches, understanding the biology of the targeted cell and the effects of these drugs is of utmost importance. Here, I will discuss important aspects of immune cell complexity, focusing on the phenotype of tumor-associated macrophages (TAMs), the impact of macrophage-targeting drugs on chemotherapy response, approaches to achieve anti-tumor immunity in poorly immunogenic tumors and the challenges to study neutrophils.

The challenging definition of macrophage functional identity

Initially, macrophages were described to have different polarization states: they could either be classically activated or alternatively activated. These terms originated from studies in the early 1990s which showed that macrophages cultured in the presence of IL-4 displayed a different phenotype as compared to ones cultured in the presence of IFNγ, which showed an "alternative" phenotype[1]. Years later, in 2000, the observation that macrophages isolated from different mouse strains had a different arginine metabolism which influenced lymphocytes to produce either Th1 or Th2 cytokines, led to the M1/M2 dichotomy[2]. Although the authors, who described these macrophage phenotypes in the original report, discussed the possibility of a "continuum of phenotypes between M1 and M2 macrophages", the M1/M2 dichotomy dominated the macrophage field for almost two decades. However, this binary generalization is rather limiting and unlikely to occur in a complex *in vivo* system. In fact, macrophages are one of the most plastic cells of the immune system. Based on *in vitro* experiments we now know that macrophages can change their phenotype based on various stimuli they receive in the environment[3]. This dynamic behavior of macrophages is critical for the protection against several insults for which a quick adaptation and response is necessary. To solve the complexity of macrophage definition, it was proposed that, besides an accurate description of the methodology used, studies should define these cells by the stimulus they receive[4]. For example, macrophages stimulated *in vitro* with IL-4 would be termed M(IL-4). Although this terminology would be useful for *in vitro* experiments, this nomenclature based on the type of activator would be challenging for *in vivo* studies, as multiple and unforeseeable mediators might be responsible for shaping the macrophage phenotype. Because of the effects that different stimuli have on the phenotype and function of macrophages, the local environment where they reside plays an important role in shaping their phenotype. An elegant study by Lavin *et al*. showed that transplantation of differentiated peritoneal macrophages into the alveolar cavity resulted in a transcriptomic switch that closely resembled the profile of lung macrophages[5]. These data reiterate the plasticity of fully differentiated macrophages that can reshape and acquire a different transcriptomic identity based on the tissue environment.

The M1/M2 terminology also became popular in the cancer field where it was used to define TAMs as pro-tumoral (M2) or anti-tumoral TAMs (M1)[6]. Interestingly, single-cell RNA-sequencing of immune cells isolated from human breast tumors revealed

the co-existence of M1 and M2 signatures in the same macrophage[7], strengthening the concept of a continuum of activation states as opposed to the static M1/M2 paradigm. This concept of plasticity implies that distinct TMEs differently affect TAM phenotype. To test this hypothesis, in **chapter 3** of this thesis, we isolated TAMs from the mammary tumors of two genetically engineered mouse models (GEMMs), in which macrophages and cancer cells co-evolve mimicking the human situation. While *K14cre;Cdh1$^{F/F}$;Trp53$^{F/F}$* (KEP) mammary tumors[8] resemble an invasive lobular carcinoma (ILC) histotype of breast cancer, the *MMTV-NeuT* (NeuT) tumors, which overexpress an activated form of *neu*, model HER2^{+} breast cancer[9]. Interestingly, the transcriptomic profile of TAMs from the KEP and the NeuT model were found to be more similar to macrophages of the mammary gland compared to macrophages that reside in other tissues, like the spleen and bone marrow, indicating that the tissue of origin dictates macrophage identity. Indeed, we observed that these TAMs have a common signature probably related to the mammary tissue where they arose. Nevertheless, we also identified a unique signature for both TAMs, strengthening the concept that distinct tumor milieus differently influence the macrophage transcriptomic profile. Several reasons may explain the different macrophage reprograming, including the genetic make-up of the tumor, the histological subtype of the tumor, and/or the presence of different stromal characteristics like fibroblasts and collagen fibers. Expanding this analysis to additional GEMMs for mammary tumorigenesis could identify tumor characteristics that associate with similar TAM transcriptomic profiles. In addition, it would be interesting to perform the same computational analysis on macrophages isolated from different tumor stages to obtain a dynamic overview on how particular features are gained, lost or changed during tumor growth. Importantly, with our analysis we only focused on the *inter*-tumoral heterogeneity of macrophages between tumor models. It may also be interesting to address the *intra*-tumoral diversity of macrophages by single cell RNA-sequencing and spatial transcriptomic[10], in order to assess how the macrophage profile changes based on location (*e.g.*: centre, rim, vicinity to necrotic areas) or contact with neighbouring cells.

Although RNA sequencing is a powerful tool it is important to consider that these results on TAM phenotype provide only descriptive data and not functional information. Nevertheless, the potential functionality of these cells could be extrapolated from transcriptomic analysis. For example, TAMs from the NeuT model, and to a lesser extent also from the KEP model, upregulate genes involved in angiogenesis-related processes, suggesting that these macrophages may support tumor growth by secreting growth factors and promoting angiogenesis. In addition, gene expression data may also provide some insights on the biology of TAMs. In preclinical models, TAMs were demonstrated to originate from circulating CCR2^{+} monocytes in the *MMTV-PyMT* mouse model for breast cancer[11], while in the *MMTVneu* model, which bears the unactivated form of HER2, the increased accumulation of TAMs in the tumors was the result of major local proliferation[12]. In **chapter 3** of this thesis, we observed that TAMs isolated from the KEP model are highly proliferative compared to TAMs from the NeuT model, suggesting that in KEP tumors TAMs may originate from local proliferation rather than differentiation of monocytes. These data highlight that different, and probably multiple, mechanisms can give rise to TAMs and future studies should assess whether the transcriptomic

profile of macrophages can determine their ontogeny.
In **chapter 3** of this thesis we show that the specific gene signature of TAMs from the KEP tumors associates with poor survival in two separate cohorts of ILC patients, while the specific gene signature of TAMs from the NeuT tumors fails to do so in the same groups of patients. These findings were quite surprising as our signature, derived from a pure TAM population, was applied to the transcriptome profile of bulk tumor samples containing multiple different cell types. This association may suggest that this novel set of genes derived from murine macrophages could have prognostic value. However, it is important to note that more studies should confirm the value of the KEP TAM signature in predicting outcome and response to specific type of therapies. For example, it would be interesting to assess whether patients with tumors enriched in this signature would benefit from the treatment with macrophage-targeting agents. In addition, it would be interesting to apply the core signature of TAMs from the NeuT model to gene expression data from $HER2^+$ breast cancer patients, and perform the same analysis. It should be noted that in other breast cancer models, two populations of intratumoral macrophages are found and distinguished based on CD11b expression[11,12]. Differently from the KEP tumors which contains only $CD11b^{high}$ macrophages (**chapter 5** of this thesis), NeuT tumors display both macrophage populations, although with some variability. To fairly compare these two models, only $CD11b^{high}$ macrophages were analyzed in our study. However, both macrophage signatures of TAMs from the NeuT model should be tested for their ability to predict survival in $HER2^+$ patients.
In conclusion our data, together with other studies, indicate that one unique TAM phenotype does not exist; rather the plasticity of macrophages to different stimuli determines a distinct phenotype in certain environments and not in others. This diversity in TAM phenotype may have consequences for the efficacy of macrophage-targeting drugs, as targeting particular TAM phenotypes might not be therapeutically beneficial.

Targeting inflammation as an anti-cancer strategy

The importance of gaining knowledge on the therapeutic effects of CSF-1R blockade
The acknowledgment of the TME as a crucial component for tumor establishment and growth[13] and the realization that myeloid cells often facilitate tumor development formed a rationale for developing approaches to clinically target these cells. TAMs represent an important target because 1) their presence within the TME strongly associates with poor prognosis across tumor types[14], 2) they are abundant in the majority of tumor types[15], and 3) preclinical data show that they contribute to tumor growth and metastasis by supporting angiogenesis, stimulating cancer cell proliferation and migration and suppressing anti-tumor immune responses[16-21]. Approaches to therapeutically target TAMs aim at depleting the pool of macrophages, blocking their recruitment or skewing their polarization towards an anti-tumor phenotype.
Thanks to the knowledge gained over the last 40 years on macrophage biology, blocking CSF-1/CSF-1R signaling pathway, which is essential for macrophage survival, denotes an attractive strategy to eliminate macrophages and suppress tumor growth. Several therapeutic approaches aiming at interfering with this

pathway have been developed, including antibodies against the receptor (anti-CSF-1R), the ligand (anti-CSF-1), and inhibitors of the tyrosine kinase domain of CSF-1R. Monotherapy treatment with CSF-1R inhibitors exert anti-tumor effects in several preclinical models[22-30], but not in others[31], including the KEP mouse model (**chapter 5** of this thesis). These differences might reflect the different function of TAMs elicited by the distinct TME, the biology of the tumor model, or may reflect the different experimental designs used, such as the type of inhibitor, tumor stage at the start of the treatment and/or doses. Because cancer patients are often treated with chemotherapy, many preclinical studies also evaluated the effect of CSF-1R inhibition in the context of chemotherapy. Targeting the CSF-1R pathway in various experimental tumor models enhances the cytotoxic efficacy of chemotherapy[24,25,31-34], including in studies where anti-CSF-1R monotherapy does not have any effect on tumor control[31]. Indeed, in **chapter 5** of this thesis we observed that anti-CSF-1R monotherapy does not affect tumor growth in the KEP mouse model of breast cancer. However, anti-CSF-1R synergized with platinum-containing drugs, *i.e.* cisplatin and oxaliplatin, resulting in prolonged tumor-specific survival. Besides blocking the main survival signaling pathway in macrophages which results in decreased TAM numbers in some tumor settings, the secondary effects of anti-CSF-1R treatment on the TME are not fully elucidated. A better understanding of the impact of anti-CSF-1R *in vivo* may explain the therapeutic benefits achieved in combination with chemotherapeutic drugs. In this regard, **chapter 5** of this thesis describes a novel mechanism-of-action of the antibody against CSF-1R in improving cisplatin response. Anti-CSF-1R treatment induces an upregulation of type I interferon (IFN) in the KEP mammary tumor which significantly enhanced the efficacy of cisplatin. However, the increase in type I IFN does not enhance the efficacy of a different type of chemotherapeutic agent, the taxane docetaxel. A possible explanation could be that the anti-CSF-1R-induced expression of type I IFNs sensitizes tumor cells to the mechanism-of-action of platinum-containing drugs, which damage the DNA, and not of taxanes, which inhibit mitosis. In addition, it is now widely acknowledged that cytotoxic drugs exert also immunomodulatory effects, as described in **chapter 4** of this thesis. Therefore, it might be plausible that chemotherapy-induced effects on immune cells might underline the therapeutic activity of CSF-1R inhibition and cisplatin. Although promising, the number of chemotherapeutic agents tested in this study is limited, therefore correlating the synergistic effects of anti-CSF-1R with certain classes of drugs is currently not possible. Future studies should expand the number of chemotherapeutic agents to be examined, including other taxane-based chemotherapies such as paclitaxel and DNA-damaging agents that do not belong to the platinum-containing drug family, including doxorubicin and cyclophosphamide which are commonly used in the clinic. In addition, it would be interesting to assess the effect of anti-CSF-1R in combination with cisplatin on metastasis. Our study showed that anti-CSF-1R alone does not affect the metastasis-specific survival in the KEP-based model of spontaneous breast metastasis. However, as with the primary tumor growth, the combination could prolong distant metastasis free survival.

Currently, immunomodulatory drugs blocking the CSF-1/CSF-1R axis are under clinical evaluation as a monotherapy or in combination with other therapies, including chemotherapy, for several types of solid tumors[35]. Although preliminary results of phase I and II clinical trials display good tolerability to the drugs, early

results on their anti-cancer efficacy describe low and variable clinical benefits in several types of tumors[35]. Currently there are clinical trials ongoing with anti-CSF-1R in combination with paclitaxel[36], another taxane-based drug like docetaxel used in our study. However, our data suggest that this class of drug might not be suitable to achieve a synergistic therapeutic advantage. Particularly, in light of our data showing that anti-CSF-1R treatment induces type I IFN response in cancer patients, choosing the optimal cytotoxic drug is of utmost importance to maximize the effects of CSF-1R targeting agents. Interestingly, of all the tumor types tested for response to CSF-1/CSF-1R-targeting drugs, only diffuse-type tenosynovial giant cell tumor showed very encouraging results with a response rate higher than 80%[35,37]. These tumors are characterized by overexpression of CSF-1 and high numbers of CSF-1R$^+$ macrophages[38]. Although it is thought that the clinical activity of CSF-1R-targeting drugs mainly rely on blocking this signaling pathway in recruited myeloid cells, cancer cells can also express the receptor[38], raising the question on the importance of targeting this pathway in malignant cells for the outcome of the therapy.

Although our data showed that CSF-1R blockade depletes intratumoral macrophages, we also describe that a small population of intratumoral F4/80$^+$ cells expressing high levels of IFNα resists anti-CSF-1R treatment. In an attempt to identify the origin of these remaining TAMs, we showed that circulating monocytes have the potential to infiltrate the tumor of anti-CSF-1R-treated mice. However, we cannot exclude that the IFNα-producing F4/80$^+$ cells are anti-CSF-1R therapy-resistant TAMs or repolarized TAMs. Notably, in this study we used a dosing schedule of CSF-1R blocking antibody that depletes 80% of TAMs; it would be interesting to investigate whether reducing the compound dose would avoid macrophage depletion without affecting the capacity of the agent to convert the TME into a type I IFN-enriched milieu. Furthermore, of all the strategies developed to inhibit the CSF-1/CSF-1R signaling pathway, we only tested the use of the anti-CSF-1R blocking antibody, raising the question whether other compounds would also induce a type I IFN response. Another study has shown that targeting CSF-1 with a neutralizing antibody in a preclinical model for pancreatic cancer reduced macrophage numbers while concomitantly skewing their polarization status into an anti-tumor activated state[30]. Interestingly, the remaining macrophages expressed IFNα, suggesting that targeting CSF-1 or inhibiting its binding to the receptor by anti-CSF-1R treatment may trigger type I IFN signaling. In addition, in a preclinical model for glioblastoma, treatment with a small molecule inhibitor of CSF-1R did not deplete TAMs, due to tumor-derived factors that sustained their survival, but repolarized them towards a tumor-inhibiting state that resulted in improved survival[27]. Unfortunately, IFNα expression was not assessed in these macrophages. The molecular mechanisms that induce type I IFN expression in cisplatin/anti-CSF-1R-treated mice are still unknown. However, because type I IFNs are stimulated by pattern recognition receptors (PRR), I hypothesize that the newly recruited monocytes or the remaining TAMs scavenge debris, RNA or DNA released from anti-CSF-1R-mediated macrophage cell death or dying cancer cells that triggers IFNα expression.

Another aspect that was not addressed in **chapter 5** of this thesis is whether newly recruited or remaining macrophages in peripheral organs also start expressing type I IFNs and whether their overall phenotype is altered affecting their function. Beside reducing intratumoral macrophages[28], CSF-1R-targeting drugs also decreases the

number of skin macrophages in patients[39] and resident macrophages of other organs, like liver and colon, in cynomologus monkeys[28]. Data from CSF-1R-null mice revealed that tissue-resident macrophages of organs like skin and liver are depleted, while macrophages from organs such as spleen and lung are not, indicating that in these tissues other growth factors are involved in macrophage survival[40,41]. These data suggest that, if IFNα-producing macrophages derive from newly recruited monocytes, anti-CSF-1R treatment may result in monocyte influx in organs in which tissue-resident macrophages rely on CSF-1R signaling. On the other hand, *in vitro* treatment of bone marrow-derived macrophages with anti-CSF-1R showed an increase in IFNα expression, suggesting that macrophages in those organs where CSF-1R inhibition does not decrease macrophage number, may also be affected by anti-CSF-1R treatment. However, whether the recruited monocytes or resident-macrophages in peripheral organs produce type I IFN and whether IFNα prevents, in combination with cisplatin, metastasis formation still needs to be elucidated.

A fine balance between type I IFN-mediated immune-stimulation and immune-suppression

Our study demonstrates that it is pivotal to induce the adequate type of inflamed TME, *i.e.* type I IFN-enriched, in order to boost the efficacy of platinum-containing drugs in the KEP model. The discovery of type I interferon (IFN) dates back to 1957 when Isaacs and Lindenmann identified factors released upon exposure of cells to heat-inactivated influenza virus that protected or "interfered" with the replication of live viruses[42]. In humans, the type I IFN family includes 13 different IFNα proteins (14 in mice), one single IFNβ protein and other, less studied IFNs, such as IFNε and IFNω[43]. Every cell can potentially produce type I IFNs upon activation of PRRs, like toll-like receptors (TLRs) and the cyclic GMP-AMP synthase (cGAS)/stimulator of IFN genes (STING) pathway, that recognize bacterial or viral components, including DNA and RNA. Subsequently, type I IFN molecules bind to their receptor that is composed of IFNAR1 and IFNAR2 subunits, either in a heterodimer or in an IFNAR1 homodimer[43]. Upon binding, IFNs activate the kinases Janus kinase 1 (JAK1) and tyrosine kinase 2 (TYK2) which phosphorylate STAT1 and STAT2 to promote the expression of type I IFN-stimulated genes (ISGs). Type I IFN signaling is well known for its role in host defense against viruses and most of our knowledge to date derives from infection studies[43]. More recently several studies have addressed the role of type I IFN in cancer settings. Blocking type I IFN signaling by knocking-out IFNAR1 or by antibody-mediated blockade of IFNAR1 results in increased tumor development in several tumor models, including tumor cell inoculation models, methylcholanthrene (MCA)-induced sarcoma model and dextran sodium sulfate/azoxymethane (DSS/AOM)-induced colitis-associated tumorigenesis[44-48]. Type I IFNs can have direct effects on tumor progression, by inducing apoptosis or blocking proliferation in cancer cells, by inhibiting angiogenesis, or indirectly by stimulating immune cells. Like during viral infections, also in a cancer setting type I IFNs exert their main immunomodulatory effects by activating DCs and stimulating antigen cross-presentation resulting in T cell activation and consequently tumor rejection[49,50]. Type I IFN signaling is also essential for the function and survival of cytotoxic T cells[51] and NK cells[47]. Indeed, experiments with IFNAR1 KO bone marrow chimeras and tumor transplantation in IFNAR1 deficient hosts revealed that IFNAR1

signaling in hematopoietic cells is critical for engaging anti-tumor immunity[44,50]. In addition, downregulation of the transcription factor interferon regulatory factor 7 (IRF7), which induces the transcription of type I IFNs and other ISGs, and its targets in 4T1 breast cancer cells fosters metastasis to the bone through immune escape[52]. Finally, sustained activation of type I IFN signaling in chemotherapy-treated breast cancer cells induced dormancy in a T cell-dependent manner[53]. Interestingly, the dose of type I IFN seems to play a role in dictating the mechanisms by which tumors are rejected; low doses induce a T cell-mediated anti-tumor responses[54], while high doses exert anti-angiogenic effects[55]. The role of type I IFNs in hindering cancer progression raises the question on their role in therapy response. Studies have described that radiotherapy and some chemotherapeutic drugs, like anthracyclines and cyclophosphamide stimulate type I IFN production in preclinical cancer models and patients[56-59]. Importantly, the secretion of type I IFNs are critical for the therapeutic efficacy of radiotherapy and anthracyclines as their anti-cancer efficacy is lost upon blockade of type I IFN signaling[56,57,59]. Differently from these studies, **chapter 5** of this thesis shows that neither cisplatin nor docetaxel alone stimulate type I IFN expression in the KEP model. In line with this, blockade of type I IFN signaling does not affect cisplatin response. Only the synergistic effect of the cisplatin/anti-CSF-1R combination is dependent on anti-CSF-1R-induced type I IFNs. The difference in the effect of chemotherapy in inducing type I IFNs may be due to the type of chemotherapy used, the tumor model or the different composition of the TMEs.

Our work still leaves a question open: how does type I IFN exert its anti-cancer efficacy in cisplatin/anti-CSF-1R-treated mice? Our data only partially answer this question. We observed that the activity of type I IFN in combination with cisplatin is independent of $CD8^+$ T cells, as the depletion of these cells did not influence the survival of cisplatin/anti-CSF-1R-treated mice. Additional studies are required to assess the role of other cytotoxic cells, such as NK cells. Our *in vitro* results showed that IFNα might have a direct inhibitory impact on KEP cancer cells, however, the *in vivo* relevance of this is still unknown. Notably, we only tested one IFNα subtype, IFNα1, which exert inhibitory effects on KEP cell line only at high concentrations. Despite the high sequence identity, the 14 IFNα molecules qualitatively differ in their potency against viral infections[60] and in their anti-proliferative effects on cancer cells[61]. It is possible that the combinatorial activity of multiple IFNα subtypes and also IFNβ might play a role in enhancing the cisplatin effect. In this regard, MDA MB231 breast cancer cells treated with cisplatin and IFNβ displayed cell growth inhibition and apoptosis[62]. Although we did not observe an increase in apoptotic cells number in cisplatin/anti-CSF-1R-treated KEP tumors, other cell death modalities like necrosis or necroptosis may occur. In addition, because both cisplatin[63] and type I IFNs[64] have been shown to induce senescence in cancer cells, it might be interesting to assess the number of senescent cells in cisplatin/anti-CSF-1R-treated tumors, as it may explain the absence of apoptosis and the reduced proliferation observed in these tumors.

Systemic administration of recombinant type I IFN is approved for haematological diseases and for melanoma at high-risk of recurrence after surgical resection, for which modest benefits were associated with intratumoral influx of DCs and T cells[65,66]. In breast cancer patients, type I IFN gene signatures have been shown

to correlate with increased bone metastasis-free survival or with metastasis-free survival in general[52,67,68]. However, administration of recombinant type I IFN in breast cancer and ovarian patients did not give the desired results because of the severe side effects and limited survival benefits[69-71]. These data suggest that a more physiological way to induce type I IFN production might promote better anti-cancer responses. In this regard, our study suggests that CSF-1R blockade may be used as a strategy to induce intratumoral type I IFNs. Importantly, we observed an increase in ISGs in the tumor of cancer patients treated with anti-CSF-1R compared to their baseline levels. Our data also implicate the use of agents that trigger type I IFN, like STING agonists[72], in order to enhance the anti-cancer efficacy of chemotherapy, bypassing the side effects of anti-CSF-1R on tissue-resident macrophages. Notably, STING agonists are now being tested in clinical trials[73-75].

Although type I IFNs are generally thought to be beneficial for anti-tumor immunity, prolonged activation of the pathway might lead to opposite effects. Indeed, like during infections, it is crucial that, after the initial inflammatory response against the pathogens, a resolution phase takes place to restore tissue homeostasis. In this regard, type I IFNs, which are important for the initial inflammatory response, also induce immunosuppression. For example in tumor-bearing and in non-tumor-bearing mice, type I IFNs can induce the expression of programmed death-ligand 1 (PD-L1), an inhibitory molecule that prevents T cell activation, IL-10, and indoleamine 2,3 deoxygenase (IDO), an enzyme involved in tryptophan metabolism that suppresses effector T cells[76-80]. In line with this, the therapeutic blockade of PD-L1 in combination with type I IFN treatment in cell line inoculation models resulted in better tumor control compared to mice that did not received the checkpoint inhibitor[80,81]. These data raise the question of whether the prolonged type I IFN signaling achieved in the KEP mice after CSF-1R blockade might induce immunosuppressive circuits. Indeed, we found that cisplatin/anti-CSF-1R treatment in KEP mice did not unleash an anti-tumor response. In order to engage anti-tumor immunity, we had to breach through the immunosuppressive layer by further targeting immunosuppressive neutrophils in this poorly immunogenic tumor model, resulting in a T cell dependent better tumor control and extended survival. RNA-sequencing analysis on intratumoral neutrophils isolated from cisplatin/anti-CSF-1R-treated mice displayed a pronounced type I IFN signaling compared to neutrophils in cisplatin/control antibody-treated mice. These data indicate that neutrophils signal through type I IFN receptor in the TME, however whether this signaling promotes immunosuppressive abilities in these cells has not been elucidated. While some studies have suggested that type I IFNs can induce anti-tumor properties in neutrophils[82], studies in chronic infections report that a type I IFN transcriptional signature in neutrophils in malaria-infected hosts and in patients with active tuberculosis correlated with tissue damage and disease pathogenesis[83,84]. It is possible that the type of IFN molecules, the set of ISGs expressed, the abundance of the receptor on cell surface and the duration of type I IFN signaling may all play a role in determining neutrophil function in different settings. Indeed, we observed that type I IFN-producing macrophages express higher levels of PD-L1 upon anti-CSF-1R treatment, raising the question of whether it is induced by IFNα in an autocrine mechanism occurring to resolve the inflammatory responses. In conclusion, we showed that although type I IFN is important to enhance the anti-cancer efficacy of cisplatin, future studies should

address whether sustained type I IFN signaling can be detrimental in cisplatin/anti-CSF-1R-treated mice.

Targeting neutrophil-derived immunosuppression

Because of the immunosuppressive function of neutrophils in the KEP model, **chapter 5** of this thesis suggests that targeting neutrophils may be an attractive therapeutic option for cancer therapy. Indeed, a high neutrophil-to-lymphocyte ratio in the circulation of several cancer types is linked to poor prognosis in patients[85]. However, total depletion of neutrophils is not desirable as it might increase the risk of serious opportunistic infections. Current approaches under clinical evaluation aim at blocking neutrophil migration by targeting CXCR1 and CXCR2, two chemokine receptors important for neutrophil recruitment in the tumor bed[86,87]. Other attractive approaches for inhibiting neutrophils include targeting the IL1β-IL-17-G-CSF inflammatory axis that leads to neutrophil expansion in several models, including the KEP model[88]. Importantly, drugs targeting this pathway are already clinically approved for the treatment of other inflammatory conditions like psoriasis, suggesting the possibility of a quick and easy transfer of these drugs to the treatment of cancer[89]. Future clinical studies should assess the efficacy of these neutrophil-targeting agents in patients with neutrophil expansion in combination with anti-CSF-1R treatment or type I IFN-stimulating drugs and chemotherapy.

Neutrophils can exert immunosuppressive functions by several mechanisms[90]. For example, neutrophils express enzymes, such as arginase I (ARG1) and IDO, that consume amino acids important for T cell function and survival like L-arginine and tryptophan, respectively[91,92]. Also, the release of reactive oxygen species and nitric oxide by the activity of ARG1 and inducible nitric oxide synthase (iNOS) inhibits the ability of T cells to recognize the specific peptide by affecting the T cell receptor (TCR) conformational flexibility[93]. Although our group has previously reported that in the KEP-based model of spontaneous breast cancer metastasis immunosuppressive and pro-metastatic neutrophils express high levels of iNOS[88,94], additional studies are required to elucidate the mechanisms employed by neutrophils to prevent an anti-tumor immune response in cisplatin/anti-CSF-1R-treated mice.

One proposed advantage of therapies targeting the immune compartment of the TME is that, differently from cancer cells, these cells are genetically stable cells, thus less prone to acquire therapy resistance. However, considering the plasticity and versatility of the immune system, resistance mechanisms to immunomodulatory drugs may derive from compensatory inflammatory cues. In several types of tumor models, macrophage inhibition triggered an influx of neutrophils with tumor-supporting functions in the TME that reinstates tumor progression[95-98]. Some of these studies showed that neutrophils compensate for the depletion of TAMs by employing the same pro-tumoral mechanisms of TAMs, such as production of metalloproteinase-9 and activation of the PI3K signaling pathway to induce angiogenesis and immunosuppression[96,97]. Differently from these studies, our work suggests that upon CSF-1R inhibition, neutrophils do not take over macrophage activities, but, unlike macrophages, exert immunosuppressive functions. The therapeutic efficacy of targeting macrophages and neutrophils in cisplatin-treated KEP is mediated by inducing type I IFNs by intratumoral macrophages and by unleashing anti-tumor responses.

The challenge to study neutrophils in cancer

Similar to macrophages, neutrophils are highly plastic cells which dynamically adapt to changes in the environment. Reflecting the M1/M2 binary definition, it was proposed that also tumor-associated neutrophils could be described as N1 or N2 with anti- and pro-tumoral properties, respectively[99]. TGFβ was found to be the key molecule to skew neutrophils towards a N2 phenotype[99]. G-CSF is another mediator known to induce pro-metastatic neutrophils with immunosuppressive or pro-angiogenic functions[88,100-103]. Conversely, IFNβ has been reported to shift neutrophil profile towards an N1 phenotype *in vivo*[104]. *In vitro* treatment of neutrophils with a cocktail of cytokines including GM-CSF and IFNγ has been shown instead to induce the generation of neutrophils with an antigen-presenting ability[105]. Interestingly, a subset of neutrophils with antigen-presenting abilities was also found in lung cancer patients[106]. These data suggest that different stimuli may sculpt neutrophils in unique ways. Like for macrophages, a static binary state of neutrophil activation is unlikely to exist; rather, their functional identity is dynamically and continuously determined by stimuli in the environment. As a consequence, the function of neutrophils in distinct TME may differ. Although the majority of the studies demonstrate the pro-tumorigenic and pro-metastatic role of neutrophils, others report tumor-inhibiting properties[100]. Neutrophil depletion is the main strategy used by these studies to identify the function of these cells. However, current approaches are either non-specific (*e.g.*: anti-GR1 antibodies or CXCR2 antagonists) or with non-durable effects (*e.g.*: anti-Ly6G antibody or genetic model based on administration of diphtheria toxin[107]). To circumvent these issues, **chapter 6** of this thesis describes a novel mouse model for the conditional and reversible depletion of neutrophils. This model, called hMRP8-ATTAC, expresses caspase 8 fused to the FKBP domain under the control of the human MRP8 promotor, which is mainly active in neutrophils. The model relies on the administration of a chemical dimerizer which binds with high affinity to two FKBP domains, leading to the dimerization and activation of caspase 8 and resulting in apoptosis[108]. Despite the high expression of the transgene mainly in neutrophils and their reduction after dimerizer injection, we did not observe neutrophil depletion in tumor-bearing hMRP8-ATTAC mice. The challenge of depleting neutrophils is that they are relatively short-lived, they are continuously produced in the bone marrow and ablating neutrophils activates feedback mechanisms to increase granulopoiesis[100]. In tumor-bearing hosts, this phenomenon is amplified, as tumors induce high levels of G-CSF pressing the bone marrow to release new neutrophils[88]. The continuous neutrophil production and the fact that the dimerizer has a half-life of approximately 5 hours, might explain why we did not observe neutrophil ablation in tumor-bearing hMRP8-ATTAC mice. Future studies should assess whether a more constant dimerizer treatment would be more successful in reducing neutrophil numbers. In this regard, it would be interesting to investigate a dimerizer formulation to be supplied in the animal chow or in the drinking water.

Besides total ablation of neutrophils, future studies should also focus on specific gene deletion in neutrophils. For example, it was discovered that the MET proto-oncogene in neutrophils is important for their chemotaxis and anti-tumoral and anti-metastatic effects[109]. The hMRP8;Cre mouse model, in which the cre recombinase is

expressed under the control of the neutrophil-specific promotor, could be crossed with a mouse model bearing LoxP-flanked genes of interest, resulting in neutrophil-specific gene knockouts. However, the generation of these transgenic mice is time and cost-consuming. A strategy to accelerate genetic studies in neutrophils could be the *in vitro* manipulation of bone marrow progenitors in order to obtain knocked-out or knocked-down genes specifically in neutrophils followed by bone marrow reconstitution with these cells, allowing for testing in parallel the function of multiple genes of interest. These types of experiments may be used to answer some of the questions described above. For example, by knocking-out IFNAR1 specifically in neutrophils, it would be interesting to assess the effect of type I IFN signaling in the immunosuppressive abilities of neutrophils in cisplatin/anti-CSF-1R-treated mice.
In conclusion, future studies should aim at generating new *in vivo* tools for the study of neutrophils, in order to obtain a better understanding of the role played by neutrophils in different aspects of tumor biology.

Concluding remarks

The TME is a complex network in which several cell populations exert a variety of functions that can favor or limit tumor growth and progression. This thesis focuses on the complexity of myeloid cells in the TME, highlights the need to better understand the effects of immunomodulatory agents and proposes the design of combinatorial strategies targeting several aspects of the TME for the treatment of breast cancer. In particular, our data suggest that creating a favorable TME and targeting immunosuppressive cells are two steps necessary to engage anti-tumor immunity in breast cancer. In addition to targeting pro-tumoral immune cells or creating an advantageous TME for immune-stimulation, directly stimulating the anti-tumor cytotoxic activity of T cells represents an attractive strategy against cancer. One of the most studied approaches is the use of immune checkpoint inhibitors, which are blocking antibodies directed against molecules that inhibit T cell function, such as cytotoxic T-lymphocyte-associated protein 4 (CTLA-4) and programmed cell death protein 1 (PD-1) on T cells, or against one of its ligands, PD-L1, expressed by a variety of cells including myeloid cells and tumor cells[110]. The use of checkpoint inhibitors in clinical trials showed remarkable results in several types of cancer including melanoma, non-small cell lung carcinoma, Hodgkin's lymphoma and bladder cancer[111-115]. The successes of this therapeutic approach resulted in the selection of cancer immunotherapy as the breakthrough of 2013 by the journal *Science*[116] and the award of the Nobel Prize in Physiology or Medicine 2018 to James P. Allison and Tasuku Honjo for their discovery of CTLA-4 and PD-1, respectively[117]. However, not all tumor types respond equally to checkpoint inhibitors. In triple negative breast cancer (TNBC) patients, checkpoint inhibitors as monotherapies show a modest response rate that varies between 5 and 30%[118], raising the possibility that a more immunosuppressed TME and/or a lower mutational burden, as compared to other tumors types, contribute to the poor response. Further evaluation of the efficacy of checkpoint inhibitors in combination with conventional chemotherapy in breast cancer patients is currently ongoing. A phase III clinical trial in TNBC patients, showed promising results of anti-PD-L1 therapy in combination

with paclitaxel, especially in the subgroup of patients that expresses PD-L1[119]. In addition, the immunomodulatory properties of low dose chemotherapy are also appealing to be exploited in combination with immunotherapy. In this regard, a clinical trial at the NKI led by Dr. Marleen Kok in metastatic TNBC patients is evaluating the effects of five different conventional therapies, including low dose chemotherapy and radiotherapy, in conditioning the tumor microenvironment to the following treatment with checkpoint inhibitors[120,121]. In addition to conventional therapies, the efficacy of checkpoint inhibitors is currently under evaluation in combination with CSF-1R-targeting agents[35]. Results from these clinical trials will provide further information on the importance of modulating the TME in order to achieve anti-tumor immunity.

Overall in my thesis I have explored the role of myeloid cells in conventional therapy response in breast cancer. My results suggest that suppressive cells are an important roadblock for successful anti-cancer therapy. Therefore, future therapeutic approaches, including immunotherapies, should include combinational therapies that counteract myeloid cells. Additionally, this thesis highlights the importance of considering the effects of conventional therapies on intratumoral cells other than cancer cells for treatment decisions.

References

1. Stein, M., Keshav, S., Harris, N. & Gordon, S. Interleukin 4 potently enhances murine macrophage mannose receptor activity: a marker of alternative immunologic macrophage activation. *J Exp Med* **176**, 287-292 (1992).
2. Mills, C.D., Kincaid, K., Alt, J.M., Heilman, M.J. & Hill, A.M. M-1/M-2 macrophages and the Th1/Th2 paradigm. *J Immunol* **164**, 6166-6173 (2000).
3. Xue, J.*, et al.* Transcriptome-based network analysis reveals a spectrum model of human macrophage activation. *Immunity* **40**, 274-288 (2014).
4. Murray, P.J.*, et al.* Macrophage activation and polarization: nomenclature and experimental guidelines. *Immunity* **41**, 14-20 (2014).
5. Lavin, Y.*, et al.* Tissue-resident macrophage enhancer landscapes are shaped by the local microenvironment. *Cell* **159**, 1312-1326 (2014).
6. Mantovani, A., Sozzani, S., Locati, M., Allavena, P. & Sica, A. Macrophage polarization: tumor-associated macrophages as a paradigm for polarized M2 mononuclear phagocytes. *Trends Immunol* **23**, 549-555 (2002).
7. Azizi, E.*, et al.* Single-Cell Map of Diverse Immune Phenotypes in the Breast Tumor Microenvironment. *Cell* **174**, 1293-1308 e1236 (2018).
8. Derksen, P.W.*, et al.* Somatic inactivation of E-cadherin and p53 in mice leads to metastatic lobular mammary carcinoma through induction of anoikis resistance and angiogenesis. *Cancer Cell* **10**, 437-449 (2006).
9. Boggio, K.*, et al.* Interleukin 12-mediated prevention of spontaneous mammary adenocarcinomas in two lines of Her-2/neu transgenic mice. *J Exp Med* **188**, 589-596 (1998).
10. Berglund, E.*, et al.* Spatial maps of prostate cancer transcriptomes reveal an unexplored landscape of heterogeneity. *Nat Commun* **9**, 2419 (2018).
11. Franklin, R.A.*, et al.* The cellular and molecular origin of tumor-associated macrophages. *Science* **344**, 921-925 (2014).
12. Tymoszuk, P.*, et al.* In situ proliferation contributes to accumulation of tumor-associated macrophages in spontaneous mammary tumors. *Eur J Immunol* **44**, 2247-2262 (2014).
13. Maman, S. & Witz, I.P. A history of exploring cancer in context. *Nat Rev Cancer* **18**, 359-376 (2018).
14. Ruffell, B. & Coussens, L.M. Macrophages and therapeutic resistance in cancer. *Cancer Cell* **27**, 462-472 (2015).
15. Gentles, A.J.*, et al.* The prognostic landscape of genes and infiltrating immune cells across human cancers. *Nat Med* **21**, 938-945 (2015).
16. Mantovani, A., Marchesi, F., Malesci, A., Laghi, L. & Allavena, P. Tumour-associated macrophages as treatment targets in oncology. *Nat Rev Clin Oncol* **14**, 399-416 (2017).
17. Chen, Q., Zhang, X.H. & Massague, J. Macrophage binding to receptor VCAM-1 transmits survival signals in breast cancer cells that invade the lungs. *Cancer Cell* **20**, 538-549 (2011).
18. Giraudo, E., Inoue, M. & Hanahan, D. An amino-bisphosphonate targets MMP-9-expressing macrophages and angiogenesis to impair cervical carcinogenesis. *J Clin Invest* **114**, 623-633 (2004).
19. Lin, E.Y.*, et al.* Macrophages regulate the angiogenic switch in a mouse model of breast cancer. *Cancer Res* **66**, 11238-11246 (2006).
20. Qian, B.*, et al.* A distinct macrophage population mediates metastatic breast cancer cell extravasation, establishment and growth. *PLoS One* **4**, e6562 (2009).
21. Wyckoff, J.B.*, et al.* Direct visualization of macrophage-assisted tumor cell intravasation in mammary tumors. *Cancer Res* **67**, 2649-2656 (2007).
22. Candido, J.B.*, et al.* CSF1R(+) Macrophages Sustain Pancreatic Tumor Growth through T Cell Suppression and Maintenance of Key Gene Programs that Define the Squamous Subtype. *Cell Rep* **23**, 1448-1460 (2018).
23. Lohela, M.*, et al.* Intravital imaging reveals distinct responses of depleting dynamic tumor-

associated macrophage and dendritic cell subpopulations. *Proc Natl Acad Sci U S A* **111**, E5086-5095 (2014).
24. Mitchem, J.B.*, et al.* Targeting tumor-infiltrating macrophages decreases tumor-initiating cells, relieves immunosuppression, and improves chemotherapeutic responses. *Cancer Res* **73**, 1128-1141 (2013).
25. Paulus, P., Stanley, E.R., Schafer, R., Abraham, D. & Aharinejad, S. Colony-stimulating factor-1 antibody reverses chemoresistance in human MCF-7 breast cancer xenografts. *Cancer Res* **66**, 4349-4356 (2006).
26. Prada, C.E.*, et al.* Neurofibroma-associated macrophages play roles in tumor growth and response to pharmacological inhibition. *Acta Neuropathol* **125**, 159-168 (2013).
27. Pyonteck, S.M.*, et al.* CSF-1R inhibition alters macrophage polarization and blocks glioma progression. *Nat Med* **19**, 1264-1272 (2013).
28. Ries, C.H.*, et al.* Targeting tumor-associated macrophages with anti-CSF-1R antibody reveals a strategy for cancer therapy. *Cancer Cell* **25**, 846-859 (2014).
29. Strachan, D.C.*, et al.* CSF1R inhibition delays cervical and mammary tumor growth in murine models by attenuating the turnover of tumor-associated macrophages and enhancing infiltration by CD8(+) T cells. *Oncoimmunology* **2**, e26968 (2013).
30. Zhu, Y.*, et al.* CSF1/CSF1R blockade reprograms tumor-infiltrating macrophages and improves response to T-cell checkpoint immunotherapy in pancreatic cancer models. *Cancer Res* **74**, 5057-5069 (2014).
31. DeNardo, D.G.*, et al.* Leukocyte complexity predicts breast cancer survival and functionally regulates response to chemotherapy. *Cancer Discov* **1**, 54-67 (2011).
32. Olson, O.C., Kim, H., Quail, D.F., Foley, E.A. & Joyce, J.A. Tumor-Associated Macrophages Suppress the Cytotoxic Activity of Antimitotic Agents. *Cell Rep* **19**, 101-113 (2017).
33. Ruffell, B.*, et al.* Macrophage IL-10 blocks CD8+ T cell-dependent responses to chemotherapy by suppressing IL-12 expression in intratumoral dendritic cells. *Cancer Cell* **26**, 623-637 (2014).
34. Weizman, N.*, et al.* Macrophages mediate gemcitabine resistance of pancreatic adenocarcinoma by upregulating cytidine deaminase. *Oncogene* **33**, 3812-3819 (2014).
35. Cannarile, M.A.*, et al.* Colony-stimulating factor 1 receptor (CSF1R) inhibitors in cancer therapy. *J Immunother Cancer* **5**, 53 (2017).
36. NCT01494688. A Study of RO5509554 as Monotherapy and in Combination With Paclitaxel in Participants With Advanced Solid Tumors.
37. Cassier, P.A.*, et al.* CSF1R inhibition with emactuzumab in locally advanced diffuse-type tenosynovial giant cell tumours of the soft tissue: a dose-escalation and dose-expansion phase 1 study. *Lancet Oncol* **16**, 949-956 (2015).
38. West, R.B.*, et al.* A landscape effect in tenosynovial giant-cell tumor from activation of CSF1 expression by a translocation in a minority of tumor cells. *Proc Natl Acad Sci U S A* **103**, 690-695 (2006).
39. Papadopoulos, K.P.*, et al.* First-in-Human Study of AMG 820, a Monoclonal Anti-Colony-Stimulating Factor 1 Receptor Antibody, in Patients with Advanced Solid Tumors. *Clin Cancer Res* **23**, 5703-5710 (2017).
40. Dai, X.M.*, et al.* Targeted disruption of the mouse colony-stimulating factor 1 receptor gene results in osteopetrosis, mononuclear phagocyte deficiency, increased primitive progenitor cell frequencies, and reproductive defects. *Blood* **99**, 111-120 (2002).
41. Wynn, T.A., Chawla, A. & Pollard, J.W. Macrophage biology in development, homeostasis and disease. *Nature* **496**, 445-455 (2013).
42. Isaacs, A. & Lindenmann, J. Virus interference. I. The interferon. *Proc R Soc Lond B Biol Sci* **147**, 258-267 (1957).
43. McNab, F., Mayer-Barber, K., Sher, A., Wack, A. & O'Garra, A. Type I interferons in infectious disease. *Nat Rev Immunol* **15**, 87-103 (2015).
44. Dunn, G.P.*, et al.* A critical function for type I interferons in cancer immunoediting. *Nat Immunol*

6, 722-729 (2005).
45. Gresser, I., Belardelli, F., Maury, C., Maunoury, M.T. & Tovey, M.G. Injection of mice with antibody to interferon enhances the growth of transplantable murine tumors. *J Exp Med* **158**, 2095-2107 (1983).
46. Picaud, S., Bardot, B., De Maeyer, E. & Seif, I. Enhanced tumor development in mice lacking a functional type I interferon receptor. *J Interferon Cytokine Res* **22**, 457-462 (2002).
47. Swann, J.B.*, et al.* Type I IFN contributes to NK cell homeostasis, activation, and antitumor function. *J Immunol* **178**, 7540-7549 (2007).
48. Tschurtschenthaler, M.*, et al.* Type I interferon signalling in the intestinal epithelium affects Paneth cells, microbial ecology and epithelial regeneration. *Gut* **63**, 1921-1931 (2014).
49. Diamond, M.S.*, et al.* Type I interferon is selectively required by dendritic cells for immune rejection of tumors. *J Exp Med* **208**, 1989-2003 (2011).
50. Fuertes, M.B.*, et al.* Host type I IFN signals are required for antitumor CD8+ T cell responses through CD8{alpha}+ dendritic cells. *J Exp Med* **208**, 2005-2016 (2011).
51. Katlinski, K.V.*, et al.* Inactivation of Interferon Receptor Promotes the Establishment of Immune Privileged Tumor Microenvironment. *Cancer Cell* **31**, 194-207 (2017).
52. Bidwell, B.N.*, et al.* Silencing of Irf7 pathways in breast cancer cells promotes bone metastasis through immune escape. *Nat Med* **18**, 1224-1231 (2012).
53. Lan, Q.*, et al.* Type I interferon/IRF7 axis instigates chemotherapy-induced immunological dormancy in breast cancer. *Oncogene* (2018).
54. Sivick, K.E.*, et al.* Magnitude of Therapeutic STING Activation Determines CD8(+) T Cell-Mediated Anti-tumor Immunity. *Cell Rep* **25**, 3074-3085 e3075 (2018).
55. Spaapen, R.M.*, et al.* Therapeutic activity of high-dose intratumoral IFN-beta requires direct effect on the tumor vasculature. *J Immunol* **193**, 4254-4260 (2014).
56. Burnette, B.C.*, et al.* The efficacy of radiotherapy relies upon induction of type i interferon-dependent innate and adaptive immunity. *Cancer Res* **71**, 2488-2496 (2011).
57. Deng, L.*, et al.* STING-Dependent Cytosolic DNA Sensing Promotes Radiation-Induced Type I Interferon-Dependent Antitumor Immunity in Immunogenic Tumors. *Immunity* **41**, 843-852 (2014).
58. Moschella, F.*, et al.* Cyclophosphamide induces a type I interferon-associated sterile inflammatory response signature in cancer patients' blood cells: implications for cancer chemoimmunotherapy. *Clin Cancer Res* **19**, 4249-4261 (2013).
59. Sistigu, A.*, et al.* Cancer cell-autonomous contribution of type I interferon signaling to the efficacy of chemotherapy. *Nat Med* **20**, 1301-1309 (2014).
60. Koyama, T.*, et al.* Divergent activities of interferon-alpha subtypes against intracellular hepatitis C virus replication. *Hepatol Res* **34**, 41-49 (2006).
61. Tanimoto, T.*, et al.* The combination of IFN-alpha2 and IFN-alpha8 exhibits synergistic antiproliferative activity on renal cell carcinoma (RCC) cell lines through increased binding affinity for IFNAR-2. *J Interferon Cytokine Res* **27**, 517-523 (2007).
62. Ethiraj, P., Veerappan, K., Doraisami, B. & Sivapatham, S. Synergistic anti-carcinogenic effect of interferon-beta with cisplatin on human breast adenocarcinoma MDA MB231 cells. *Int Immunopharmacol* **23**, 222-228 (2014).
63. Wang, X.*, et al.* Evidence of cisplatin-induced senescent-like growth arrest in nasopharyngeal carcinoma cells. *Cancer Res* **58**, 5019-5022 (1998).
64. Katlinskaya, Y.V.*, et al.* Suppression of Type I Interferon Signaling Overcomes Oncogene-Induced Senescence and Mediates Melanoma Development and Progression. *Cell Rep* **15**, 171-180 (2016).
65. Jonasch, E. & Haluska, F.G. Interferon in oncological practice: review of interferon biology, clinical applications, and toxicities. *Oncologist* **6**, 34-55 (2001).
66. Moschos, S.J.*, et al.* Neoadjuvant treatment of regional stage IIIB melanoma with high-dose interferon alfa-2b induces objective tumor regression in association with modulation of tumor infiltrating host cellular immune responses. *J Clin Oncol* **24**, 3164-3171 (2006).

67. Callari, M.*, et al.* Subtype-dependent prognostic relevance of an interferon-induced pathway metagene in node-negative breast cancer. *Mol Oncol* **8**, 1278-1289 (2014).
68. Snijders, A.M.*, et al.* An interferon signature identified by RNA-sequencing of mammary tissues varies across the estrous cycle and is predictive of metastasis-free survival. *Oncotarget* **5**, 4011-4025 (2014).
69. Alberts, D.S.*, et al.* Randomized trial of adjuvant intraperitoneal alpha-interferon in stage III ovarian cancer patients who have no evidence of disease after primary surgery and chemotherapy: An intergroup study. *Gynecol Oncol* **100**, 133-138 (2006).
70. Hall, G.D.*, et al.* Maintenance treatment with interferon for advanced ovarian cancer: results of the Northern and Yorkshire gynaecology group randomised phase III study. *Br J Cancer* **91**, 621-626 (2004).
71. Nethersell, A., Smedley, H., Katrak, M., Wheeler, T. & Sikora, K. Recombinant interferon in advanced breast cancer. *Br J Cancer* **49**, 615-620 (1984).
72. Corrales, L.*, et al.* Direct Activation of STING in the Tumor Microenvironment Leads to Potent and Systemic Tumor Regression and Immunity. *Cell Rep* **11**, 1018-1030 (2015).
73. NCT03172936. Study of the Safety and Efficacy of MIW815 With PDR001 to Patients With Advanced/Metastatic Solid Tumors or Lymphomas.
74. NCT03010176. Study of MK-1454 Alone or in Combination With Pembrolizumab in Participants With Advanced/Metastatic Solid Tumors or Lymphomas (MK-1454-001).
75. NCT02675439. Safety and Efficacy of MIW815 (ADU-S100) +/- Ipilimumab in Patients With Advanced/Metastatic Solid Tumors or Lymphomas.
76. Huang, L.*, et al.* Cutting edge: DNA sensing via the STING adaptor in myeloid dendritic cells induces potent tolerogenic responses. *J Immunol* **191**, 3509-3513 (2013).
77. Lemos, H.*, et al.* STING Promotes the Growth of Tumors Characterized by Low Antigenicity via IDO Activation. *Cancer Res* **76**, 2076-2081 (2016).
78. Mellor, A.L.*, et al.* Cutting edge: CpG oligonucleotides induce splenic CD19+ dendritic cells to acquire potent indoleamine 2,3-dioxygenase-dependent T cell regulatory functions via IFN Type 1 signaling. *J Immunol* **175**, 5601-5605 (2005).
79. Stewart, C.A.*, et al.* Interferon-dependent IL-10 production by Tregs limits tumor Th17 inflammation. *J Clin Invest* **123**, 4859-4874 (2013).
80. Yang, X.*, et al.* Targeting the tumor microenvironment with interferon-beta bridges innate and adaptive immune responses. *Cancer Cell* **25**, 37-48 (2014).
81. Liang, Y.*, et al.* Targeting IFNalpha to tumor by anti-PD-L1 creates feedforward antitumor responses to overcome checkpoint blockade resistance. *Nat Commun* **9**, 4586 (2018).
82. Pylaeva, E., Lang, S. & Jablonska, J. The Essential Role of Type I Interferons in Differentiation and Activation of Tumor-Associated Neutrophils. *Front Immunol* **7**, 629 (2016).
83. Berry, M.P.*, et al.* An interferon-inducible neutrophil-driven blood transcriptional signature in human tuberculosis. *Nature* **466**, 973-977 (2010).
84. Rocha, B.C.*, et al.* Type I Interferon Transcriptional Signature in Neutrophils and Low-Density Granulocytes Are Associated with Tissue Damage in Malaria. *Cell Rep* **13**, 2829-2841 (2015).
85. Templeton, A.J.*, et al.* Prognostic role of neutrophil-to-lymphocyte ratio in solid tumors: a systematic review and meta-analysis. *J Natl Cancer Inst* **106**, dju124 (2014).
86. NCT02370238. A Double-blind Study of Paclitaxel in Combination With Reparixin or Placebo for Metastatic Triple-Negative Breast Cancer.
87. Schott, A.F.*, et al.* Phase Ib Pilot Study to Evaluate Reparixin in Combination with Weekly Paclitaxel in Patients with HER-2-Negative Metastatic Breast Cancer. *Clin Cancer Res* **23**, 5358-5365 (2017).
88. Coffelt, S.B.*, et al.* IL-17-producing gammadelta T cells and neutrophils conspire to promote breast cancer metastasis. *Nature* **522**, 345-348 (2015).
89. Gaffen, S.L., Jain, R., Garg, A.V. & Cua, D.J. The IL-23-IL-17 immune axis: from mechanisms to therapeutic testing. *Nat Rev Immunol* **14**, 585-600 (2014).
90. Gabrilovich, D.I., Ostrand-Rosenberg, S. & Bronte, V. Coordinated regulation of myeloid cells by

tumours. *Nat Rev Immunol* **12**, 253-268 (2012).
91. Rotondo, R.*, et al.* IL-8 induces exocytosis of arginase 1 by neutrophil polymorphonuclears in nonsmall cell lung cancer. *Int J Cancer* **125**, 887-893 (2009).
92. Yu, J.*, et al.* Myeloid-derived suppressor cells suppress antitumor immune responses through IDO expression and correlate with lymph node metastasis in patients with breast cancer. *J Immunol* **190**, 3783-3797 (2013).
93. Nagaraj, S.*, et al.* Altered recognition of antigen is a mechanism of CD8+ T cell tolerance in cancer. *Nat Med* **13**, 828-835 (2007).
94. Kersten, K.*, et al.* Mammary tumor-derived CCL2 enhances pro-metastatic systemic inflammation through upregulation of IL1beta in tumor-associated macrophages. *Oncoimmunology* **6**, e1334744 (2017).
95. Nywening, T.M.*, et al.* Targeting both tumour-associated CXCR2(+) neutrophils and CCR2(+) macrophages disrupts myeloid recruitment and improves chemotherapeutic responses in pancreatic ductal adenocarcinoma. *Gut* **67**, 1112-1123 (2018).
96. Pahler, J.C.*, et al.* Plasticity in tumor-promoting inflammation: impairment of macrophage recruitment evokes a compensatory neutrophil response. *Neoplasia* **10**, 329-340 (2008).
97. Rivera, L.B.*, et al.* Intratumoral myeloid cells regulate responsiveness and resistance to antiangiogenic therapy. *Cell Rep* **11**, 577-591 (2015).
98. Swierczak, A.*, et al.* The promotion of breast cancer metastasis caused by inhibition of CSF-1R/CSF-1 signaling is blocked by targeting the G-CSF receptor. *Cancer Immunol Res* **2**, 765-776 (2014).
99. Fridlender, Z.G.*, et al.* Polarization of tumor-associated neutrophil phenotype by TGF-beta: "N1" versus "N2" TAN. *Cancer Cell* **16**, 183-194 (2009).
100. Coffelt, S.B., Wellenstein, M.D. & de Visser, K.E. Neutrophils in cancer: neutral no more. *Nat Rev Cancer* **16**, 431-446 (2016).
101. Kowanetz, M.*, et al.* Granulocyte-colony stimulating factor promotes lung metastasis through mobilization of Ly6G+Ly6C+ granulocytes. *Proc Natl Acad Sci U S A* **107**, 21248-21255 (2010).
102. Shojaei, F.*, et al.* Bv8 regulates myeloid-cell-dependent tumour angiogenesis. *Nature* **450**, 825-831 (2007).
103. Waight, J.D., Hu, Q., Miller, A., Liu, S. & Abrams, S.I. Tumor-derived G-CSF facilitates neoplastic growth through a granulocytic myeloid-derived suppressor cell-dependent mechanism. *PLoS One* **6**, e27690 (2011).
104. Andzinski, L.*, et al.* Type I IFNs induce anti-tumor polarization of tumor associated neutrophils in mice and human. *Int J Cancer* **138**, 1982-1993 (2016).
105. Takashima, A. & Yao, Y. Neutrophil plasticity: acquisition of phenotype and functionality of antigen-presenting cell. *J Leukoc Biol* **98**, 489-496 (2015).
106. Singhal, S.*, et al.* Origin and Role of a Subset of Tumor-Associated Neutrophils with Antigen-Presenting Cell Features in Early-Stage Human Lung Cancer. *Cancer Cell* **30**, 120-135 (2016).
107. Reber, L.L.*, et al.* Neutrophil myeloperoxidase diminishes the toxic effects and mortality induced by lipopolysaccharide. *J Exp Med* **214**, 1249-1258 (2017).
108. Pajvani, U.B.*, et al.* Fat apoptosis through targeted activation of caspase 8: a new mouse model of inducible and reversible lipoatrophy. *Nat Med* **11**, 797-803 (2005).
109. Finisguerra, V.*, et al.* MET is required for the recruitment of anti-tumoural neutrophils. *Nature* **522**, 349-353 (2015).
110. Ribas, A. & Wolchok, J.D. Cancer immunotherapy using checkpoint blockade. *Science* **359**, 1350-1355 (2018).
111. Ansell, S.M.*, et al.* PD-1 blockade with nivolumab in relapsed or refractory Hodgkin's lymphoma. *N Engl J Med* **372**, 311-319 (2015).
112. Eggermont, A.M.*, et al.* Prolonged Survival in Stage III Melanoma with Ipilimumab Adjuvant Therapy. *N Engl J Med* **375**, 1845-1855 (2016).
113. Eggermont, A.M.M.*, et al.* Adjuvant Pembrolizumab versus Placebo in Resected Stage III Melanoma. *N Engl J Med* **378**, 1789-1801 (2018).

114. Hellmann, M.D.*, et al.* Nivolumab plus Ipilimumab in Lung Cancer with a High Tumor Mutational Burden. *N Engl J Med* **378**, 2093-2104 (2018).
115. Powles, T.*, et al.* MPDL3280A (anti-PD-L1) treatment leads to clinical activity in metastatic bladder cancer. *Nature* **515**, 558-562 (2014).
116. Couzin-Frankel, J. Breakthrough of the year 2013. Cancer immunotherapy. *Science* **342**, 1432-1433 (2013).
117. The Nobel Prize in Physiology or Medicine 2018. NobelPrize.org. Nobel Media AB 2019. Sun. 13 Jan 2019. https://www.nobelprize.org/prizes/medicine/2018/summary/.
118. Polk, A., Svane, I.M., Andersson, M. & Nielsen, D. Checkpoint inhibitors in breast cancer - Current status. *Cancer Treat Rev* **63**, 122-134 (2018).
119. Schmid, P.*, et al.* Atezolizumab and Nab-Paclitaxel in Advanced Triple-Negative Breast Cancer. *N Engl J Med* **379**, 2108-2121 (2018).
120. Kok, M.*, et al.* Adaptive phase II randomized trial of nivolumab after induction treatment in triple negative breast cancer (TONIC trial): Final response data stage I and first translational data. **36**, 1012-1012 (2018).
121. https://clinicaltrials.gov/ct2/show/NCT02499367. Nivolumab After Induction Treatment in Triple-negative Breast Cancer (TNBC) Patients (TONIC).

CHAPTER 8

Addenda

English Summary
Dutch Summary
Acknowledgements
Curriculum Vitae
Publications

English Summary

The recognition that non-cancer cells infiltrate tumors and critically contribute to cancer biology, brought large attention in the cancer-research field to the interplay between cancer and non-cancer cells[1]. The tumor microenvironment (TME) includes several cell populations, such as endothelial cells, fibroblasts and immune cells, and their mediators, which play a pivotal role in tumor development, progression and therapy response. Interestingly, immune cells play a paradoxical role in tumors. While some immune cells, like $CD8^+$ T cells and NK cells, can recognize and kill cancer cells, other cells like macrophages and neutrophils can promote tumor development and progression, and facilitate metastasis.

Macrophages represent an important component of the tumor microenvironment and they have been the subject of a large body of studies aimed at understanding their contribution to tumor progression and therapy response[2]. Historically, tumor-associated macrophages (TAMs) were described as being either anti-tumoral (M1) or pro-tumoral (M2) and were distinguished based on the expression of a few markers, however, it is now clear that TAM phenotype and function is far more complex than this binary definition[3,4]. Macrophages are very plastic myeloid cells that dynamically and continuously adapt their phenotype based on the stimuli they receive from their environment. Because different tumors have distinct TMEs, there is an emerging realization that one single definition of TAMs does not exist; rather, TAMs from distinct tumor types do not have the same phenotype and function. However, a direct comparison of the transcriptome of TAMs isolated from distinct breast cancer subtypes have not been performed yet. Thus, one of the hypothesis we follow in this thesis is that interrogation of transcriptional profiles of TAMs from different breast cancer subtypes might be of relevance and have prognostic value.

Because macrophages exert tumor-supporting functions in various preclinical models[5] and are often associated with poor prognosis in several human cancer types, immunomodulatory agents that target TAMs have been developed and are currently being evaluated in clinical trials[6]. One approach to target TAMs is by interfering with the Colony Stimulating Factor-1 (CSF1)/CSF-1 receptor (CSF-1R) signaling pathway, which is vital for macrophages, using, for example, an antagonistic antibody against CSF-1R[7]. In order to maximize the success of macrophage-targeting compounds it is of utmost importance to understand the effects of these drugs on the targeted cells and on cancer behavior, and to identify the optimal partner among the available conventional anti-cancer therapies. As such, part of this thesis aims at investigating how to maximize the efficacy of anti-CSF-1R treatment by combining it with chemotherapeutic agents and to unravel the mechanisms that lead to therapeutic benefit.

Besides macrophages, neutrophils have also been shown to be important in cancer progression and metastasis formation[8]. They are often found increased in cancer patients and a high neutrophil-to-lymphocytes ratio in the circulation predicts poor survival in several types of cancer[9,10]. Furthermore, chemotherapy-induced neutropenia in breast cancer patients correlates with a better prognosis[11,12]. Therefore, a better understanding on the role of neutrophils in chemotherapy response is necessary to improve anti-cancer efficacy. In order to do so, in this thesis, we generate a new mouse model for the conditional depletion of neutrophils.

The overall aim of the work described in this thesis is to gain novel insights into the complexity of immune cells, in particular of macrophages and neutrophils, in the context of breast cancer. How tumors influence TAM phenotype and how immune cells affect chemotherapy response are key questions addressed in this thesis.

To study intratumoral immune cells, in **chapter 2** we describe a method to isolate immune cell populations from freshly harvested tissues. This method is based on antibody-mediated enrichment of immune cells by magnetic cell sorting followed by purification of selected immune cell populations with multi-color flow cytometry-based sorting. We used this approach in **chapter 3**, where we isolated TAMs from two distinct genetically engineered mouse models for mammary tumorigenesis, *i.e.* the *K14cre;Cdh1$^{F/F}$;Trp53$^{F/F}$* and *MMTV-NeuT* models, which resemble human invasive lobular carcinoma (ILC) and HER2-overexpressing breast tumors, respectively[13,14]. Although bioinformatics analyses of these TAM populations identified a common gene signature suggesting that TAMs from different models may have common phenotypes and functions, **chapter 3** also shows that breast cancer subtype-specific core signatures exist in TAMs, indicating that distinct TMEs differentially dictate the transcriptional profile of TAMs. Interestingly, a selection of genes specific for the *K14cre;Cdh1$^{F/F}$;Trp53$^{F/F}$* model correlated with poor survival in two cohorts of ILC patients.

Chemotherapy is the mainstay treatment for most cancer types. Chemotherapeutic drugs do not only kill cancer cells, but also influence the number and the phenotype of immune cells. Understanding how different chemotherapeutic agents impact the immune system could facilitate the rational design of combination therapies. In **chapter 4**, we review the effects of chemotherapeutic drugs on immune cells and we propose that those chemotherapeutic drugs that relieve immunosuppression may be combined with immunotherapeutic compounds in order to maximize the activity of the latter.
Besides affecting the immune system, the therapeutic efficacy of chemotherapeutic agents is influenced by immune cells. In particular macrophages have been shown to counteract the anti-cancer effects of several chemotherapeutic drugs. By using a macrophage-targeting agent, anti-CSF-1R, in the spontaneous *K14cre;Cdh1$^{F/F}$;Trp53$^{F/F}$* model for breast cancer, we showed in **chapter 5** of this thesis that CSF-1R inhibition enhances chemotherapy efficacy in a drug dependent manner. We reported that anti-CSF-1R synergizes with platinum-containing drugs, like cisplatin, but not docetaxel, highlighting the importance of optimally matching these compounds with the correct cytotoxic drug. In addition, we mechanistically discovered that CSF-1R inhibition stimulates intratumoral type I interferon signaling which is essential for the synergistic anti-cancer effect of cisplatin and anti-CSF-1R combination. We also demonstrated that further targeting immunosuppressive neutrophils is essential to engage a successful anti-tumor immunity in a poorly immunogenic tumor model.

Thus far, the most commonly used methods to study neutrophils rely on depleting the population or blocking their recruitment. However, the current strategies are either not specific for neutrophils or have short-term efficacy. Therefore, there

is a clear need for genetic models that allow long-term neutrophil depletion in a conditional and reversible fashion. In **chapter 6** we describe the development and characterization of the hMRP8-ATTAC (human migration inhibitory factor-related protein 8-Apoptosis Through Targeted Activation of Caspase 8) model[15], a newly generated genetic mouse model for the conditional and reversible depletion of neutrophils. Upon injection with a chemical dimerizer, the transgene carrying a caspase 8-FKBP fusion protein is activated and apoptosis is induced mainly in neutrophils. Although this approach successfully reduces neutrophils in a homeostatic condition, it fails to do so in tumor-bearing mice, indicating that improvements are required to sustain an efficacious neutrophil ablation in a chronically inflamed context.

Chapter 7 contains the general discussion where I contextualize the findings of this thesis with the current literature and I provide my point of view on the future of my research.

In conclusion, the work described here highlights the importance of targeting myeloid cells to engage an anti-tumor immune response in the context of chemotherapy. In addition, it prompts to explore some aspects of the effects of conventional therapies and of newly developed drugs, such as their impact on the microenvironment, in order to fully exploit their anti-tumor efficacy.

References

1. Maman, S. & Witz, I.P. A history of exploring cancer in context. *Nat Rev Cancer* **18**, 359-376 (2018).
2. Cassetta, L. & Pollard, J.W. Targeting macrophages: therapeutic approaches in cancer. *Nat Rev Drug Discov* (2018).
3. DeNardo, D.G. & Ruffell, B. Macrophages as regulators of tumour immunity and immunotherapy. *Nat Rev Immunol* (2019).
4. Mantovani, A., Sozzani, S., Locati, M., Allavena, P. & Sica, A. Macrophage polarization: tumor-associated macrophages as a paradigm for polarized M2 mononuclear phagocytes. *Trends Immunol* **23**, 549-555 (2002).
5. Mantovani, A., Marchesi, F., Malesci, A., Laghi, L. & Allavena, P. Tumour-associated macrophages as treatment targets in oncology. *Nat Rev Clin Oncol* **14**, 399-416 (2017).
6. Cannarile, M.A*., et al.* Colony-stimulating factor 1 receptor (CSF1R) inhibitors in cancer therapy. *J Immunother Cancer* **5**, 53 (2017).
7. Ries, C.H*., et al.* Targeting tumor-associated macrophages with anti-CSF-1R antibody reveals a strategy for cancer therapy. *Cancer Cell* **25**, 846-859 (2014).
8. Coffelt, S.B., Wellenstein, M.D. & de Visser, K.E. Neutrophils in cancer: neutral no more. *Nat Rev Cancer* **16**, 431-446 (2016).
9. Templeton, A.J*., et al.* Prognostic role of neutrophil-to-lymphocyte ratio in solid tumors: a systematic review and meta-analysis. *J Natl Cancer Inst* **106**, dju124 (2014).
10. Wei, B*., et al.* The neutrophil lymphocyte ratio is associated with breast cancer prognosis: an updated systematic review and meta-analysis. *Onco Targets Ther* **9**, 5567-5575 (2016).
11. Han, Y*., et al.* Prognostic value of chemotherapy-induced neutropenia in early-stage breast cancer. *Breast Cancer Res Treat* **131**, 483-490 (2012).
12. Ma, R.M*., et al.* Prognostic Value of Chemotherapy-Induced Neutropenia at the First Cycle in Invasive Breast Cancer. *Medicine (Baltimore)* **95**, e3240 (2016).
13. Boggio, K*., et al.* Interleukin 12-mediated prevention of spontaneous mammary adenocarcinomas in two lines of Her-2/neu transgenic mice. *J Exp Med* **188**, 589-596 (1998).
14. Derksen, P.W*., et al.* Somatic inactivation of E-cadherin and p53 in mice leads to metastatic lobular mammary carcinoma through induction of anoikis resistance and angiogenesis. *Cancer Cell* **10**, 437-449 (2006).
15. Pajvani, U.B*., et al.* Fat apoptosis through targeted activation of caspase 8: a new mouse model of inducible and reversible lipoatrophy. *Nat Med* **11**, 797-803 (2005).

Nederlandse Samenvatting

De bevinding dat niet-getransformeerde cellen tumoren infiltreren en bijdragen aan de biologie van kanker, heeft geleid tot veel aandacht voor onderzoek naar de interactie tussen kanker- en niet-kanker cellen[1]. Het micro-milieu van tumoren (TME) bestaat uit verschillende cel populaties zoals endotheel cellen, fibroblasten en immuuncellen, welke een belangrijke rol spelen in tumor- ontwikkeling en progressie, maar ook bij de therapeutische respons op anti-kanker therapieën. Opvallend is dat juist immuuncellen een paradoxale rol hebben in tumoren. Terwijl sommige immuuncellen (zoals $CD8^+$ T lymfocyten en NK cellen), kankercellen kunnen herkennen en doden, kunnen andere immuuncellen (zoals macrofagen en neutrofielen), tumor- ontwikkeling, groei en uitzaaiing bevorderen.

Macrofagen maken een belangrijk deel uit van de TME van tumoren, en zijn onderwerp geweest van tal van studies gericht op het begrijpen van hun rol in tumorprogressie en therapie respons[2]. Van oudsher werden tumor-geassocieerde macrofagen (TAMs) beschreven als antitumoraal (M1) of pro-tumoraal (M2) en onderscheidden op basis van de expressie van enkele markers. Echter, het is nu duidelijk dat het fenotype en de functie van TAMs veel complexer is dan deze binaire definitie doet lijken[3,4]. Macrofagen zijn plastische myeloide cellen, die continu hun fenotype aanpassen op basis van signalen die ze uit hun micro-milieu ontvangen. Omdat verschillende tumoren ook verschillen in hun bijhorende micro-milieu, is het idee ontstaan dat een enkele definitie van een TAM niet bestaat, en dat TAMs uit verschillende tumoren dus ook niet per definitie dezelfde functie en fenotype hebben. Een directe vergelijking van het transcriptoom van TAMs geïsoleerd uit verschillende subtypes borstkanker is echter nog niet uitgevoerd. Een van de hypotheses in dit proefschrift is daarom ook dat onderzoek naar de transcriptionele profielen van TAMs uit verschillende borstkanker subtypes relevant kan zijn, en kan bijdragen aan het stellen van een betere prognose.

In verschillende pre-klinische modellen is aangetoond dat macrofagen tumor-ondersteunende functies hebben[5]. Daarnaast zijn macrofagen geassocieerd met een slechte prognose in verscheidene humane kankers. Om deze redenen worden immuno-modulatoire medicijnen, gericht op het depleteren van macrofagen, momenteel geëvalueerd in klinische trials[6]. Een manier om TAMs te depleteren is door te interfereren met de Colony Stimulating Factor-1 (CSF1)/CSF1 receptor (CSF-1R) signalerings route, welke van vitaal belang is voor macrofagen. Dit is bijvoorbeeld mogelijk met het gebruik van agonistische antilichamen tegen CSF-1R[7]. Om het succes van op macrofaag gerichte medicijnen te maximaliseren, is het uitermate belangrijk om de effecten van deze medicijnen op macrofagen en de kanker te begrijpen, maar ook om optimale medicijncombinaties te vinden, gebruikmakend van conventionele therapieën. Als zodanig, is een deel van het onderzoek beschreven in dit proefschrift erop gericht om uit te zoeken hoe de effectiviteit van anti-CSF-1R door combinaties met chemotherapieën gemaximaliseerd kan worden. Ook worden de achterliggende mechanismes aangehaald.
Naast macrofagen, zijn neutrofielen ook belangrijk voor kankerprogressie en de formatie van metastases[8]. Neutrofiel niveaus zijn vaak verhoogd in kankerpatiënten

en een hoge neutrofiel-tot-lymfocyt ratio in circulatie is voorspellend voor een slechtere overleving in verschillende kankertypes[9,10]. Bovendien correleert chemotherapie-geïnduceerde neutropenie in borstkanker patiënten met een betere prognose[11,12]. Daarom is een beter begrip van de rol van neutrofielen op de chemotherapie respons nodig om de anti-kanker effectiviteit van deze medicijnen te verbeteren. Om dat te kunnen doen, beschrijven we in deze thesis een nieuw muismodel voor de conditionele depletie van neutrofielen.
Het algemene doel van het werk in dit proefschrift is om nieuwe inzichten te vergaren in de complexiteit van immuuncellen, met een focus op macrofagen en neutrofielen, in de context van borstkanker. Hoe tumoren het fenotype van TAMs kunnen beïnvloeden, en hoe immuuncellen de respons op chemotherapie beïnvloeden, zijn de hoofdvragen van deze thesis.

Om intratumorale immuuncellen te bestuderen beschrijven we in **hoofdstuk 2** een methode om immuuncelpopulaties te verkrijgen uit vers geïsoleerd weefsel. Deze methode is gebaseerd op antilichaam-gemedieerde verrijking van immuuncellen met magnetische cel sortering, gevolgd door purificatie van de geselecteerde populatie met multi-color flow cytometry-based sorting.

We gebruiken deze aanpak in **hoofdstuk 3**, waar we TAMs isoleren van twee verschillende genetisch gemanipuleerde muismodellen voor borsttumor ontwikkeling, namelijk, de *K14cre;Cdh1$^{F/F}$;Trp53$^{F/F}$* en *MMTV-NeuT* modellen[13,14]. Deze modellen lijken respectievelijk op humaan invasief lobulair carcinoma (ILC) en HER2^{+} borst tumoren. Bio-informatische analyse van TAM populaties uit deze modellen identificeert een overlappende gen-signatuur, erop duidend dat TAMs uit verschillende modellen ook een overlappend fenotype en functie kunnen hebben. Echter, uit **hoofdstuk 3** blijkt dat er borstkanker subtype specifieke gen-signaturen bestaan, toch indicerend dat verschillende TMEs ook op verschillende manieren het transcriptionele profiel van TAMs dicteren. Interessant genoeg, een selectie van genen specifiek voor het *K14cre;Cdh1$^{F/F}$;Trp53$^{F/F}$* model, correleerde met een slechte overleving van ILC patiënten in twee cohorten.

Chemotherapie is nog steeds de meest gebruikelijke behandeling voor de meeste kankertypes. Chemotherapeutische medicijnen doden kankercellen niet alleen, maar beïnvloeden ook het aantal en fenotype van immuuncellen. Begrip over hoe verschillende chemotherapieën het immuunsysteem beïnvloeden, kan het maken van rationele keuzes voor combinatietherapieën faciliteren. In **hoofdstuk 4** volgt een review over de effecten van chemotherapie op immuuncellen, en stellen we voor dat chemotherapieën die immunosuppressie verlichten, gecombineerd kunnen worden met immuno-therapeutische medicijnen, om het effect van deze te versterken. Naast het feit dat chemotherapieën immuuncellen beïnvloeden, hebben immuuncellen zelf ook een invloed op de therapeutische effectiviteit van deze medicijnen. Het is in het bijzonder bekend dat macrofagen het anti-tumor effect van verschillende chemotherapieën kan tegenwerken. Door een macrofaag depleterend medicijn te gebruiken, anti-CSF-1R, in het *K14cre;Cdh1$^{F/F}$;Trp53$^{F/F}$* model voor spontane borstkanker, laten we in **hoofdstuk 5** van deze thesis zien dat CSF-1R inhibitie de effectiviteit van chemotherapie versterkt, afhankelijk van het type

chemotherapie. We beschrijven dat anti-CSF-1R synergistisch werkt met platinum-houdende medicijnen, zoals cisplatin. We hebben geen synergie gevonden met bijvoorbeeld docetaxel, wat het belang aangeeft om de juiste medicijnen met elkaar te combineren. Daarnaast hebben we ontdekt dat CSF-1R inhibitie type 1 interferon signalering stimuleert in de tumor, wat essentieel is voor het geobserveerde anti-kanker effect van de combinatie cisplatin met anti-CSF-1R. Ook demonstreren we dat verdere depletie van immunosuppressieve neutrofielen van essentieel belang is om een succesvolle anti-tumor respons op gang te brengen in een immunogeen zwak model.

Tot zover zijn de meest gebruikelijke methodes om neutrofielen te bestuderen het depleteren van de populatie, of hun rekrutering te blokkeren. Huidige strategieën hiervoor zijn echter niet specifiek voor neutrofielen, of slechts voor een korte termijn. Daarom is er een duidelijke behoefte aan genetische modellen voor lange termijn neutrofiel depletie, op een conditionele en reversibele manier. In **hoofdstuk 6** beschrijven we de ontwikkeling en karakterisatie van het hMRP8-ATTAC (human migration inhibitory factor-related protein 8-Apoptosis Through Targeted Activation of Caspase 8) model[15]. Dit is een nieuw gegenereerd genetisch muismodel, voor de conditionele en reversibele depletie van neutrofielen. Wanneer een chemische dimerizer wordt geïnjecteerd, wordt het transgen dat het caspase-8-FKBP fusie-eiwit draagt geactiveerd, met apoptose voornamelijk in neutrofielen tot gevolg. Alhoewel deze methode neutrofielen reduceert onder homeostatische condities, gebeurt dit niet in tumor-dragende dieren. Dit geeft aan dat verbeteringen aan het model nodig zijn om een efficiënte neutrofiel depletie te behouden, in de context van chronische inflammatie.

Hoofdstuk 7 bevat een generieke discussie waarin ik de bevindingen uit dit proefschrift in de context van de huidige literatuur plaats, en vervolgens mijn standpunten beschrijf over de toekomst van mijn onderzoek.

References

1. Maman, S. & Witz, I.P. A history of exploring cancer in context. *Nat Rev Cancer* **18**, 359-376 (2018).
2. Cassetta, L. & Pollard, J.W. Targeting macrophages: therapeutic approaches in cancer. *Nat Rev Drug Discov* (2018).
3. DeNardo, D.G. & Ruffell, B. Macrophages as regulators of tumour immunity and immunotherapy. *Nat Rev Immunol* (2019).
4. Mantovani, A., Sozzani, S., Locati, M., Allavena, P. & Sica, A. Macrophage polarization: tumor-associated macrophages as a paradigm for polarized M2 mononuclear phagocytes. *Trends Immunol* **23**, 549-555 (2002).
5. Mantovani, A., Marchesi, F., Malesci, A., Laghi, L. & Allavena, P. Tumour-associated macrophages as treatment targets in oncology. *Nat Rev Clin Oncol* **14**, 399-416 (2017).
6. Cannarile, M.A*., et al.* Colony-stimulating factor 1 receptor (CSF1R) inhibitors in cancer therapy. *J Immunother Cancer* **5**, 53 (2017).
7. Ries, C.H*., et al.* Targeting tumor-associated macrophages with anti-CSF-1R antibody reveals a strategy for cancer therapy. *Cancer Cell* **25**, 846-859 (2014).
8. Coffelt, S.B., Wellenstein, M.D. & de Visser, K.E. Neutrophils in cancer: neutral no more. *Nat Rev Cancer* **16**, 431-446 (2016).
9. Templeton, A.J*., et al.* Prognostic role of neutrophil-to-lymphocyte ratio in solid tumors: a systematic review and meta-analysis. *J Natl Cancer Inst* **106**, dju124 (2014).
10. Wei, B*., et al.* The neutrophil lymphocyte ratio is associated with breast cancer prognosis: an updated systematic review and meta-analysis. *Onco Targets Ther* **9**, 5567-5575 (2016).
11. Han, Y*., et al.* Prognostic value of chemotherapy-induced neutropenia in early-stage breast cancer. *Breast Cancer Res Treat* **131**, 483-490 (2012).
12. Ma, R.M*., et al.* Prognostic Value of Chemotherapy-Induced Neutropenia at the First Cycle in Invasive Breast Cancer. *Medicine (Baltimore)* **95**, e3240 (2016).
13. Boggio, K*., et al.* Interleukin 12-mediated prevention of spontaneous mammary adenocarcinomas in two lines of Her-2/neu transgenic mice. *J Exp Med* **188**, 589-596 (1998).
14. Derksen, P.W*., et al.* Somatic inactivation of E-cadherin and p53 in mice leads to metastatic lobular mammary carcinoma through induction of anoikis resistance and angiogenesis. *Cancer Cell* **10**, 437-449 (2006).
15. Pajvani, U.B*., et al.* Fat apoptosis through targeted activation of caspase 8: a new mouse model of inducible and reversible lipoatrophy. *Nat Med* **11**, 797-803 (2005).

Acknowledgments

The completion of this thesis could have not been possible without the help of many people who inspired me, supported me and motivated me. For that I feel very lucky.

First of all, I would like to express my deepest gratitude for you Karin for the opportunity you gave me to work in your lab. You have been a great mentor who always motivated me, challenged me and helped me grow into the scientist I became.

To my great paranimfen - Kim, you have been such a huge support during these years both in the lab and in the office. I couldn't have done it without you!
Hannah, you are the flow cytometry goddess! Thank you for your invaluable advices but also for the non-scientific – mainly cat-related – chats!
To the paranimf behind the scene - Max, you have been such an incredible friend and colleague. Thank you for the many favors I asked you!

Tisee, Lisanne, do you remember all the experiments you helped me with? I do! Thank you so much for all the help during these years.

Seth, thank you very much for guiding me during my first steps as a PhD student… and for your patience! I am very happy I had the possibility to work with you and learn from you.

Kelly, I had a great time with you in the lab and I am very happy we are still seeing each other in the US!

Kevin, you are a brilliant scientist and I'm sure you'll do great! Thank you for all the times you calmed me down and for all the laughs we had together.

Danique, Olga, Anni, Lorenzo, Antoinette, Ewald, Chris, Noor, thank you so much for the help in the lab and for the great fun we had together!

Chris D., we overlapped in the lab for far too short, but be assured that I will always ask myself "what's the question?". Metamia, after so many years of work I cannot believe our story is published! We did a great job and I am happy we meet again in New York!

Sander, I very much appreciate the time you took to answer my two million questions on bioinformatics. Thank you!

Feline, Mirjam and Bianca, thank you for the fun we had together!

To the whole B3 and C2, thank you very much for the useful and critical discussions we had over the years and for the great time we had at the social events. You have made my time in Amsterdam a great one!

I also wish to thank the many PIs I had the opportunity to interact with: Jannie Borst, Jos Jonkers, Hein the Riele, Heinz Jacobs, Ton Schumacher, Leila Akkari, Pia Kvistborg, Marleen Kok and Joachim Schultze, thank you for the critical discussions and for your useful advices on my project and on my career.

A special thanks to the very talented Giovanni for designing this cool cover and to Agnese and Camilla for being always present despite the distance.

Mamma, papa', grazie per il sostegno che mi avete sempre dimostrato, per aver provato a capire il mio lavoro e per avermi sempre incoraggiato nella mia carriera.

Richi, grazie per starmi accanto e per credere sempre in me, anche in quei momenti in cui penso di non farcela. Amsterdam e il dottorato sono stati una bellissima esperienza perche' c'eri tu vicino a me.

Curriculum Vitae

Camilla Salvagno was born on March, the 2nd 1987 in Venice, Italy. In 2006, she completed her secondary education at the scientific high school "Leopardi - Majorana" in Pordenone, Italy. In September 2006, she started her bachelor studies in Medical Biotechnology at the University of Milan, Italy, that she finalized in 2009 with a thesis on the oxidative stress response of myoblasts derived from facioscapulohumeral Muscular Dystrophy (FSHD) under the supervision of Prof. Dr. Enrico Ginelli. In 2009, she was admitted at Vita-Salute San Raffaele University in Milan, Italy, where she obtained her master Degree in Medical, Molecular and Cellular Biotechnology. She graduated in 2012 with a thesis investigating an intracerebral gene therapy approach for the treatment of leukodystrophies in the laboratory of Dr. Angela Gritti. After that, she briefly continued her research in the lab of Dr. Angela Gritti as post-graduate fellow. In February 2013, she started her PhD work in the laboratory of Prof. Dr. Karin de Visser at the Netherlands Cancer Institute in Amsterdam, the Netherlands, working on the role of the tumor microenvironment in breast cancer development and therapy response. Results of her studies are presented in this thesis. Camilla is continuing her training in cancer immunology in the laboratory of Dr. Juan Cubillos-Ruiz, at Weill Cornell Medicine in New York, USA, where she will be studying how the endoplasmic reticulum stress in immune cells impacts on tumor biology.

Publications

Salvagno, C., Ciampricotti, M., Tuit, S., Hau, C. S., van Weverwijk, A., Coffelt, S. B., Kersten, K., Vrijland, K., Kos, K., Ulas, T., Song, J. Y., Ooi, C. H., Ruttinger, D., Cassier, P. A., Jonkers, J., Schultze, J. L., Ries, C. H. & de Visser, K. E. Therapeutic targeting of macrophages enhances chemotherapy efficacy by unleashing type I interferon response. *Nat Cell Biol* **21**, 511-521, doi:10.1038/s41556-019-0298-1 (2019).

Kersten, K., Coffelt, S. B., Hoogstraat, M., Verstegen, N. J. M., Vrijland, K., Ciampricotti, M., Doornebal, C. W., Hau, C. S., Wellenstein, M. D., **Salvagno, C**., Doshi, P., Lips, E. H., Wessels, L. F. A. & de Visser, K. E. Mammary tumor-derived CCL2 enhances pro-metastatic systemic inflammation through upregulation of IL1beta in tumor-associated macrophages. *Oncoimmunology* **6**, e1334744, doi:10.1080/2162402X.2017.1334744 (2017).

Salvagno, C. & de Visser, K.E. Purification of Immune Cell Populations from Freshly Isolated Murine Tumors and Organs by Consecutive Magnetic Cell Sorting and Multi-parameter Flow Cytometry-Based Sorting. *Methods Mol Biol* **1458**, 125-135 (2016).

Kersten, K.*, **Salvagno, C***. & de Visser, K.E. Exploiting the Immunomodulatory Properties of Chemotherapeutic Drugs to Improve the Success of Cancer Immunotherapy. *Front Immunol* **6**, 516 (2015). **Equal contribution*

Lattanzi, A., **Salvagno, C**., Maderna, C., Benedicenti, F., Morena, F., Kulik, W., Naldini, L., Montini, E., Martino, S. & Gritti, A. Therapeutic benefit of lentiviral-mediated neonatal intracerebral gene therapy in a mouse model of globoid cell leukodystrophy. *Hum Mol Genet* **23**, 3250-3268, doi:10.1093/hmg/ddu034 (2014).